PERTURBER AND TEMPERATURE DEPENDENCE OF COLLISION-INDUCED LIGHT SCATTERING FOR SPHERICAL TOP MOLECULES

A Thesis
Submitted to the Faculty of Graduate Studies
The University of Manitoba

In Partial Fulfillment
of the Requirements for the Degree
Doctor of Philosophy

by

© SALAH MOHAMED EL-SHEIKH

February, 1989

National Library of Canada | Bibliothèque nationale du Canada

Canadian Theses Service | Service des thèses canadiennes

Ottawa, Canada
K1A 0N4

The author has granted an irrevocable non-exclusive licence allowing the National Library of Canada to reproduce, loan, distribute or sell copies of his/her thesis by any means and in any form or format, making this thesis available to interested persons.

L'auteur a accordé une licence irrévocable et non exclusive permettant à la Bibliothèque nationale du Canada de reproduire, prêter, distribuer ou vendre des copies de sa thèse de quelque manière et sous quelque forme que ce soit pour mettre des exemplaires de cette thèse à la disposition des personnes intéressées.

The author retains ownership of the copyright in his/her thesis. Neither the thesis nor substantial extracts from it may be printed or otherwise reproduced without his/her permission.

L'auteur conserve la propriété du droit d'auteur qui protège sa thèse. Ni la thèse ni des extraits substantiels de celle-ci ne doivent être imprimés ou autrement reproduits sans son autorisation.

ISBN 0-315-51571-6

Canada

PERTURBER AND TEMPERATURE DEPENDENCE OF COLLISION-INDUCED LIGHT SCATTERING FOR SPHERICAL TOP MOLECULES

BY

SALAH MOHAMED EL-SHEIKH

A thesis submitted to the Faculty of Graduate Studies of the University of Manitoba in partial fulfillment of the requirements of the degree of

DOCTOR OF PHILOSOPHY

© 1989

Permission has been granted to the LIBRARY OF THE UNIVERSITY OF MANITOBA to lend or sell copies of this thesis, to the NATIONAL LIBRARY OF CANADA to microfilm this thesis and to lend or sell copies of the film, and UNIVERSITY MICROFILMS to publish an abstract of this thesis.

The author reserves other publication rights, and neither the thesis nor extensive extracts from it may be printed or otherwise reproduced without the author's written permission.

ACKNOWLEDGEMENTS

I would like to express my sincere gratitude to my advisor, Dr. G.C. Tabisz, for suggesting the topic, as well as for his skillful guidance and patience throughout the course of this work.

I would like also to thank Dr. R.T. Pack for providing us with advice and subroutines to develop the intermolecular potential for SF_6-Xe.

ABSTRACT

Collision-induced light scattering (CILS) refers to the Rayleigh and Raman spectral features forbidden by the symmetry of a free molecule, but which appear in the scattering from dense media through molecular interactions.

In order to avoid complications from allowed rotational Raman lines, molecules of high symmetry (spherical top) were chosen for the present study.

The two- and three-body (CILS) spectra of both pure octahedral molecules (SF_6), and tetrahedral molecules (CF_4) at 295 K have been determined experimentally. As well, the two-body spectra of these systems perturbed by inert gases have been measured.

Classical line shape calculations were performed for the free-free interactions (translational spectrum), and a model was used to calculate the effects of bound dimers. Comparison between the two-body experimental and theoretical spectra showed a very good agreement at low frequency shifts where the collision-induced rotational Raman scattering has a negligible effect. This agreement was best in the cases of SF_6 mixtures with inert gases because of the availability of good intermolecular potentials.

At higher frequency shifts, higher order polarizabilities played a role, the dipole-octopole polarizability $\underset{\sim}{E}$ in the case of octahedral molecules, and both the dipole-quadrupole $\underset{\sim}{A}$ and the dipole-octopole $\underset{\sim}{E}$ polarizabilities in the case of tetrahedral molecules. The intensity and the shape of the rotational spectra were accounted for well by theory. The values of the polarizabilities found were

E = 10.7 ± 2.5 $\mathring{A}^5$ for SF_6, and A = 2.5 ± 0.3 $\mathring{A}^4$, E = 2.5 ± 0.3 $\mathring{A}^5$ for CF_4. The CILS spectrum of SF_6-Xe, together with both the values of the diffusion coefficient and the second virial coefficient, were used in developing a new M2SV intermolecular potential for SF_6-Xe.

A temperature study of the CILS of CH_4 was performed in the range 130-295 K. The model for the pair polarizability anisotropy with no adjustable parameters still holds at lower temperatures. Calculations for both the induced translational and rotational scattering worked well over this wide temperature range. Values of the dipole-quadrupole polarizability A of 0.88 ± 0.03 $\mathring{A}^4$ and the dipole-octopole polarizability E of 2.5 ± 0.26 $\mathring{A}^5$ were found.

TABLE OF CONTENTS

LIST OF FIGURES

LIST OF TABLES

CHAPTER 1

INTRODUCTION

Raman scattering is named after the Indian scientist C.V. Raman, who first observed this phenomenon in liquids in 1928.

In the spectrum of the inelastically scattered radiation from molecules, the new frequencies constitute Raman lines, or bands. Raman bands at frequencies less than the incident frequency $\tilde{\nu}_0$ are referred to as Stokes $(\tilde{\nu}_0-\tilde{\nu}_\mu)$ bands, and those at frequencies greater than the incident frequency as Antistokes $(\tilde{\nu}_0+\tilde{\nu}_\mu)$ bands. The scattering of radiation without change of frequency is called Rayleigh scattering.

The scattering radiation in general has polarization characteristics different from those of the incident radiation, and both the intensity and the polarization of the scattered radiation depends on the direction of observation.

Collision induced light scattering (CILS) refers to the Rayleigh and Raman spectral features forbidden by the symmetry of a free molecule, but which appear in the scattering from dense media through molecular interactions. In case of only two interacting molecules, the electric field of the incident light induces a dipole moment in one molecule of the pair; the total field acting on its neighbour, to the first order, is the field of this induced dipole plus the external field, which is called the dipole-induced-dipole interaction. CILS was discovered in 1967 by Thibeau (Thibeau, 1968).

The first experiments on interaction induced Raman scattering (Tabisz, 1979) were performed in the mid-seventies (Holzer and leDuff,

1974; Holzer and Ouillon, 1971, 1976) on the molecules of CF_4, SF_6 and CO_2. They explained their observation of the depolarized component of the ν_1 vibrational bands by a dipole-induced-dipole (DID) mechanism. Thibeau et al. (1977) elucidated this mechanism, making a thorough and general comparison between the depolarization ratio for Rayleigh and for Raman scattering by a fluid composed of isotropic molecules. Such an approach, however could not explain the observation of completely forbidden vibrational bands.

Samson, Pasmanter and Ben-Reuven (1976; Samson and Ben-Reuven, 1976) proposed a theory to account for these which formally included effects due to dipole-quadrupole $\underset{\sim}{A}$ and electric dipole-magnetic dipole $\underset{\sim}{G}$ polarizabilities. This theory has not been developed to the point at which it is useful for analysis of experiments. At this time, Buckingham and Ladd (1976) extended the theory of collison-induced absorption in the far infrared region to include the contribution of the dipole moment induced in a molecule by the gradient of the field due to the permanent multipole moments of its neighbours. A theory of induced pure rotational scattering was then developed by Buckingham and Tabisz (1977, 1978). A recent computer search (Frommhold, 1987), showed that 500 papers dealing with the collision induced Rayleigh and Raman spectra by gases and condensed matter have appeared from 1967 until the end of 1987.

Collision induced light scattering (CILS) is a general effect; it appears in the spectra of isotropic and anisotropic molecules in the gas, liquid, and solid state phase. The interest in CILS lies in the fact that it exists because of collisions and is, in principal, a source of information on molecular interactions and dynamics in dense media.

The purpose of this thesis is to study the CILS for spherical top isotropic molecules in the gas phase (octahedral molecules (SF_6), and tetrahedral molecules (CF_4 and CH_4)), and to deal with some of the persisting problems that one has in investigating the spectra of those molecules. Some of these problems are as follows:

(1) There is perhaps no adequate potential to describe SF_6-SF_6 interactions.

(2) The existence in the literature of two sets of parameters for a potential for SF_6-Kr mixture.

(3) There is no good potential for SF_6-Xe mixture.

(4) A discrepancy between the theoretical calculations and the experimental spectrum in the case of CF_4 (measured previously in this laboratory) exists possibly because of an impurity in the sample.

(5) Detailed study of CILS as a function of temperature has never been done systematically.

A number of experiments are conceived and performed in this study in order to deal with these problems:

(1) The spectrum of SF_6-SF_6 is measured twice to obtain a reliable experimental spectrum to compare with various calculations using different potentials.

(2) Spectra are taken for SF_6 mixtures:

(i) SF_6-Xe

(ii) SF_6-Kr

(iii) SF_6-Ar

(iv) SF_6-Ne

(3) The spectra of CF_4 to re-investigate the CF_4 problem are recorded, these are

(i) CF_4-CF_4

(ii) CF_4-Ar.

In addition, experiments were performed in Firenze (Italy) by the group at CNR. In particular, spectra for CH_4 were studied as a function of temperature from 295 K to 130 K. These data are compared with a series of calculations.

In the case of SF_6-SF_6, an HFD form is fit to the Neumann numerical potential, and calculations performed with it agree well with the experimental data (see Chapter 4). There are good potentials available for SF_6-Kr, SF_6-Ar, SF_6-Ne from the Pack group which help to obtain a firm value for the dipole-octopole polarizability (E) for SF_6. In the case of SF_6-Kr, we do the calculations using the two available sets of parameters, compare the theoretical spectra with the experimental one, and are able to make a distinction between these potentials.

In the case of SF_6-Xe, through cooperation with Pack and the use of available data (virial coefficient, diffusion coefficient and the CILS spectrum as a third property), a new potential is developed for SF_6-Xe.

In the case of CF_4, the new series of experiments enable us to obtain better agreement between the theoretical and experimental spectra, especially at high frequency shifts. This spectrum together with the CF_4-Ar spectrum, enable us to find refined values for the dipole-quadrupole A and the dipole octopole E polarizabilities for

CF_4.

In the case of CH_4 as a function of temperature, two models are tried to explain the induced translational spectrum, one of them works well. The dimer contribution as a function of temperature is studied. A model to explain the rotational scattering works well over the entire temperature range. Values of the dipole-quadrupole and the dipole-octopole polarizability for CH_4 are determined.

This thesis is divided into eight chapters:

Chapter 1. Introduction.

Chapter 2. The theory of collision-induced translational and rotational scattering is discussed in detail; the dimer calculations are described and the different forms of potentials used in the calculations are presented.

Chapter 3. The experimental set-up, data collection and data analysis for both pure and perturbed molecular interactions are detailed.

Chapter 4. The generation of theoretical spectra and the comparison between the theory and experiments for both pure and perturbed octahedral molecules are discussed.

Chapter 5. The development for an M2SV potential for SF_6-Xe is described.

Chapter 6. Calculations of theoretical spectra and comparison between the theoretical and experimental spectra for both pure and perturbed tetrahedral molecules form the subject here.

Chapter 7. Detailed calculations and analysis for CH_4 spectra in the range 130-295 K are presented.

Chapter 8. Conclusions.

CHAPTER 2

THEORY OF COLLISION INDUCED SCATTERING

In the study of molecular interactions, we are normally concerned with the difference between the energy of a group of molecules (usually a pair) and the energy of separate molecules for fixed molecular positions and orientations.

This interaction energy is usually small compared to the molecular electronic and vibrational energies, but it may be much larger than the difference between the rotational energy levels; the rotational and translational motions of interacting molecules can, therefore, be very different from those of the free molecule. The basic problem is the evaluation of the energy as a function of relative molecular positions and orientations. When this has been solved, the effects of the interaction can be determined by considering the translational and rotational motions.

In some cases this is a formidable task but often the occupied states have energy separations that are small compared to $k_B T$ and a classical treatment suffices.

This chapter is concerned with the interaction of molecules, as perceived through features of their scattered light spectrum.

The chapter will be divided into three sections:

1. Translational spectrum.
2. Dimer or long-lived cluster spectrum.
3. Rotational spectrum.

2.1 THE TRANSLATIONAL SPECTRUM

We consider the collision-induced light scattering by a pair of molecules, neglecting the internal degrees of freedom of the interacting molecules.

2.1.1 The Pair Polarizability

The polarizability of a pair of widely separated molecules has the value $(\alpha_{01} + \alpha_{02})$ where α_{01}, α_{02} are the polarizabilities of the two isolated molecules. However, when the separation of the two molecules is small enough, the polarizability will be different from the sum of the isolated molecular polarizabilities due to the interaction. The dominant interaction leading to this effect is the so-called dipole-induced-dipole (DID) mechanism.

2.1.1a The Dipole-Induced-Dipole Model (Tabisz, 1979; Silberstein, 1917)

The electric field of the incident light induces a dipole moment in one molecule of the pair. To first order, the total field acting on its neighbour is then the field of this induced dipole plus the external field. The interaction may be taken to higher orders, wherein the field of the dipole induced in molecule 2 acts back on molecule 1, etc. This effect can be described as follows and the situation is shown in Fig. 2.1:

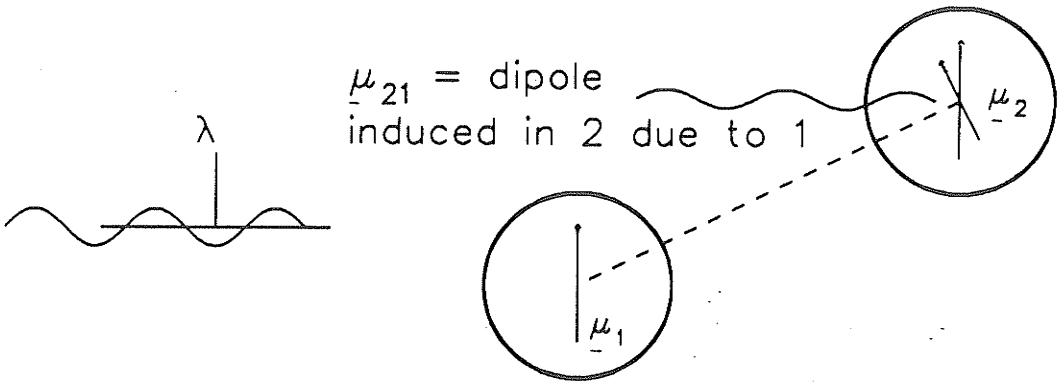

Figure 2.1

For a spherical molecule, the dipole moment $\underline{\mu}$ is given by

$$\underline{\mu} = \alpha_0 \underline{F}_0 \tag{2.1}$$

where α_0 is the polarizability of the isolated molecule and F_0 is the external field.

In cases of two non-interacting molecules:

$$\underline{\mu} = \alpha_{01} \underline{F}_0 + \alpha_{02} \underline{F}_0 \cdot \tag{2.2}$$

If the two molecules are interacting, the dipole moment will be given by,

$$\underline{\mu} = \alpha_1 \underline{F}_1 + \alpha_2 \underline{F}_2 \tag{2.3}$$

where α_1, α_2 are different from α_{10}, α_{20} and the total field acting on each molecule will be given by

$$\underline{F}_1 = \underline{F}_0 + \underline{F}_{12} , \qquad \underline{F}_2 = \underline{F}_0 + \underline{F}_{21} \tag{2.4}$$

where $\underline{F}_{12}$ is the field at 1 of the dipole induced in 2 and is given by

$$\underline{F}_{12} = \frac{3\underline{n}_{21}\,(\underline{\mu}_2 \cdot \underline{n}_{21}) - \underline{\mu}_2}{r^3} \tag{2.5}$$

and $\underline{n}_{21}$ is the unit vector pointing from 2 to 1.

Similarly

$$\underline{F}_{21} = \frac{3\underline{n}_{12}\,(\underline{\mu}_1 \cdot \underline{n}_{12}) - \underline{\mu}_1}{r^3} \tag{2.6}$$

With $\underline{n}_{21} \parallel \underline{F}_0$,

$$\underline{F}_{12} = \frac{2\underline{\mu}_2}{r^3} \quad \text{and} \quad \underline{F}_{21} = \frac{2\underline{\mu}_1}{r^3} \tag{2.7}$$

where $$\underline{\mu}_2 = \alpha_2\,\underline{F}_2 \ , \qquad \underline{\mu}_1 = \alpha_1\,\underline{F}_1 \ . \tag{2.8}$$

The polarizability in a direction parallel to the incident field is given by (Silberstein, 1917)

$$\alpha_{\parallel} = \frac{\underline{\mu}}{\underline{F}_0} = \frac{\alpha_1\,\underline{F}_1 + \alpha_2\,\underline{F}_2}{\underline{F}_0}$$

$$= \alpha_1 + \alpha_2 + \frac{4\alpha_1\,\alpha_2\,(r^3 + \alpha_1 + \alpha_2)}{r^6 - 4\alpha_1\,\alpha_2} \ . \tag{2.9}$$

For $\underline{n}_{21} \perp \underline{F}_0$, the polarizability in a direction $\perp$ to the incident field is given by

$$\alpha_{\perp} = \alpha_1 + \alpha_2 - \frac{\alpha_1\,\alpha_2\,(2r^3 - \alpha_1 - \alpha_2)}{(r^6 - \alpha_1\,\alpha_2)} \ . \tag{2.10}$$

In case of two similar molecules

$$\alpha_{\parallel} = 2\alpha_0 + \frac{4\alpha_0^2}{r^3} + \frac{8\alpha_0^3}{r^6} + \frac{16\alpha_0^4}{r^9} + \ldots \qquad (2.11)$$

$$\alpha_{\perp} = 2\alpha_0 - \frac{2\alpha_0^2}{r^3} + \frac{2\alpha_0^3}{r^6} - \frac{2\alpha_0^4}{r^9} + \ldots \qquad (2.12)$$

where r is the distance between the two molecules; then the isotropic and the anisotropic parts of the pair polarizability tensor are given by

$$\bar{\alpha}(r) = \frac{\alpha_{\parallel} + 2\alpha_{\perp}}{3} = 2\alpha_0 + \frac{4\alpha_0^3}{r^6} + \frac{4\alpha_0^4}{r^9} + \ldots \qquad (2.13)$$

$$\beta(r) = \alpha_{\parallel} - \alpha_{\perp} = \frac{6\alpha_0^2}{r^3} + \frac{6\alpha_0^3}{r^6} + 18\,\frac{\alpha_0^4}{r^9} + \ldots \qquad (2.14)$$

To first order the incremental polarizability, $\Delta\alpha(r) = \alpha_{12} - \alpha_1 - \alpha_2$, is completely anisotropic where α_{12} is the total polarizability of the interacting molecules; $\beta(r) = 6\alpha_0^2/r^3$, which provides a major (usually the principal) contribution to $\Delta\alpha(r)$ for gases.

2.1.1b Other Contributions to Molecule-Molecule Interactions

(i) Electron Overlap Interaction: The distortion of the electron clouds during close collision of molecules gives a negative contribution to the total incremental polarizability. Because the volume occupied by the electrons will be reduced when the electrons are more tightly confined, they move less in response to an applied field and hence the polarizability is reduced. O'Brien et al. (1973) completed Hartee-Fock calculations on $(He)_2$ at several intermolecular

distances. They found that $\alpha_{\perp}(r) - 2\alpha_{He}$ is always negative and decreases with increasing r and that $\alpha_{\parallel}(r) - 2\alpha_{He}$ is positive over the range of r studied, initially increasing and then decreasing with decreasing r. The incremental anisotropy, $\alpha_{\parallel}(r) - \alpha_{\perp}(r)$ is nearly zero beyond r = 8 a.u.; they find that $[\beta(r) - \frac{6\alpha_0^2}{r^3}]$ has an exponential form.

(ii) Electron Density Fluctuations: The term in the molecular pair polarizability due to electron density fluctuations is analogous to the London dispersion which arises because the electrons are not static within the molecule. At any given moment the electron density distribution within the molecule may differ from its time-averaged value, with the result that the net dipole moment of the atom fluctuates rapidly about zero. The instantaneous dipole moment on the atom tends to induce a parallel dipole moment in any neighbouring molecules. Two parallel dipoles always attract and the time-averaged effect of the correlated fluctuations is a net attraction between the charge distribution.

Certain and Fortune (1971) apply variational methods to obtain the coefficients in the r^{-6} term for $(He)_2$ and got different values than the classical values for both $\bar{\alpha}$ and β (Eqns. 2.13 and 2.14).

To account for both contributions $\beta(r)$ has been written as

$$\beta(r) = \frac{6\alpha_0^2}{r^3} + Ar^{-6} - B \exp(-r/r_0) \qquad (2.15)$$

A, B and r_0 are constants which can be determined using the three lowest even experimental moments of the spectral profile of the resultant light scattering.

Work has been done for Ar (Bafile et al., 1983), Kr, and Xe (Barocchi et al., 1983) and CH_4 (Meinander et al., 1985), and it seems that the numerical values of the three parameters are very sensitive to the input values of the moments, but the corresponding functions $\beta(r)$ are really very similar, except for very small values of r. Therefore a new model was developed in which two of the parameters are fixed by theoretical considerations.

2.1.1c <u>**A New Model for $\beta(r)$ and The Scaling Law**</u> (Meinander et al., 1986)

A simple model for the parameter (A) of model (2.15), has been derived by Buckingham (1956)

$$A = 6\alpha_0^3 + \frac{\gamma\, C_6}{3\alpha_0} \qquad (2.16)$$

where γ is the hyperpolarizability and C_6 is the first dispersion force coefficient.

The value of A for the noble gases and for CH_4 using Eqn. (2.16) is within the range of the A values obtained by model (2.15) using different experimental data (Barocchi and Zoppi, 1978).

Tha value of A can therefore be fixed as determined by the model of Buckingham.

The value for $X_0 = \frac{r_0}{r_m}$ has been fixed at the value $X_0 = 0.09531$, where r_m is the separation at which the intermolecular potential energy attains its minimum value, using the ab initio calculations of $\beta(r)$ for He by Dacre (1982). We are thus left with only one adjustable parameter in our model for $\beta(r)$, the parameter B, which we determine using the first few even moments of the measured spectrum.

It is of interest that the reduced parameter $B^* = \frac{Br_m^3}{6\alpha_0^2}$ is very similar for Ne, Ar, Kr, Xe and CH_4 (Meinander et al., 1986). Within the uncertainties, a common reduced value of $B^* = 2600 \pm 200$ would seem to be applicable to all five systems and perhaps can be used for other gases. The final form for the anisotropy is then

$$\beta(r) = \frac{6\alpha_0^2}{r^3} + (6\alpha_0^3 + \frac{\gamma C_6}{3\alpha_0}) \bar{r}^6 - (2600) (\frac{6\alpha_0^2}{r_m^3}) \exp (\frac{r}{0.09531\ r_m}) \tag{2.17}$$

where all the parameters are known.

2.1.2 Line Shape Analysis (Meinander and Tabisz, 1986)

At moderate pressures, the CILS spectrum is determined by binary interactions only and is proportional to the Fourier transform of the pair correlation function c(t):

$$D_{II}(\omega) \propto \int_{-\infty}^{\infty} dt \exp(-i\omega t)\, c(t) \tag{2.18}$$

with $$c(t) = \langle \alpha_{xz}(t)\, \alpha_{xz}(0) \rangle ,$$

where $\alpha_{xz}(t) = \alpha_{xz}(\underline{r}(t))$ is the xz component of the polarizability tensor of the interacting molecular pair in a space fixed coordinate system. This function can be expressed in terms of the dependence of the pair polarizability anisotropy $\beta(r)$, and on the motion of the atoms, which is governed by the intermolecular potential $U(\underline{r})$. The time dependence of $\alpha_{xz}(t)$ can be explicitly described by specifying the functional dependence $\underline{r}(t)$. The function $\underline{r}(t)$ can be evaluated by transforming the two-body problem to an equivalent one-body problem as follows.

If we consider the encounter of two masses m_a and m_b whose coordinate vectors in the laboratory frame are $\underline{r}_a$, and $\underline{r}_b$, then the vector for the centre of mass $\underline{r}_c$ is

$$\underline{r}_c = \frac{m_a \underline{r}_a + m_b \underline{r}_b}{m_a + m_b} \quad . \tag{2.19}$$

We may introduce the separation vector $\underline{r} = \underline{r}_a - \underline{r}_b$. The situation is as shown in Fig. 2.2.

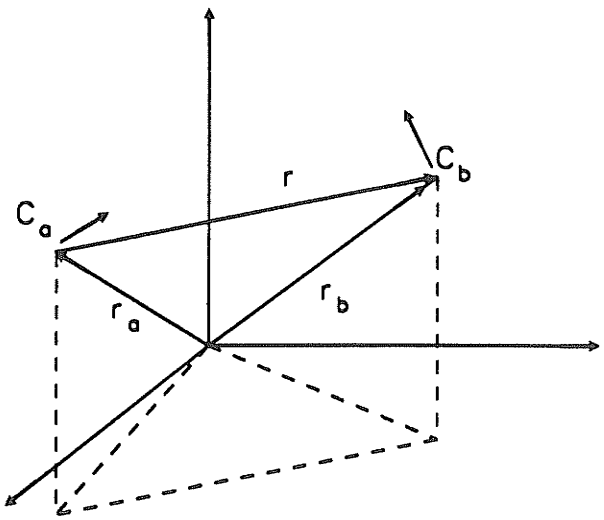

Figure 2.2

Applying Newton's equations of motion to each particle we have

$$\underline{F} = m_a \frac{d\underline{C}_a}{dt}$$

$$-\underline{F} = m_b \frac{d\underline{C}_b}{dt} \tag{2.20}$$

assuming a spherically symmetrical potential.

Here $\underline{C}_a$, and $\underline{C}_b$ are the respective velocities of a and b. It is clear from Eqns. (2.19) and (2.20) that

$$\underline{a}_c = \frac{d\underline{C}_c}{dt} = \frac{d^2\underline{r}_c}{dt^2} = 0$$

that is, the centre of mass moves with a constant velocity $\underline{C}_c$. The relative acceleration of the two particles can be written using Eqn. (2.20) as

$$\frac{d}{dt}\left(\frac{d\underline{r}}{dt}\right) = \frac{d\underline{C}}{dt} = \frac{d\underline{C}_a}{dt} - \frac{d\underline{C}_b}{dt} = \left(\frac{1}{m_a} + \frac{1}{m_b}\right)\underline{F} = \frac{\underline{F}}{\mu} \qquad (2.21)$$

where μ is the reduced mass of the system.

Eqn. (2.21) defines the relative motion of a and b, which is confined to a plane containing both particles and their centre of mass. In the centre-of-mass frame, the relative motion of the two particles is thus equivalent to the motion of a single particle of mass μ in the central force field $\underline{F}$, i.e. under the influence of the potential $U(\underline{r})$, (Fig. 2.3).

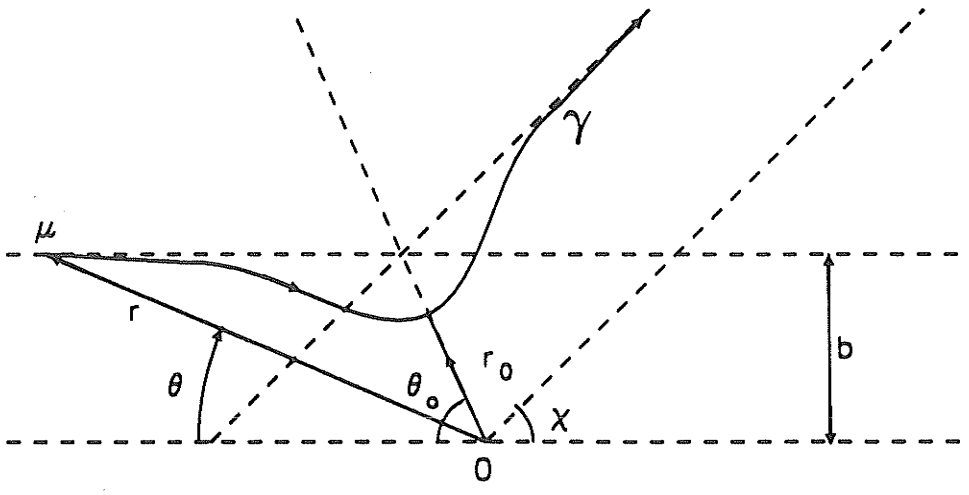

Figure 2.3

The vector $\underline{r}$ joins the centre of mass O to the position of the particle of mass μ, which follows the trajectory γ. The angle between $\underline{r}$ and the initial direction of motion is called the orientation angle θ. This has the value θ_0 at the distance of closest approach. The impact parameter b, is the distance of closest approach in the absence of the potential $U(\underline{r})$ and, hence in the absence of any deflection.

The dynamics of this collision may be described by considering the conservation of both energy E and angular momentum L in the system as follows:

$$E = \frac{1}{2}\mu v_0^2 = \frac{1}{2}\mu v^2 + U(r) = \frac{1}{2}\mu \dot{r}^2 + \frac{1}{2}\frac{L^2}{\mu r^2} + U(r) \qquad (2.22)$$

$$L = \mu r^2 \dot{\theta} = \mu b v_0 \qquad (2.23)$$

where v_0 is the initial velocity.

Solving Eqns. (2.22) and (2.23), one can get

$$\frac{\dot{r}}{v_0} = [1 - (\frac{b}{r})^2 - \frac{U(r)}{E}]^{\frac{1}{2}} \qquad (2.24)$$

$$\dot{\theta} = \frac{b v_0}{r^2} \qquad (2.25)$$

These equations can be integrated to obtain $\underline{r}(t)$.

Once $\underline{r}(t)$ is known, together with U(r), the explicit time dependence of the polarizability $\alpha(t)$ can be found. The incident light is along the x axis with its electric vector polarized in the z direction and observations are made in the z direction. The differential scattering cross-section for a single similar pair of interacting molecules per unit frequency and unit solid angle is

given by (Bafile et al., 1983)

$$\frac{d^2\sigma_{II}}{d\Omega\, d\nu_s} = 2K_0 K_s^3 \int_{-\infty}^{\infty} dt \exp(-i\omega t) < \alpha_{xz}(t)\, \alpha_{xz}(0) > \quad (2.26)$$

where K_0 and K_s are the wave vectors of the incoming and scattering light respectively, and

$$< \alpha_{xz}(t)\, \alpha_{xz}(0) > = \int_0^{\infty} dv \int_0^{\infty} db \int_{\gamma(v,b)} dr\, P(v)\, P(b,r(\tau))$$

$$\alpha_{xz}(t+\tau)\, \alpha_{xz}(\tau) \quad (2.27)$$

where $P(v)dv$ is the probability that the relative velocity is between v and v+dv

$P(b, r(\tau))\, db\, dr$ is the probability that the impact parameter is between b and b+db where the initial distance of the pair is between $r(\tau)$ and $r(\tau)+dr$ and the integration is extended to all possible $r(\tau)$ on the trajectories $\gamma(v,b)$.

For a system of volume V at thermal temperature T, $P(v)$ is the Maxwell distribution of the relative velocity v, and

$$P(b, r(\tau))\, db\, dr = \frac{2\pi\, bv}{V} d\tau\, db \quad (2.28)$$

Using Eqns. (2.27), (2.28) and the convolution theory, Eqn. (2.26) becomes

$$\frac{d^2\sigma_{II}}{d\Omega \cdot d\nu_s} = \frac{2K_0 K_s^3}{V} \int_0^\infty dv\, P(v) \int_0^\infty db\, 2\pi bv$$

$$\left| \int_{-\infty}^{\infty} dt \exp(-i\omega t)\, \alpha_{xz}(t) \right|^2 \qquad (2.29)$$

Rewriting Eqn. (2.29) using the intrinsic variables $r(t)$ and $\theta(t)$ of the colliding pair and defining the depolarized spectrum $D_{II}(\omega)$ as

$$D_{II}(\omega) = V \frac{d^2\sigma_{II}}{d\Omega\, d\nu_s} \qquad (2.30)$$

we get

$$D_{II}(\omega) = \frac{2}{15} K_0 K_s^3 \int_0^\infty dv\, P(v) \int_0^\infty db\, 2\pi bv\, \Gamma(\omega) \qquad (2.31)$$

where

$$\Gamma(\omega) = 1.5 \left\{ \int_0^\infty \beta(t) \cos [2\theta(t) + \omega t]\, dt \right\}^2 \qquad (2.32)$$

$$+ \left\{ \int_0^\infty \beta(t) \cos\omega t\, dt \right\}^2 + 1.5 \left\{ \int_0^\infty \beta(t) \right.$$

$$\left. \cos [2\theta(t) - \omega t]\, dt \right\}^2$$

The computation (Bafile et al., 1983) of the CILS can be performed using Eqns. (2.31) and (2.32).

The integrations in Eqn. (2.32) are performed along the trajactory of the interacting molecules, starting from the point of closest approach a, which is a solution of the equation

$$0 = 1 - \frac{2}{mv^2}\ U(a) \tag{2.33}$$

The accuracy of the trajectories was checked by comparison with the function

$$\theta(r) = b \int_a^r dr\ \bar{r}^2 \left[1 - b^2\ \bar{r}^2 - \frac{U(r)}{E}\right]^{-\frac{1}{2}} \tag{2.34}$$

The integrands of Eqn. (2.32) are computed as products of slowly varying functions $f_i(\beta,\theta)$ with $\sin(\omega t)$ or $\cos(\omega t)$ (Meinander et al., 1986). For time steps $\Delta t \leq \pi/\omega$, seventh degree interpolation polynomials reproducing the integrands and their first three time derivatives at the end points, are integrated analytically. For higher frequencies $\Delta t >> \pi\omega$, the time steps are divided into sub-intervals of π/ω. The intensity at $\omega = 0$ is obtained easily during the calculations of the trajectories by setting $\omega = 0$ in Eqn. (2.32).

Classical spectral line shapes are symmetric, i.e.

$$D(-\omega) = D(\omega) \tag{2.35}$$

Usually the wings of induced spectra extend to energies greater than thermal energies, i.e. $\hbar\omega \geq k_B T$, where k_B and T are the Boltzman constant and the temperature. Accordingly, the principle of detailed balance (Poll, 1980; Borysow and Frommhold, 1983) causes observed profiles to be asymmetric, i.e.

$$D_{exp}(-\omega) = \exp\left(-\hbar\omega/k_B T\right)\ D_{exp}(\omega) \tag{2.36}$$

It is believed that this defect of the classical profile calculation can be corrected by desymmetrizing (Borysow and Frommhold, 1983; Poll and Hunt, 1981) classical line shapes for comparison with measurements, by multiplying the classical profile by the factor

$$2\,[1 - \exp\,[-\hbar\omega/k_B T]]^{-1}$$

which leaves the even moments of the profile unchanged and valid for the first order in h (Barocchi et al. 1982). The even spectral moments are given by

$$M_{2n} = \int_0^\infty D(\omega)\,\omega^{2n}\,d\omega \qquad (2.37)$$

with n = 0, 1, 2, ...

which we use as a check for the correctness of the calculated profile, by comparison with the theoretical moments obtained from the sum formulae (see section 2.2).

It should be noted that calculations, using Eqn. (2.32), do not include the contributions from bound or semi-bound trajectories.

The computation of the intensity at 40 different frequencies (Stokes side) requires about 17 minutes of CPU time on the Amadahl 470/V8 Computer.

2.1.3 The Intermolecular Potential U(r)

The intermolecular potential in general includes both isotropic and anisotropic interactions, but in our purely translational spectrum we will be dealing with spherical top molecules, for which the anisotropic part (as in CH_4) is small. We fit the total potential to an isotropic form (as will be discussed in detail in Chapter 7).

The interaction potentials used in our computation can be expressed by an analytical function. For the present calculations the following potential functions were used.

In the case of SF_6, CF_4 and their mixtures, isotropic potentials were used.

(i) SF_6-SF_6 Interactions - Two different intermolecular potentials were tested.

(1) Lennard-Jones 28-7 - The potential is given by

$$U_{28\text{-}7}(r) = \frac{(4)^{4/3}}{3} \varepsilon \left(\left(\frac{\sigma}{r}\right)^{28} - \left(\frac{\sigma}{r}\right)^{7} \right) \qquad (2.38)$$

where (i) $r_m = 4.999$ Å, $\varepsilon/k_B = 439$ K (McCoubrey and Singh, 1959).(MC)

(ii) $r_m = 5.4305$ Å, $\varepsilon/k_B = 404$ K (Powels et al., 1983).(PS)

(2) Neumann Potential - Since there were numerical data available for a site-site potential that Pleich had used to determine the value of the dipole-octopole polarizability E, (Neumann, 1984), we decided to employ this potential as well.

The data are listed in Table 2.1.

Fitting the data to the Hartree-Fock (HFD) form, namely

$$U(x) = A_0 x^{A_1} e^{-A_2 x} - (C_6 x^{-6} + C_8 x^{-8} + C_{10} x^{-10}) F(D) \qquad (2.39)$$

where

$$F(D) = 1 \qquad x \geq D = 1.28$$

$$= e^{-(\frac{1.28}{x} - 1)^2} \qquad x < D$$

TABLE 2.1

Neumann Potential Data for SF_6-SF_6

r (Å)	U(r) (K)	r (Å)	U(r) (K)
4.0	4195.15	7.2	-57.57
4.1	2797.15	7.3	-52.25
4.2	1809.81	7.4	-47.49
4.3	1109.45	7.5	-43.24
4.4	622.469	7.6	-39.42
4.5	288.779	7.7	-36.00
4.6	60.9057	7.8	-32.93
4.7	-94.436	7.9	-30.17
4.8	-199.09	8.0	-27.66
4.9	-267.44	8.1	-25.39
5.0	-309.6	8.2	-23.35
5.1	-332.26	8.3	-21.49
5.2	-340.25	8.4	-19.82
5.3	-337.57	8.5	-18.30
5.4	-327.43	8.6	-16.91
5.5	-312.03	8.7	-15.62
5.6	-292.87	8.8	-14.47
5.7	-271.18	8.9	-13.40
5.8	-248.27	9.0	-12.44
5.9	-225.37	9.1	-11.57
6.0	-203.41	9.2	-10.74
6.1	-182.91	9.3	-10.00
6.2	-164.17	9.4	-9.32
6.3	-147.22	9.5	-8.69
6.4	-132.03	9.6	-8.11
6.5	-118.46	9.7	-7.57
6.6	-106.42	9.8	-7.08
6.8	-86.18	10.0	-6.21
6.9	-77.73		
7.0	-70.2		
7.1	-63.52		

and using a library program (ZxSSQ), which employed a Levenberg-Marquardt method, we find the constants

$$A_0 = 0.147976 \times 10^7 \text{ K}$$
$$A_1 = -0.114067$$
$$A_2 = 14.50061$$
$$C_6 = 0.6776507 \text{ K}$$
$$C_8 = 0.7963240 \text{ K}$$
$$C_{10} = 0.3656460 \text{ K}$$

which fit the data very accurately as shown in Fig. 2.4.

(ii) For SF_6-Kr, SF_6-Ar, and SF_6-Ne Mixtures: Pack et al. (1982, 1984) have reported the most accurate interatomic potentials yet for these systems. In the M3SV form, (the potential is shown in Fig. 2.5) viz:

$$U_i(r) = \varepsilon_i \{\exp[-2\alpha_i (r-r_{mi})] - 2\exp[-\alpha_i (r-r_{mi})]\} \quad \begin{matrix} r \leq r_0 & i = I \\ r_0 \leq r \leq r_m & i = II \\ r_m \leq r \leq r_1 & i = III \end{matrix} \qquad (2.40)$$

$$U_{Iv} = \beta_1 + (x-x_1)\{\beta_2 + (x-x_2)[\beta_3 + (x-x_1)\beta_4]\} \quad r_1 \leq r \leq r_2$$

$$U_v = -C_6 r^{-6} - C_8 r^{-8} - C_{10} r^{-10} \quad r \geq r_2$$

where $\varepsilon_{II} = \varepsilon_{III} = \bar{\varepsilon}$

$r_{mII} = r_{mIII} = \bar{r}_m$

$$\varepsilon_I = \bar{\varepsilon}\ \alpha_{II}/\alpha_I$$

$$r_0 = \bar{r}_m - \alpha_{II}^{-1} \ln 2$$

$$r_{mI} = r_0 + \alpha_I^{-1} \ln 2$$

$$x = \frac{r}{r_{min}}$$

$$r_1 = r_m + \alpha_{III}^{-1} \ln 2$$

$$\beta_1 = U(x_1)$$

$$\beta_2 = (x_2-x_1)^{-1} [U(x_2) - \beta_1]$$

$$\beta_3 = (x_2-x_1)^{-1} [\frac{\partial U}{\partial x}|_{x_1} - \beta_2]$$

and

$$\beta_4 = (x_2-x_1)^{-1} \{(x_2-x_1)^{-1} [\frac{\partial U}{\partial x}|_{x_2} - \beta_2] - \beta_3\}$$

The data for the isotropic potential is given in Table 2.2. (The dimensions of the first seven parameters are in Hartree a.u., the last two are dimensionless).

(iii) SF_6-Xe Mixture - For this mixture there was no potential available. We tried the combination rules given by Pena et al. (1982) for two L-J (12-6) potentials for SF_6 and Xe.

The combination rules are

$$\sigma_{12}^6 = \frac{(I_1 + I_2)}{2(\varepsilon_1 \varepsilon_2 \sigma_1^6 \sigma_2^6 I_1 I_2)^{\frac{1}{2}}} (\beta_1 \beta_2)^6 \langle\beta\rangle_m ,$$

$$\varepsilon_{12}^6 = \frac{2(\varepsilon_1 \varepsilon_2 \sigma_1^6 \sigma_2^6 I_1 I_2)^{\frac{1}{2}}}{(I_1 + I_2)\sigma_{12}^6} \quad . \tag{2.41}$$

TABLE 2.2

The Parameters of M3SV Potential for SF_6-Kr, SF_6-Ar, and SF_6-Ne

Parameter	SF_6 Ne	SF_6 Ar	D SF_6 Kr	S
$\bar{\varepsilon}$	$(3.52\pm0.02)\times10^{-4}$	$(7.5\pm0.1)\times10^{-4}$	$(8.6\pm0.1)\times10^{-4}$	$(8.0\pm0.1)\times10^{-4}$
$\bar{r}_m$	8.128±0.005	8.39±0.02	8.72±0.02	8.81±0.02
$\alpha_I=\alpha_{II}$	0.88±0.01	0.97±0.03	0.84±0.02	0.89±0.02
α_{III}	0.85±0.02	0.88±0.03	0.84±0.02	0.89±0.02
C_6	76.4±13	252±10	320±10	277±8
C_8	1505	6100	9000	9000
C_{10}	34000	180000	270000	270000
x_1	infl. pt.	infl. pt.	infl. pt.	infl. pt.
x_2	1.55	1.4	1.4	1.4

I_1, I_2 are the ionization potentials for SF_6 and Xe and are equal to 19.3 and 12.127 e.v. respectively.

For Xe $\quad \varepsilon_1/k_B = 222.43$ K $\quad\quad \sigma_1 = 4.105$ Å

For SF_6 $\quad \varepsilon_2/k_B = 182$ K $\quad\quad \sigma_2 = 6.631$ Å

$$\beta_1 = (\varepsilon_1 \sigma_1^{12})^{1/13} \qquad \beta_2 = (\varepsilon_2 \sigma_2^{12})^{1/13} \tag{2.42}$$

In our case

$$\langle\beta\rangle_{m'} = \sqrt{\beta_1 \beta_2} \tag{2.43}$$

which gives $\sigma_{12} = 4.997875$ Å, $\varepsilon_{12}/k_B = 190.72522$ K

and

$$U(r) = 4\varepsilon_{12} \left[\left(\frac{\sigma_{12}}{r}\right)^{12} - \left(\frac{\sigma_{12}}{r}\right)^{6} \right] .$$

This method provided a potential which yielded spectra in poor agreement compared with the experiment. Cooperation with Pack to develop an M3SV potential for this system ensued and will be discussed in Chapter 5.

(iv) CF_4-CF_4 Interaction - A L-J (12-6) potential was used in the form

$$U(r) = 4\varepsilon \left[\left(\frac{\sigma}{r}\right)^{12} - \left(\frac{\sigma}{r}\right)^{6} \right] , \qquad (2.44)$$

$\varepsilon/k_B = 152.5$ K, $\sigma = 4.7$ Å (MacCormack and Schneider, 1951)

(v) CF_4-Ar Mixture - Two potentials were used:

(1) A simple combination rule gives

$$\varepsilon = \sqrt{\varepsilon_1 \varepsilon_2} \qquad \sigma = \frac{\sigma_1 + \sigma_2}{2} \qquad (2.45)$$

(2) The combination rules by Pena et al. (1982) were tried for two L-J (12-6) potentials for CF_4 and Ar.

The parameters required are:

For CF_4 $\varepsilon_1/k_B = 152.5$ K $\sigma = 4.7$ Å

For Ar $\varepsilon_2/k_B = 123.29$ K $\sigma = 3.41169$ Å

$I(Ar) = 15.775$ e.v. $I(CF_4) = 17.8$ e.v.

These give (1) $\sigma_{12} = 4.0558$ Å, $\varepsilon_{12}/k_B = 137.119$ K

(2) $\sigma_{12} = 4.0056$ Å, $\varepsilon_{12}/k_B = 136.62$ K

(vi) CH_4-CH_4 - An HFD modified potential (Meinander and Tabisz, 1983) had been developed in this laboratory and was used to construct an isotropic effective potential at different temperatures.

2.2 DIMER CONTRIBUTION

In this thesis, the term dimers refers to a metastable bound pair of molecules held together by van der Waals forces.

Our computer code, which is based on classical physics, at present does not include the effects of bound dimers in the calculation of the spectral profile. The contribution from these states to the spectrum is small at room temperature for rare gases and limited to low frequency shifts. The spectrum can conveniently be established from calculation of the spectral moments of these contributions.

The first four even moments for the two-body interaction including the dimer contribution have been calculated from the following expressions (Barocchi and Zoppi, 1980). The first three are quantum mechanically corrected (Barocchi et al., 1981).

$$M_0' = \frac{2V}{15} K_0^4 \langle \beta^2 \rangle_0$$

$$M_2' = 2V \frac{k_B T}{15 M} K_0^4 \langle (\beta')^2 + 6 \frac{\beta^2}{r^2} \rangle_0$$

$$\begin{aligned} M_4' = \frac{2}{15} V K_0^4 \{ & (\frac{K_B T}{M})^2 \langle 3 (\beta'')^2 + 4 \frac{\beta' \beta''}{r} - 12 \frac{\beta \beta''}{r^2} + 32 (\frac{\beta'}{r})^2 \\ & - 96 \frac{\beta \beta'}{r^3} + 120 \frac{\beta^2}{r^4} \rangle_0 - 2 \frac{k_B T}{M} \langle \frac{U' \beta''}{M} (\beta'' + 2 \frac{\beta'}{r} - 6 \frac{\beta}{r^2} \rangle_0 \\ & + \langle (\frac{U' \beta'}{M})^2 \rangle_0 \} \end{aligned} \tag{2.46}$$

$$M_6' = \frac{2V}{15} K_0^4 \left(\frac{k_B T}{M}\right)^3 < [15(\beta''')^2 + 360 \left(\frac{\beta''}{r}\right)^2 + 3648 \left(\frac{\beta'}{r^2}\right)^2 + 9000 \left(\frac{\beta}{r^3}\right)^2$$

$$- 1584 \frac{\beta''}{r} \frac{\beta'}{r^2} + 1776 \frac{\beta''}{r} \frac{\beta}{r^3} - 10992 \frac{\beta'}{r^2} \frac{\beta}{r^3}] + \frac{U''}{k_B T} [15 (\beta'')^2 + 102 \left(\frac{\beta'}{r}\right)^2$$

$$- 144 \frac{\beta'}{r} \frac{\beta}{r^2}] + \frac{U'''}{k_B T} [6 \beta' \beta''] + \left(\frac{U''}{k_B T}\right)^2 (\beta')^2 >_0 \quad .$$

$$M_{2n} = \frac{15}{2} \frac{1}{K_0^4} M_{2n}'$$

Here $\beta(r)$ may be obtained from Eqn. (2.17) and $U(r)$ from section 2.1.3. The primes indicate first, second and third derivative with respect to the pair distance r. k_B is the Boltzman constant, T is the temperature and μ is the reduced mass of the pair of atoms or molecules. The averages indicate:

$$<\ldots>_0 = \frac{4\pi}{V} \int_0^\infty dr\, r^2\, g_0(r) \qquad (2.47)$$

where the pair distribution function is taken in zeroth order, $g_0(r) = \exp(-U(r)/k_B T)$.

The difference between these moments and the moments calculated from the translational spectrum $I(\omega)$ using Eqn. (2.37) gives the dimer contribution. Prengel and Gornall (1976) have shown that the dimer spectrum for CH_4 is roughly gaussian at low frequencies with a long high frequency tail. Recently Leduff et al. (1987) observed a maximum in the Xe spectra at 153 K at low frequency shifts which is due to the contribution of dimers. This is difficult to detect due to the stray light at low frequencies. Accordingly, we have estimated the dimer spectrum associated with these moments by fitting the different moments to a gaussian plus an exponential.

$$I(\omega) = I_1 \exp(-\lambda_1 \omega) + I_2 \exp(-\lambda_2 \omega^2) \tag{2.48}$$

Using the first four even moments M_0, M_2, M_4 and M_6, one can find I_1, λ_1, I_2, λ_2 and the approximate form of the dimer spectrum.

2.3 COLLISION INDUCED ROTATIONAL SCATTERING

In the first part of this chapter, we considered collision induced light scattering by a pair of molecules, neglecting the internal degrees of freedom of the interacting molecules. In this part we will now consider the way in which higher order polarizabilities can lead to a rotational Raman spectrum from colliding isotropic molecules. The mechanism we will present is essentially the result of the work done by Buckingham and Tabisz (1978), which explains why higher intensities are observed in experiments than predicted by the DID model, especially at high frequency shifts. We will be dealing with isotropic spherical top molecules (SF_6, CF_4 and CH_4).

The total dipole moment $\mu^{(i)}$, quadrupole moment $\Theta^{(i)}$ and octopole moment $\Omega^{(i)}$ of a single molecule i in an external field F and field gradients F', F", can be written as follows (Buckingham, 1967)

$$\begin{aligned}
\mu_\alpha^{(i)} &= \mu_\alpha^{(0)(i)} + \alpha_{\alpha\beta}^{(i)} F_\beta + \frac{1}{2} \beta_{\alpha\beta\gamma}^{(i)} F_\beta F_\gamma + \frac{1}{6} \gamma_{\alpha\beta\gamma\delta}^{(i)} F_\beta F_\gamma F_\delta \\
&\quad + \frac{1}{3} A_{\alpha\beta\gamma}^{(i)} F'_{\beta\gamma} + \frac{1}{15} E_{\alpha\beta\gamma\delta}^{(i)} F''_{\beta\gamma\delta} + \ldots \\
\Theta_{\alpha\beta}^{(i)} &= \Theta_{\alpha\beta}^{(0)(i)} + A_{\alpha\beta\gamma}^{(i)} F_\gamma + C_{\alpha\beta\gamma\delta}^{(i)} F'_{\gamma\delta} + \ldots
\end{aligned} \tag{2.49}$$

$$\Omega^{(i)}_{\alpha\beta\gamma} = \Omega^{(0)(i)}_{\alpha\beta\gamma} + E^{(i)}_{\alpha\beta\gamma\delta} F_\delta + \ldots$$

The subscripts refer to components of the tensors in a Cartesian reference frame. The superscript zero denotes a permanent moment, and

$\underset{\sim}{\alpha}$ is the dipole polarizability, previously referred to as the polarizability.

$\underset{\sim}{\beta}, \underset{\sim}{\gamma}$, ... etc. are hyperpolarizabilities describing departures from a linear polarization law.

$\underset{\sim}{A}$ is the dipole-quadrupole polarizability, determining both the dipole induced by a field gradient and the quadrupole induced by a uniform field.

$\underset{\sim}{E}$ is the dipole-octopole polarizability.

$\underset{\sim}{C}$ is the quadrupole-quadrupole polarizability.

For the present case (spherical top molecules)

(a) In the case of tetrahedral molecules

$$\mu^{(0)}_\alpha = \Theta^{(0)}_{\alpha\beta} = 0$$

$$A_{\alpha\beta\gamma} = A\,(i_\alpha\, j_\beta\, k_\gamma + i_\alpha\, j_\gamma\, k_\beta + i_\beta\, j_\gamma\, k_\alpha + i_\beta\, j_\alpha\, k_\gamma + i_\gamma\, j_\alpha\, k_\beta + i_\gamma\, j_\beta\, k_\alpha) \tag{2.50}$$

$$E_{\alpha\beta\gamma\delta} = \frac{5}{2} E\,[i_\alpha\, i_\beta\, i_\gamma\, i_\delta + j_\alpha\, j_\beta\, j_\gamma\, j_\delta + k_\alpha\, k_\beta\, k_\gamma\, k_\delta - \frac{1}{5}(\delta_{\alpha\beta}\,\delta_{\gamma\delta} + \delta_{\alpha\gamma}\,\delta_{\beta\delta} + \delta_{\alpha\delta}\,\delta_{\beta\gamma})\,] \tag{2.51}$$

(b) In the case of octahedral molecules

$$\mu_\alpha^{(0)} = \Theta_{\alpha\beta}^{(0)} = \Omega_{\alpha\beta\gamma}^{(0)} = 0$$

$$A_{\alpha\beta\gamma} = 0 , \qquad E_{\alpha\beta\gamma\delta} \quad \text{is given by Eqn. (2.51)} \tag{2.52}$$

We will write the expressions for spherical top molecules, and take the tetrahedral and octahedral molecules as special cases. The field and its gradients are given by

$$\begin{aligned} F_\beta &= T_{\beta\gamma}\, \mu_\gamma + \ldots \\ F'_{\beta\gamma} &= -T_{\beta\gamma\delta}\, \mu_\delta - \ldots \\ F''_{\beta\gamma\delta} &= T_{\beta\gamma\delta\eta}\, \mu_\eta + \ldots \end{aligned} \tag{2.53}$$

where $$T_{\alpha\beta\gamma\ldots\nu}\,(r^{-1}) = (4\pi\varepsilon_0)^{-1}\, \nabla_\alpha\, \nabla_\beta\, \nabla_\gamma \ldots \nabla_\nu (r^{-1}) \tag{2.54}$$

and

$$T_{\underline{\alpha\beta\gamma\ldots\nu}}\,(r_{12}^{-1}) = (-1)^n\, T_{\alpha\beta\gamma\ldots\nu}\,(r_{21}^{-1})$$

where $\nabla_\alpha = \partial/\partial r_\alpha$

For convenience we will take $(4\pi\varepsilon_0)^{-1} = 1$

From Eqns. (2.49), (2.50), (2.53) and (2.54), one can rewrite the equation for the total dipole moment as

$$
\begin{aligned}
\mu_\alpha &= \mu_\alpha^{(1)} + \mu_\alpha^{(2)} \\
&= \alpha_1 \left(\xi_\alpha + T_{\alpha\gamma}\, \mu_\gamma^{(2)} + \frac{1}{3} T_{\alpha\gamma\delta}\, \Theta_{\gamma\delta}^{(2)} + \frac{1}{15} T_{\alpha\gamma\delta\varepsilon}\, \Omega_{\gamma\delta\varepsilon}^{(2)} + \ldots\right) \\
&+ \frac{1}{3} A_{\alpha\beta\gamma}^{(1)} \left(- T_{\beta\gamma\delta}\, \mu_\delta^{(2)} - \frac{1}{3} T_{\beta\gamma\delta\varepsilon}\, \Theta_{\delta\varepsilon}^{(2)} - \frac{1}{15} T_{\beta\gamma\delta\varepsilon\partial}\, \Omega_{\delta\varepsilon\partial}^{(2)} \ldots\right) \\
&+ \frac{1}{15} E_{\alpha\beta\gamma\delta}^{(1)} \left(T_{\beta\gamma\delta\varepsilon}\, \mu_\varepsilon^{(2)} + \frac{1}{3} T_{\beta\gamma\delta\varepsilon\partial}\, \Theta_{\varepsilon\partial}^{(2)} + \frac{1}{15} T_{\beta\gamma\delta\varepsilon\partial\eta}\, \Omega_{\partial\eta\xi}^{(2)} + \ldots\right) \\
&+ \alpha_2 \left(\xi_\alpha + T_{\alpha\gamma}\, \mu_\gamma^{(1)} - \frac{1}{3} T_{\alpha\gamma\delta}\, \Theta_{\gamma\delta}^{(1)} + \frac{1}{15} T_{\alpha\gamma\delta\varepsilon}\, \Omega_{\gamma\delta\varepsilon}^{(1)} - \ldots\right) \\
&+ \frac{1}{3} A_{\alpha\beta\gamma}^{(2)} \left(T_{\beta\gamma\delta}\, \mu_\delta^{(1)} - \frac{1}{3} T_{\beta\gamma\delta\varepsilon}\, \Theta_{\delta\varepsilon}^{(1)} + \frac{1}{15} T_{\beta\gamma\delta\varepsilon\partial}\, \Omega_{\delta\varepsilon\partial}^{(1)} \ldots\right) \\
&+ \frac{1}{15} E_{\alpha\beta\gamma\delta}^{(2)} \left(T_{\beta\gamma\delta\varepsilon}\, \mu_\varepsilon^{(1)} - \frac{1}{3} T_{\beta\gamma\delta\varepsilon\partial}\, \Theta_{\varepsilon\partial}^{(1)} + \frac{1}{15} T_{\beta\gamma\delta\varepsilon\partial\eta}\, \Omega_{\partial\eta\xi}^{(1)} + \ldots\right)
\end{aligned}
\tag{2.55}
$$

where ξ_α is the external field.

The light scattering is conventionally described in terms of the pair polarizability tensor $\alpha_{\alpha\omega}$

$$
\begin{aligned}
\alpha_{\alpha\omega} &= \frac{\partial \mu_\alpha}{\partial \xi_\omega} = (\alpha_1 + \alpha_2)\, \delta_{\alpha\omega} + 2\alpha_1 \alpha_2\, T_{\alpha\omega} \\
&+ \frac{1}{3} T_{\alpha\gamma\delta} \left(\alpha_1 A_{\gamma\delta\omega}^{(2)} - \alpha_2 A_{\gamma\delta\omega}^{(1)}\right) + \frac{1}{3} T_{\beta\gamma\omega} \left(\alpha_1 A_{\alpha\beta\gamma}^{(2)} - \alpha_2 A_{\alpha\beta\gamma}^{(1)}\right) \\
&+ \frac{1}{15} T_{\alpha\gamma\delta\varepsilon} \left(\alpha_1 E_{\gamma\delta\varepsilon\omega}^{(2)} + \alpha_2 E_{\gamma\delta\varepsilon\omega}^{(1)}\right) + \frac{1}{15} T_{\beta\gamma\delta\omega} \left(\alpha_1 E_{\alpha\beta\gamma\delta}^{(2)} + \alpha_2 E_{\alpha\beta\gamma\delta}^{(2)}\right) \\
&- \frac{1}{9} T_{\beta\gamma\delta\varepsilon} \left(A_{\alpha\beta\gamma}^{(1)} A_{\delta\varepsilon\omega}^{(2)} + A_{\alpha\beta\gamma}^{(2)} A_{\delta\varepsilon\omega}^{(1)}\right) \\
&+ \frac{1}{225} T_{\beta\gamma\delta\varepsilon\phi\eta} \left(E_{\alpha\beta\gamma\delta}^{(1)} E_{\varepsilon\phi\eta\omega}^{(2)} + E_{\alpha\beta\gamma\delta}^{(2)} E_{\varepsilon\phi\eta\omega}^{(1)}\right)
\end{aligned}
\tag{2.56}
$$

$$+ \frac{1}{45} T_{\beta\gamma\delta\varepsilon\partial} \left(E^{(1)}_{\alpha\beta\gamma\delta} A^{(2)}_{\varepsilon\partial\omega} - E^{(2)}_{\alpha\beta\gamma\delta} A^{(1)}_{\varepsilon\partial\omega}\right)$$

$$+ \frac{1}{45} T_{\beta\gamma\delta\varepsilon\partial} \left(E^{(1)}_{\delta\varepsilon\partial\omega} A^{(2)}_{\alpha\beta\gamma} - E^{(2)}_{\delta\varepsilon\partial\omega} A^{(1)}_{\alpha\beta\gamma}\right)$$

$$+ \ldots$$

The scattered intensity is dependent on $\langle \alpha_{\alpha\omega} \alpha_{\alpha'\omega'} \rangle$ where the angular brackets denote an average over all orientations of molecule 1 and 2 and of the intermolecular vector $\underline{r}$.

$$\langle \alpha_{\alpha\omega} \alpha_{\alpha'\omega'} \rangle = (\alpha_1+\alpha_2)^2 \delta_{\alpha\omega} \delta_{\alpha'\omega'} + 2(\alpha_1+\alpha_2) \alpha_1 \alpha_2 \langle \delta_{\alpha\omega} T_{\alpha'\omega'}$$

$$+ \delta_{\alpha'\omega'} T_{\alpha\omega} \rangle + \alpha_1^2 \alpha_2^2 \langle T_{\alpha\omega} T_{\alpha'\omega'} \rangle$$

$$+ \text{single A transition term} \qquad (2.57)$$

$$+ \text{single E transition term}$$

$$+ \text{double A transition term}$$

$$+ \text{AE transition term (evaluated here for the first time)}$$

$$+ \text{double E transition term (evaluated here for the first time)}$$

$$+ \ldots$$

We will derive the first four terms, and give the values for the rest.

The first term gives the polarized Rayleigh scattering. The second term is equal to

$$T_{\alpha\omega} = \nabla_\alpha \nabla_\omega r^{-1} = \frac{3R_\alpha R_\omega}{r^5} - \frac{\delta_{\alpha\omega}}{r^3} \qquad (2.58)$$

$$\langle T_{\alpha\omega} \rangle = \left\langle \frac{3R_\alpha R_\omega}{r^5} - \frac{\delta_{\alpha\omega}}{r^3} \right\rangle$$

$$= \frac{3\ 1/3\ \delta_{\alpha\omega}}{r^3} - \frac{\delta_{\alpha\omega}}{r^3} = 0 \qquad (2.59)$$

The third term represents the translational DID spectrum. The isotropic part of the multiplication of two second-rank tensors can be written in the form

$$\langle T_{\alpha\omega}\ T_{\alpha'\omega'} \rangle = A_1\ \delta_{\alpha\omega}\ \delta_{\alpha'\omega'} + A_2\ \delta_{\alpha\alpha'}\ \delta_{\omega\omega'} + A_3\ \delta_{\alpha\omega'}\ \delta_{\alpha'\omega} \qquad (2.60)$$

If $\alpha = \alpha'$ $\omega = \omega'$

$$0 = 9A_1 + 3A_2 + 3A_3 \qquad \text{(i)}$$

If $\alpha = \omega'$ $\alpha' = \omega$

$$\langle T_{\alpha\omega}\ T_{\alpha\omega} \rangle = 3A_1 + 9A_2 + 3A_3 \qquad \text{(ii)}$$

If $\alpha = \omega$ $\alpha' = \omega'$

$$\langle T_{\alpha\omega}\ T_{\alpha\omega} \rangle = 3A_1 + 3A_2 + 9A_3 \qquad \text{(iii)}$$

where A_1, A_2, and A_3 are constants.

Solving (i), (ii), (iii) and using

$$\langle \underbrace{T_{\alpha\beta\gamma\ldots\eta}}_{n}\ T_{\alpha\beta\gamma\ldots\eta} \rangle = \frac{(2n)!}{2^n}\ \overline{r^{-(2n+2)}}$$

$$\therefore \langle T_{\alpha\omega}\ T_{\alpha'\omega'} \rangle = \left(\frac{4!}{2^2}\ \overline{r^{-6}}\right) \frac{1}{30} \left(-2\ \delta_{\alpha\omega}\ \delta_{\alpha'\omega'} + 3\delta_{\alpha\alpha'}\ \delta_{\omega\omega'} + 3\delta_{\alpha\omega'}\delta_{\alpha'\omega}\right)$$

Then the DID term will be equal to

$$4\,\frac{6}{30}\,\alpha_1^2\,\alpha_2^2\,\overline{r^{-6}}\,(-2\delta_{\alpha\omega}\,\delta_{\alpha'\omega'}+3\delta_{\alpha\alpha'}\,\delta_{\omega\omega'}+3\delta_{\alpha\omega'}\,\delta_{\alpha'\omega})$$

$$=\frac{4}{5}\,\alpha_1^2\,\alpha_2^2\,\overline{r^{-6}}\,(-2\delta_{\alpha\omega}\,\delta_{\alpha'\omega'}+3\delta_{\alpha\alpha'}\,\delta_{\omega\omega'}+3\delta_{\alpha\omega'}\,\delta_{\alpha'\omega}) \qquad [I]$$

where $\overline{r^{-n}} = \int_0^\infty r^{-n}\,r^2\,e^{-U(r)/k_BT}\,dr$

The fourth term (single A) is the first induced rotational contribution and is equal to

$$=\frac{1}{9}\,\alpha_1^2\,\{\,\langle T_{\alpha\gamma\delta}\,T_{\alpha'\gamma'\delta'}\rangle\,\langle A^{(2)}_{\omega\gamma\delta}\,A^{(2)}_{\omega'\gamma'\delta'}\rangle$$

$$+\langle T_{\alpha\gamma\delta}\,T_{\beta'\gamma'\omega'}\rangle\,\langle A^{(2)}_{\gamma\delta\omega}\,A^{(2)}_{\alpha'\beta'\gamma'}\rangle+\langle T_{\beta\gamma\omega}\,T_{\beta'\gamma'\omega'}\rangle \qquad (2.61)$$

$$\langle A^{(2)}_{\alpha\beta\gamma}\,A^{(2)}_{\alpha'\beta'\gamma'}\rangle+\langle T_{\beta\gamma\omega}\,T_{\alpha'\gamma'\delta'}\rangle\,\langle A^{(2)}_{\beta\gamma\alpha}\,A^{(2)}_{\gamma'\delta'\omega'}\rangle\,\}$$

$$+\frac{1}{9}\,\alpha_2^2\,\{\ \text{similar terms with } (2)\Leftrightarrow(1)\,\}$$

We can see that the first and the third terms are similar and that the second and the fourth terms are similar too. We will calculate the first term using the identities

$$\langle A^{(2)}_{\alpha\beta\gamma}\,A^{(2)}_{\alpha'\beta'\gamma'}\rangle = 12A^{2}_{(2)}\,\langle i_\alpha\,i_{\alpha'}\,j_\beta\,j_{\beta'}\,k_\gamma\,k_{\gamma'}\rangle+24A^{2}_{(2)}$$

$$\langle i_\alpha\,i_{\beta'}\,j_\beta\,j_{\alpha'}\,k_\gamma\,k_{\gamma'}\rangle \qquad (2.62)$$

where

$$\langle i_\alpha\,i_{\alpha'}\,j_\beta\,j_{\beta'}\,k_\gamma\,k_{\gamma'}\rangle=\frac{8}{105}\,\delta_{\alpha\alpha'}\,\delta_{\beta\beta'}\,\delta_{\gamma\gamma'}-\frac{1}{42}\,\{\,\delta_{\alpha\alpha'}$$

$$(\delta_{\beta\gamma}\,\delta_{\beta'\gamma'}+\delta_{\beta\gamma'}\,\delta_{\beta'\gamma})+\delta_{\beta\beta'}\,(\delta_{\alpha\gamma}\,\delta_{\alpha'\gamma'}+\delta_{\alpha\gamma'}\,\delta_{\alpha'\gamma})$$

$$+ \delta_{\gamma\gamma'} (\delta_{\alpha\beta} \delta_{\alpha'\beta'} + \delta_{\alpha\beta'} \delta_{\beta\alpha'}) \} + \frac{1}{105} \{\delta_{\alpha\beta} \delta_{\alpha'\gamma} \delta_{\beta'\gamma'}$$

$$+ \delta_{\alpha\beta} \delta_{\alpha'\gamma'} \delta_{\beta'\gamma} + \delta_{\alpha\beta'} \delta_{\alpha'\gamma} \delta_{\beta\gamma'} + \delta_{\alpha\beta'} \delta_{\alpha'\gamma'} \delta_{\beta\gamma} + \delta_{\alpha\gamma} \delta_{\alpha'\beta} \delta_{\beta'\gamma'}$$

$$+ \delta_{\alpha\gamma} \delta_{\alpha'\beta'} \delta_{\beta\gamma'} + \delta_{\alpha\gamma'} \delta_{\alpha'\beta} \delta_{\beta'\gamma} + \delta_{\alpha\gamma'} \delta_{\alpha'\beta'} \delta_{\beta\gamma} \}$$

and a similar expression for $\langle i_\alpha j_{\beta'} j_\beta j_{\alpha'} k_\gamma k_{\gamma'} \rangle$; from Eqns. (2.61) and (2.62) the first term can be rewritten in the form

$$\langle T_{\alpha\gamma\delta} T_{\alpha'\gamma'\delta'} \rangle \langle A^{(2)}_{\omega\gamma\delta} A^{(2)}_{\omega'\gamma'\delta'} \rangle = 12A^{2(2)} \{ (\frac{10}{105} - \frac{3}{42})\delta_{\alpha\alpha'}$$

$$\langle T_{\omega\delta\varepsilon} T_{\omega'\gamma\delta} \rangle + (\frac{8}{105} - \frac{4}{42}) \langle T_{\alpha\omega\delta} T_{\alpha'\omega'\delta} \rangle + (\frac{20}{105} - \frac{6}{42}) \langle T_{\alpha\omega'\delta} T_{\alpha'\omega\delta} \rangle \} \tag{2.63}$$

As in Eqn. (2.60), one can write

$$\langle T_{\alpha\omega\delta} T_{\alpha'\omega'\delta} \rangle = A_1 \delta_{\alpha\omega} \delta_{\alpha'\omega'} + A_2 \delta_{\alpha\alpha'} \delta_{\omega\omega'} + A_3 \delta_{\alpha\omega'} \delta_{\alpha'\omega}$$

Using the same method, one can get

$$\langle T_{\alpha\omega\delta} T_{\alpha'\omega'\delta} \rangle = (\frac{(6!)}{2^3} \overline{r^{-8}}) \frac{1}{30} (-2\delta_{\alpha\omega} \delta_{\alpha'\omega'} + 3\delta_{\alpha\alpha'} \delta_{\omega\omega'}$$

$$+ 3\delta_{\alpha\omega'} \delta_{\alpha'\omega}) \tag{2.64}$$

and with the identity

$$\langle T_{\underbrace{\alpha\beta\gamma\ldots\nu}_{n}} T_{\underbrace{\eta\beta\gamma\ldots\nu}_{n}} \rangle = \frac{(n+1)\ (2n!)}{2^{n+1}} (\frac{(n+2)\ R_\alpha R_\eta + nR^2 \delta_{\alpha\eta}}{\overline{r^{2n+6}}})$$

$$T_{\omega\gamma\delta}\, T_{\omega'\gamma\delta} = \frac{(3)\,(4!)}{2^3}\ \left(\frac{4/3\ \delta_{\omega\omega'} + 2\delta_{\omega\omega'}}{\overline{r^8}}\right) \qquad (2.65)$$

$$= 30\delta_{\omega\omega'}\ \overline{r^{-8}} \quad .$$

By substituting Eqns. (2.64) and (2.65) into Eqn. (2.63) we get

$$\therefore \langle T_{\alpha\gamma\delta}\ T_{\alpha'\gamma'\delta'}\rangle \langle A_{\omega\gamma\delta}\ A_{\omega'\gamma'\delta'}\rangle = 12A^{2}(2)\ \overline{r^{-8}}\ \{\ \frac{102}{105}\ \delta_{\alpha\alpha'}\ \delta_{\omega\omega'}$$

$$+ \frac{57}{105}\ \delta_{\alpha\omega}\ \delta_{\alpha'\omega'} - \frac{48}{105}\ \delta_{\alpha\omega'}\ \delta_{\alpha'\omega}\ \} \quad .$$

Now, the 1st term + 3rd term $= 24A^{2}(2)\ \overline{r^{-8}}\ \{\ \frac{102}{105}\ \delta_{\alpha\alpha'}\ \delta_{\omega\omega'}$

$$+ \frac{57}{105}\ \delta_{\alpha\omega}\ \delta_{\alpha'\omega'} - \frac{48}{105}\ \delta_{\alpha\omega'}\ \delta_{\alpha'\omega}\}$$

Similarly, we can show that the 2nd term is equal to

$$= 12A^{2}(2)\ \overline{r^{-8}}\ \{\frac{-48}{105}\ \delta_{\alpha\alpha'}\ \delta_{\omega\omega'} + \frac{57}{105}\ \delta_{\alpha\omega}\ \delta_{\alpha'\omega'} + \frac{102}{105}\ \delta_{\alpha'\omega}\ \delta_{\alpha\omega'}\ \}$$

and the 2nd term + fourth term

$$= 24A^{2}(2)\ \overline{r^{-8}}\ \{\frac{-48}{105}\ \delta_{\alpha\alpha'}\ \delta_{\omega\omega'} + \frac{57}{105}\ \delta_{\alpha\omega}\ \delta_{\alpha'\omega'} + \frac{102}{105}\ \delta_{\alpha'\omega}\ \delta_{\alpha\omega'}\ \} \quad .$$

Then the contribution from the single A term

$$= \frac{1}{9}\ \alpha_1^2\ (24)\ A^{2}(2)\ \overline{r^{-8}}\ \{\frac{54}{105}\ \delta_{\alpha\alpha'}\ \delta_{\omega\omega'} + \frac{114}{105}\ \delta_{\alpha\omega}\ \delta_{\alpha'\omega'} + \frac{54}{105}\ \delta_{\alpha'\omega}\ \delta_{\alpha\omega'}\}$$

$$+ \frac{1}{9}\ \alpha_2^2\ (24)\ A^{2}(1)\ \overline{r^{-8}}\ \{\ \frac{54}{105}\ \delta_{\alpha\alpha'}\ \delta_{\omega\omega'} + \frac{114}{105}\ \delta_{\alpha\omega}\ \delta_{\alpha'\omega'} + \frac{54}{105}\ \delta_{\alpha'\omega}\ \delta_{\alpha\omega'}\}$$

$$= \frac{16}{105} \overline{r^{-8}} \{\alpha_1^2 A^{(2)2} + \alpha_2^2 A^{(1)2}\} \{9\delta_{\alpha\alpha'} \delta_{\omega\omega'} + 9\delta_{\alpha'\omega} \delta_{\alpha\omega'}$$

$$+ 19\delta_{\alpha\omega} \delta_{\alpha'\omega'}\} \quad . \qquad \text{(II)}$$

Similarly, one can evaluate the contributions from the single E term, double A term, AE term and the double E term.

Contribution from single E term:

$$= \frac{1}{9} [(\alpha_1 E_2)^2 + (\alpha_2 E_1)^2] \overline{r^{-10}} (30\delta_{\alpha\omega} \delta_{\alpha'\omega'} + 11\delta_{\alpha\alpha'} \delta_{\omega\omega'}$$

$$+ 11\delta_{\alpha\omega'} \delta_{\alpha'\omega}) \quad . \qquad \text{(III)}$$

Contribution from double A term:

$$= \frac{64}{5} (A_1 A_2)^2 \overline{r^{-10}} (-\frac{472}{945} \delta_{\alpha\omega} \delta_{\alpha'\omega'} + \frac{983}{945} \delta_{\alpha\alpha'} \delta_{\omega\omega'}$$

$$+ \frac{983}{945} \delta_{\alpha\omega'} \delta_{\alpha'\omega}) \quad . \qquad \text{(IV)}$$

Contribution from AE term:

$$= \overline{r^{-12}} \{A_1^2 E_2^2 + A_2^2 E_1^2\} \{\frac{232}{21} \delta_{\alpha\alpha'} \delta_{\omega\omega'} + \frac{232}{21} \delta_{\alpha\omega'} \delta_{\alpha'\omega}$$

$$- \frac{40}{7} \delta_{\alpha\omega} \delta_{\alpha'\omega'}\} \quad . \qquad \text{(V)}$$

Contribution from double E term:

$$= \overline{r^{-14}} E_1^2 E_2^2 \{\frac{17589}{315} \delta_{\alpha\alpha'} \delta_{\omega\omega'} + \frac{17589}{315} \delta_{\alpha\omega'} \delta_{\alpha'\omega} - \frac{9405}{315} \delta_{\alpha\omega} \delta_{\alpha'\omega'}\} \quad .$$

$$\text{(VI)}$$

If we consider a particular scattering geometry, in which the incident light is along the x-axis with its electric vector polarized in the z direction and observations are made in the z direction, then our interest will be in $\langle\alpha^2_{xz}\rangle$:

$$\alpha = \alpha' = x \qquad\qquad \omega = \omega' = z$$

and

$$\delta_{\alpha\alpha'} = \delta_{\omega\omega'} = 1 \tag{2.66}$$

$$\delta_{\alpha\omega'} = \delta_{\alpha'\omega} = \delta_{\alpha\omega} = \delta_{\alpha'\omega'} = 0$$

$$\langle\alpha^2_{xz}\rangle = \frac{12}{5}(\alpha_1\,\alpha_2)^2\,\overline{r^{-6}} + \frac{48}{35}[(\alpha_1\,A_2)^2 + (\alpha_2\,A_1)^2]\,\overline{r^{-8}}$$

$$+ \frac{11}{9}[(\alpha_1\,E_2)^2 + (\alpha_2\,E_1)^2]\,\overline{r^{-10}} + \frac{62912}{4725}(A_1\,A_2)^2\,\overline{r^{-10}} \tag{2.67}$$

$$+ \frac{232}{21}\,\overline{r^{-12}}\,(A_1^2\,E_2^2 + A_2^2\,E_1^2) + \frac{5863}{105}\,\overline{r^{-14}}\,(E_1\,E_2)^2 + \ldots$$

Of course, in this equation the first term is the first order DID. A fuller description of the pure translational includes the r^{-6} **&exponential** terms in Eqn. (2.17).

This is a general expression for the interaction of two tetrahedral molecules, neglecting all the polarizabilities of higher order than the dipole-octopole polarizability.

It is of interest to determine the depolarization ratio $\rho = \langle\alpha^2_{xz}\rangle/\langle\alpha^2_{zz}\rangle$.

First, one can write a similar expression for $\langle\alpha^2_{zz}\rangle$

$$\alpha = \alpha' = \omega = \omega' = z$$

$$\langle\alpha_{zz}^2\rangle = (\alpha_1 + \alpha_2)^2 + \frac{16}{5}(\alpha_1\,\alpha_2)^2\,\overline{r^{-6}} + \frac{592}{105}[(\alpha_1\,A_2)^2 + (\alpha_2\,A_1)^2]\,\overline{r^{-8}}$$

$$+ \frac{52}{9}[(\alpha_1\,E_2)^2 + (\alpha_2\,E_1)^2]\,\overline{r^{-10}} + \frac{95616}{4725}(A_1\,A_2)^2\,\overline{r^{-10}} \qquad (2.68)$$

$$+ \frac{344}{21}[(A_1\,E_2)^2 + A_2\,E_1)^2]\overline{r^{-12}} + \frac{8591}{105}(E_1\,E_2)^2\,\overline{r^{-14}} + \ldots$$

For the tetrahedral-atom interaction

$$A_2 = E_2 = 0$$

$$\langle\alpha_{xz}\rangle^2 = \frac{12}{5}(\alpha_1\,\alpha_2)^2\,\overline{r^{-6}} + \frac{48}{35}(\alpha_2\,A_1)^2\,\overline{r^{-8}} + \frac{11}{9}(\alpha_2\,E_1)^2\,\overline{r^{-10}} + \ldots \qquad (2.69)$$

$$\langle\alpha_{zz}\rangle^2 = (\alpha_1 + \alpha_2)^2 + \frac{16}{5}(\alpha_1\,\alpha_2)^2\,\overline{r^{-6}} + \frac{592}{105}(\alpha_2\,A_1)^2\,\overline{r^{-8}}$$

$$+ \frac{52}{9}(\alpha_2\,E_1)^2\,\overline{r^{-10}} + \ldots \qquad (2.70)$$

For the octahedral-octahedral interaction

$$A_1 = A_2 = 0$$

$$\langle\alpha_{xz}^2\rangle = \frac{12}{5}(\alpha_1\,\alpha_2)^2\,\overline{r^{-6}} + \frac{11}{9}[(\alpha_1\,E_2)^2 + (\alpha_2\,E_1)^2]\,\overline{r^{-10}}$$

$$+ \frac{5863}{105}(E_1\,E_2)^2\,\overline{r^{-14}} + \ldots \qquad (2.71)$$

$$\langle\alpha_{zz}^2\rangle = (\alpha_1 + \alpha_2)^2 + \frac{16}{5}(\alpha_1\,\alpha_2)^2\,\overline{r^{-6}} + \frac{52}{9}[(\alpha_1\,E_2)^2$$

$$+ (\alpha_2\,E_1)^2]\,\overline{r^{-10}} + \frac{8591}{105}(E_1\,E_2)^2\,\overline{r^{-14}} + \ldots \qquad (2.72)$$

For the octahedral-atom interaction

$$A_1 = 0$$

$$A_2 = E_2 = 0$$

$$\langle \alpha_{xz}^2 \rangle = \frac{12}{5} (\alpha_1 \alpha_2)^2 \overline{r^{-6}} + \frac{11}{9} (\alpha_2 E_1)^2 \overline{r^{-10}} + \ldots \quad (2.73)$$

$$\langle \alpha_{zz}^2 \rangle = (\alpha_1 + \alpha_2)^2 + \frac{14}{5} (\alpha_1 \alpha_2)^2 \overline{r^{-6}} + \frac{52}{9} (\alpha_2 E_1)^2 \overline{r^{-10}} + \ldots (2.74)$$

The depolarization ratios are

$$\rho_A = \frac{48}{35} \frac{105}{592} = \frac{9}{37} = 0.243$$

$$\rho_E = \frac{11}{9} \frac{9}{52} = 0.212$$

$$\rho_{AA} = \frac{62912}{4725} \frac{4725}{62912} = 0.658$$

$$\rho_{AE} = \frac{232}{21} \frac{21}{344} = 0.6744$$

$$\rho_{EE} = \frac{5863}{105} \frac{105}{8591} = 0.6824$$

where ρ_A is the depolarization ratio considering the αA term only, and so on.

2.3.1 Still Higher Order Polarizabilities

This section will put some light on still higher order polarizabilities (higher than the dipole-octopole polarizability $\underset{\sim}{E}$), and their effect.

Eqn. (2.55) can be rewritten to include higher order polarizabilities, and the dipole moment will be given (in a symbolic manner, with the neglect of numerical coefficients) by

$$\mu^i = (\alpha_1 \alpha_2)\, r^{-3} + (A_1 \alpha_2 + \alpha_1 A_2)\, r^{-4} + (\alpha_2 E_1 + A_1 A_2 + \alpha_1 E_2)\, r^{-5}$$
$$+ (\alpha_2 F_1 + E_1 A_2 + A_1 E_2 + \alpha_1 F_2 + \alpha_1^2 \alpha_2) r^{-6}$$
$$+ (\alpha_2 H_1 + F_1 A_2 + E_1 E_2 + A_1 F_2 + \alpha_1 H_2 + \alpha_1^2 A_2 + A_1 \alpha_1 \alpha_2)\, r^{-7}$$
$$+ (\alpha_1 \alpha_1 C_2 + \alpha_2 \alpha_2 C_1 + \ldots)\, r^{-8} + \ldots \qquad (2.75)$$

where F is the dipole-hexadecapole polarizability
H is the dipole-2^5 pole polarizability, and
C is the quadrupole-quadrupole polarizability

Fieschi and Fumi (1953), using the inspection method, found that F has 10 independent non-zero elements for tetrahedral symmetry, and H has 31 independent non-zero elements for both tetrahedral and octahedral symmetries. It is known that C (Buckingham, 1967) has 2 independent non-zero components for both symmetries of interest here. So, instead of including contributions of F, H, and C which will make the actual analysis of data impossible, one can try to calculate the effect of neglecting them.

We will take octahedral molecules, where F = 0, and include terms to H in Eqn. (2.72), getting

$$\langle \alpha_{xz}^2 \rangle = \frac{12}{5} (\alpha_1 \alpha_2)^2 \overline{r^{-6}} + \frac{11}{9} [(\alpha_1 E_2)^2 + (\alpha_2 E_1)^2] \overline{r^{-10}} \qquad (2.76)$$
$$+ \{ \frac{5863}{105} E_1^2 E_2^2 + L [(\alpha_2 H_2)^2 + (\alpha_2 H_1)^2] \} \overline{r^{-14}}$$
$$+ M [(\alpha_1 \alpha_1 C_2)^2 + (\alpha_2 \alpha_2 C_1)^2] \overline{r^{-16}} + \ldots$$

Calculation showed that the double E spectrum is a broad flat feature. The spectrum of the αH function will have $\Delta J = 5$ and $\Delta J = 6$ branches; its major effect is at frequencies higher than those at which intensity could be detected in our experiments with octahedral molecules (higher than 100 cm^{-1}). Assuming that the two coefficients of $\overline{r^{-14}}$ are equal, the effect of including the αH term is about 1% of the induced rotational intensity.

In the case of tetrahedral molecules (especially CH_4), where the spectrum is very broad $\simeq$ 600 cm^{-1}, the ratio of $\frac{(\alpha A \text{ term})}{(\alpha F \text{ term})}$ is about 10^3, assuming that A and F have the same order of magnitude and almost constant for the temperature range (130-295 K). So, the neglect of F and H does not affect our calculations of the rotational intensity by more than 1%.

The quadrupole-quadrupole polarizability C has the coefficient $\overline{r^{-16}}$ and its effect is smaller than that of F and H at temperatures of 300 K and below.

2.3.2 Rotational Spectrum

In the calculation of the spectral distribution, we must consider the rotational states of the two molecules. The transition probabilities are given by the matrix elements:

$$| \langle J_1', J_2' | \alpha_{\alpha\beta} | J_1, J_2 \rangle |^2 \qquad (2.77)$$

where $\alpha_{\alpha\beta}$ is the pair polarizability and J_i , J_i' represent the initial and final rotational states of the i-th molecule. The normalized symmetric-top wave function (Rose, 1959) for a molecule in a rotational state J is

$$\psi_{Jk_m} = \sqrt{\frac{2J+1}{8\pi^2}}\ D^{J*}_{mk}\ (\Omega)\ , \tag{2.78}$$

where $D^{J}_{mk}\ (\Omega)$ is the Wigner rotation matrix, m is the quantum number associated with the projection of the angular momentum of J on the space-fixed axis and k is the quantum number associated with the projection of J on the molecule-fixed axis. Both k and m have (2J+1) components and each rotational state J is thus $(2J+1)^2$ degenerate (in the rigid-rotor approximation). To evaluate the matrix elements, the pair polarizability is written in a spherical tensor form using the Stone expressions (Stone, 1975, 1976). The terms in Eqn. (2.67) that depend only on the isotropic polarizabilities α_i do not give rise to a rotational spectrum. For example, the single A transition term gives rise to a matrix element of the form

$$|\langle J_1' J_2' | D^{3*}_{m2}\ (\Omega_j) - D^{3*}_{m-2}\ (\Omega_j) | J_1 J_2\rangle|\ , \tag{2.79}$$

from which one obtains the following inequalities and selection rules

$$\begin{aligned} &|\langle J_1', J_2'|\ J_1, J_2\rangle|^2 \neq 0 \rightarrow \Delta J_i = 0 \\ &|\langle J_1' J_2'|\ D^{3*}_{m2}\ (\Omega_j - D^{3*}_{m-2}\ (\Omega_j)|\ J_1 J_2|^2 \neq 0 \rightarrow \Delta J_j = 0, \pm 1, \pm 2, \pm 3, \\ &(J_j + J_j \geq 3)\ . \end{aligned} \tag{2.80}$$

Similarly, the single E transition term gives rise to a matrix element of the form

$$|\langle J_1' J_2' |\ \tfrac{1}{6}\left[\left(\tfrac{14}{5}\right)^{\frac{1}{2}} D^{4*}_{m0}\ (\Omega) + D^{4*}_{m4}\ (\Omega) + D^{4*}_{m-4}\ (\Omega)\right]|\ J_1 J_2\rangle\ , \tag{2.81}$$

from which one obtains the selection rules

$$\Delta J_i = 0 \qquad \Delta J_j = 0, \pm 1, \pm 2, \pm 3, \pm 4 \ (J_j + J_j' \geq 4). \tag{2.82}$$

For double A, the selection rules are

$$\begin{aligned} \Delta J_i &= 0, \pm 1, \pm 2, \pm 3 \qquad (J_i + J_i' \geq 3) \\ \Delta J_j &= 0, \pm 1, \pm 2, \pm 3 \qquad (J_j + J_j' \geq 3) \ . \end{aligned} \tag{2.83}$$

For AE transition term, the selection rules are

$$\begin{aligned} \Delta J_i &= 0, \pm 1, \pm 2, \pm 3 \qquad (J_i + J_i' \geq 3) \\ \Delta J_j &= 0, \pm 1, \pm 2, \pm 3, \pm 4 \qquad (J_j + J_j' \geq 4). \end{aligned} \tag{2.84}$$

For double E transition term, the selection rules are

$$\begin{aligned} \Delta J_i &= 0, \pm 1, \pm 2, \pm 3, \pm 4 \qquad (J_i + J_i' \geq 4) \\ \Delta J_j &= 0, \pm 1, \pm 2, \pm 3, \pm 4 \qquad (J_j + J_j' \geq 4). \end{aligned} \tag{2.85}$$

The different selection rules lead to different rotational Raman shifts

$$\Delta\omega_{rot} = [F(J_1') - F(J_1)] - [F(J_2') - F(J_2)] \ . \tag{2.86}$$

For spherical top molecules in the rigid rotor approximation

$$F(J) = B\ J(J+1) \tag{2.87}$$

and

$$\therefore \Delta\omega_{rot} = B_1[J_1'(J_1'+1) - J_1(J_1+1)] - B_2[J_2'(J_2'+1) - J_2(J_2+1)]$$

The spectral intensity (Stokes) resulting from rotational transitions $J_1', J_2' \leftarrow J_1, J_2$, is proportional to

$$\Gamma(J_1', J_2', J_1, J_2) = \omega_R^4 (2J_1' + 1)(2J_2' + 1)(2J_1 + 1)(2J_2 + 1)$$

$$\times \exp\{(-J_1(J_1 + 1) B_1 + J_2(J_2 + 1) B_2) \hbar C / k_B T\} \qquad (2.88)$$

where $\omega_R = \omega_0 - \Delta\omega_{rot}$

ω_0 is the frequency of the incident light, and B_i is the rotational constant of molecule i.

To obtain the spectral distribution from the selection rules and the expression for $\Gamma(J_1, J_2, J_1', J_2')$, we compute the positions (according to Eqn. (2.86)) and the relative intensities of all the spectral lines arising from a given term of $\langle\alpha^2\rangle$, and then normalize the intensity of their sum to the experimental spectrum. Finally, we must remember that because of the dependence of the pair polarizability on the intermolecular separation r, each line will be broadened by the translational motion of the molecules. Posch (1982) has computed the shape of the translational broadening function associated with an interaction characterized by a tensor of rank ℓ and varying with $r^{-(\ell+1)}$; the broadening increases in width with increasing ℓ. Taking the experimentally estimated exponential decay function for the r^{-3} interaction of the pure translational spectrum, and through the calculations of Posch, we estimate the corresponding decay constants for single $A(r^{-4})$, and

double A and single $E(r^{-5})$ transitions. Corresponding decay constants for the mixture spectra were determined from their $\frac{1}{\sqrt{\mu}}$ dependence.

Figure 2.4

Neumann intermolecular potential data and the fitted HFD potential.

FIGURE 2.4

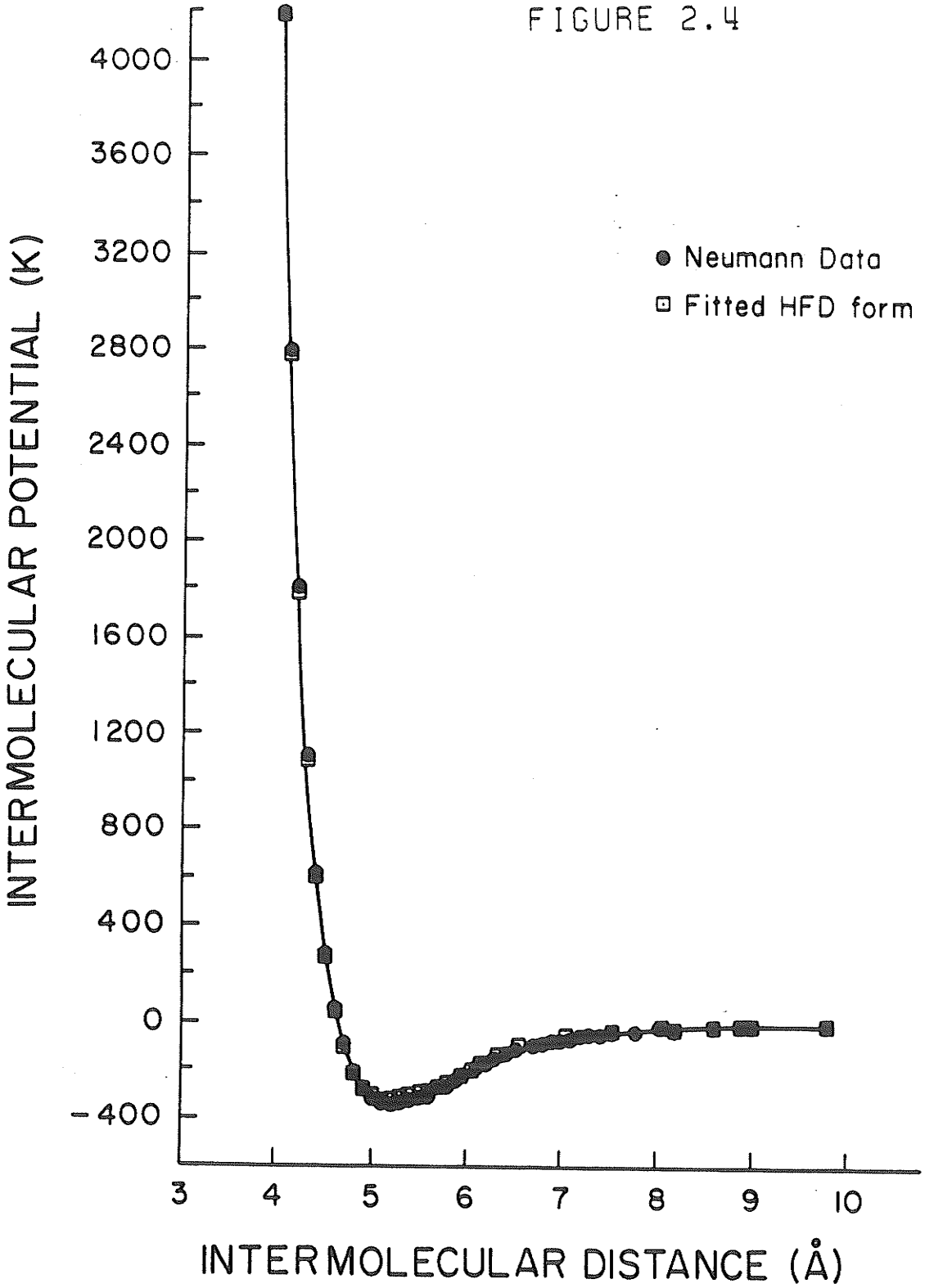
INTERMOLECULAR POTENTIAL (K)
4000
3600
3200
2800
2400
2000
1600
1200
800
400
0
-400
3
4
5
6
7
8
9
10
INTERMOLECULAR DISTANCE (Å)
Neumann Data
Fitted HFD form

Figure 2.5

The M3SV intermolecular potential

FIGURE 2.5

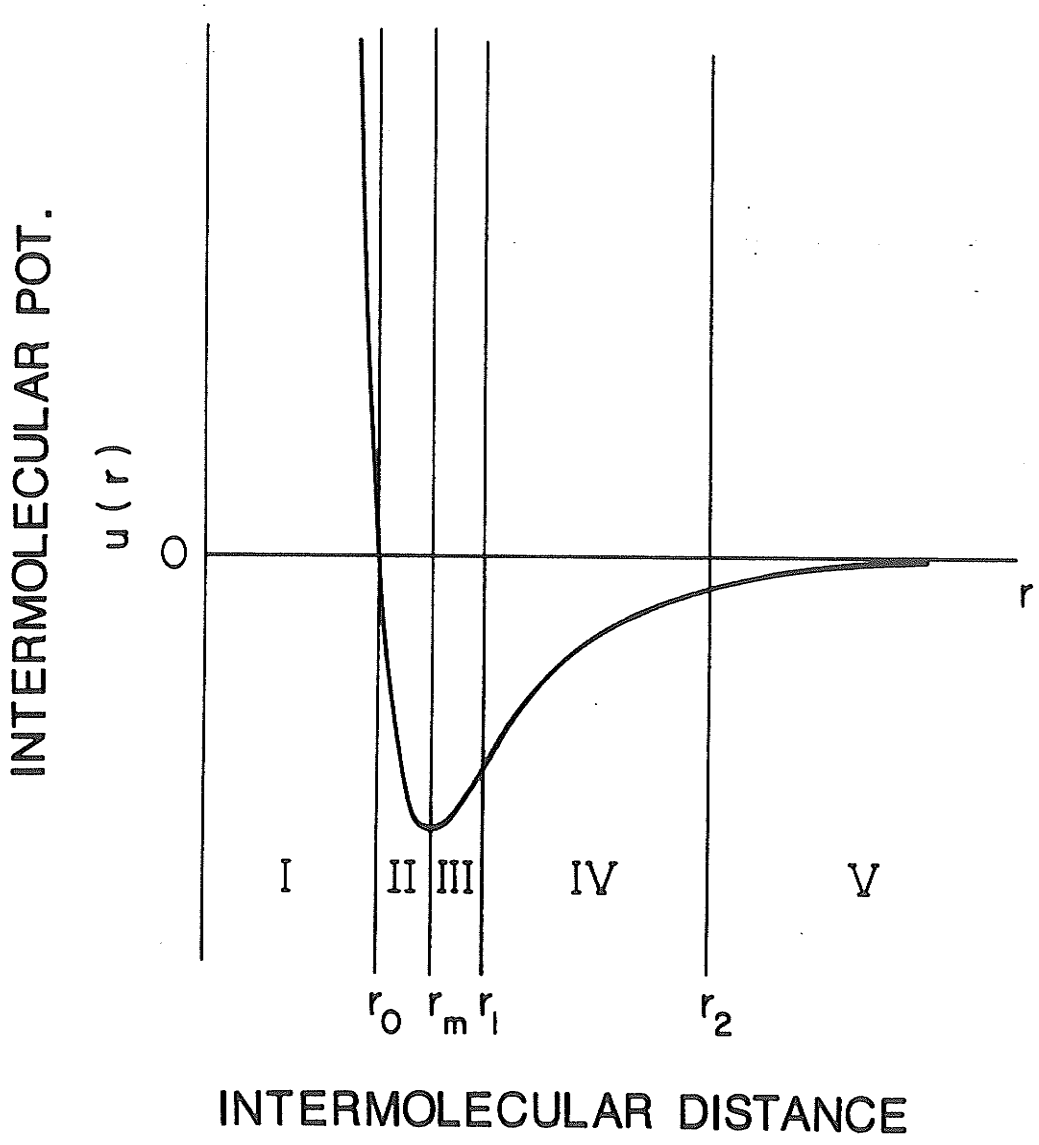

THF M3SV INTERMOLECULAR POTENTIAL FORM

CHAPTER 3

EXPERIMENT AND DATA ANALYSIS

3.1 EXPERIMENT

The experiment consists in sending a beam of light, generated by a laser, through a sample of gas and measuring (with a spectrometer) the intensity and spectral distribution of the light scattered at right angles to the beam direction. The experimental set-up is almost the same as that reported previously in the theses of Shelton (1979), Penner (1983) and myself (El-Sheikh, 1985) and is as shown in Fig. 3.1.

The light beam is generated by an Ar-ion laser [1]. The laser has a prism in the resonant cavity to force operation on one line. Power is of the order of 3.0 watts at a current of 35 amperes. A half-wave plate [2] is used to rotate the polarization of the beam to the correct orientation and is followed by a Nicol prism [2] which removes the unwanted polarization component. The beam is then reflected vertically upwards by a prism and focused by a 10 cm focal lens placed just below the cell [9].

The light scattered by the gas is collected and focused on the entrance slit of the spectrometer using two 20 cm focal length collection and focusing lenses mounted on a translating stage [3].

The spectrum is scanned by a tandem Czerny-turner double monochromator [8] (Jarrell-Ash series 25-100) as shown in Fig. 3.2. The two monochromators are mounted one above the other and the light path in the second monochromator is the same as in the first, but in the opposite direction; this system improves stray-light rejection

over a single monochromator. Light enters through slit (A) and passes to a collimating mirror (B) where it is reflected as parallel light to a plane grating (C). The dispersed light, still parallel, but with separate wavelengths diverging, is reflected back to the camera mirror (D). Here light is deflected 90° by mirror (E), through the intermediate slit (F) to an additional 45° mirror (G) where it is deflected to the lower monochromator (which is mainly the same as the upper one) and finally to the exit slit. The light emerging from the double monochromator is focused on to the photocathode of an RCA C31034 photomultiplier tube [4]. The pulses from the photomultiplier tube are amplified and stored in a multi-channel analyzer [5] from which the spectra are obtained by counting the number of photons received at each frequency. The equipment for filling the sample cell is contained in the area [7].

3.2 IMPURITIES

The reason for repeating the two experiments on SF_6-SF_6 and CF_4-CF_4 which were done previously in our laboratory (Shelton, 1979), is that the impurities in these early experiments were high. Some of these impurities came with the sample and one was added to the sample for intensity normalization. For example, CF_4 was contaminated with 0.2% air. This air impurity has a rotational band due to O_2 and N_2 scattering at 60 cm^{-1} which could affect the rotational wing of the induced spectrum. As well, these impurities in the molecules could interact with CF_4 molecules to give a contribution to the intensity of the total induced spectrum.

In the present work, the air impurity was less than 0.03%,

which was almost ten times less than before.

In the earlier work another impurity (H_2) was added before to the sample for intensity normalization. Again, this could interact with CF_4 to affect the intensity.

In this work, the intensity normalization procedure did not require an internal foreign calibration standard (see Section 3.3.1a).

The purities of the samples used in the present study are: SF_6 99.99%, CF_4 99.9%, Xe 99.99%, Kr 99.995%, Ar 99.9995% and Ne 99.999%.

3.3 RAW DATA AND DATA ANALYSIS

The experiment has two conflicting goals: measurement of the very weak spectrum at high frequency shifts and measurement of the spectrum near $\omega = 0$ in spite of the bright Rayleigh line. To obtain the CILS spectrum near $\omega = 0$, one must use a narrow spectral slit width so that only a small portion of the spectrum is obliterated by the instrumentally broadened Rayleigh line. Since the detected signal increases as the square of the spectral slit width, measurement at large frequency shifts will be favoured by wide slits. So, the only way to reconcile these conflicting requirements is to make separate scans with narrow and wide slits, for the small and large frequency shift regions of the spectrum, respectively.

Seven different experiments have been performed in our laboratory, in the range of frequency shifts 0-100 cm^{-1}, at different pressures.

In this thesis, pressures are given in p.s.i.:

1 p.s.i. = 0.68027 kPa

The total pressure range investigated in the experiment is 150 p.s.i. to 600 p.s.i. ≈ 100 kPa to 400 kPa.

3.3.1 Similar Molecules

(i) SF_6-SF_6

Scans were taken in the range 0-100 cm^{-1} with a 2 cm^{-1} slit width, in the range 0-30 cm^{-1} with 0.75 cm^{-1} slit, and in the range 475-565 cm^{-1} for intensity normalization purposes. This experiment was done twice, in order to gauge the limits of the experimental error, and the possible sources of that error. Shelton and Ulivi (1988) had measured carefully the intensity ratio of the ν_5 SF_6 vibrational band at 525 cm^{-1} to the S(1) line for H_2. The ratio was used hereafter for intensity normalization.

(a) SF_6 (I) - The experiment was performed in the pressure range 167-288 p.s.i.

(b) SF_6 (II) - The experiment was performed in the pressure range 165-309 p.s.i.

(ii) CF_4-CF_4

The same spectral parameters as for SF_6 were used, except that the range 590-710 cm^{-1} was recorded for normalization.

The experiment was done at the pressures: 363, 343, 327, 307, 283, 268, 252, 227, 210 and 187 p.s.i.

The densities were calculated using the second and third virial coefficients (Dymond, 1969) from the virial equation

$$P = \frac{RT}{V}\left[1 + \frac{B}{V} + \frac{C}{V^2} + \ldots\right] \qquad (3.1)$$

where

$\frac{1}{V} = \rho$ is the molecular density in moles/cm^3

P = the pressure in atm.

T = the temperature in K

B and C = the second and the third virial coefficient of the gas in cm^3/mole and $cm^6/mole^2$ respectively, and

R = the universal gas constant.

Then

$$P = 355.089\ [\rho + B\rho^2 + C\rho^3 + \ldots]\ \text{p.s.i.}$$

where

for SF_6

$B = -282\ cm^3/mole$ $\qquad$ $C = 21.4 \times 10^3\ cm^6/mole^2$

and for CF_4

$B = -88.3\ cm^3/mole$ $\qquad$ $C = 6070\ cm^6/mole^2$.

The densities corresponding to the pressures used were as follows:

For SF_6

(a) the range was 0.56-1.15 mole/litre, and

(b) the range was 0.545-1.3 mole/litre.

For CF_4, they were

1.13, 1.06, 1.01, 0.94, 0.86, 0.81, 0.76, 0.68, 0.6 and 0.55 mole/litre.

3.3.1a Normalization of Data

Since experimental conditions vary from day to day, causing changes in line intensities, data taken for the spectrum under experimental consideration must be normalized. For this purpose, the intensity of the depolarized ν_5 vibration line at 525 cm^{-1} was used in the case of SF_6, and the ν_4 vibration line at 631 cm^{-1} in the case of CF_4. The area of these lines were checked at every pressure, and to calibrate the spectrum on an absolute scale, the 560 cm^{-1} S(1) line for H_2 was used.

We will take SF_6 as an example. The same procedure is followed for CF_4. The intensity of an allowed line is proportional to the density, so one can write the following equation:

$$\frac{\int I_{SF_6}(500)}{\int I_{H_2}(560)} = \frac{\omega_0(\omega_0 + 500)^3 \, Q_{SF_6} \, \rho_{SF_6}}{\omega_0(\omega_0 + 560)^3 \, Q_{H_2} \, \rho_{H_2}} = K_1 \qquad (3.2)$$

where ω_0 is the frequency of the incident light, and

$$Q_{H_2} = \frac{(J+1)\,(J+2)}{(2J+1)\,(2J+3)} \frac{\beta_{H_2}^2}{10} \quad n(J)$$

and $\beta_{H_2} = 0.316$ $\mathring{A}^3$; for the S(1) line J = 1 and n(1) = 0.6585.

From Eqn. (3.2)

$$Q_{SF_6} = K_1 \frac{\omega_0(\omega_0 + 560)^3}{\omega_0(\omega_0 + 500)^3} Q_{H_2} \frac{\rho_{H_2}}{\rho_{SF_6}} \tag{3.3}$$

For a CILS run at density ρ_x

$$\frac{\int I_{SF_6}(CILS)}{\int I_{SF_6}(500)} = \frac{\omega_0(\omega_0 + \omega_{CILS})^3 Q_{SF_6}(CILS)\, F(\rho_x)}{\omega_0(\omega_0 + 500)^3\, Q_{SF_6}\, \rho_x} = K_2 \tag{3.4}$$

From Eqns. (3.3) and (3.4)

$$Q_{SF_6}(CILS) = K_1 K_2 \frac{(\omega_0 + 560)^3 \rho_x}{(\omega_0 + CILS)^3} \frac{Q_{H_2} \rho_{H_2}}{\rho_{SF_6}} \tag{3.5}$$

From Eqns. (3.4) and (3.5)

$$I_{SF_6}(CILS) = \omega_0(\omega_0 + 560)^3 Q_{H_2} \rho_x K_1 K_2 \frac{\rho_{H_2}}{\rho_{SF_6}} \quad . \tag{3.6}$$

Eqn. (3.6) is used to put the intensity on an absolute scale.

3.3.1b Data Analysis

The normalized intensities at different frequency shifts were plotted as a function of density to check if the intensity varied smoothly with density within experimental error. As a result of this test, data at several pressures were not used further in the analysis.

Reasons for these points falling off the curve are probably related to the fact that the experimental conditions change with time. For example, the laser power beam position could have shifted.

It was therefore felt that it was not appropriate to use the defective points for the analysis.

For example, in the case of SF_6-SF_6, the following densities only were used

(I) 1.15, 1.0, 0.72, 0.64, and 0.56 mole/litre.

(II) 1.3, 1.16, 1.02, 0.88, 0.65, and 0.545 mole/litre.

In the case of CF_4, all the runs were used.

The intensity $I(\omega)$ at each frequency ω for densities less than 2 mole/litre, may be expressed by a virial expansion as a function of density, in the form

$$I(\omega) = I^{(2)}(\omega)\ \rho^2 + I^{(3)}(\omega)\ \rho^3 + \ldots \qquad (3.7)$$

The ρ^2 term describes the two-body correlation spectrum and the ρ^3 term describes the three-body correlation spectrum. So, fitting our 2 cm^{-1} spectra with the above equation in the range 6-70 cm^{-1}, one can separate contributions of two and three body interactions.

To obtain information near $\omega = 0$, we used both 2 cm^{-1} and 0.75 cm^{-1} spectra in the range 6-20 cm^{-1}. Analysis shows that the ratio of intensities of the two sets of measurements in that range follows a straight line, with different constants at each pressure.

Extrapolating the 0.75 cm^{-1} spectra using the constants at each pressure enables us to obtain the two-body spectrum within 2 cm^{-1} from the laser line. A gaussian is then fit to the data within 5 cm^{-1} from the laser line to determine the spectrum until $\omega = 0$.

The two-body spectrum for SF_6 and CF_4 is shown in Figures 3.3 (a,b) and 3.4, and listed in Tables 3.1 (I,II) and 3.2 respectively.

TABLE 3.1 (I)

The Two-Body Spectrum of SF_6-SF_6 (I)

Frequency (cm^{-1})	Intensity ($Å^6$)	Frequency (cm^{-1})	Intensity ($Å^6$)
4.0	0.168×10^{-2}	38.0	0.251
5.0	0.1293	39.0	0.239
6.0	0.9654×10^{-3}	40.0	0.2052
7.0	0.6909	41.0	0.1874
8.0	0.4871	42.0	0.1703
9.0	0.3421	43.0	0.1524
10.0	0.2453	44.0	0.1338
11.0	0.1881	47.0	0.973×10^{-6}
12.0	0.1497	48.0	0.865
13.0	0.1150	52.0	0.667
14.0	0.93×10^{-4}	54.0	0.448
15.0	0.7583	56.0	0.42
16.0	0.6428	58.0	0.3406
17.0	0.5314	64.0	0.29
18.0	0.4459	66.0	0.254
19.0	0.3703	68.0	0.22
20.0	0.3005		
21.0	0.2586		
22.0	0.2049		
23.0	0.1793		
24.0	0.1491		
25.0	0.127		
27.0	0.959×10^{-5}		
28.0	0.8164		
29.0	0.751		
30.0	0.6055		
31.0	0.559		
32.0	0.5		
33.0	0.379		
34.0	0.369		
36.0	0.292		

TABLE 3.1 (II)

The Two-Body Spectrum of SF_6-SF_6 (II)

Frequency (cm^{-1})	Intensity ($Å^6$)
4.0	0.1618×10^{-2}
6.0	0.942×10^{-3}
8.0	0.4746
10.0	0.257
12.0	0.152
14.0	0.1008
16.0	0.661×10^{-4}
18.0	0.45
20.0	0.305
22.0	0.2162
24.0	0.1643
26.0	0.1186
28.0	0.8673×10^{-5}
30.0	0.5773
32.0	0.5029
34.0	0.3569
36.0	0.2997
38.0	0.258
44.0	0.1289
47.0	0.9628×10^{-6}
50.0	0.763
53.0	0.482
56.0	0.39
60.0	0.312

TABLE 3.2

The Two-Body Spectrum of CF_4-CF_4

Frequency (cm^{-1})	Intensity ($\AA^6$)
4.0	0.203×10^{-3}
6.0	0.1535
8.0	0.9942×10^{-4}
10.0	0.6183
12.0	0.4499
14.0	0.314
16.0	0.2082
18.0	0.1442
20.0	0.997×10^{-5}
24.0	0.482
26.0	0.387
30.0	0.238
33.0	0.181
38.0	0.122
41.0	0.90×10^{-6}
44.0	0.77
48.0	0.56
52.0	0.438
55.0	0.36
58.0	0.306
60.0	0.258

The three-body of the first run for SF_6 was available in a larger frequency range and was taken for further analysis.

Figures. 3.5 and 3.6 show the three-body spectrum for SF_6 and CF_4 respectively.

3.3.2 Mixtures

The two-body spectra for the five following mixtures -

(i) SF_6 - Xe

(ii) SF_6 - Kr

(iii) SF_6 - Ar

(iv) SF_6 - Ne

(v) CF_4 - Ar

have been obtained using the following procedure. Three different spectra needed to be taken for each mixture. For example, in the case of SF_6-Ar, a SF_6-SF_6, Ar-Ar and SF_6-Ar mixture spectra were taken. The pressure for SF_6 was fixed and different pressures for Ar were used for analysis. To determine the number density of Ar in the SF_6-Ar mixture, a small filling apparatus was used to fill the cell as shown in Fig. 3.7.

At the start, Ar, at a pressure X_1 atmospheres is in the cell, while valves 2 and 3 are closed. Then all the valves are closed except valve 3 which is opened to evacuate the system. Then valve 4 only is open and the pressure of the gauge changes to X_2. From X_1 and X_2 and the virial coefficients for Ar, one can find ρ_1 and ρ_2, and then the ratio of volumes of the cell and the tubes

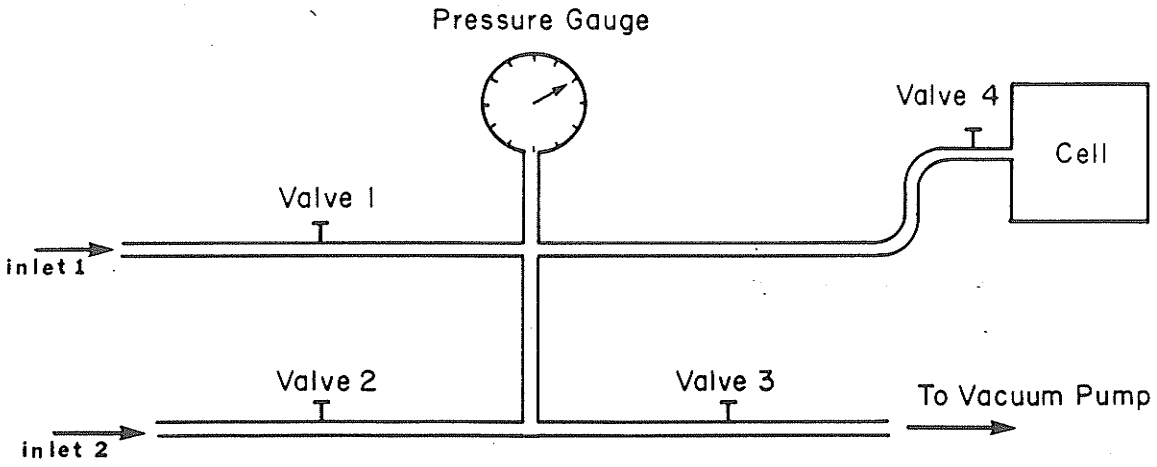

Figure 3.7

$$R = \frac{V_{tubes}}{V_{cell}} = \frac{\rho_1}{\rho_2} - 1 \quad . \tag{3.8}$$

This is done four times and an average taken for R. Once this is done, Ar is let out of the system and valve 3 is opened to evacuate the system.

SF_6 is let into the cell, at a certain known pressure, through valve 1, and then all the valves are closed except valve 3 to evacuate the system.

Ar is let into the system through valve 2 at pressure (P_{Ar_1}). Valve 4 is then opened and closed quickly, allowing some of the Ar gas to enter the cell and mix with SF_6. The reading of the gauge is reduced to (P_{Ar_2}).

From R, P_{Ar_1} and P_{Ar_2}, the number density of Ar in the cell can be found as follows:

ρ_{Ar_1} and ρ_{Ar_2} are determined from the virial coefficients for Ar, and the number density of Ar atoms that pass into the cell

$$= \rho_{Ar_1} V_{tubes} - \rho_{Ar_2} V_{tubes}$$

Thus the number of Ar atoms in the cell is given by

$$\rho_{Ar} = (\rho_{Ar_1} - \rho_{Ar_2}) \frac{V_{tubes}}{V_{cell}}$$

$$= (\rho_{Ar_1} - \rho_{Ar_2}) R$$

and so on. Increasing the pressure of Ar in the tubes and opening V_4 to let more Ar in, we can do the experiment at different densities of Ar.

Scans were taken for:

(i) SF_6-SF_6 in the range 0-100 cm^{-1} with a 2 cm^{-1} slit width, in the range 0-30 cm^{-1} with a 0.75 cm^{-1} slit width, and in the range 475-565 cm^{-1} for normalization.

(ii) Ar-Ar (perturber) in the range 0-100 cm^{-1} with a 2 cm^{-1} slit width, and in the range 0-30 cm^{-1} with a 0.75 cm^{-1} slit width.

(iii) SF_6-Ar in the same ranges as (i).

The densities for the systems studied were as follows:

(i) SF_6-Xe

SF_6 - SF_6 at pressure 192 p.s.i.

Xe - Xe at pressure 310 p.s.i.

SF_6 - Xe the densities for Xe were 0.065, 0.103, 0.151, 0.220, 0.280, 0.32, 0.422, 0.53 and 0.616 mole/litre.

(ii) SF_6-Kr

SF_6 - SF_6 at pressure 192 p.s.i.

Kr - Kr at pressure 270 p.s.i.

SF_6 - Kr the densities for Kr were 0.058, 0.092, 0.158, 0.214, 0.226, 0.269, 0.316 and 0.363 mole/litre.

(iii) SF_6-Ar

SF_6 - SF_6 at pressure 192 p.s.i.

Ar - Ar at pressure 556 p.s.i.

SF_6 - Ar the densities of Ar were 0.324, 0.445, 0.538, 0.697, 0.823, .836, 0.942, 0.974, 1.016 and 1.065 mole/litre.

(iv) SF_6-Ne

In this case we used wider slits (3 cm^{-1} rather than 2 cm^{-1}), because the intensity of the scattering from Ne was very weak.

SF_6 - SF_6 at pressure 192 p.s.i.

Ne - Ne at pressure 373 p.s.i.

SF_6 - Ne the densities for Ne were 0.127, 0.258, 0.306, 0.350, 0.417, 0.480, 0.567, 0.626 and 0.677 mole/litre.

(v) CF_4-Ar

CF_4 - CF_4 at pressure 187 p.s.i.

Ar - Ar at pressure 363 p.s.i.

CF_4 - Ar the densities for Ar are 0.048, 0.121, 0.168, 0.212, 0.259, 0.303 and 0.350 mole/litre.

3.3.2a Data Normalization

We followed similar procedures, as for the scattering by like molecules, for normalization.

3.3.2b Data Analysis

The intensity of the mixture is due, not only to the interaction of like molecules, but to the interaction of different molecules also. We can write the total intensity as

$$I_{tot.} = (I^{(2)} \rho_1^2 + I^{(3)} \rho_1^3) + (I^{(2')} \rho_2^2 + I^{(3')} \rho_2^3)$$

$$+ (I^{(2")} \rho_1 \rho_2 + I^{(3")} \rho_1 \rho_2^2 + I^{(3"')} \rho_1^2 \rho_2) + \ldots \qquad (3.9)$$

where $I^{(2)}$ and $I^{(3)}$ are the two and three-body for molecule 1

$I^{(2')}$ and $I^{(3')}$ are the two and three-body for molecule 2

$I^{(2")}$ is the two-body interaction of molecules 1 and 2.

The last two terms in the third bracket are the interaction between one molecule of the first kind and two molecules of the second kind and vice versa.

Eqn. (3.9) can be rewritten in the form

$$\frac{I_{tot.} - (I^{(2)} \rho_1^2 + I^{(3)} \rho_1^3) - (I^{(2)} \rho_2^2 + I^{(3)} \rho_2^3)}{\rho_1 \rho_2} \qquad (3.10)$$

$$= I^{(2")} + I^{(3")} \rho_2 + I^{(3"')} \rho_1 + \ldots$$

$I^{(2")}$ is the two-body spectrum of the mixture.

$I^{(3")}$ and $I^{(3"')}$ could not be identified in the analysis because of limits on the numerical precision of the experiments. These terms were neglected for further analysis. Some theoretical justification is given in Chapter 4 in the case of SF_6, and in Chapter 6 in the case of CF_4.

The two-body spectra for SF_6-Xe, SF_6-Kr, SF_6-Ar, SF_6-Ne, and CF_4-Ar are shown in Figs. 3.8-3.12 and listed in Tables 3.3-3.7 respectively.

TABLE 3.3

The Two-Body Spectrum of SF_6-Xe

Frequency (cm^{-1})	Intensity ($\AA^6$)
6.0	0.9503×10^{-3}
8.0	0.537
10.0	0.338
12.0	0.235
14.0	0.162
16.0	0.115
18.0	0.71×10^{-4}
20.0	0.576
22.0	0.417
25.0	0.263
26.0	0.245
28.0	0.165
30.0	0.1465
32.0	0.1087
34.0	0.905×10^{-5}
36.0	0.734
38.0	0.47
42.0	0.302
44.0	0.228
46.0	0.1741
48.0	0.125
50.0	0.1008
54.0	0.669×10^{-6}

TABLE 3.4

The Two-Body Spectrum of SF_6-Kr

Frequency (cm^{-1})	Intensity ($\AA^6$)
4.0	0.69×10^{-3}
6.0	0.484
8.0	0.3305
10.0	0.2
12.0	0.132
14.0	0.806×10^{-4}
16.0	0.6067
18.0	0.413
20.0	0.278
22.0	0.2175
25.6	0.131
27.6	0.892×10^{-5}
31.6	0.573
34.0	0.45
36.4	0.367
38.0	0.3
40.0	0.238
42.0	0.196
44.0	0.168
46.0	0.133
48.4	0.124
50.0	0.1009
55.0	0.6105×10^{-6}
59.0	0.45
62.0	0.345

TABLE 3.5

The Two-Body Spectrum of SF_6-Ar

Frequency (cm^{-1})	Intensity ($\AA^6$)
4.0	0.268×10^{-3}
5.8	0.24
6.4	0.21
8.4	0.1706
10.0	0.1132
12.4	0.715×10^{-4}
14.8	0.547
15.6	0.425
17.2	0.342
18.8	0.3079
20.0	0.235
22.4	0.185
25.0	0.133
28.4	0.97×10^{-5}
30.4	0.71
31.4	0.61
33.0	0.53
33.8	0.455
35.4	0.4
37.0	0.335
40.0	0.28
42.0	0.1961
43.6	0.1665
46.0	0.1412
50.0	0.1104
52.0	0.855×10^{-6}
56.0	0.693
64.0	0.337
66.0	0.2873

TABLE 3.6

The Two-Body Spectrum of SF_6-Ne

Frequency (cm^{-1})	Intensity ($\mathring{A}^6$)
9.2	0.6842×10^{-5}
12.	0.4964
14.4	0.447
17.6	0.222
23.2	0.199
25.2	0.1324
28.0	0.901
30.0	0.735×10^{-6}
32.0	0.609
36.0	0.402
39.2	0.303
42.8	0.250
45.0	0.213
49.0	0.15
53.2	0.1104

TABLE 3.7

The Two-Body Spectrum of CF_4-Ar

Frequency (cm^{-1})	Intensity ($\AA^6$)
4.0	0.6197×10^{-4}
6.0	0.4722
8.0	0.37
10.0	0.2919
12.0	0.2422
14.0	0.2025
16.0	0.1658
18.0	0.1264
20.0	0.9702×10^{-5}
22.0	0.76
24.0	0.6051
28.0	0.4669
32.0	0.267
35.0	0.194
38.0	0.1448
42.0	0.1189
45.0	0.9307×10^{-6}
50.0	0.6542
52.0	0.5628
53.0	0.525
57.0	0.4153
62.0	0.298

Figure 3.1

The set-up of the experiment.

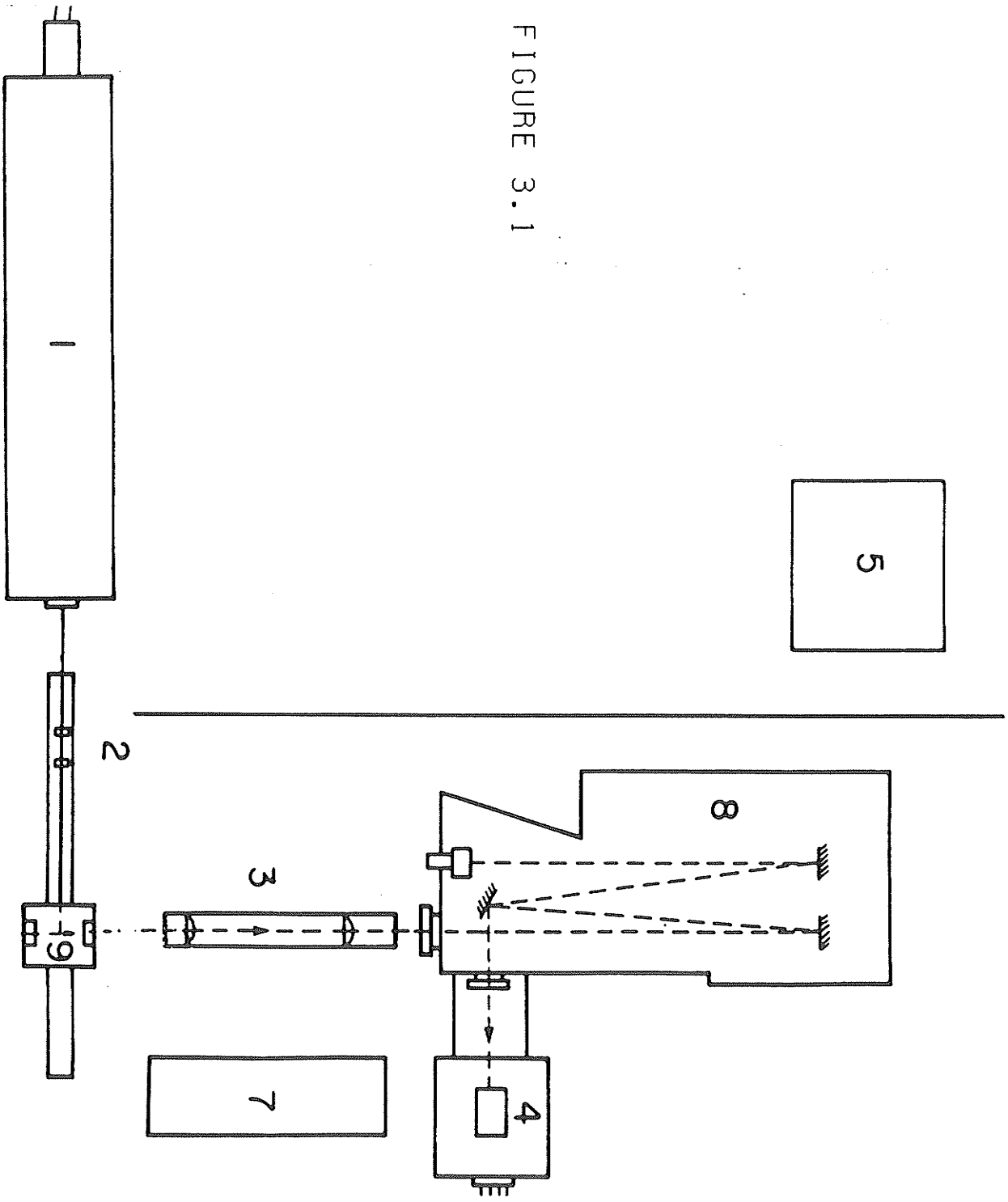

FIGURE 3.1

Figure 3.2

The spectrometer (double monochromator).

FIGURE 3.2

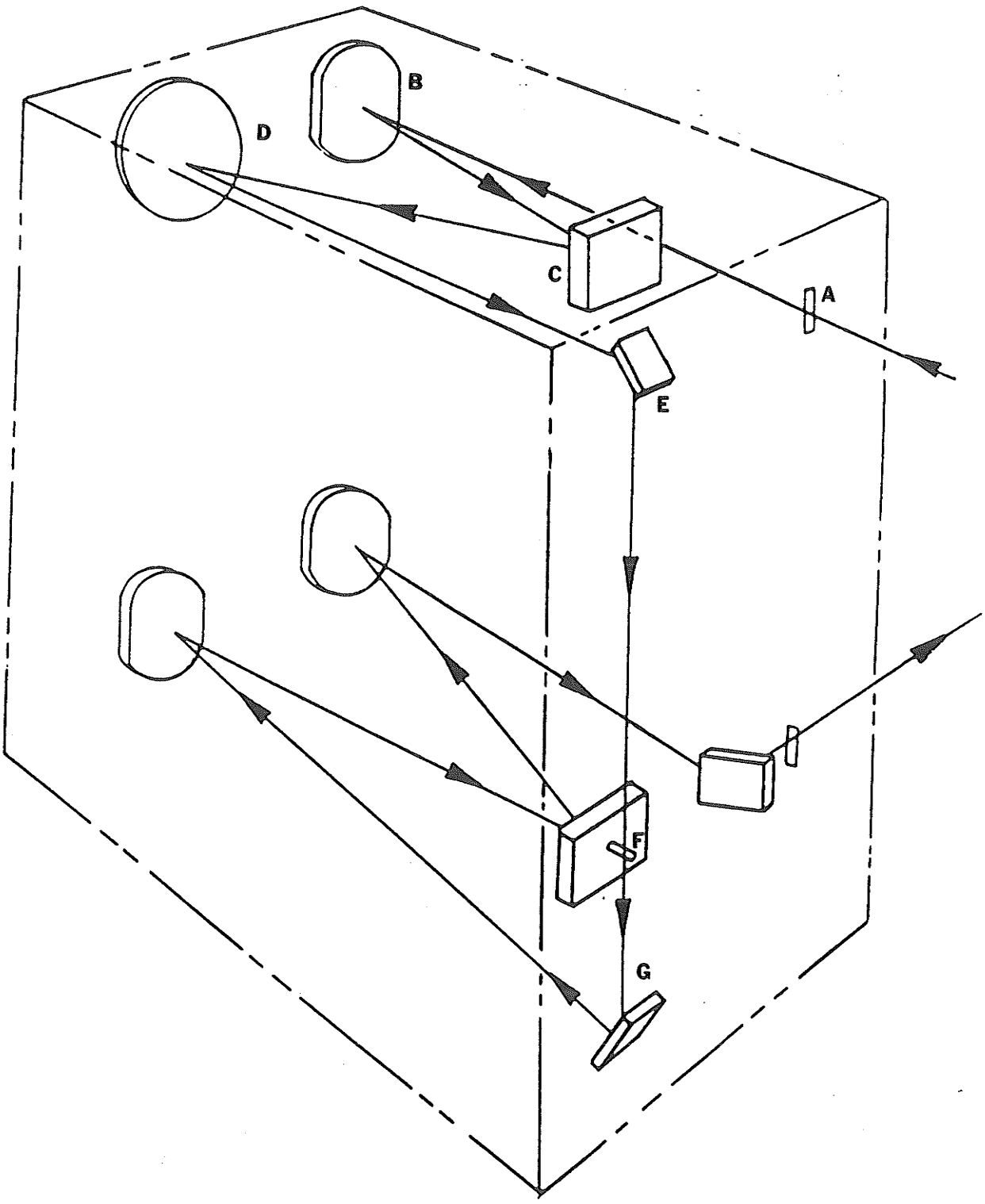

Figures 3.3a, b, and 3.4

Figure 3.3a The experimental two-body spectrum of SF_6-SF_6 (I).

Figure 3.3b The experimental two-body spectrum of SF_6-SF_6 (II).

Figure 3.4 The experimental two-body spectrum of CF_4-CF_4.

FIGURE 3.3.a

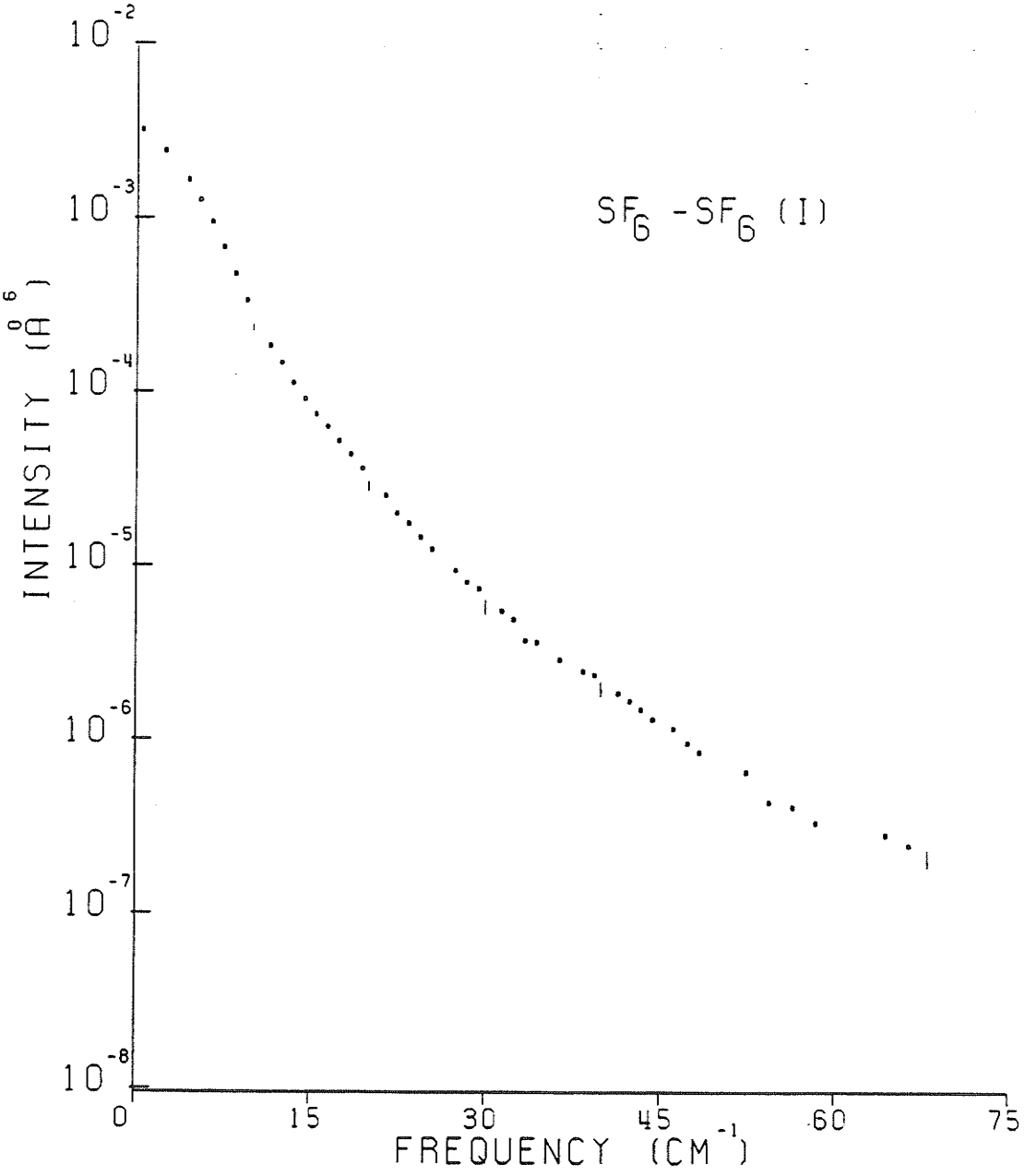
$SF_6 - SF_6$ (I)
INTENSITY ($\AA^6$)
10^{-2}
10^{-3}
10^{-4}
10^{-5}
10^{-6}
10^{-7}
10^{-8}
0
15
30
45
60
75
FREQUENCY (CM^{-1})

FIGURE 3.3.b

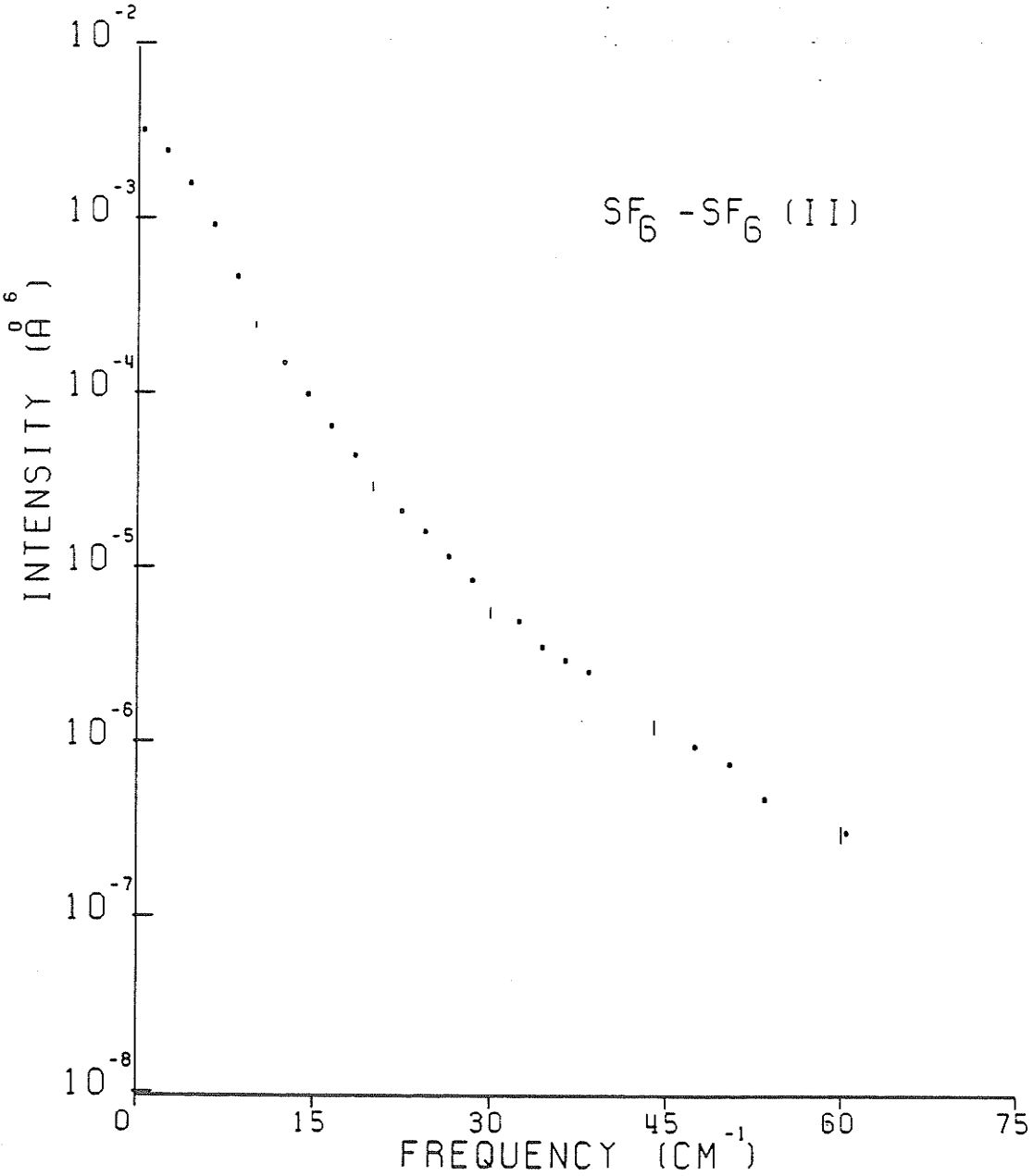
$SF_6 - SF_6$ (II)
INTENSITY ($\AA^6$)
10^{-2}
10^{-3}
10^{-4}
10^{-5}
10^{-6}
10^{-7}
10^{-8}
0
15
30
45
60
75
FREQUENCY (CM^{-1})

FIGURE 3.4

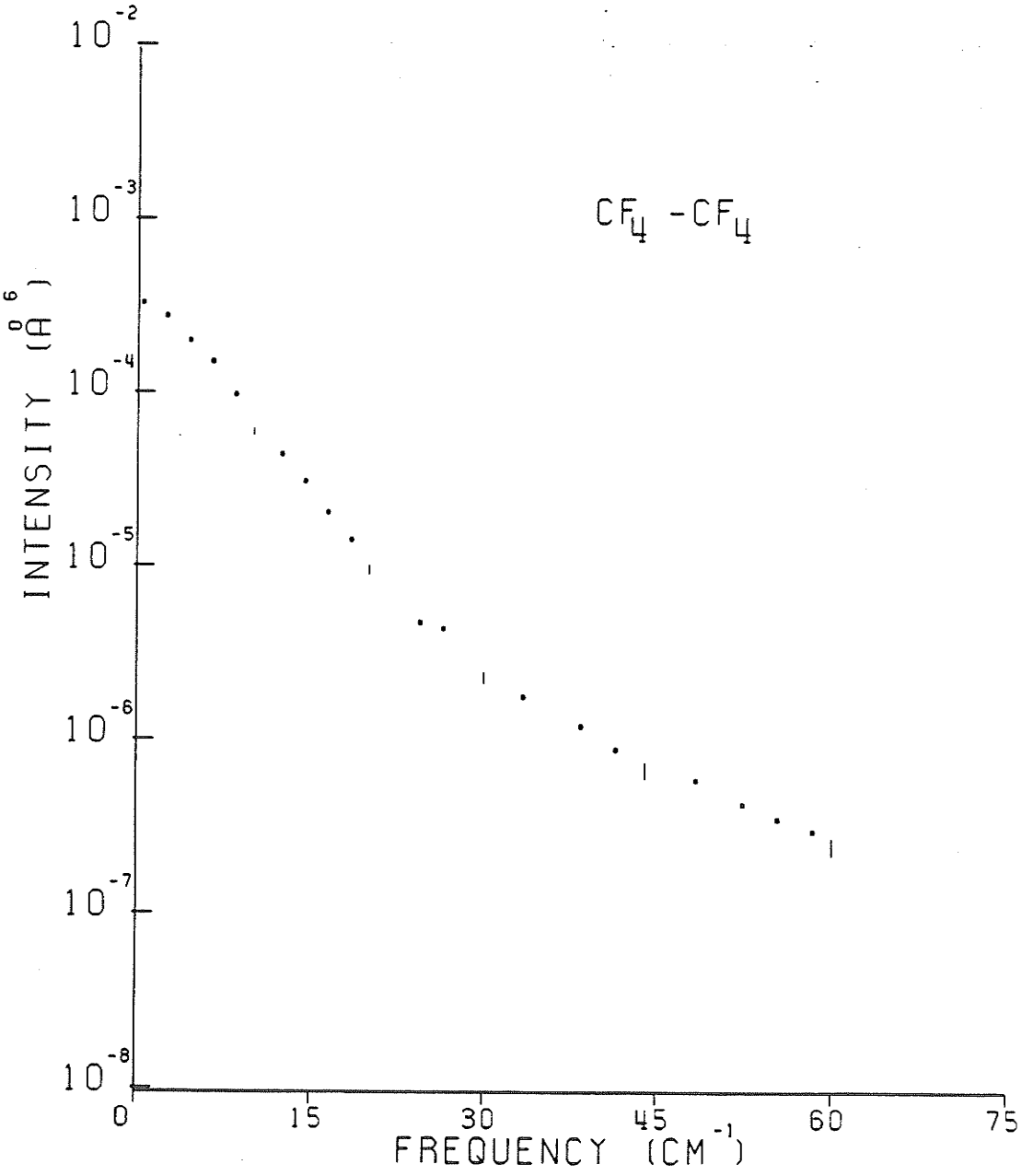
10^{-2}
10^{-3}
10^{-4}
10^{-5}
10^{-6}
10^{-7}
10^{-8}
INTENSITY ($A^{o\,6}$)
CF_4 - CF_4
0
15
30
45
60
75
FREQUENCY (CM^{-1})

Figures 3.5-3.6

Figure 3.5 The experimental three-body spectrum of SF_6-SF_6.

Figure 3.6 The experimental three-body spectrum of CF_4-CF_4.

FIGURE 3.5

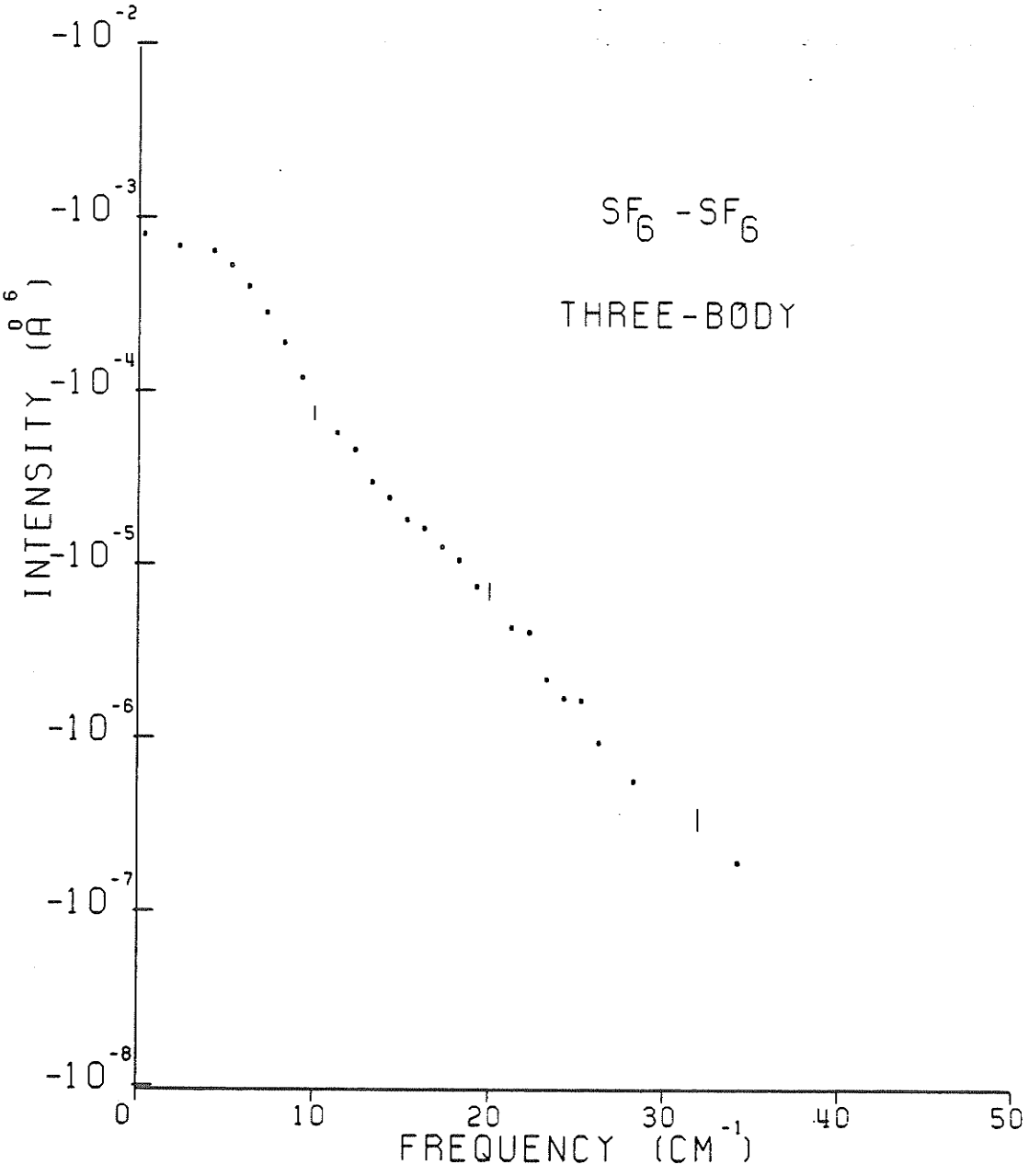
SF_6 -SF_6
THREE-BODY
INTENSITY (A^6)
-10^{-2}
-10^{-3}
-10^{-4}
-10^{-5}
-10^{-6}
-10^{-7}
-10^{-8}
0
10
20
30
40
50
FREQUENCY (CM^{-1})

FIGURE 3.6

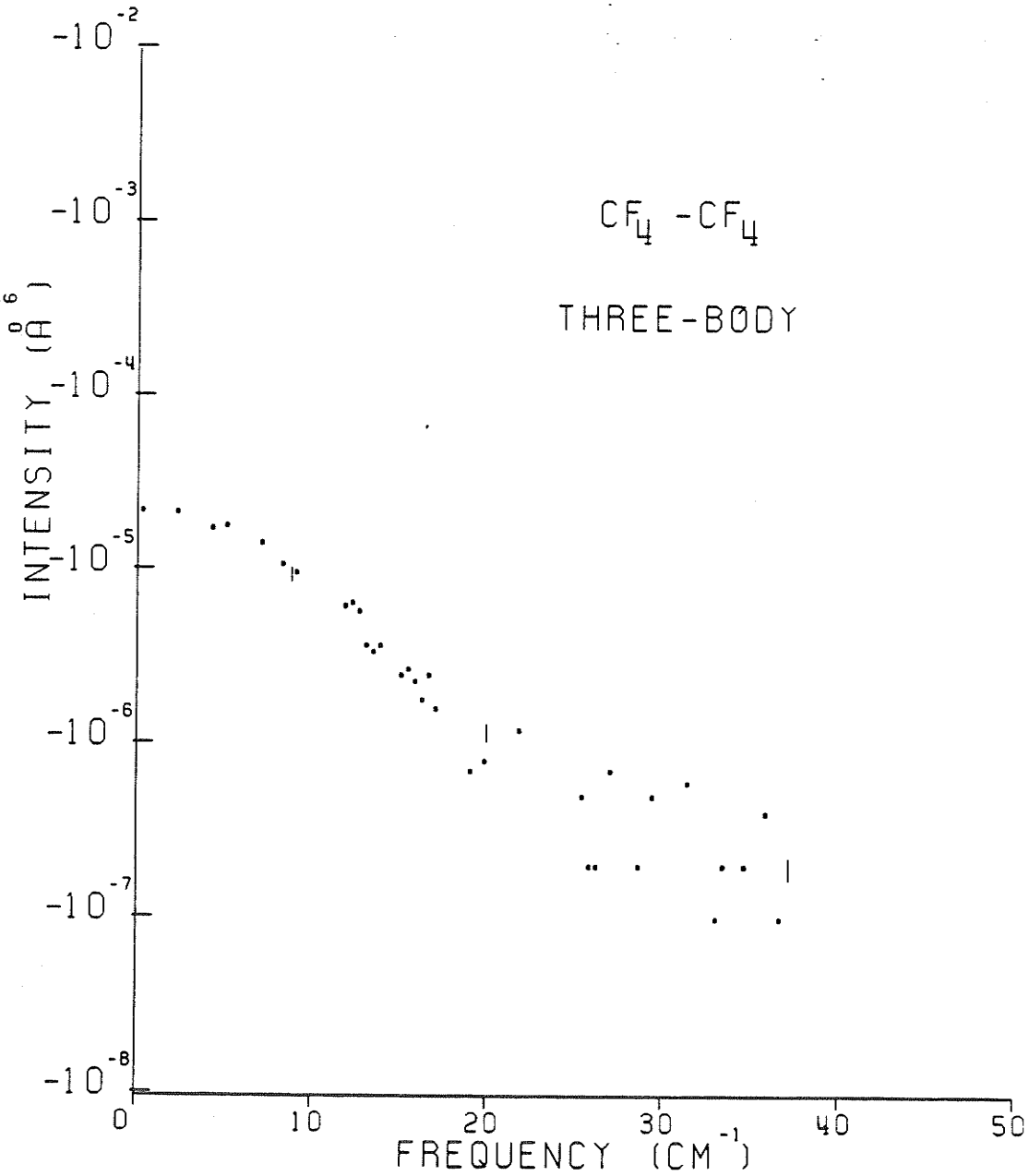
CF_4 - CF_4
THREE-BODY
INTENSITY ($\AA^6$)
-10^{-2}
-10^{-3}
-10^{-4}
-10^{-5}
-10^{-6}
-10^{-7}
-10^{-8}
0
10
20
30
40
50
FREQUENCY (CM^{-1})

Figures 3.8-3.12

Figure 3.8 The experimental two-body spectrum of SF_6-Xe.

Figure 3.9 The experimental two-body spectrum of SF_6-Kr.

Figure 3.10 The experimental two-body spectrum of SF_6-Ar.

Figure 3.11 The experimental two-body spectrum of SF_6-Ne.

Figure 3.12 The experimental two-body spectrum of CF_4-Ar.

FIGURE 3.8

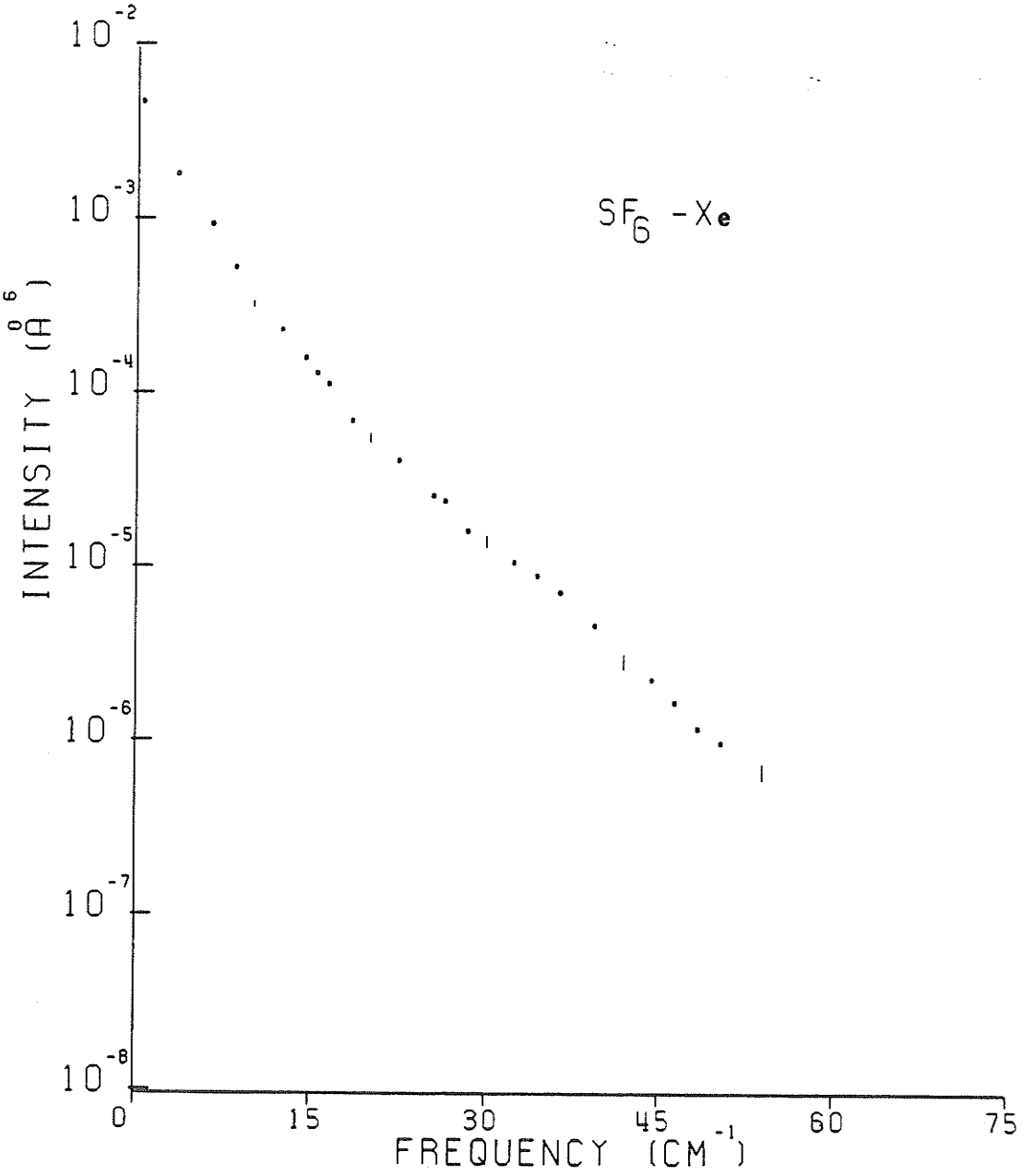
$SF_6 - Xe$
INTENSITY (A^6)
10^{-2}
10^{-3}
10^{-4}
10^{-5}
10^{-6}
10^{-7}
10^{-8}
0
15
30
45
60
75
FREQUENCY (CM^{-1})

FIGURE 3.9

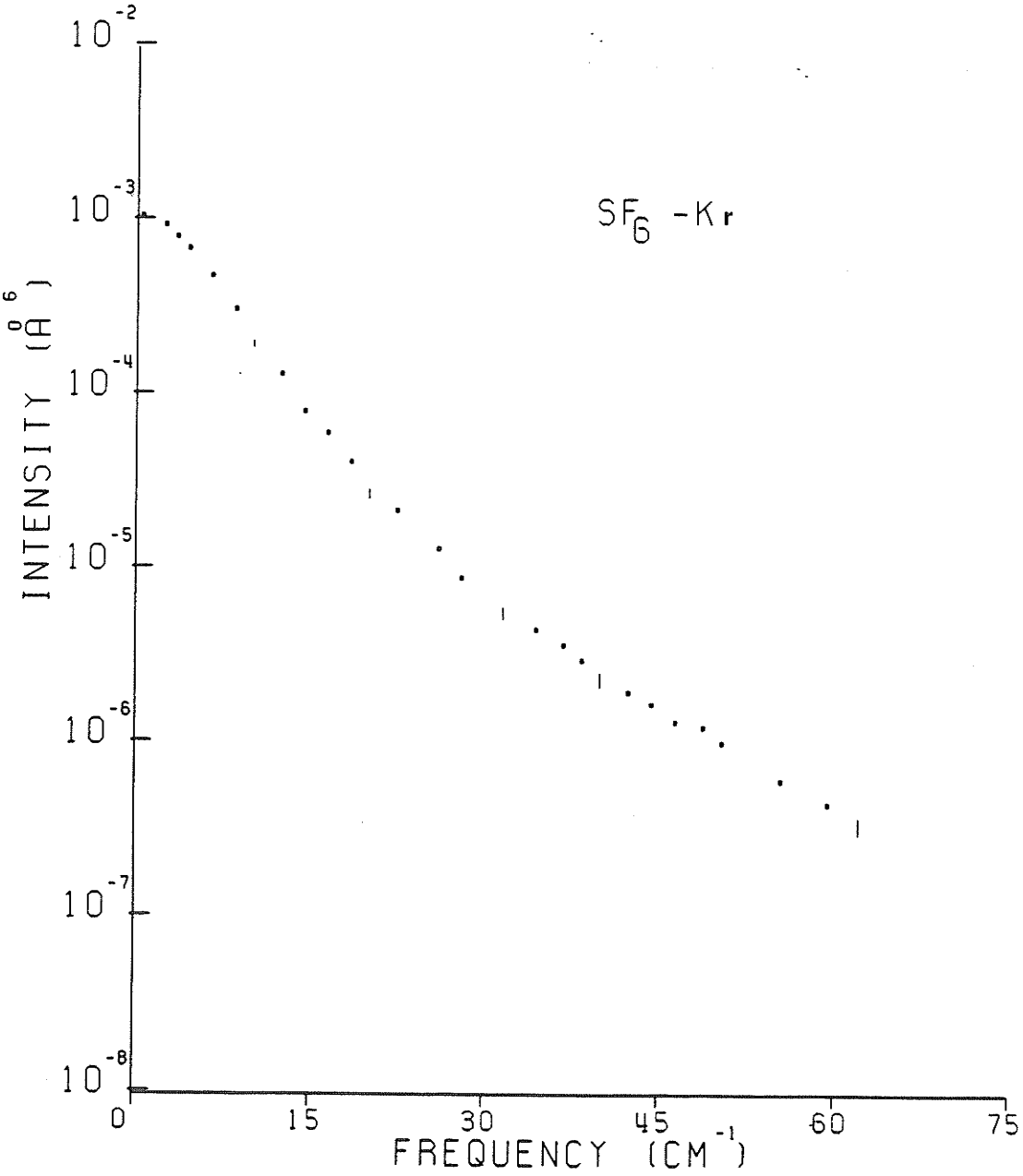
SF_6 -Kr
INTENSITY (A^6)
10^{-2}
10^{-3}
10^{-4}
10^{-5}
10^{-6}
10^{-7}
10^{-8}
0
15
30
45
60
75
FREQUENCY (CM^{-1})

FIGURE 3.10

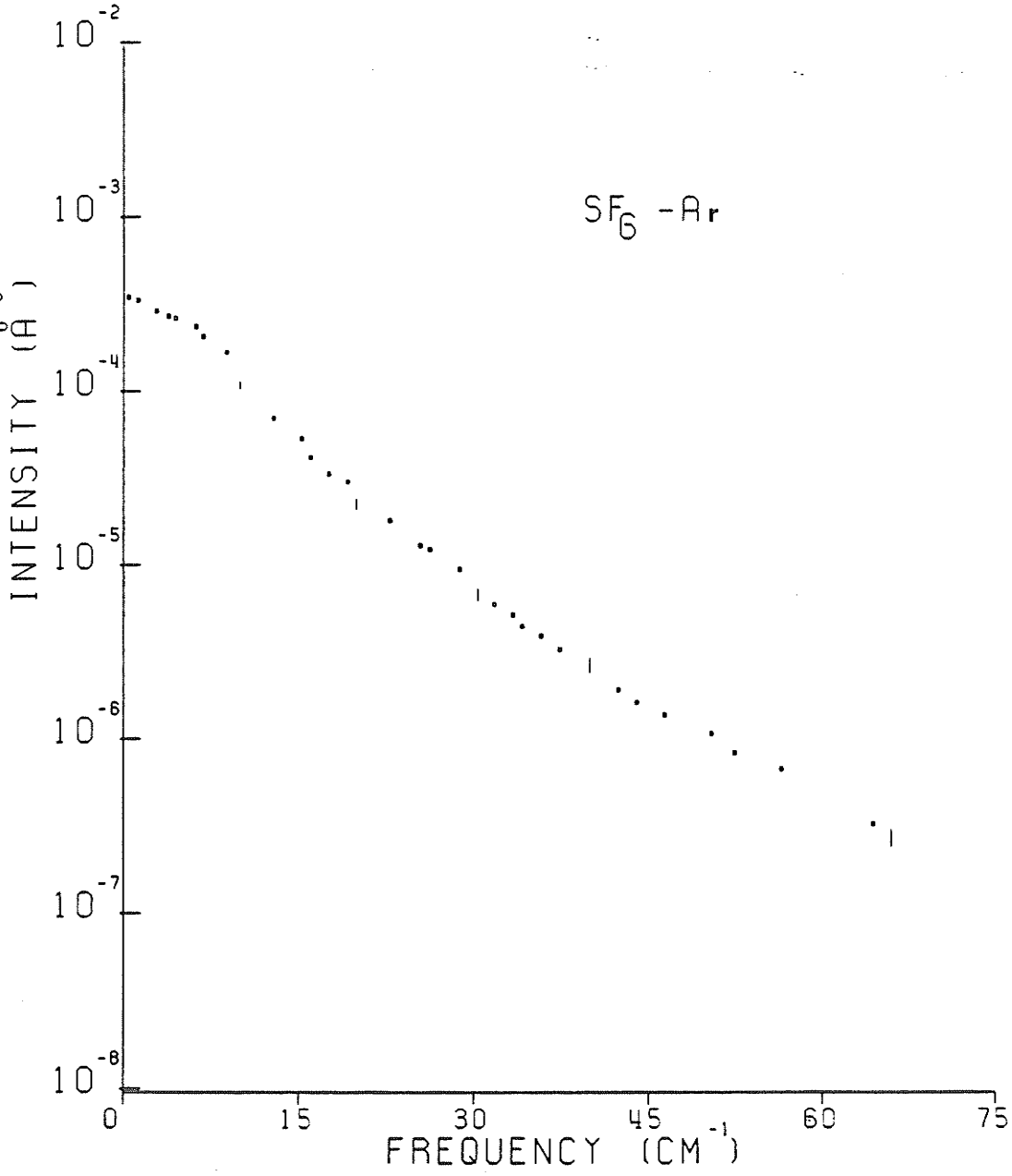
SF_6 -Ar
INTENSITY ($A^{\circ 6}$)
10^{-2}
10^{-3}
10^{-4}
10^{-5}
10^{-6}
10^{-7}
10^{-8}
0
15
30
45
60
75
FREQUENCY (CM^{-1})

FIGURE 3.11

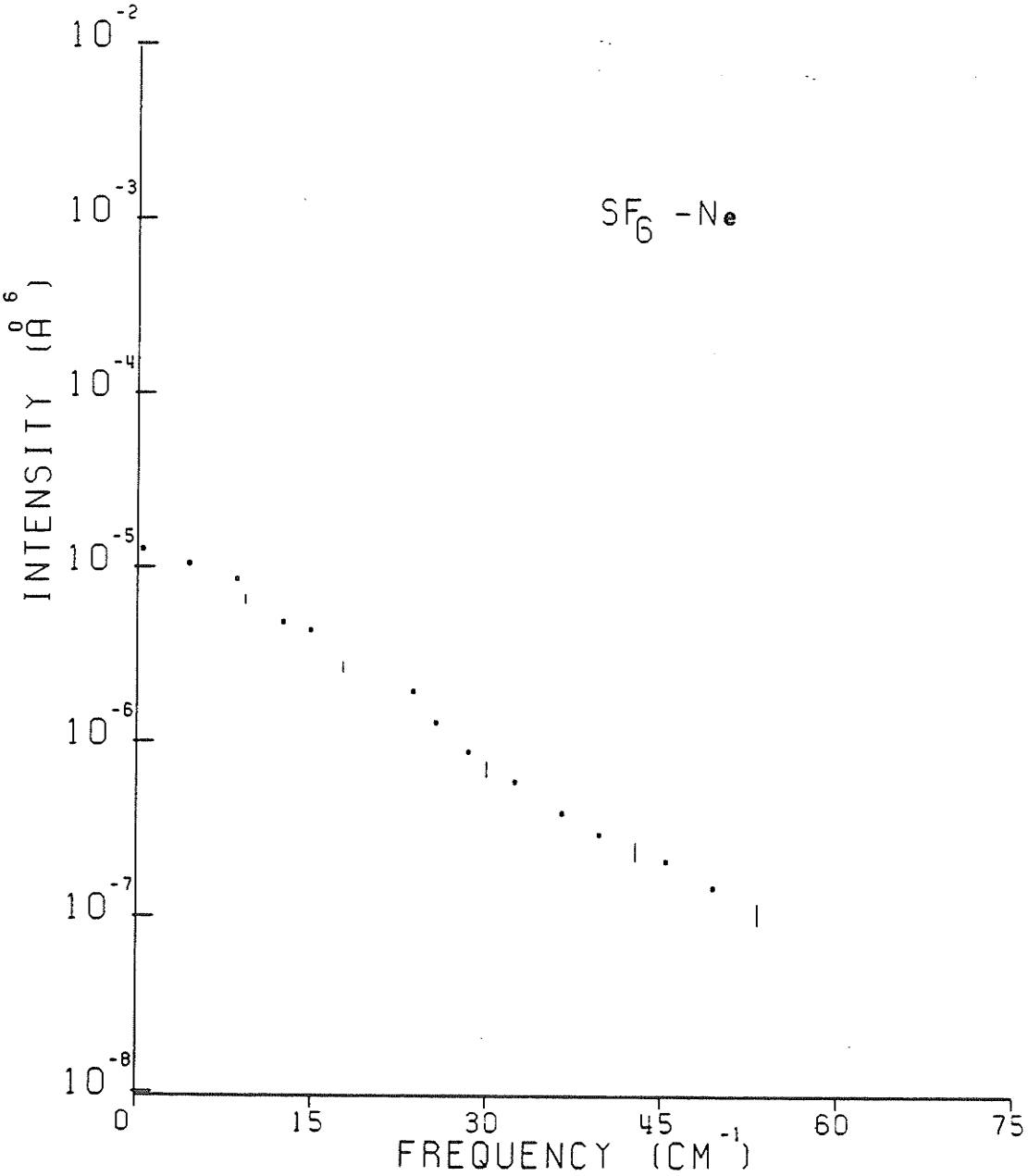
SF_6 -Ne
INTENSITY ($\AA^6$)
10^{-2}
10^{-3}
10^{-4}
10^{-5}
10^{-6}
10^{-7}
10^{-8}
0
15
30
45
60
75
FREQUENCY (CM^{-1})

FIGURE 3.12

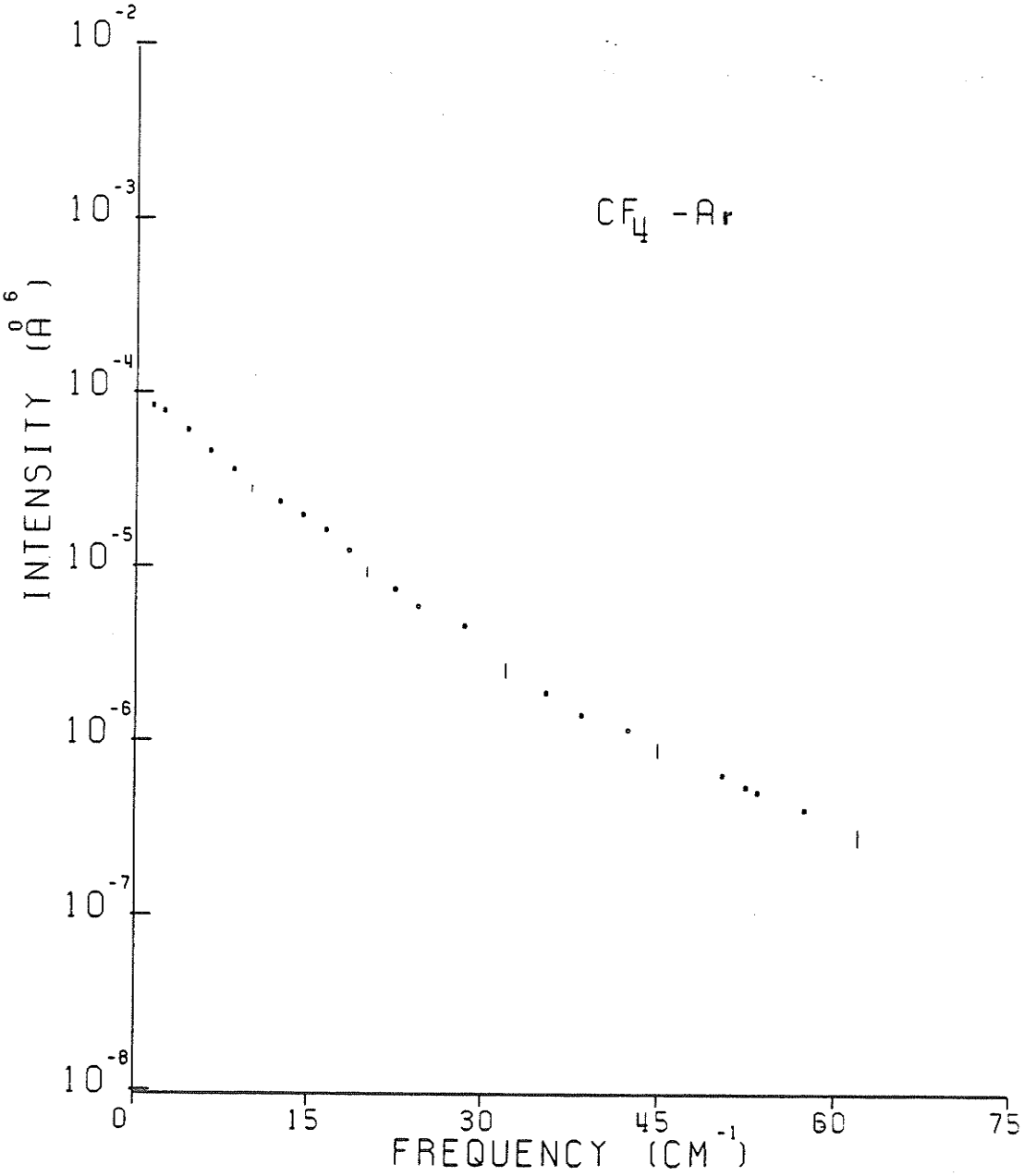
10^{-2}
10^{-3}
10^{-4}
10^{-5}
10^{-6}
10^{-7}
10^{-8}
INTENSITY (A^6)
CF_4 -Ar
0
15
30
45
60
75
FREQUENCY (CM^{-1})

CHAPTER 4

OCTAHEDRAL MOLECULES

In molecular gases, the intensity of the collison induced light scattering is proportional to the square of the anisotropy $\beta(r)$, and is larger than predicted by the DID model where $\beta(r)$ is given by Eqn. (2.14), or the anisotropy corrected for electron overlap given by Eqn. (2.17). Buckingham and Tabisz (1978) proposed a mechanism which is a generalization of the DID effect. The intensity of CILS is given by Eqn. (2.67), the first term corresponds to the first order DID effect, which gives the dominant contribution to the scattered intensity at low frequency shifts, the rest of the terms correspond to the intensity of the induced rotational scattering. Since octahedral molecules have a centre of symmetry, the dipole-quadrupole polarizability $\underset{\sim}{A}$ vanishes, and the dipole-octopole effect gives the main contribution to collision induced rotational Raman scattering.

Our interest in this chapter is the dipole-octopole polarizability $\underset{\sim}{E}$ of SF_6. As mentioned in Chapter 2, one can calculate the translational spectrum using Eqns. (2.31) and (2.32) once the anisotropy and the intermolecular potential are known.

Table 4.1 shows the parameters that were used in calculating the translational spectra for SF_6-SF_6, SF_6-Kr, SF_6-Ar, and SF_6-Ne.

The moments from the translational spectra (TR) and from the sum rules (SR) can be evaluated using Eqns. (2.37) and (2.46) respectively (the first three even SR moments are quantum mechanically corrected).

TABLE 4.1

The Values of the Polarizability and Hyperpolarizability for SF_6, Kr, Ar, and Ne

	α ($\mathring{A}^3$)		γ ($C^4 M^4 J^{-3} \times 10^{-62}$)	
SF_6	4.549	Watson and Ramaswamy, (1936)	12.0	Kielich (1969)
Kr	2.54	Meinander et al. (1985)	14.0	Shelton (1986)
Ar	1.679	Dalgarno and Kingston (1960)	7.3	Buckingham and Dummer (1968)
Ne	0.3989	Meinander et al. (1985)	0.44	Shelton and Lu (1988)

Table 4.2 shows the values of the moments, using the different potentials mentioned in Chapter 2.

It is clear from Table 4.2 that the moments calculated from the sum rule are higher than those of the translational spectrum. This result is expected since the sum rule expressions for the moments include the dimer contribution. In fact, the difference between those moments gives the moments due to the dimer interactions. One can use that difference with Eqn. (2.48) to calculate the dimer spectra for the different species. If the two spectra are added, translational plus dimer, and compared with the experimental spectrum, one will find an excess in intensity of the experimental spectrum, especially at high frequency shifts which is due to the collision induced rotational spectrum. (In this case, it is mainly due to the dipole-octopole polarizability E).

TABLE 4.2

The First Four Even Moments Calculated from the Translational Spectrum and from the Sum Rule for SF_6-SF_6, SF_6-Kr, SF_6-Ar, and SF_6-Ne

			$M_0(\text{Å}^9)$	$M_2(\text{Å}^9\text{PS}^{-2})$	$M_4(\text{Å}^9\text{PS}^{-4})$	$M_6(\text{Å}^9\text{PS}^{-6})$
SF_6-SF_6	HFD	TR	712.35	986.09	0.1017759×10^5	0.1010342×10^7
		SR	1058.33	1143.21	0.1107228×10^5	0.1055745×10^7
	MC	TR	656.67	949.36	0.135154×10^5	0.1082222×10^7
		SR	1167.03	1302.44	0.1854561×10^5	0.17994157×10^7
	PS	TR	554.80	794.58	0.1578177×10^5	0.2194837×10^7
		SR	931.11	1013.49	0.1890082×10^5	0.2394980×10^7
SF_6-Kr	D	TR	322.78	884.35	0.2253744×10^5	0.2335921×10^7
		SR	448.25	993.91	0.2413713×10^5	0.2435917×10^7
	S	TR	309.28	781.713	0.1873883×10^5	0.192513×10^7
		SR	402.70	851.05	0.198975×10^5	0.200795×10^7
SF_6-Ar		TR	159.85	769.73	0.3873442×10^5	0.9140079×10^7
		SR	202.22	831.98	0.4190311×10^5	0.9678816×10^7
SF_6-Ne		TR	9.78	72.75	0.4043358×10^4	0.7450079×10^6
		SR	10.91	82.90	0.5652674×10^4	0.1432258×10^7

Figs. 4.1-4.7 show the translational, dimer, and the experimental spectra for SF_6-SF_6 (HFD, MC, PS), SF_6-Kr (D, S), SF_6-Ar, and SF_6-Ne respectively.

It is clear from the figures that the dimer has an effect only at low frequency shifts ($\leq 30\ cm^{-1}$).

The rotational spectrum (normalized to unity) can be

calculated using Eqns. (2.87) and (2.88). The rotational constant for SF_6 is B = 0.095 cm^{-1}, so the rotational lines are closely spaced. Each rotational δ-function is broadened (Posch, 1982) with a translational broadening function associated with an interaction characterized by a tensor of rank 4 and varying as r^{-5}. The width of the lines due to $\underset{\sim}{E}$ were estimated from the experimental exponential decay function for the r^{-3} interaction of the pure translational spectrum and scaled to r^{-5} through the calculation of Posch. A gaussian of HWHM of 5 cm^{-1} was thus used for the broadening function; the widths were assumed to vary as $\frac{1}{\sqrt{\mu}}$ for the mixture cases.

If one multiplies the normalized spectrum with the factor:

$$\frac{22}{9}\alpha^2 E^2 \overline{r^{-10}} + \frac{5863}{105} E^4 \overline{r^{-14}}, \text{ (mentioned in Eqn. (2.71))},$$

in the case of SF_6-SF_6,
and with the factor

$$\frac{11}{9}\alpha_2^2 E_1^2 \overline{r^{-10}}, \text{ (mentioned in Eqn. (2.73))},$$

in the case of mixtures, one can get the value of E by fitting the rotational spectrum to the difference between the experimental and the sum of the (translational + dimer) spectrum.

Different cases will be treated separately in the next section.

4.1 OCTAHEDRAL-OCTAHEDRAL INTERACTIONS (SF_6-SF_6)

In the case of SF_6-SF_6, we performed the experiment twice and found about 4% difference between the intensities of the two-body

spectra. Both were separately used for analysis and the individual values of E were then averaged.

4.1.1 HFD Potential

Figs. 4.8 and 4.9 show the translational, rotational, total theoretical, and the experimental spectra for both experiments (I) and (II) respectively. The values of E obtained were as follows:

$$(I) \quad E_1 = 9.6 \pm 1.8 \ \text{Å}^5$$
$$(II) \quad E_2 = 9.2 \pm 1.5 \ \text{Å}^5$$

The average of E is $9.4 \pm 1.65 \ \text{Å}^5$.

The error mentioned above includes both the experimental and the statistical errors.

4.1.2 MC Potential

Figs. 4.10 and 4.11 show the same spectra for this case. The values of E obtained were:

$$(I) \quad E_1 = 6.2 \pm 1.8 \ \text{Å}^5$$
$$(II) \quad E_2 = 5.9 \pm 1.7 \ \text{Å}^5$$

The average is $E = 6.05 \pm 1.75$.

4.1.3 PS Potential

Again Figs. 4.12 and 4.13 show the spectra for this case. The values of E were as follows:

$$(I) \quad E_1 = 8.8 \pm 2 \ \text{Å}^5$$
$$(II) \quad E_2 = 8.2 \pm 2 \ \text{Å}^5$$

The average of E is 8.5 ± 2 $\mathring{A}^5$.

To compare these three potentials, we calculate a measure of success of the fit between the experimental and the theoretical spectra, in the frequency range where the potential is a crucial factor in determining the theoretical spectrum (10-25 cm^{-1}), i.e. a region where the free-free translational spectrum rather than the dimer spectrum dominates the profile.

$$\delta_j^2(\text{CILS}) = \frac{1}{n_j} \sum_{i=1}^{n_j} \bar{\Delta}_{ji}^{-2} (P_{ji} - P_{ij})^2 \qquad (4.1)$$

where n_j is the number of frequencies used, $\bar{\Delta}_{ji}$ is the experimental percentage error at each frequency, and $(P_{ji}-P_{ij})$ is the ratio $(\frac{\text{experimental-theoretical}}{\text{experimental}})$ for the intensities at a particular frequency.

A value of $\delta < 1$, means that the difference between the experimental and theoretical spectra is less than the experimental error and the fit is excellent. Table 4.3 shows the values of δ(CILS) for the three potentials.

From Table 4.3 the HFD potential seems to be the best available potential for SF_6, though we believed at the outset that there is no truly refined potential for SF_6-SF_6 as yet. This circumstance lay behind the idea of using the SF_6 mixtures to determine E since for these there exists the good potentials determined by Pack.

TABLE 4.3

Comparison of δ (CILS) for HFD, Mc, and PS Potentials

		δ(CILS)
HFD	(I)	1.58
	(II)	1.81
MC	(I)	1.92
	(II)	2.04
PS	(I)	3.24
	(II)	3.5

TABLE 4.4

δ(CILS) for the Three Mixtures SF_6-Kr, SF_6-Ar, and SF_6Ne

		δ(CILS)
SF_6-Kr	D	0.957
	S	2.5
SF_6-Ar		0.8865
SF_6-Ne		1.28

4.2 OCTAHEDRAL-ATOM INTERACTIONS (SF_6-Kr, SF_6-Ar, and SF_6-Ne)

Table 4.4 shows the values of δ(CILS) for the three mixtures.

In the case of SF_6-Kr, the theoretical spectra were calculated using the two available potentials (D and S). We decided to consider D only for further analysis for two reasons. The first one is that the value of δ(CILS) for S was very high. Secondly, the two potentials were determined using two different sets of data for the interaction second virial coefficient, S, from only the data of the Santafa group (Santafa, 1978); D from the data of the Dunlop group (Martin et al., 1982). The latter agrees with the data measured by B. Schram (Pack et al., 1982). The CILS experiment then could be regarded as a test for the reliability of an intermolecular potential.

The actual experimental error in the case of SF_6-Ne was higher than that for SF_6-Ar and SF_6-Kr, but we used the same error in calculating δ(CILS) in all three cases for comparison purposes. Taking that higher experimental error into consideration, the fit of SF_6-Ne is not worse than the other two mixtures.

Figs. 4.14-4.16 show the good agreement between the theoretical and experimental spectra for the three mixtures. The values of E obtained were:

$$E = 12.9 \pm 2\ \text{Å}^5 \qquad SF_6\text{-Kr}$$
$$= 10.2 \pm 4\ \text{Å}^5 \qquad SF_6\text{-Ar}$$
$$= 11.3 \pm 5\ \text{Å}^5 \qquad SF_6\text{-Ne}$$

The uncertainty in the value of E increases as the polarizability of the perturber decreases, because the signal at high frequency shifts is weaker and the statistical error is higher.

In the case of SF_6-Xe, there was no intermolecular potential available. So, at first, two L-J (6-12) potentials for SF_6-SF_6 (Sigmund et al., 1972) and for Xe-Xe were used with the combination rules (Pena et al., 1982), but the difference between the experimental and theoretical spectra was very high. Hence we developed a new M3SV intermolecular potential for this mixture which leads to a value of E = 8.3 ± 3 $\mathring{A}^5$. The specifying of the potential will be discussed in detail in Chapter 5.

Table 4.5 shows the values of E, obtained in this and other studies.

Another comparison was made between the total theoretical and experimental spectra for all cases by calculating the same kind of δ given by Eqn. (4.1), but for the full frequency range of the spectra (0-70 cm^{-1}). Table 4.6 shows this comparison.

It is clear from Tables 4.3, 4.4 and 4.6 that not only is the HFD potential for SF_6-SF_6 better in the range 10-25 cm^{-1}, but also in the total frequency range. For SF_6-Kr and SF_6-Ar, the values are a little bit higher than for those in the limited frequency range.

4.3 EXPERIMENTAL MOMENTS

Another measure of agreement between the theoretical and experimental spectra is the zeroth moment. Since the experimental spectrum is measured at the Stokes side, we have to calculate the spectrum at the Anti-Stokes side using the relation:

TABLE 4.5

Value of |E|

Group	Method	|E| $\mathring{A}^5$
Present work	Experimental	
	(i) SF_6-SF_6	
	(1) HFD	9.4±1.65
	(2) MC	6.05±1.75
	(3) PS	8.5±2
	(ii) SF_6-Xe	8.3±3
	(iii) SF_6-Kr	12.9±2
	(iv) SF_6-Ar	10.2±4
	(v) SF_6-Ne	11.3±5
	Average =	10.7±2.5*
Shelton and Tabisz (1980)	Experimental	< 20
Buckingham and Tabisz (1978)	Bond-polarizability calculations	20
Neumann (1984)	Applequist's atom dipole interaction calculations	9.456
Pleich (1983)	Experiment	< 9
El-Sheikh et al. (1985) (after revised analysis)	Experiment SF_6-SF_6	8.5

Note

* The L-J and PS cases are neglected in this average because of the high values of δ(CILS)

TABLE 4.6

δ(total) for SF_6-SF_6, SF_6-Kr, SF_6-Ar, and SF_6-Ne

		δ(total
SF_6-SF_6 HFD	(1)	1.059
	(2)	0.944
MC	(1)	1.552
	(2)	1.358
PS	(1)	1.979
	(2)	1.775
SF_6-Kr		0.024
SF_6-Ar		0.9908
SF_6-Ne		1.246

$$I(-\omega) = \exp(-\hbar\omega/k_B T)\ I(\omega)$$

Integrating over the available range of the experimental data one can calculate the zeroth experimental moment. The m^{th} spectral moment of the n-body spectrum is defined as:

$$M_m^n = \int_{-\infty}^{\infty} \omega^m\ I^n\ (\omega)\ d\omega \quad .$$

Usually it is possible to determine the zeroth, second, fourth, and sixth moments for the two-body spectrum. The zeroth and second moments were calculated for the available three body spectra.

To calculate the zeroth moment, extrapolation is necessary to zero frequency as mentioned in Chapter 3. For higher moments, extrapolation is needed at high frequency shifts. This can be done by adding the theoretical translational spectrum plus the rotational spectrum corresponding to each case. The error is taken as greater than or equal to the area of the extrapolated portion of the curve.

4.3.1 The Two-Body Experimental Moments

To compare the two-body experimental and theoretical moments, one has to calculate the total theoretical moment, i.e. the moment calculated from the sum rule (translational + dimer) plus the moment due to the rotational spectrum.

The moments due to the rotational spectrum were calculated using the formula

$$M_n = \int_{-\infty}^{\infty} R(\omega)\ \omega^n\ d\omega$$

where $R(\omega)$ is the intensity of the rotational spectrum at a frequency ω.

Table 4.7 shows a comparison between the experimental and theoretical zeroth moment.

The error in the zeroth experimental moment was estimated as one third of the area extrapolated to zero frequency, whereas the extrapolated area at high frequency shifts have an effect of less than 0.01% of the zeroth moment.

Table 4.7 shows best agreement between the experimental and theoretical zeroth moment for the HFD potential in case of SF_6-SF_6.

TABLE 4.7

Comparison Between the Experimental and Theoretical Zeroth Moment of the Two-Body Spectrum for SF_6-SF_6, SF_6-Kr, SF_6-Ar, and SF_6-Ne

		$M_0(\text{Å}^9)$		
		Theoretical (SR)	Total Theoretical	Experimental
SF_6-SF_6	HFD (I)	1058.34	1064.95	1048.48±222
	(II)		1064.43	1037.48±221
	MC (I)	1167.04	1170.22	1048.47±222
	(II)		1169.83	1037.46±221
	PS (I)	931.12	934.38	1048.48±222
	(II)		934.00	1037.47±221
SF_6-Kr		448.26	451.63	474.78±108
SF_6-Ar		202.22	203.6	206.72±17.5
SF_6-Ne		10.91	11.0	10.65±1.9

In the case of mixtures, there is good agreement in all cases.

Table 4.8 shows a comparison of the same type, for higher moments.

The effect of collision induced rotational spectrum becomes more important the higher the order of the moments. The error in calculating M_2 is small, about 10%, which made M_2 a candidate for comparison between the theoretical and experimental spectra. Table 4.8 shows a good agreement in general for M_2.

The error due to high frequency extrapolation is very high for M_4 and M_6.

TABLE 4.8

Comparison Between the Experimental and Theoretical Higher Moments of the Two-Body Spectrum for SF_6-SF_6, SF_6-Kr, SF_6-Ar, and SF_6-Ne

			Theoretical (SR)	Total Theoretical	Experimental
SF_6-SF_6		HFD (I)	1143.21	1331.076	1359.89±125
		(II)		1315.197	1366.88±122
	M_2	MC (I)	1302.44	1391.787	1357.9±123
		(II)		1381.396	1364.73±120
		PS (I)	1013.49	1105.45	1360.39±125
		(II)		1094.66	1367.29±123
		HFD (I)	0.1107228×10^5	26532.33	27049±4796
				25225.8	26163±4465
	M_4	MC (I)	0.1854561×10^5	25898.03	26638±4421
		(II)		25043.1	25764±4203
		PS (I)	0.1890082×10^5	26503.65	31871 ± 9649
		(II)		25580.57	31004±9419
		HFD (I)	0.1055795×10^7	0.30927×10^7	$(0.29163 \pm 0.1508) \times 10^7$
		(II)		0.29205×10^7	$(0.29302 \pm 0.14306) \times 10^7$
	M_6	MC (I)	0.16994157×10^7	0.266813×10^7	$(0.4279 \pm 0.2878) \times 10^7$
		(II)		0.255546×10^7	$(0.41049 \pm 0.2826) \times 10^7$
		PS (I)	0.239498×10^7	0.339206×10^7	$(0.3265 \pm 0.3251) \times 10^7$
		(II)		0.3275041×10^7	$(0.32633 \pm 0.325) \times 10^7$

SF_6-Kr	M_2	993.91	1088.96	11242±133
	M_4	24137.13	31959.11	30549±5764
	M_6	0.2435917×10^7	0.346646×10^7	$(0.28245 \pm 0.1564) \times 10^7$
SF_6-Ar	M_2	831.987	870.99	821.86±51.5
	M_4	41905.11	45115.18	38838±15040
	M_6	0.9678816×10^7	0.101017×10^7	$(0.80553 \pm 0.628) \times 10^7$
SF_6-Ne	M_2	82.9	85.61	82.06±1.1
	M_4	5652.67	5875.69	5382±2404
	M_6	0.1432258×10^7	0.14616×10^7	$(0.1316 \pm 0.1075) \times 10^7$

Note

The units are M_2 ($\mathring{A}^9$ PS^{-2}), M_4 ($\mathring{A}^9$ PS^{-4}), and M_6 ($\mathring{A}^9$ PS^{-6}).

TABLE 4.9

Comparison Between the Experimental and Theoretical Zeroth and Second Moments of the Three-Body Spectrum for SF_6-SF_6 in This and Other Studies

Group	Method	$M_0(\text{Å}^9)$	$M_2(\text{Å}^9\ PS^{-2})$
This work	Experimental	286.1±46	344.75±30
Shelton et al. (1982)	Experimental	349 ±66	373.55±19
Shelton et al. (1982)	Calculations using Mc potential	184.36	280.16

4.3.2 The Three-Body Experimental Moment

The zeroth and second frequency moments are compared with calculations based on a pair-wise additive triplet cluster polarizability (Barocchi et al., 1977).

Table 4.9 shows a comparison of the zeroth and second moments if the experimental and theoretical spectra of this and other studies for SF_6-SF_6.

Table 4.9 shows reasonable agreement between this work and the calculations, having in mind that the Mc potential is not the best available potential for SF_6-SF_6.

The ratio of M_0^3/M_0^2 is about 20% for SF_6-SF_6.

This result justifies the neglect of the three-body mixture spectrum in the data analysis.

In the case of mixtures (Section 3.2.2b), the intensity

of the two-body spectra of any of the mixtures studied is less than the intensity of the two-body spectrum of SF_6-SF_6 because α_{SF_6} is higher than α of the perturbers used.

So too the three-body of any of the mixtures is less intense than the three-body spectrum of SF_6-SF_6. The intensity of the three-body mixture spectrum is thus very small. The procedure of subtraction used in the analysis of the raw data to obtain the total mixture spectrum (Eqn. 3.10) resulted in large statistical error and made the determination of the three-body spectrum of the mixture impossible within the precision of the experiment.

4.4 CONCLUSIONS

(1) The HFD potential is the best available potential for SF_6-SF_6 interactions for the following reasons:-

  (i) δ(CILS) is the best in the HFD case,

  (ii) δ(total) is the best in the HFD case,

  (iii) The value of E obtained with it agrees with the value calculated by Neumann.

(2) In the analysis of the mixtures, the error due to the full normalization procedure (like subtraction of three spectra) was not taken into account when calculating δ(CILS) and δ(total), which makes the values of δ that we got upper limits.

(3) The expression for the quantum mechanical correction for M_6 is not available and thus made the calculations of the dimer spectrum not very accurate at high frequencies.

(4) The average value of E for SF_6 is 10.7 ± 2.5 $\mathring{A}^5$. The average value and the error were calculated from the different values of E obtained using different perturbers and different potentials.

(5) The lower limit of the average value of E includes the values obtained by Neumann and Pleich.

Figures 4.1-4.3

Figures 4.1-4.3 show the experimental two-body spectra of SF_6-SF_6 (I) and SF_6-SF_6 (II), with the translational and dimer calculations using the different potentials HFD, MC, and PS.

. The experimental two-body spectrum.

□ The theoretical translational spectrum.

⊙ The theoretical dimer spectrum.

FIGURE 4.1.a

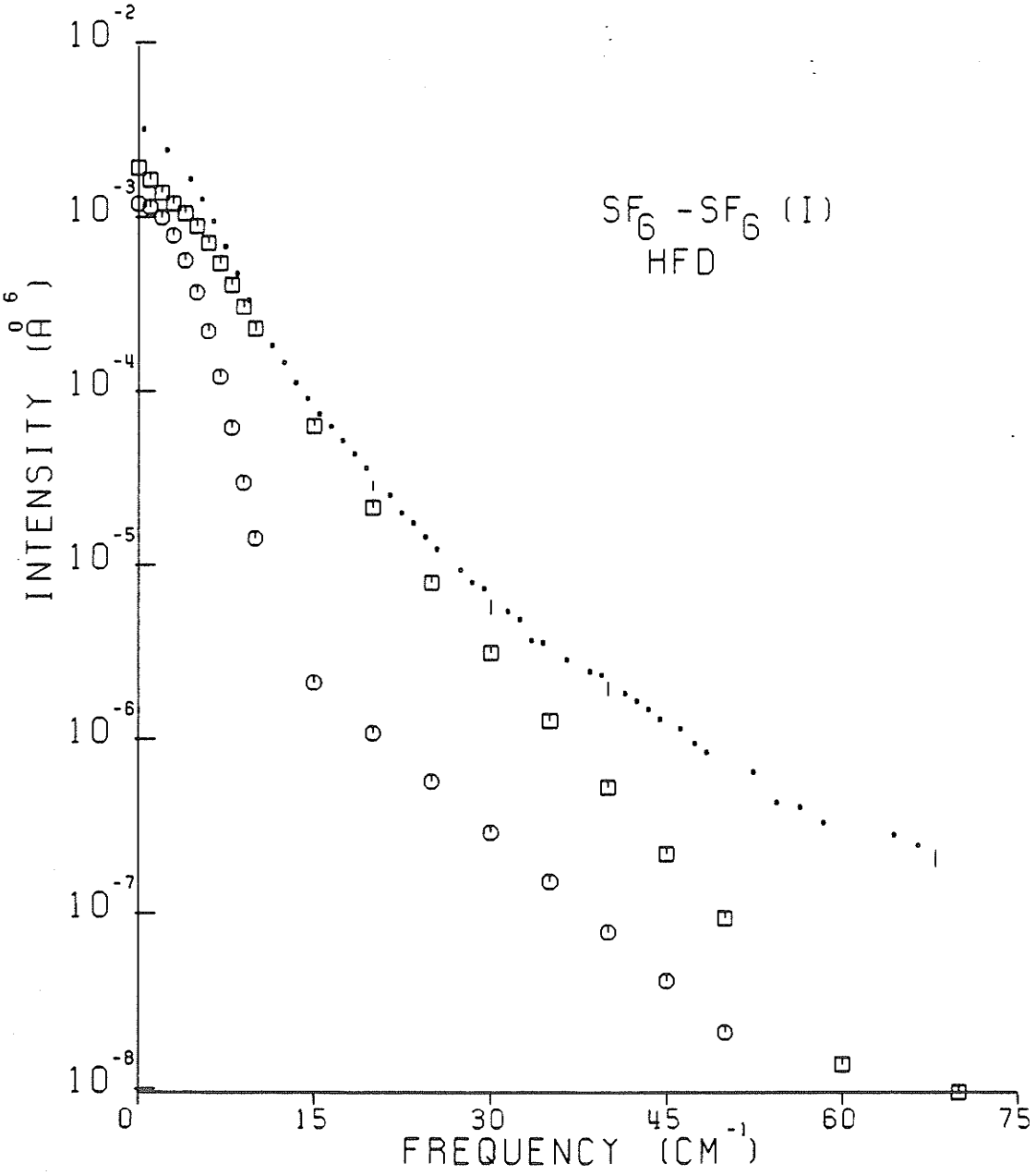
$SF_6 - SF_6$ (I)
HFD
INTENSITY ($\AA^6$)
10^{-2}
10^{-3}
10^{-4}
10^{-5}
10^{-6}
10^{-7}
10^{-8}
0
15
30
45
60
75
FREQUENCY (CM^{-1})

FIGURE 4.1.b

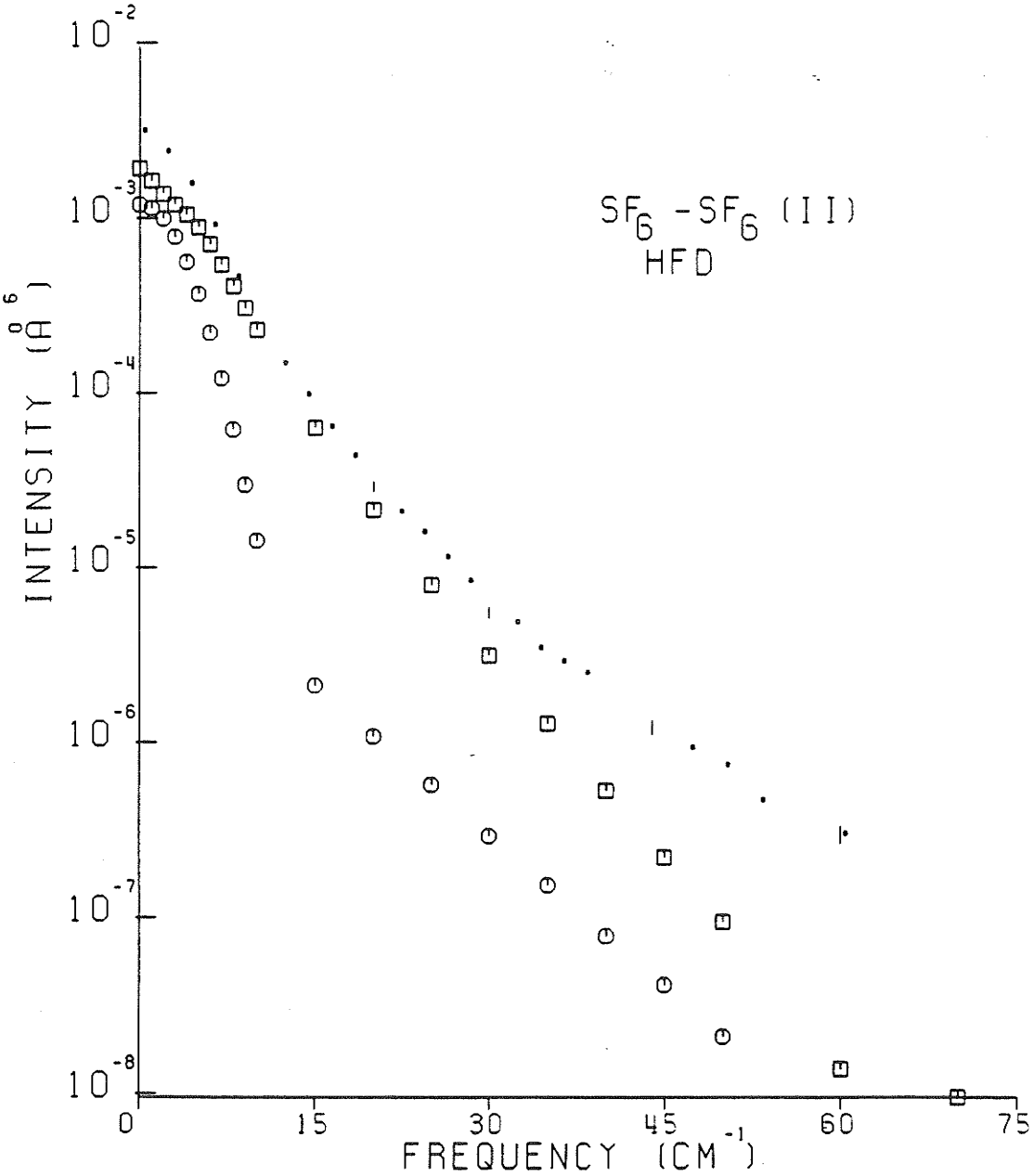
10^{-2}
10^{-3}
10^{-4}
10^{-5}
10^{-6}
10^{-7}
10^{-8}
INTENSITY (A^6_0)
$SF_6 - SF_6$ (II)
HFD
0
15
30
45
60
75
FREQUENCY (CM^{-1})

FIGURE 4.2.a

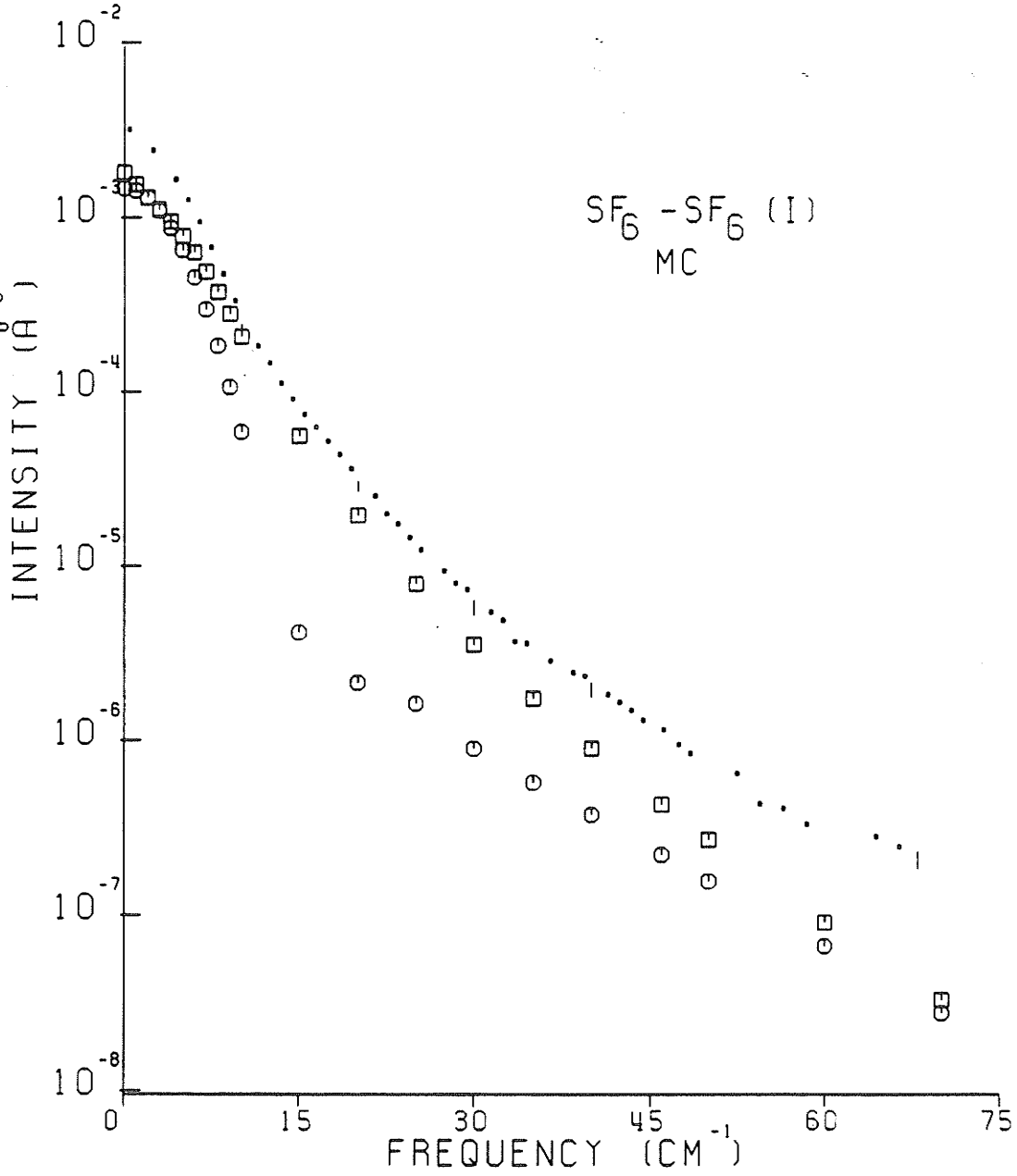
10^{-2}
10^{-3}
10^{-4}
10^{-5}
10^{-6}
10^{-7}
10^{-8}
INTENSITY (A^6)
SF_6 - SF_6 (I)
MC
0
15
30
45
60
75
FREQUENCY (CM^{-1})

FIGURE 4.2.b

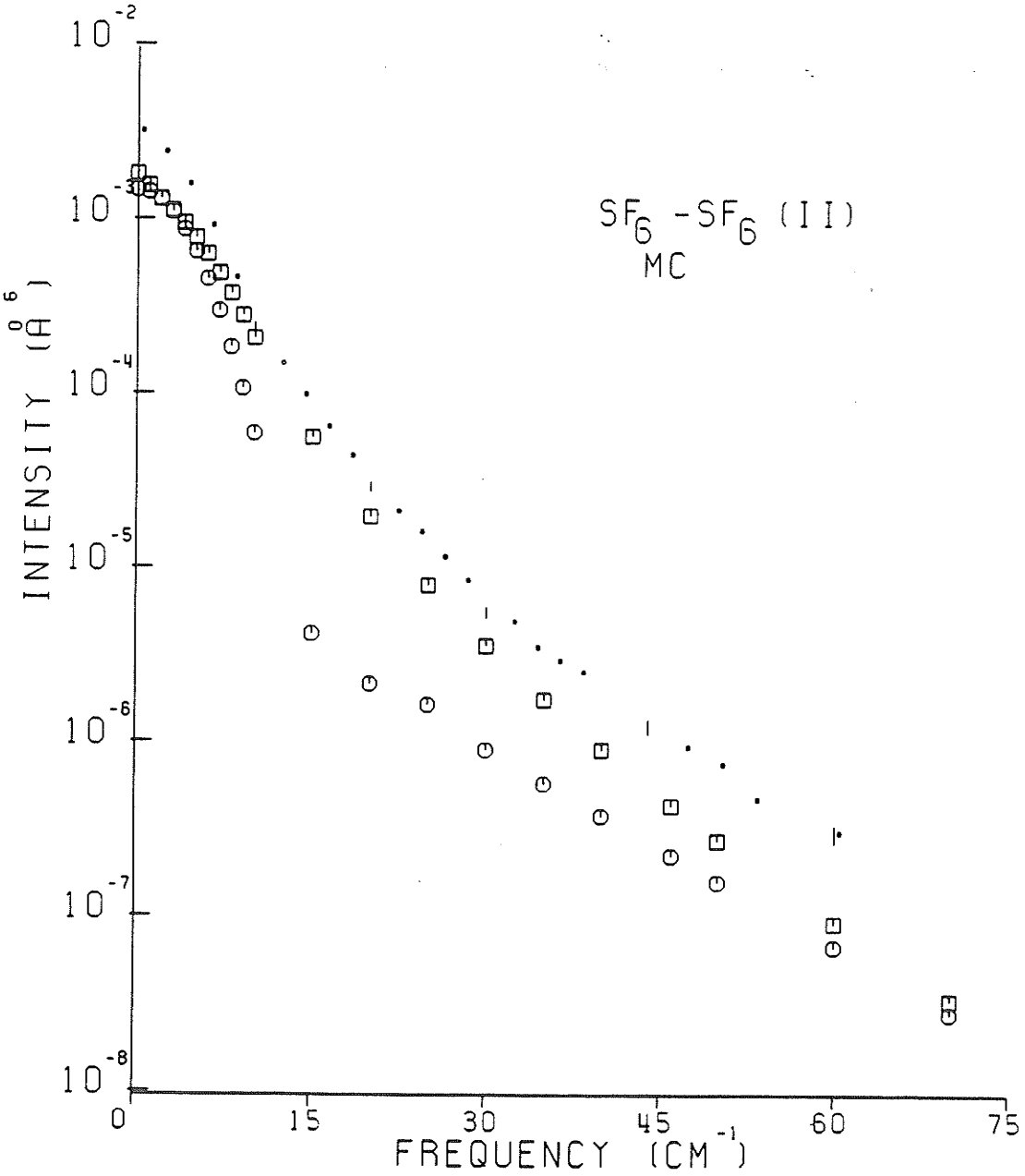
$SF_6 - SF_6$ (II)
MC
INTENSITY (A^6)
10^{-2}
10^{-3}
10^{-4}
10^{-5}
10^{-6}
10^{-7}
10^{-8}
0
15
30
45
60
75
FREQUENCY (CM^{-1})

FIGURE 4.3.a

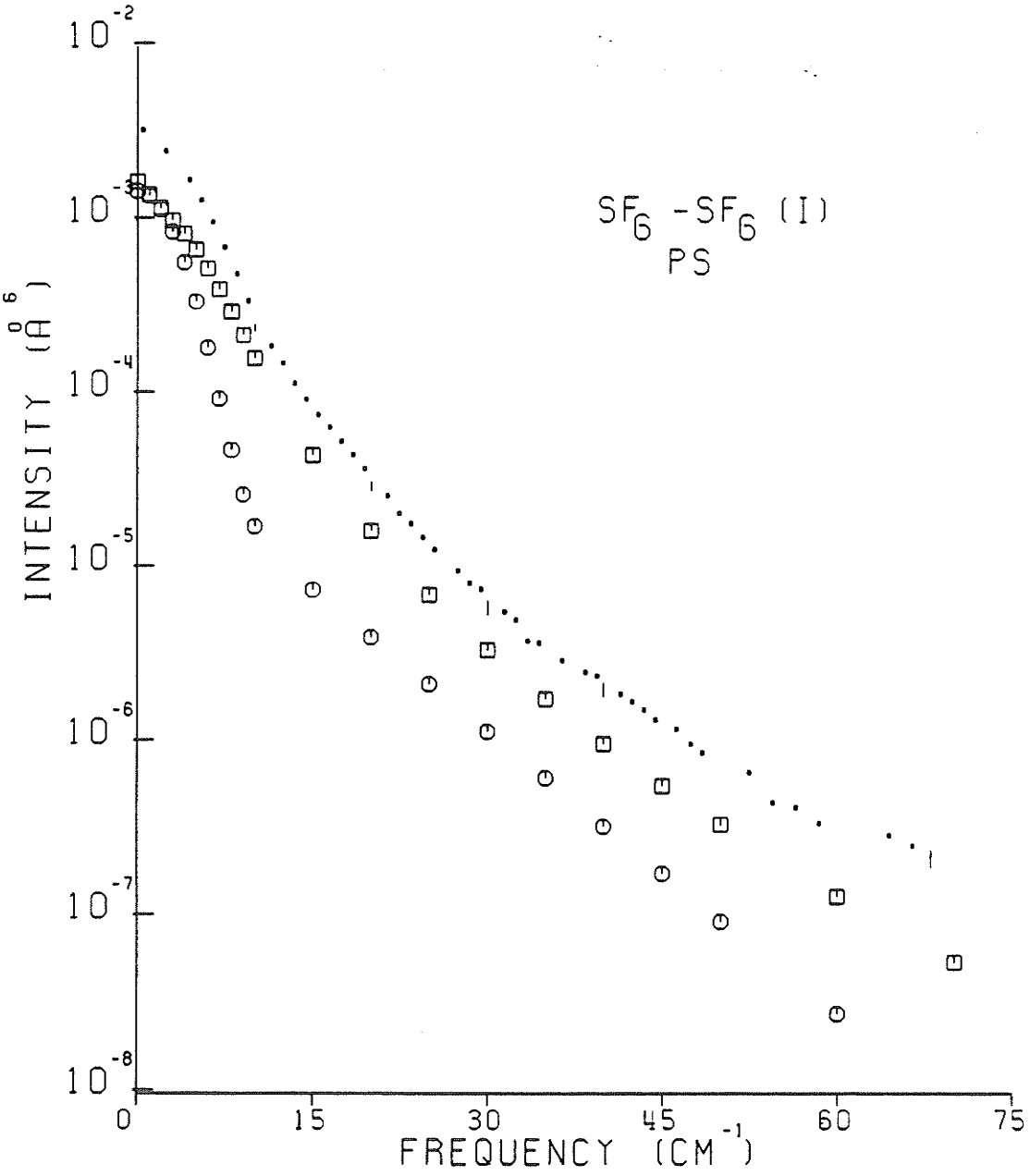
10^{-2}
10^{-3}
10^{-4}
10^{-5}
10^{-6}
10^{-7}
10^{-8}
INTENSITY ($A^{0\,6}$)
SF_6 - SF_6 (I)
PS
0
15
30
45
60
75
FREQUENCY (CM^{-1})

FIGURE 4.3.b

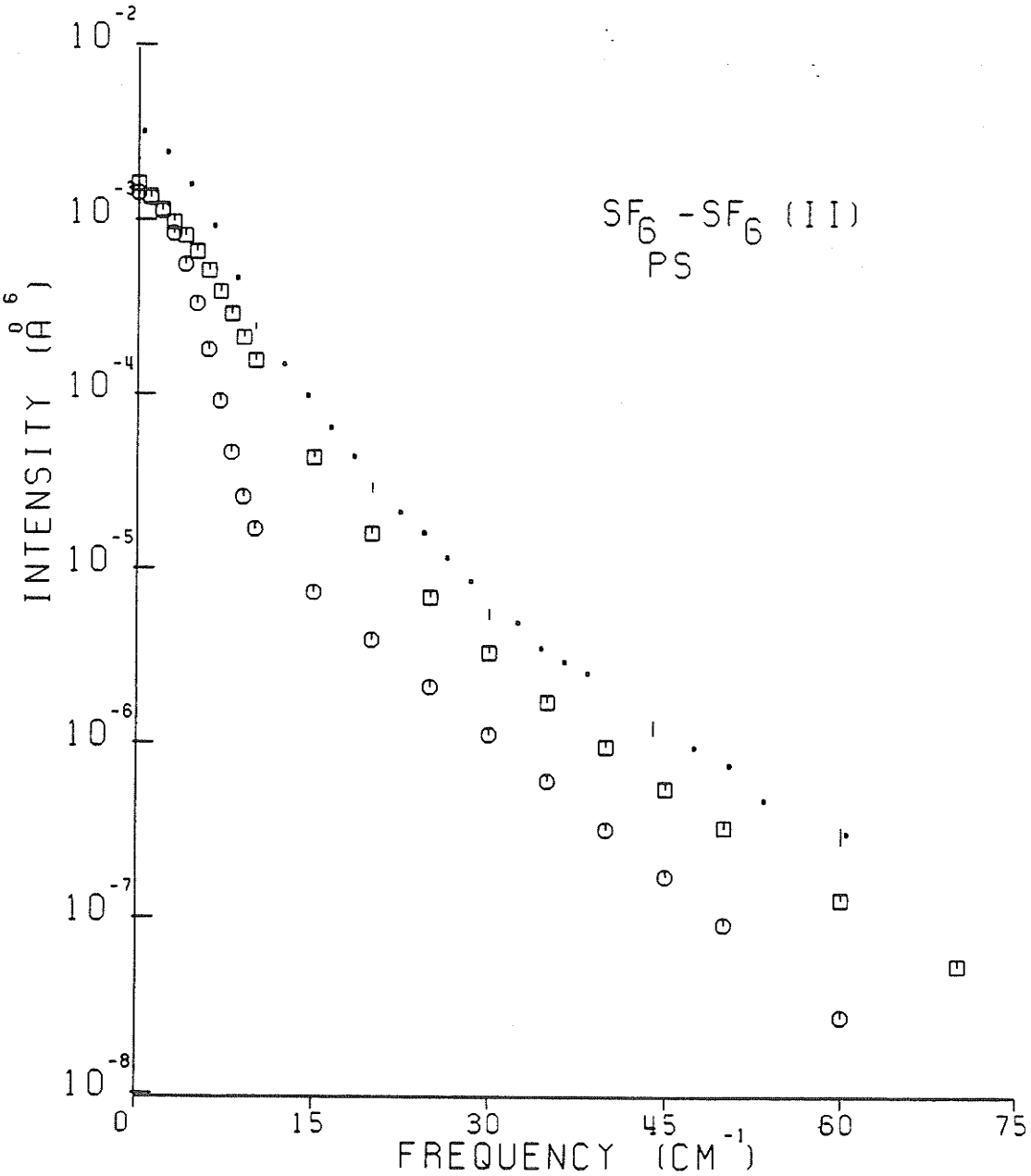
10^{-2}
10^{-3}
10^{-4}
10^{-5}
10^{-6}
10^{-7}
10^{-8}
INTENSITY ($\AA^6$)
$SF_6 - SF_6$ (II)
PS
0
15
30
45
60
75
FREQUENCY (CM^{-1})

Figures 4.4-4.7

Figures 4.4-4.7 show the experimental two-body, translational, and dimer spectra for SF_6-Kr (D,S), SF_6-Ar, and SF_6-Ne respectively.

. The experimental two-body spectrum.

◻ The theoretical translational spectrum.

◷ The theoretical dimer spectrum.

FIGURE 4.4

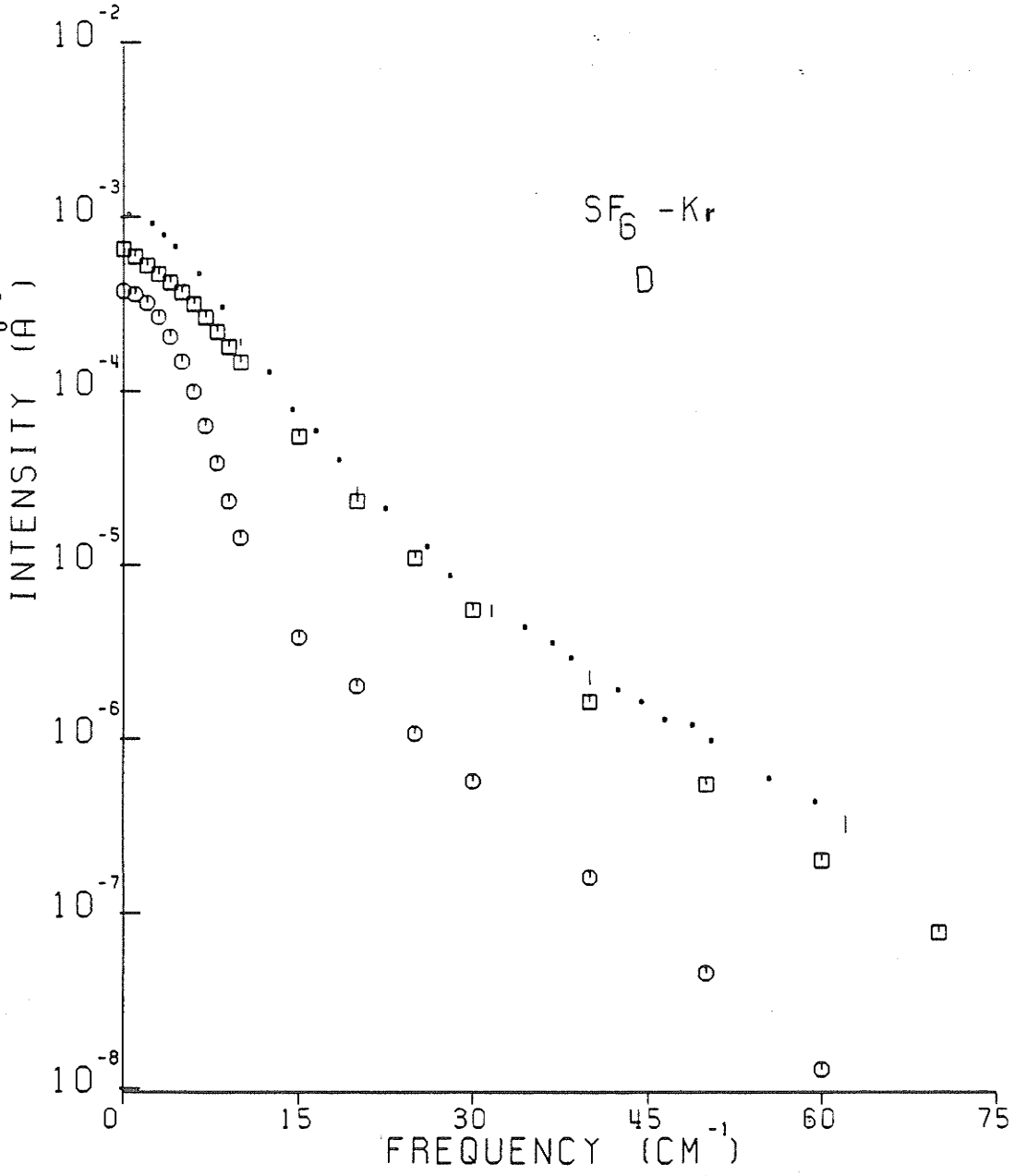
10^{-2}
10^{-3}
10^{-4}
10^{-5}
10^{-6}
10^{-7}
10^{-8}
INTENSITY (A^6)
SF_6 -Kr
D
0
15
30
45
60
75
FREQUENCY (CM^{-1})

FIGURE 4.5

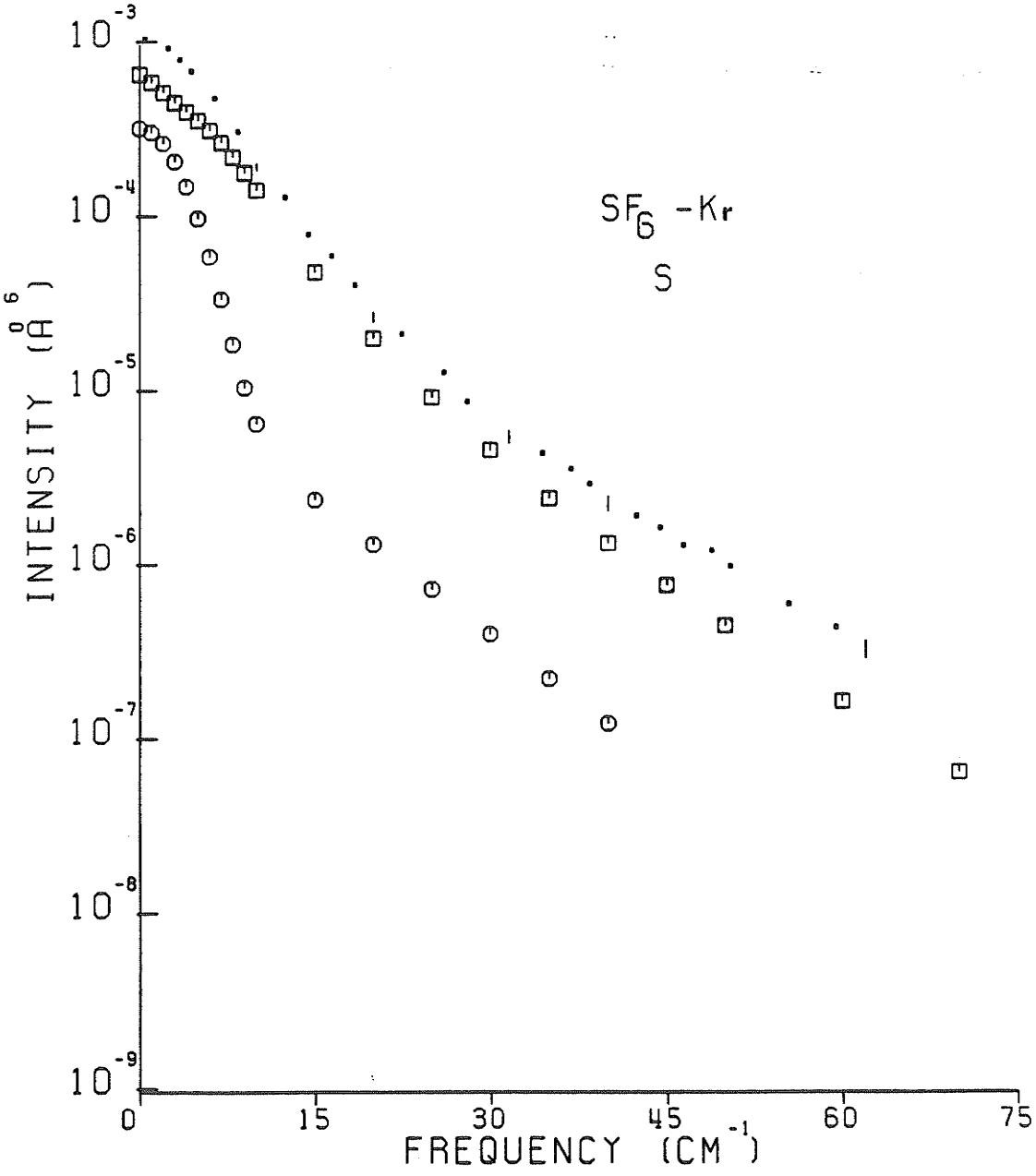
SF_6 -Kr
S
INTENSITY (A^6)
10^{-3}
10^{-4}
10^{-5}
10^{-6}
10^{-7}
10^{-8}
10^{-9}
0
15
30
45
60
75
FREQUENCY (CM^{-1})

FIGURE 4.6

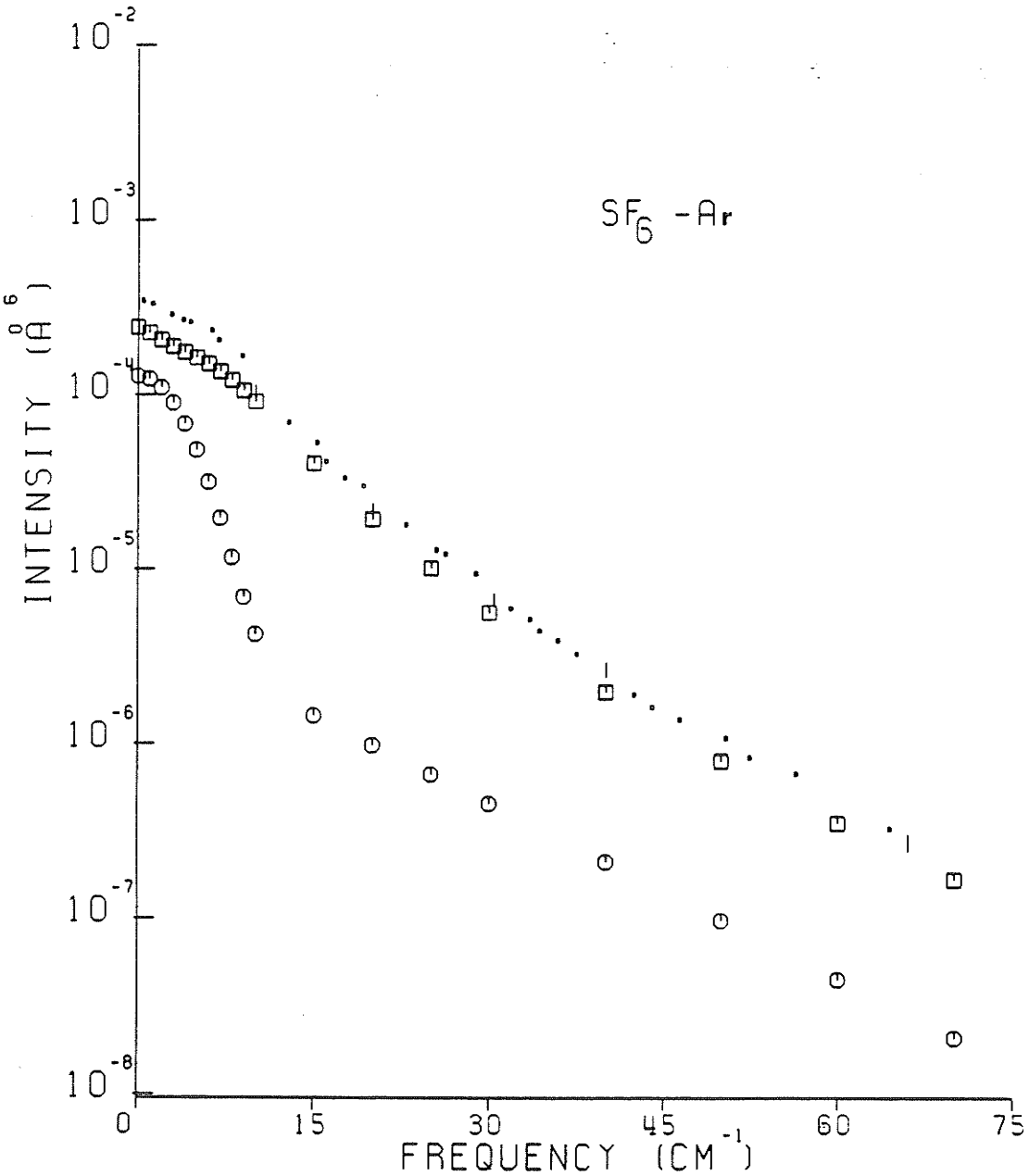
SF_6 -Ar
INTENSITY ($\AA^6$)
10^{-2}
10^{-3}
10^{-4}
10^{-5}
10^{-6}
10^{-7}
10^{-8}
0
15
30
45
60
75
FREQUENCY (CM^{-1})

FIGURE 4.7

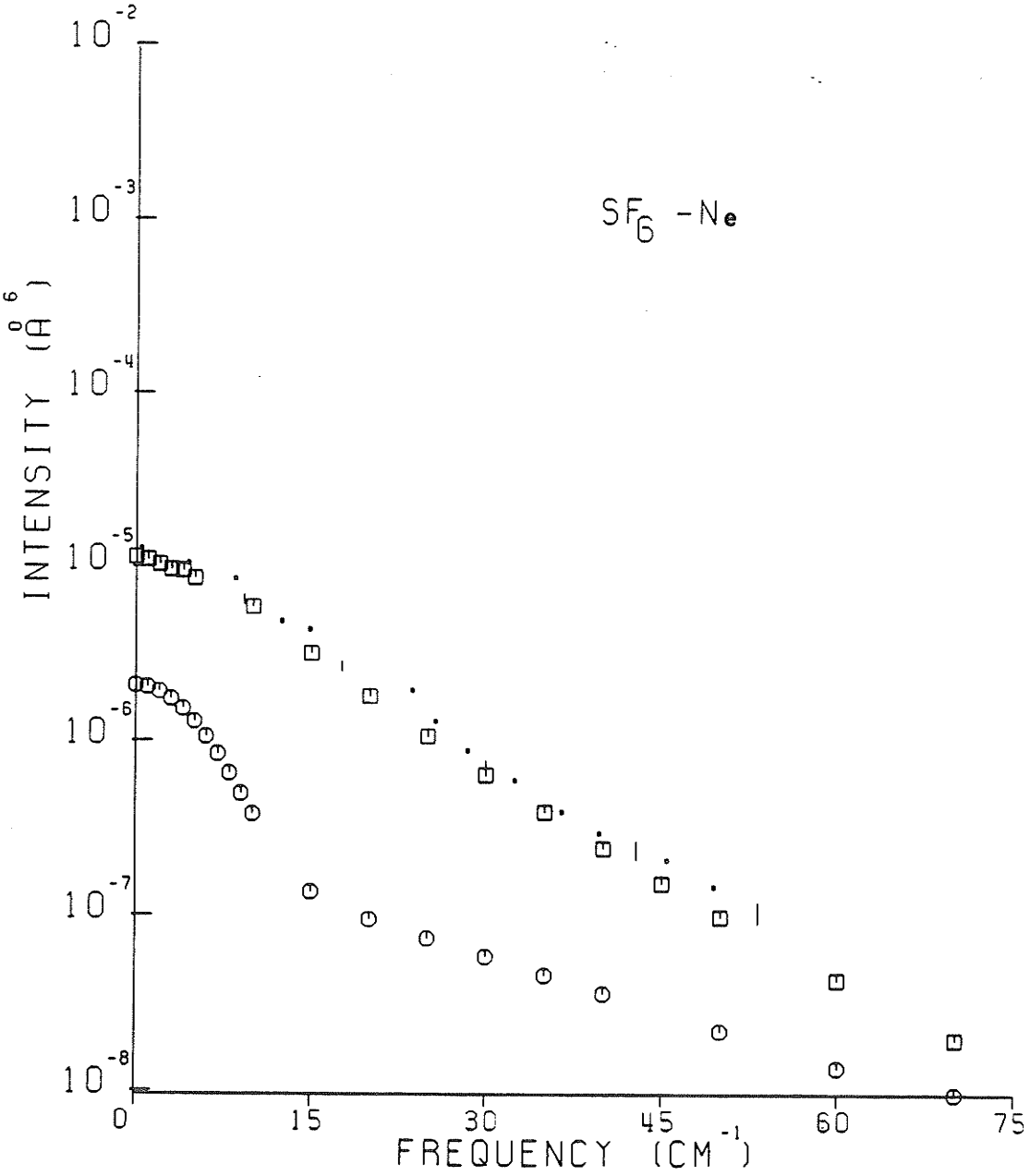
SF_6 -Ne
INTENSITY ($\AA^6$)
10^{-2}
10^{-3}
10^{-4}
10^{-5}
10^{-6}
10^{-7}
10^{-8}
0
15
30
45
60
75
FREQUENCY (CM^{-1})

Figures 4.8-4.16

Figures 4.8-4.16 show the experimental two-body, total theoretical, translational, and rotational spectra.

Figure 4.8	SF_6-SF_6 (I), using HFD potential.
Figure 4.9	SF_6-SF_6 (II), using HFD potential.
Figure 4.10	SF_6-SF_6 (I), using MC potential.
Figure 4.11	SF_6-SF_6 (II), using MC potential.
Figure 4.12	SF_6-SF_6 (I), using PS potential.
Figure 4.13	SF_6-SF_6 (II), using PS potential.
Figure 4.14	SF_6-Kr, using M3SV potential.
Figure 4.15	SF_6-Ar, using M3SV potential.
Figure 4.16	SF_6-Ne, using M3SV potential.
.	The experimental two-body spectrum.
-	The total theoretical spectrum.
□	The theoretical translational spectrum.
*	The theoretical rotational spectrum.

FIGURE 4.8

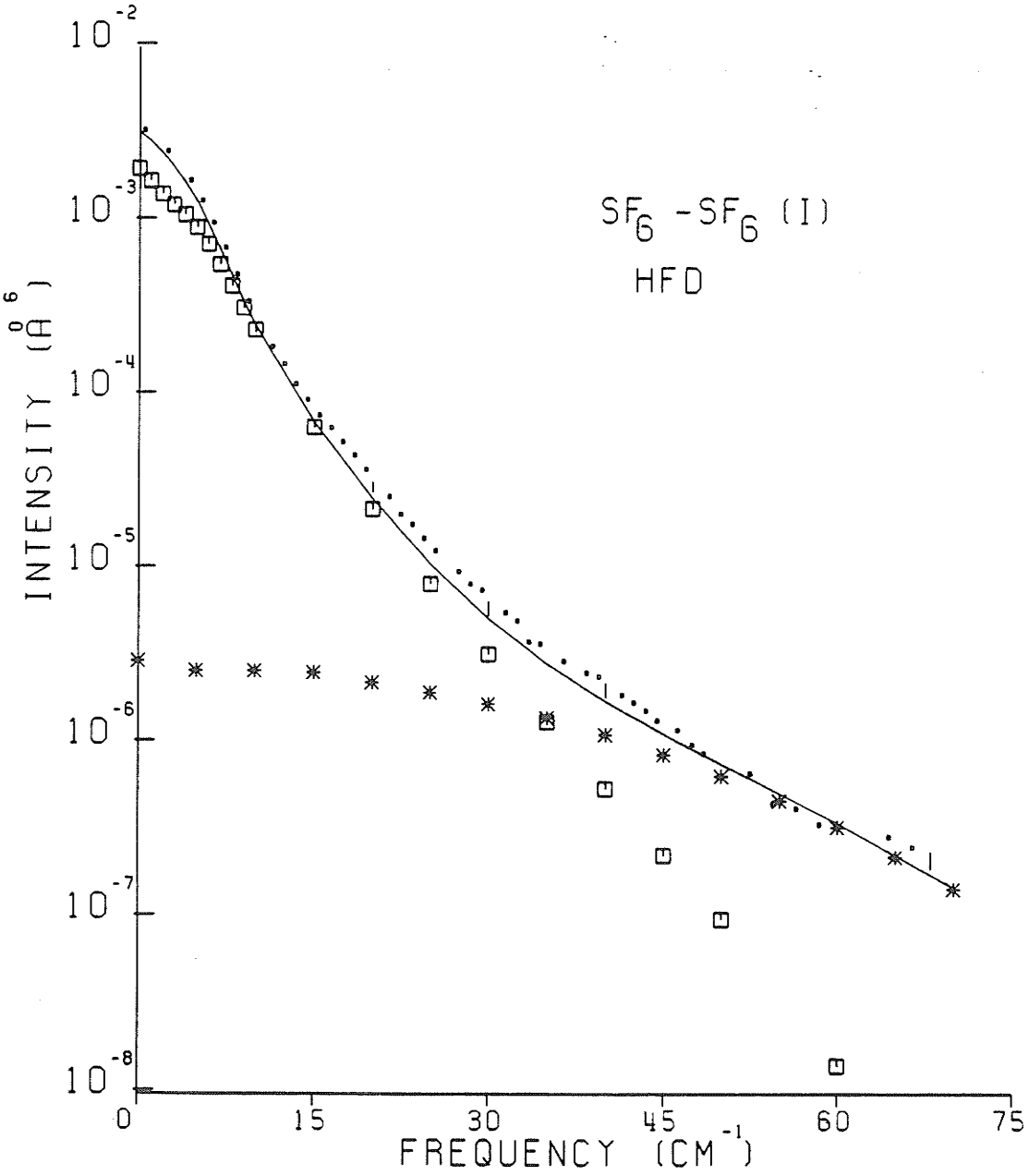
$SF_6 - SF_6$ (I)
HFD
INTENSITY (A^{06})
10^{-2}
10^{-3}
10^{-4}
10^{-5}
10^{-6}
10^{-7}
10^{-8}
0
15
30
45
60
75
FREQUENCY (CM^{-1})

FIGURE 4.9

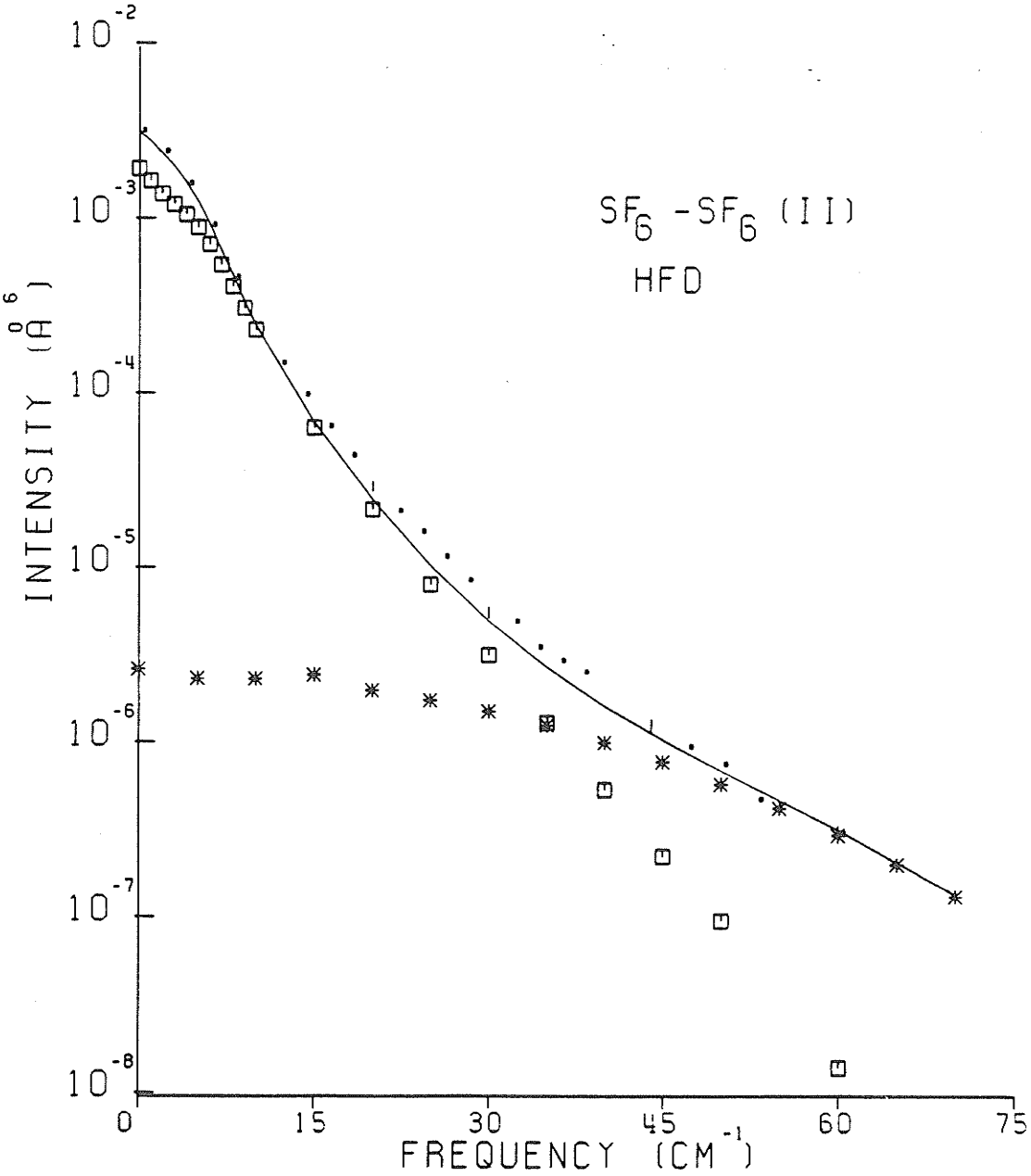
$SF_6 - SF_6$ (II)
HFD
INTENSITY (A^6)
10^{-2}
10^{-3}
10^{-4}
10^{-5}
10^{-6}
10^{-7}
10^{-8}
0
15
30
45
60
75
FREQUENCY (CM^{-1})

FIGURE 4.10

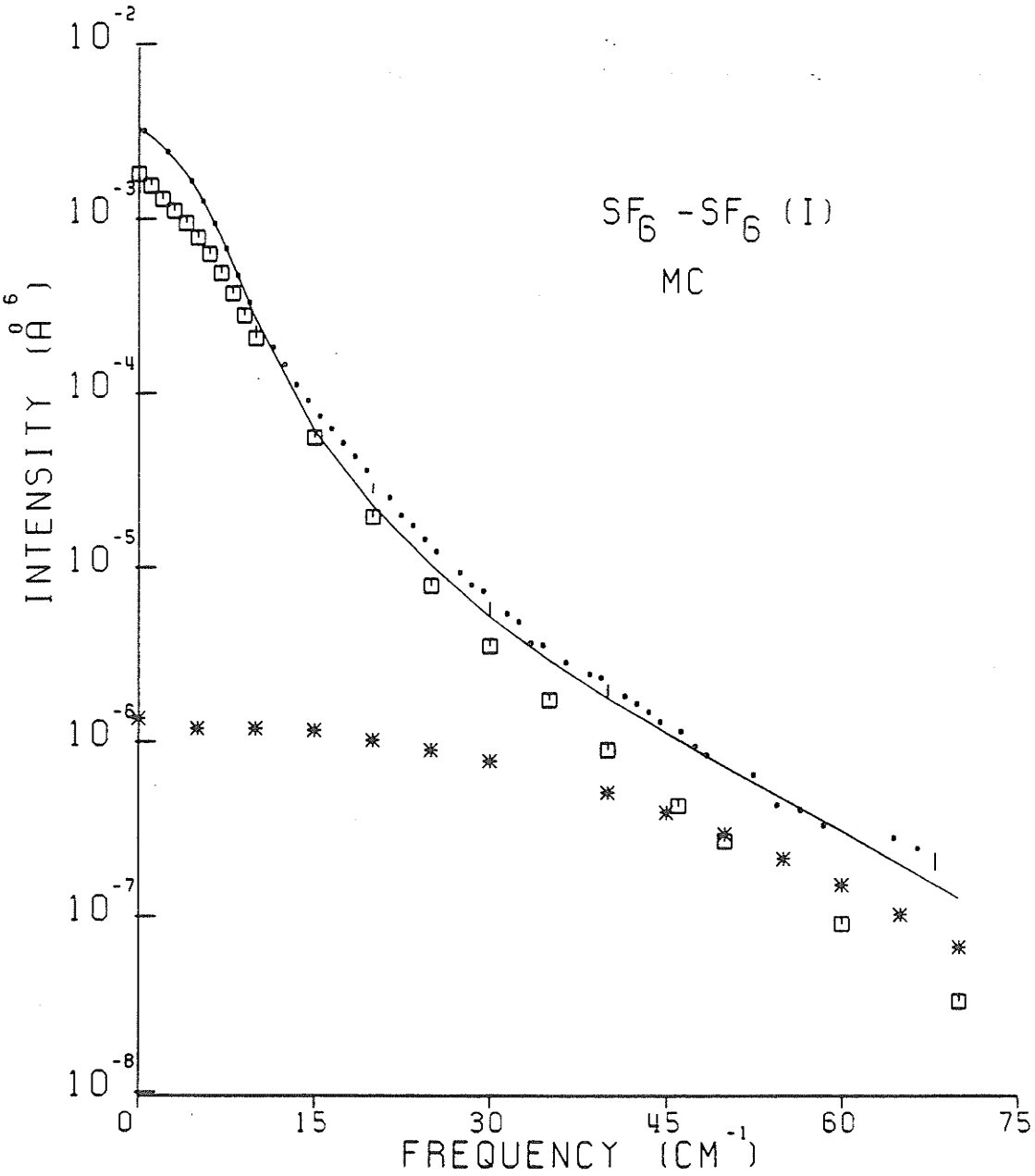
$SF_6 - SF_6$ (I)
MC
INTENSITY (A^6)
10^{-2}
10^{-3}
10^{-4}
10^{-5}
10^{-6}
10^{-7}
10^{-8}
0
15
30
45
60
75
FREQUENCY (CM^{-1})

FIGURE 4.11

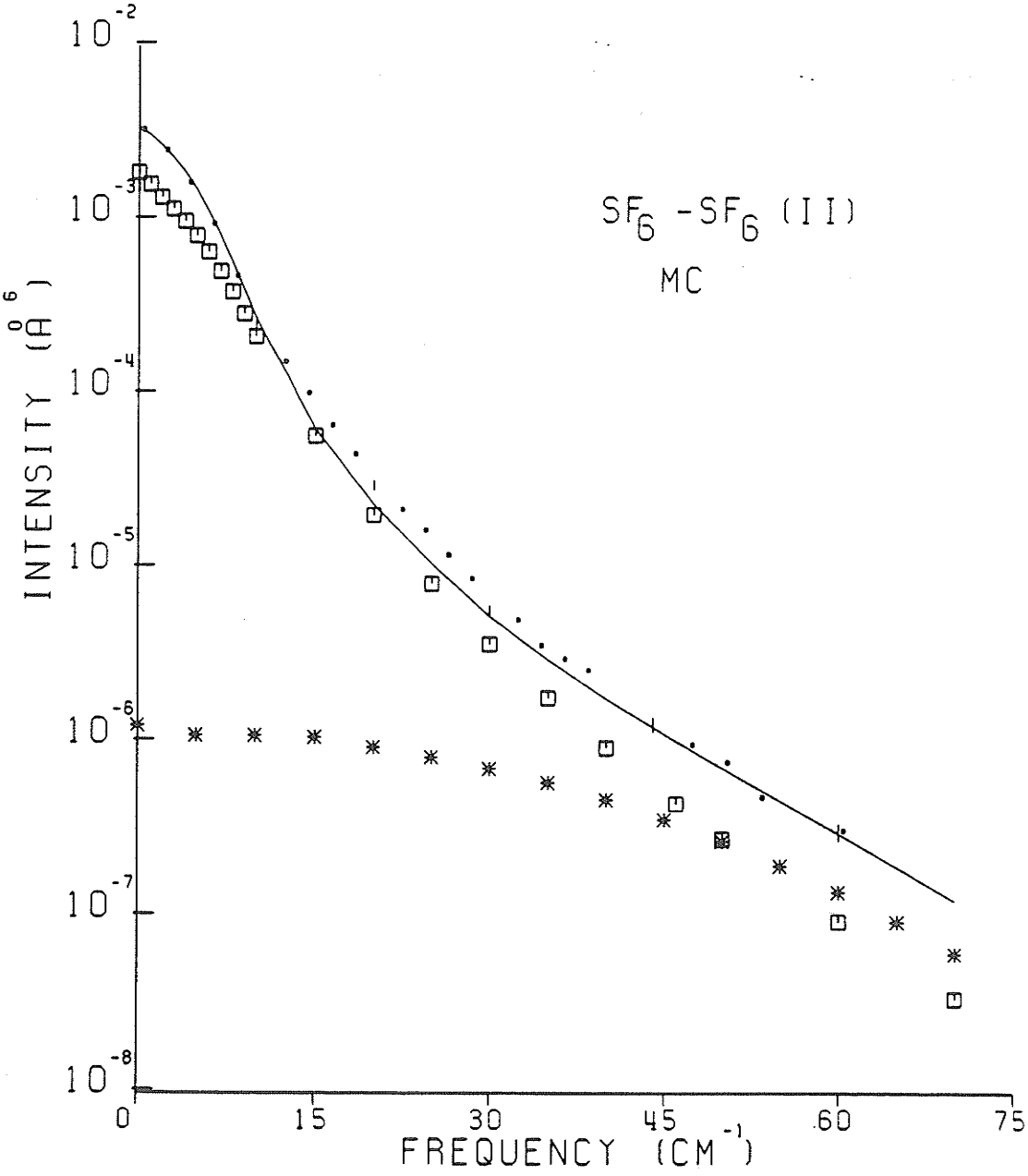
$SF_6 - SF_6$ (II)
MC
INTENSITY (A^6)
10^{-2}
10^{-3}
10^{-4}
10^{-5}
10^{-6}
10^{-7}
10^{-8}
0
15
30
45
60
75
FREQUENCY (CM^{-1})

FIGURE 4.12

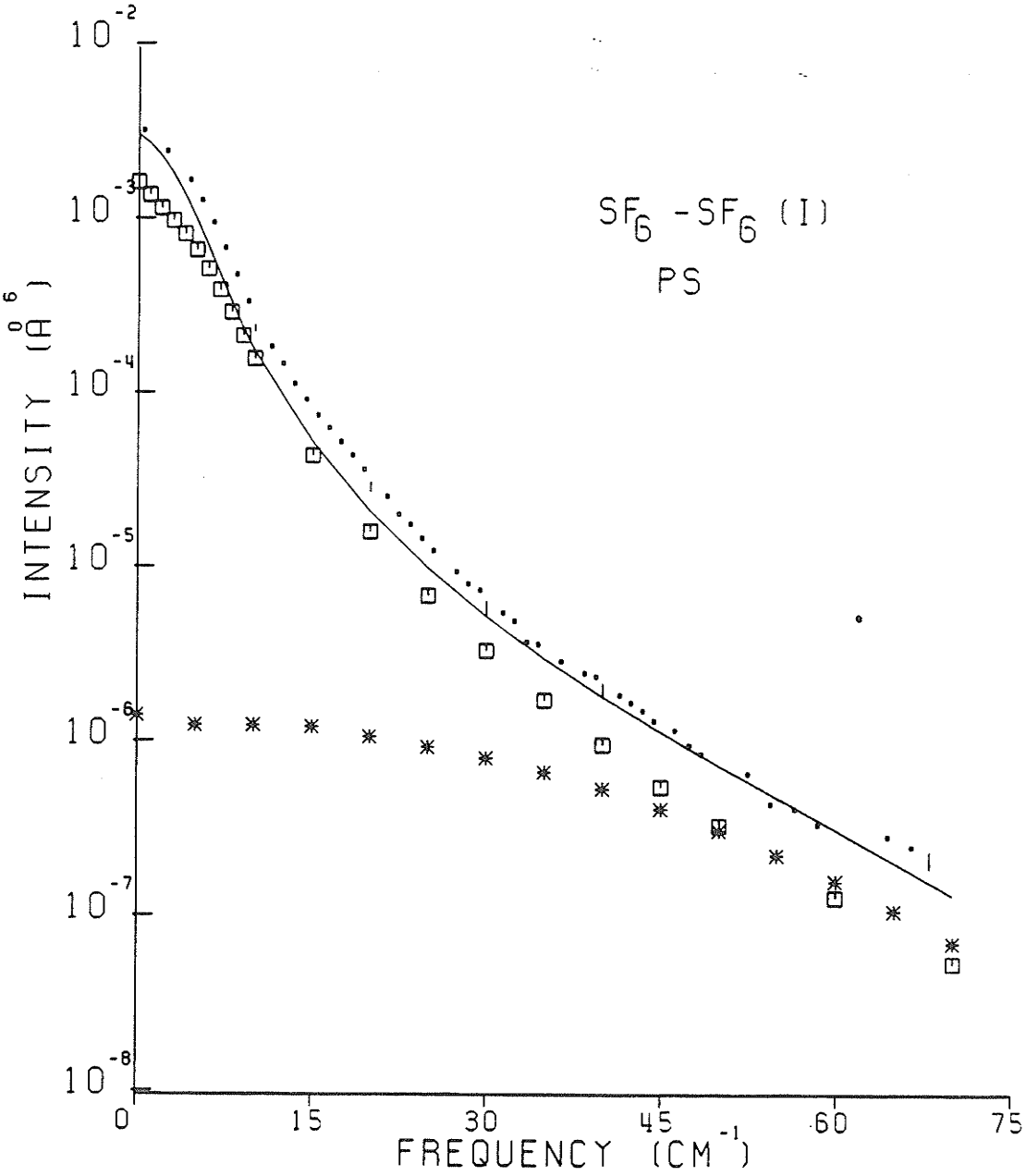
$SF_6 - SF_6$ (I)
PS
INTENSITY (A^6)
10^{-2}
10^{-3}
10^{-4}
10^{-5}
10^{-6}
10^{-7}
10^{-8}
0
15
30
45
60
75
FREQUENCY (CM^{-1})

FIGURE 4.13

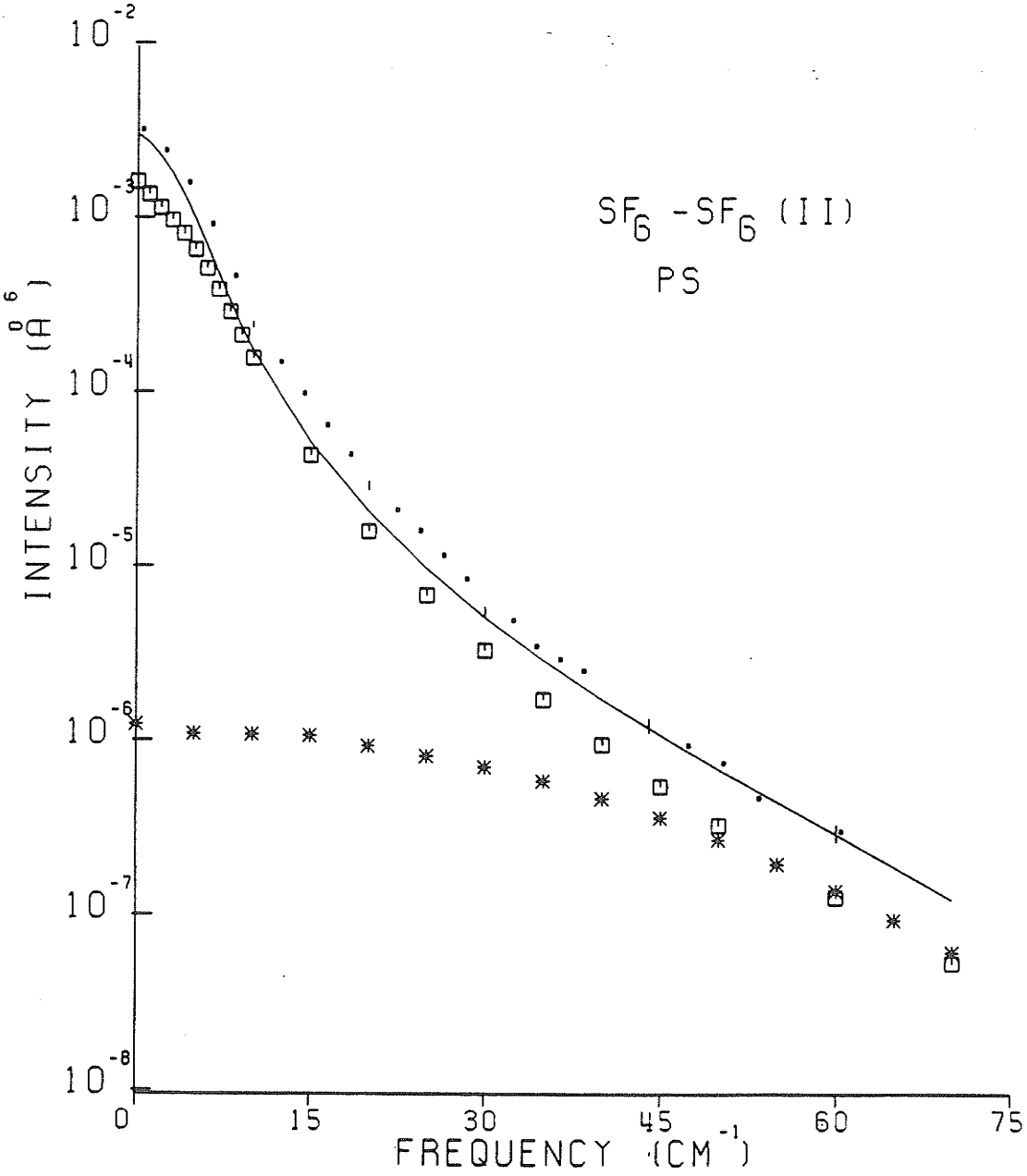
$SF_6 - SF_6$ (II)
PS
INTENSITY (A^6)
10^{-2}
10^{-3}
10^{-4}
10^{-5}
10^{-6}
10^{-7}
10^{-8}
0
15
30
45
60
75
FREQUENCY (CM^{-1})

FIGURE 4.14

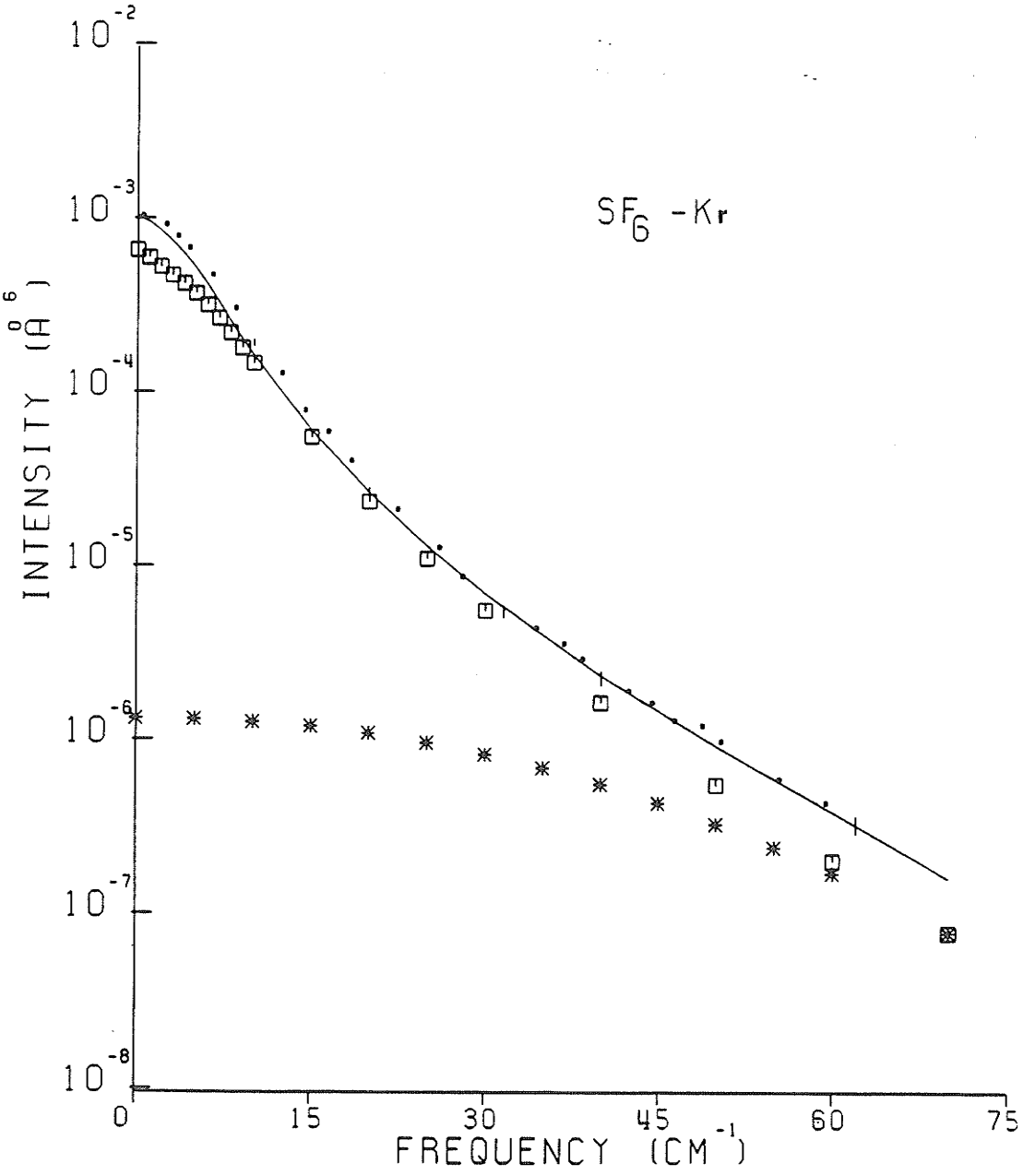
SF_6 -Kr
INTENSITY (A^6)
10^{-2}
10^{-3}
10^{-4}
10^{-5}
10^{-6}
10^{-7}
10^{-8}
0
15
30
45
60
75
FREQUENCY (CM^{-1})

FIGURE 4.15

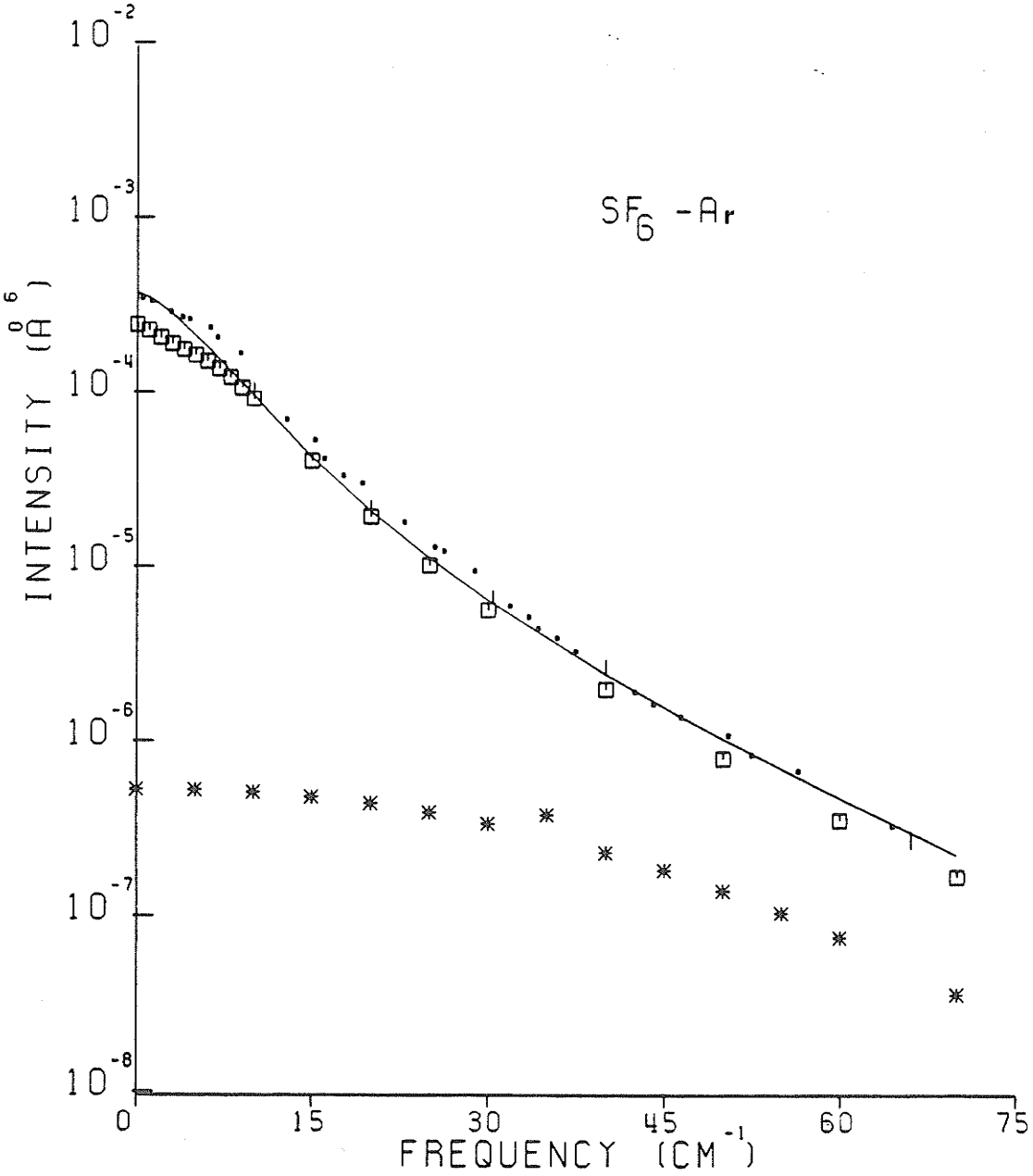
SF_6 -Ar
INTENSITY ($A^{\circ 6}$)
10^{-2}
10^{-3}
10^{-4}
10^{-5}
10^{-6}
10^{-7}
10^{-8}
0
15
30
45
60
75
FREQUENCY (CM^{-1})

FIGURE 4.16

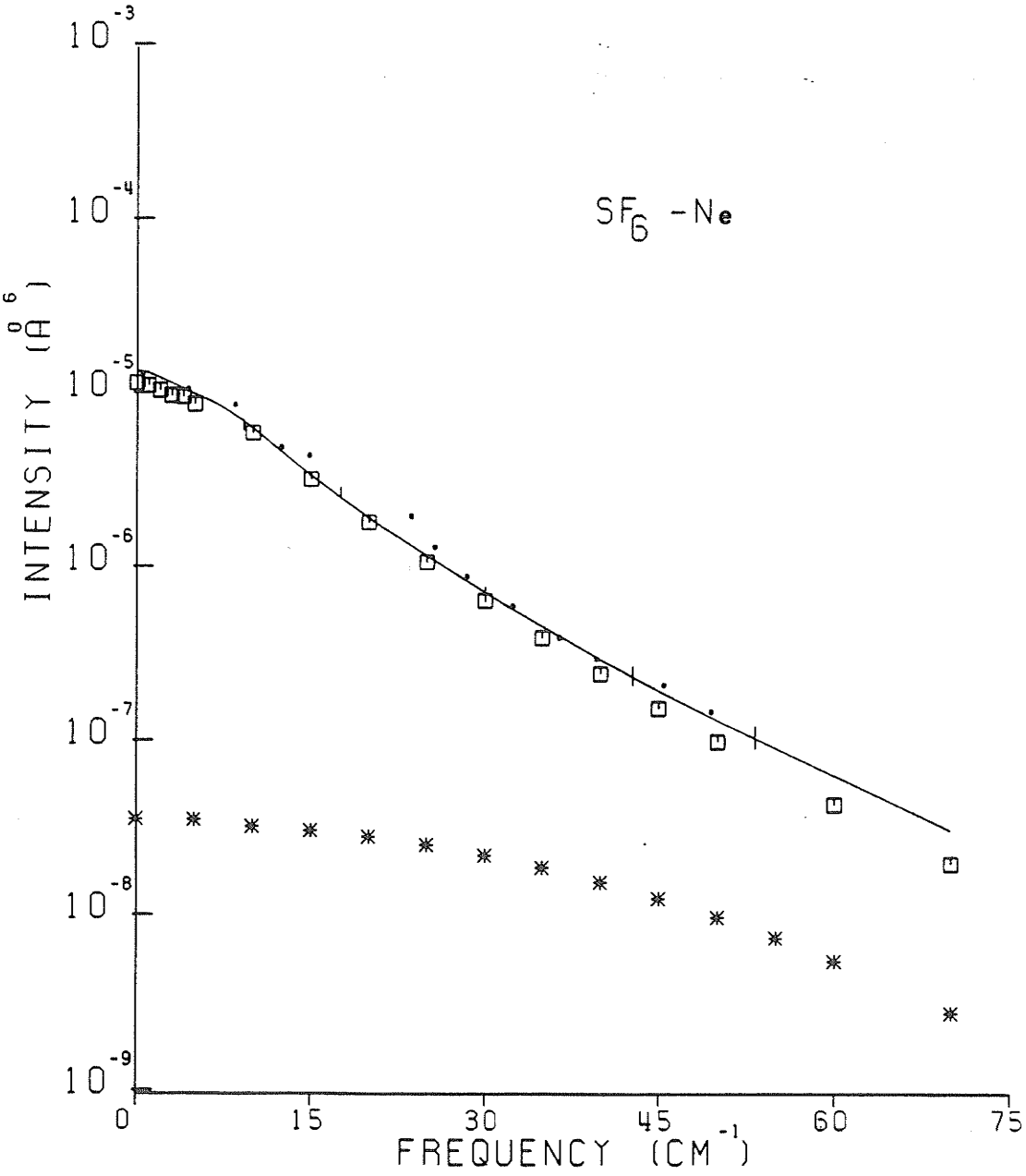
SF_6 -Ne
INTENSITY (A^6)
10^{-3}
10^{-4}
10^{-5}
10^{-6}
10^{-7}
10^{-8}
10^{-9}
0
15
30
45
60
75
FREQUENCY (CM^{-1})

CHAPTER 5

INTERMOLECULAR POTENTIAL FOR SF_6-Xe

The potential energy function $U(\underline{r})$ is a way to represent the force between two molecules (Maitland et al. 1981).

We will start with the simplest possible situation in which two atoms, a and b, each composed of a positively charged nucleus surrounded by a negatively charged, spherically symmetric electron cloud, interact. When the two atoms are infinitely separated, they do not interact at all and the total energy of the two-atom systems, E_{tot}, is just the sum of the energies of the individual atoms.

$$E_{tot}\ (\infty) = E_a + E_b \tag{5.1}$$

If the atoms are separated by a finite distance r, the interaction between them provides an extra contribution to the total energy of the system.

$$E_{tot}\ (r) = E_a + E_b + U(r) \tag{5.2}$$

From Eqns. (5.1) and (5.2) one can get:

$$U(r) = E_{tot}\ (r) - E_{tot}\ (\infty) \tag{5.3}$$

The intermolecular pair potential thus describes the departure of the total energy of the two atom system from its value when the two atoms are infinitely separated. This energy difference is numerically equal to the work done in bringing the two atoms from infinite separation to the separation r and is given by

$$U(r) = \int_{r}^{\infty} F(r)\, dr \qquad (5.4)$$

where $F(r)$ is the force acting between the two atoms at the separation r.

Fig. 5.1 shows the general form of the intermolecular potential energy function for atoms.

There is a strong repulsive force at short range and an attractive force at long range. In terms of the potential energy $U(r)$ this behaviour corresponds to large, positive energies at small separations and negative energies at long range, the two extreme regions being joined by a function with a single negative minimum. The separation at which the potential energy is zero is σ; the separation at which the energy attains its minimum value is r_{min}, and the minimum energy itself is $-\varepsilon$; ε is called the well depth.

In the more general problem of the interaction of two molecules which lack spherical symmetry, the intermolecular energy depends not only upon the intermolecular separation, but also upon the relative orientation. Usually the procedure to generate an intermolecular potential for a certain interaction is to assume a suitable form for the potential for this interaction, with primary values for the parameters of the potential, and try to calculate a property that is known experimentally, fitting the parameters to this property. Accordingly the parameters depend on the type of experiment used, and if one tries to calculate another property dependent upon the same interaction, sometimes one will find a discrepancy between the calculation and the measurement.

It seems that certain regions of the potential are more sensitive to certain properties than other regions. Fitting all

known properties simultaneously will generate a potential that can calculate accurately another unknown property of the interaction.

5.1 SOURCES OF INFORMATION ABOUT INTERMOLECULAR POTENTIALS

Crossed molecular beam measurements of differential cross sections (DCS), viscosity, pressure virial coefficients (Pack et al., 1982) and diffusion coefficients (Pack et al., 1984) have been used by Pack to determine intermolecular potentials for SF_6 mixtures.

There was no available intermolecular potential for SF_6-Xe, but the ones developed by Pack for other mixtures were very reliable. We therefore contacted Dr. R.T. Pack at the Los Alamos National Laboratory, Division of Theoretical Chemistry and together decided to collaborate to develop a new potential for SF_6-Xe. The only available data for this mixture were the virial coefficient (Martin et al., 1982) and the diffusion coefficient (private communication by Pack). Our CILS SF_6-Xe data was used as a third property to refine the potential.

Subroutines to calculate the interaction virial coefficient and the diffusion coefficient through collision integrals for octahedral-atom interactions were generously offered by Pack and sent via BITNET network. These also calculated the value of δ for each property and the total value of δ. Together with our program for the classical line shape calculations, we were able to fit the three properties simultaneously to obtain the potential parameters which minimized the value of δ.

5.2 CALCULATIONS

The form of the spherical limit potential used is the same as in Eqn. (2.40). The anisotropic potential is different in that ε and r_{min} are angle dependent. Their angular dependence is described by the following equations:

$$\varepsilon = \bar{\varepsilon} \left[1 + a_4 T_4 + a_6 T_6 + \ldots\right] \tag{5.5}$$

$$r_m = \bar{r}_m \left[1 + b_4 T_4 + a_6 T_6 + \ldots\right] \tag{5.6}$$

where T_n are the spherical tensors that transform as A_{1g} (the completely symmetric irreducable representation of the group O_h).

Thus a_4, a_6, b_4, and b_6 are parameters to be determined.

The number of parameters to be fitted is twelve [$\bar{\varepsilon}$, $\bar{r}_m$, α_I, α_{II}, α_{III}, C_6, C_8, C_{10}, a_4, a_6, b_4, and b_6]. The first five usually are adjusted to obtain a reasonably good fit with the anisotropic parameters zero. This was done to keep the anisotropy parameters from serving merely to make up deficiencies in the spherical limit of the potential. Final adjustment of all parameters were made using the anisotropic potential form. The properties calculated were as detailed in the following paragraphs.

5.2.1 Interaction Second Virial Coefficient

The virial coefficients of gas mixtures are related to the gas composition and to the intermolecular potential energy function which characterize the different type of interactions which can occur. For a binary mixture the second virial coefficient is given by:

$$\beta_m = x_1^2 \beta_{11} + 2x_1 x_2 \beta_{12} + x_2^2 \beta_{22} \qquad (5.7)$$

where β_m is the virial coefficient of a mixture containing mole fractions x_i of component i. β_{11} and β_{22} are the second virial coefficients of the pure components, and β_{12}, the interaction second virial coefficient, is related to the pair potential $U_{12}(r)$ by:

$$\beta_{12}(T) = \frac{1}{2} \int dr \, [1 - \exp[-U_{12}(r) / k_B T]] \qquad (5.8)$$

The interaction second virial coefficient β_{12} is sensitive to the size r_m and to the volume of the attractive well of the potential (Pack et al., 1982).

5.2.2 Diffusion Coefficient

The binary diffusion coefficient D_{12} is an important transport property for the investigation of intermolecular forces, and is defined by Fick's law

$$J_1 = -D_{12} \frac{\partial n_1}{\partial \underline{r}} \qquad (5.9)$$

where J_1 is the number flux of species 1 in an isothermal binary mixture subject to a gradient of the number density, n_1, of species 1. It can be shown that the diffusion coefficient is given in a first order by the expression (Parker and Pack, 1978).

$$D_{A,BC} = [3k_B T / 16 n\mu \, \Omega^{(1,1)}_{A,BC}] \qquad (5.10)$$

Here μ is the reduced mass of the two species, and the collision integral $\Omega^{(1,1)}_{A,BC}$ is given by (Monchick et al., 1963, Monchick and Green, 1975 and Hirschfolder et al., 1954)

$$\Omega^{n,s}_{A,BC} = \frac{1}{2}\left(\frac{k_B T}{2\mu\pi}\right)^{\frac{1}{2}} \frac{1}{(k_B T)^{s+2}} \int_0^{\alpha} d\varepsilon\, \varepsilon^{S+1} e^{-\varepsilon/k_B T} Q^n(\varepsilon) \tag{5.11}$$

where ε is the incident kinetic energy $= \frac{h^2 K^2}{2\mu}$. $Q^n(\varepsilon)$ is given by:

$$Q^n(\varepsilon) = \frac{1}{2} \int_{-1}^{1} Q^n(\varepsilon; \gamma)\, d\,\mathrm{Cos}\,\gamma \tag{5.12}$$

where

$$Q^n(\varepsilon; \gamma) = \frac{4\pi}{K_\varepsilon^2} \sum_{\ell} (\ell+1) \sin^2[\eta_{\ell+1}(\gamma) - \eta_\ell(\gamma)] \tag{5.13}$$

The diffusion coefficient is most sensitive to the well of the potential from r_m to the point when the potential is repulsive.

5.2.3 CILS Spectrum

The translational and the dimer spectra were calculated for SF_6-Xe as for the other mixtures for SF_6 (see Chapter 4).

The CILS data are most sensitive to the region near $r = \sigma$ (Birnbaum and Cohen, 1975).

5.2.4 Data

(a) Interaction Second Virial Coefficient

The experimental data used were (Martin et al., 1982):

T(K)	β_{12} (cm^3/mole)
290.0	-171.0
300.0	-157.6
320.0	-133.0

(b) Diffusion Coefficient

The experimental data used were (private communication by Pack)

T(K)	D (cm^2/sec)
278.18	0.403
288.28	0.428
300.0	0.460
311.18	0.4895
323.18	0.5287

(c) CILS Data

The absolute intensity of the spectrum as a function of frequency is shown in Fig. 3.8. The frequency range 10-25 cm^{-1} was used for comparison with the calculated spectrum. Here the intermolecular potential and the form of $\beta(r)$ are the main factors affecting the spectrum as explained in Section 4.1.

5.3 PROCEDURE AND RESULTS

There were too many parameters to try to vary them all simultaneously ($\bar{\varepsilon}$, $\bar{r}_m$, α_I, α_{II}, α_{III}, C_6, C_8, C_{10}, a_4, a_6, b_4 and b_6). We started first by setting all the anisotropic parameters

equal to zero ($a_4 = a_6 = b_4 = b_6 = 0$), and

$$\alpha = \alpha_I = \alpha_{II} = \alpha_{III} \qquad \text{(MSV potential)}$$

and also by keeping C_6, C_8, and C_{10} constants, the values of which were suggested by Pack.

With assumed values for $\bar{\varepsilon}$, $\bar{r}_m$, and α, the three properties were calculated at the experimental points. Then, the dimensionless mean square deviation δ^2, from the j^{th} experiment, was calculated from Eqn. (4.1). Then an overall dimensionless root mean square deviation was obtained from

$$\delta = \left[\frac{1}{3} \sum_{j=1}^{3} \delta_j^2\right]^{\frac{1}{2}} \tag{5.14}$$

and the calculations were iterated to minimize this overall δ. Thus $\bar{r}_m$, $\bar{\varepsilon}$, and α were changed cyclically until a minimum was reached. Then the anisotropic parameters a_4, a_6, b_4 and b_6 were permitted to play a role. Starting with assumed values we changed their values until a minimum for δ was recorded. Then we returned to change $\bar{r}_m$, $\bar{\varepsilon}$, and α and so on, until we determined that the δ obtained was the true minimum. Finally we changed the parameter scheme to $\alpha_I = \alpha_{II} \neq \alpha_{III}$ and repeated the procedure until we got a minimum value for δ.

To prevent improper weighting of one experiment relative to the others, it is important that the uncertainties Δ_{ji} on the experimental data be as realistic as possible and contain an estimate of the maximum systematic error limit as well as statistical errors. The uncertainties used were, for the virial coefficient, $\pm$ 2 cm^3/mole,

for the diffusion coefficient 0.4%, and for the CILS spectrum, a variable in the range of 5-10%, depending on the frequency shift.

The parameters obtained for the potentials are listed in Table 5.1.

The dimensions of the first seven parameters are in Hartree a.u., and the last six are dimensionless.

Table 5.2 shows the values of δ as defined in Eqn. (4.1) for the diffusion coefficient, virial coefficient, and for the CILS experiment and an overall δ as defined in Eqn. (5.14).

Another approach was taken, keeping $\alpha_I = \alpha_{II} = \alpha_{III}$ as a constant and changing $\bar{r}_m$, and $\bar{\varepsilon}$ only, at first with $a_4 = a_6 = b_4 = b_6 = 0$. Then changing the anisotropic parameters a_4, a_b, b_4, and b_6 following the same procedure mentioned before, one gets the following parameters listed in Table 5.3.

The dimension of the first seven parameters are in Hartree a.u., and the last six are dimensionless. These parameters give the values for δ as shown in Table 5.4.

In the calculation of the value of δ(CILS), the statistical error was not included. So the value of δ(CILS) can be taken as an upper limit, and so also the value of δ(total).

Comparing Tables 5.2 and 5.4, one can see that the M2SV spherical limit potential is better than the MSV spherical limit one, but the MSV anisotropic potential is better than the M2SV anisotropic potential. But from a careful look we see that changing $\bar{\varepsilon}$ and $\bar{r}_m$ only means that we did not get the absolute minimum and

TABLE 5.1

The Parameters for the M2SV Potential for SF_6-Xe
(see Eqn. 2.40)

$\bar{\varepsilon}$	0.00101
$\bar{r}_m$	8.983
$\alpha_I = \alpha_{II}$	0.787
α_{III}	0.808
C_6	396.8
C_8	10600
C_{10}	320000
X_1	inflection pt.
X_2	1.45
a_4	-0.33
a_6	0.38
b_4	0.087
b_6	-0.011

Note: The dimension of the first seven parameters are in Hartree a.u., and the last six are dimensionless

TABLE 5.2

The Values of δ for the M2SV Potential

	Spherical Limit	Anisotropic
δ(diffusion coefficient)	1.4512	1.4285
δ(virial coefficient)	0.6848	0.62226
δ(CILS)	0.945	0.945
δ(total)	1.07516	1.05211

TABLE 5.3

The Parameters for an MSV Potential for SF_6-Xe
(see Eqn. 2.40)

$\bar{\varepsilon}$	0.00101
$\bar{r}_m$	8.98
$\alpha_I = \alpha_{II} = \alpha_{III}$	0.8
C_6	396.8
C_8	10600
C_{10}	320000
X_1	inflection pt.
X_2	1.45
a_4	-0.47
a_6	0.37
b_4	0.088
b_6	0.02

TABLE 5.4

The Values of δ for the MSV Potential

	Spherical Limit	Anisotropic
δ(diffusion coefficient)	1.6025	1.347
δ(virial coefficient)	0.6209	0.6038
δ(CILS)	0.857	0.857
δ(total)	1.108	0.9856

the anisotropic parameters were serving to fill the inadequacy of the spherical limit potential. So, we think the M2SV potential is the one to use.

The measurement of the total differential cross section would lead certainly to a still improved potential, especially at small separation.

Figs. 5.2-5.4 show the experimental and the theoretical values for the diffusion coefficient, virial coefficient, and for the CILS spectrum for the M2SV potential.

Figure 5.1

The intermolecular potential energy function for atoms.

FIGURE 5.1

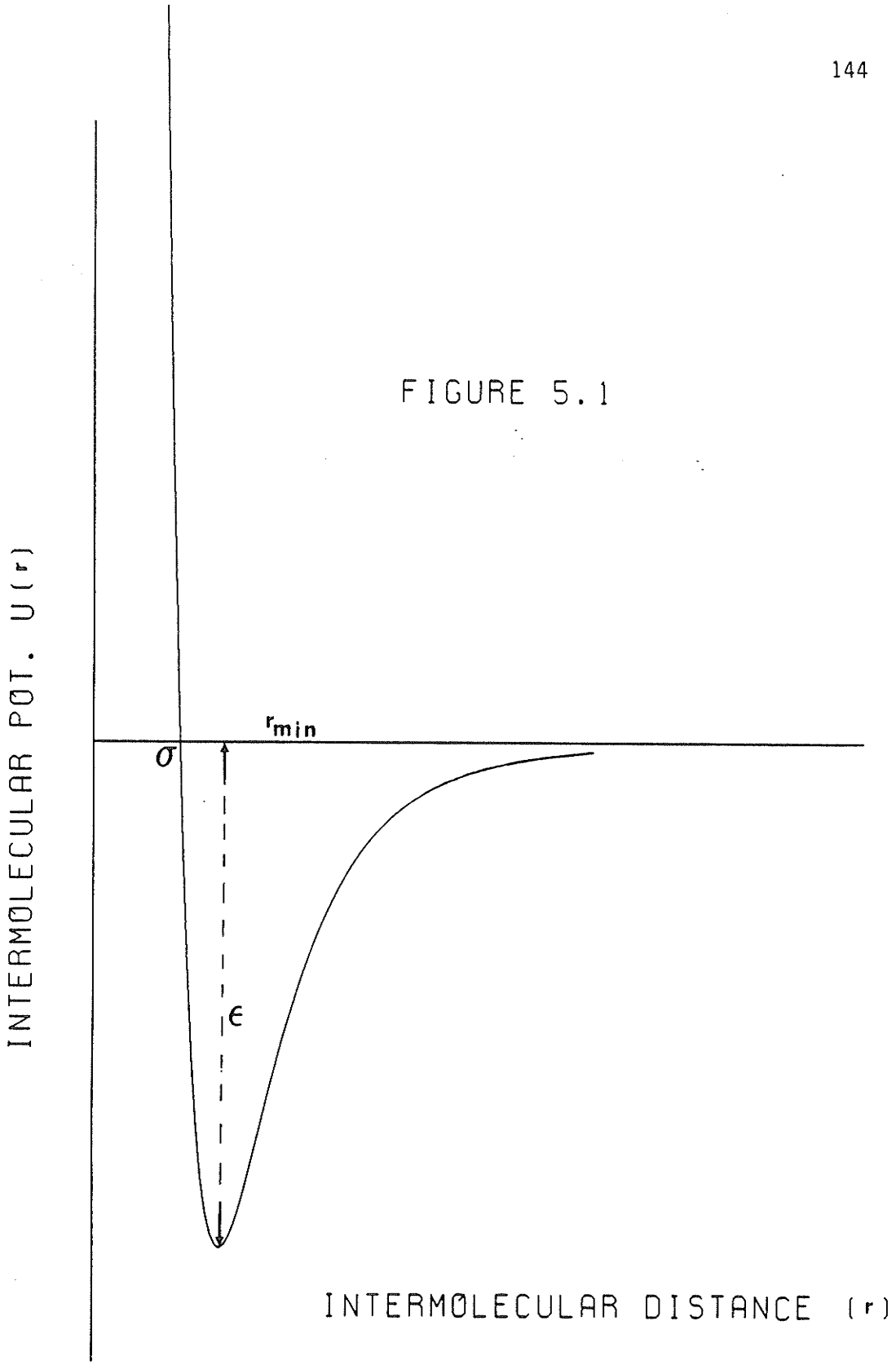
INTERMOLECULAR POT. U(r)
r_{min}
σ
ϵ
INTERMOLECULAR DISTANCE (r)

Figure 5.2

Figure 5.2 A comparison between the experimental and theoretical diffusion coefficient at different temperatures for SF_6-Xe.

. The experimental measurement

* The theoretical calculation.

FIGURE 5.2

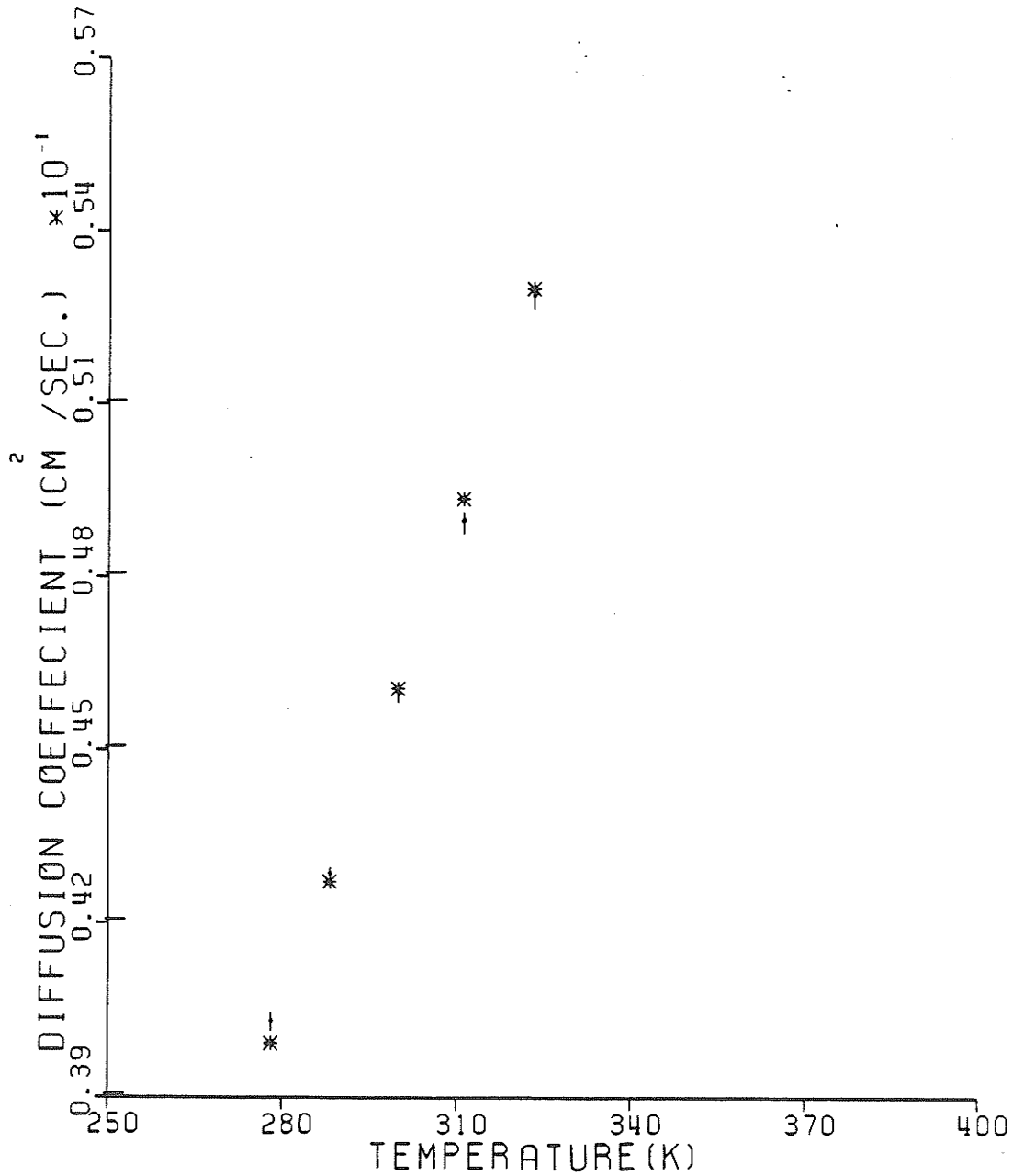
DIFFUSION COEFFECIENT (CM /SEC.) *10⁻¹
0.39
0.42
0.45
0.48
0.51
0.54
0.57
250
280
310
340
370
400
TEMPERATURE(K)

Figure 5.3

Figure 5.3 A comparison between the experimental and theoretical calculations for the second virial coefficient at different temperatures for SF_6-Xe.

. The experimental measurement.

* The theoretical calculation.

FIGURE 5.3

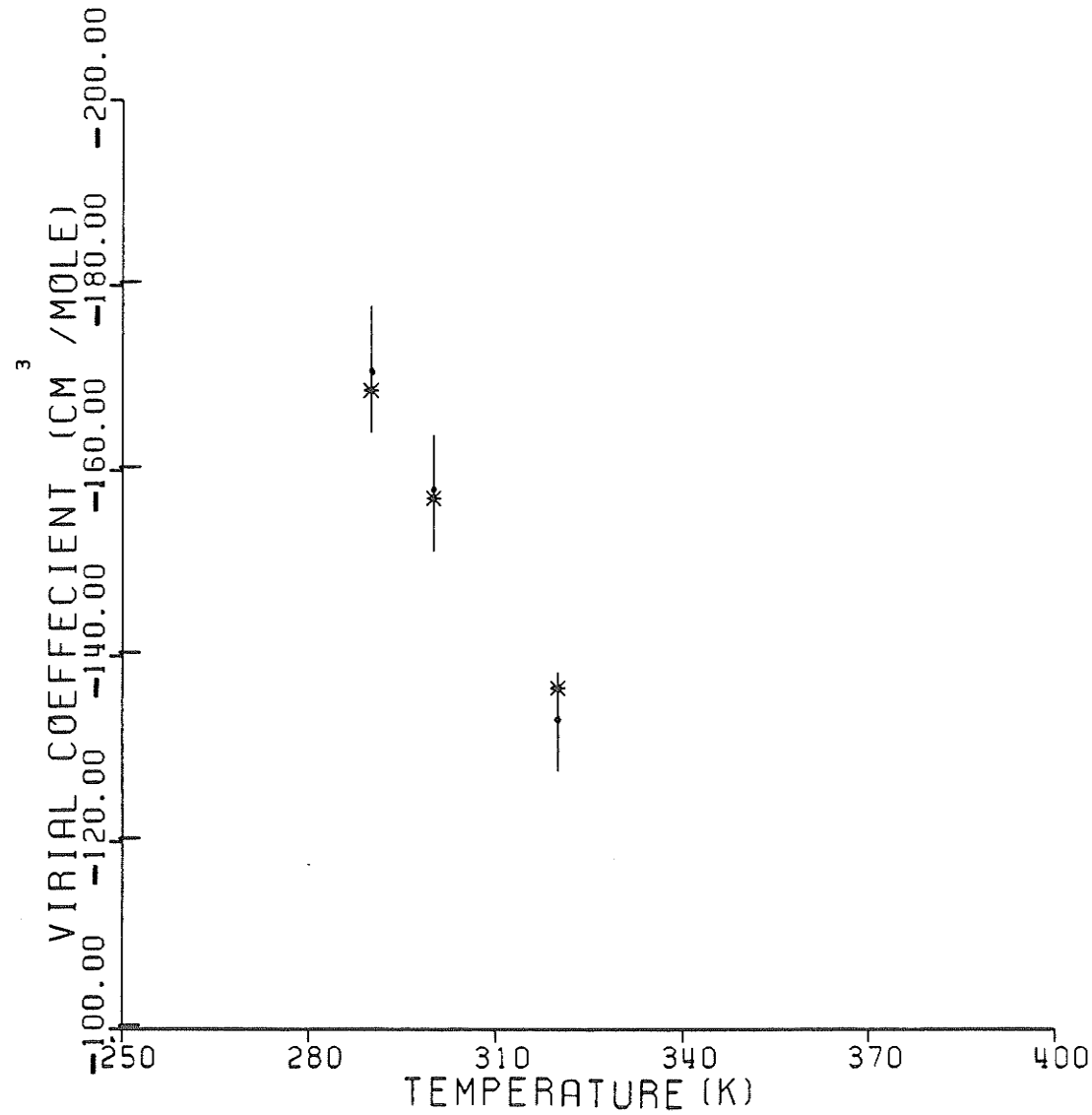
VIRIAL COEFFECIENT (CM /MOLE)
3
-100.00
-120.00
-140.00
-160.00
-180.00
-200.00
250
280
310
340
370
400
TEMPERATURE (K)

Figure 5.4

Figure 5.4 A comparison between the experimental CILS and the total theoretical spectra for SF_6-Xe.

. The experimental spectrum.

- The total theoretical spectrum.

FIGURE 5.4

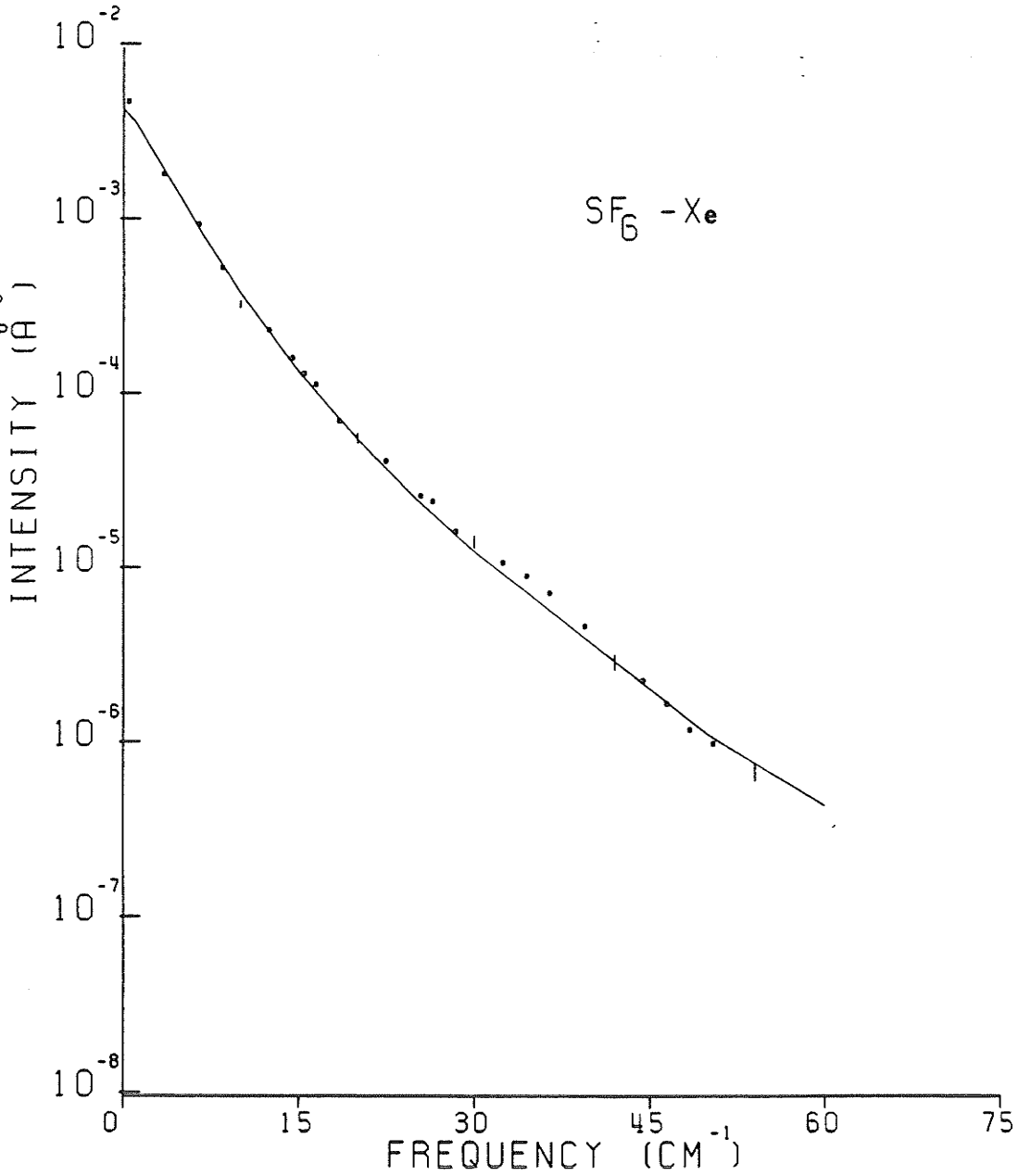
$SF_6 - Xe$
INTENSITY (A^6)
10^{-2}
10^{-3}
10^{-4}
10^{-5}
10^{-6}
10^{-7}
10^{-8}
0
15
30
45
60
75
FREQUENCY (CM^{-1})

CHAPTER 6

TETRAHEDRAL MOLECULES

The collision-induced light scattering spectrum arises from an incremental polarizability induced in a cluster of interacting molecules. The collision-induced Rayleigh wing in molecular spectra is broader than predicted by the DID and overlap contribution Eqn. (2.17). The additional intensity comes from rotational contributions as indicated in Eqn. (2.67), where the first term corresponds to the first order DID interaction and the rest of the terms represent the collision induced rotational scattering by tetrahedral molecules. Our interest in this chapter is in both the dipole-quadrupole polarizability $\underset{\sim}{A}$ and the dipole-octopole polarizability $\underset{\sim}{E}$ for CF_4. Two experiments have been done in our laboratory, namely, CF_4-CF_4 and CF_4-Ar. The first system had been studied before in our laboratory (Shelton and Tabisz, 1980). The reason for repeating this experiment is that the air impurity in the gas was high at that time, and the difference between the experimental and theoretical zeroth moment that agreed best was still 60% of the theoretical moment, with the values of A = 2.2 $\mathring{A}^4$ and E = 2.2 $\mathring{A}^5$.

Gharbi and Leduff (1980) have done the same experiment, but they calculated only the theoretical translational spectrum. They had good agreement at low frequency shifts, which encouraged us to use the same type of potential.

The other experiment, a mixture of CF_4 with Ar was done to provide additional data for refinement of the values of A and E we got from the CF_4-CF_4 experiment.

6.1 THEORETICAL SPECTRA

The translational spectra were calculated using the following parameters in Eqns. (2.31) and (2.32)

$$\alpha_{CF_4} = 2.937\ \mathring{A}^3 \quad \text{(Watson and Ramaswamy, 1936)}$$

$$\gamma_{CF_4} = 6.0 \times 10^{-62}\ C^4\ m^4\ J^{-3} \quad \text{(Lu and Shelton, 1987)}$$

The values for Ar were mentioned in Table 4.1.

The moments from both the computed translational spectra and from the sum rules for both CF_4-CF_4 and CF_4-Ar were calculated. In the case of CF_4-Ar, both combination rules were used. Table 6.1 shows the values of the zeroth, second, fourth and sixth moments for CF_4-CF_4 and CF_4-Ar.

TABLE 6.1

The Zeroth, Second, Fourth, and Sixth Moments for CF_4-CF_4, CF_4-$Ar^{(1)}$, and CF_4-$Ar^{(2)}$

		M_0	M_2	M_4	M_6
CF_4-CF_4	TR	126.54	284.82	5079.1	0.3454617×10^6
	SR	145.72	291.96	5118.8	0.3900088×10^6
CF_4-$Ar^{(1)}$	TR	45.17	169.94	4985.77	0.5310704×10^6
	SR	50.98	173.08	5025.3	0.5747376×10^6
CF_4-$Ar^{(2)}$	TR	69.86	368.53	16807.01	0.3034866×10^7
	SR	78.82	376.1	17225.96	0.3099724×10^7

CF_4-$Ar^{(1)}$ will refer to the simple combination rules.

CF_4-$Ar^{(2)}$ will refer to the combination rules by Pena.

As previously (Chapter 4), the differences in the moments were used to calculate the dimer spectra.

Figs. 6.1-6.3 show the translational, dimer and experimental spectra for CF_4-CF_4, CF_4-$Ar^{(1)}$, and CF_4-$Ar^{(2)}$ respectively.

The rotational spectra were calculated using the rotational constant B = 0.185 cm^{-1} for CF_4 and the values A = 2.2 $\mathring{A}^4$ and E = 2.2 $\mathring{A}^5$, having in mind that in the case of CF_4-Ar, $A_2 = E_2 = 0$ for Ar, Eqn. (2.67) and Eqn. (2.69) were used for the two cases, respectively.

Figs. 6.4-6.6 show the translational, rotational, total theoretical and experimental spectra for CF_4-CF_4, CF_4-$Ar^{(1)}$ and CF_4-$Ar^{(2)}$ respectively.

A good fit between the experimental and theoretical spectra with these values for A and E is obtained in the case of CF_4-CF_4. Values of A = 6 $\mathring{A}^4$, E = 6 $\mathring{A}^5$ for CF_4-$Ar^{(1)}$ and A = 2.8 $\mathring{A}^4$, E = 2.8 $\mathring{A}^5$ for CF_4-$Ar^{(2)}$ were required to obtain a good fit.

Another check was made by calculating δ(CILS) for all cases

$$\delta(CF_4\text{-}CF_4) = 1.84$$
$$\delta(CF_4\text{-}Ar^{(1)}) = 3.78$$
$$\delta(CF_4\text{-}Ar^{(2)}) = 1.96$$

which shows that the use combination rules by Pena are better than just the use of the simple combination rules.

Table 6.2 shows the values of A and E from this and other studies.

Another comparison between the total theoretical and experimental spectra is achieved by calculating δ(total).

TABLE 6.2

The Values of A and E for CF_4 in This and Other Studies

Group	Method	A	E
This Work CF_4-CF_4	Experimental	2.2	2.2
CF_4-$Ar^{(1)}$	Experimental	6.0	6.0
CF_4-$Ar^{(2)}$	Experimental	2.8	2.8
	Average* =	2.5 ± 0.3	2.5 ± 0.3
Buckingham and Tabisz (1978)	Bond polarizability model	2.2	
Shelton and Tabisz (1980)	Experimental	≤ 2.2	≤ 10

* Values for CF_4-$Ar^{(1)}$ were neglected because of the high value of δ(CILS). The error calculated is the average deviation.

TABLE 6.3

A Comparison Between the Values of δ(total) for CF_4-CF_4, CF_4-$Ar^{(1)}$, and CF_4-$Ar^{(2)}$

	δ(total)
CF_4-CF_4	0.893
CF_4-$Ar^{(1)}$	2.152
CF_4-$Ar^{(2)}$	1.288

Table 6.3 shows this comparison for CF_4-CF_4, CF_4-$Ar^{(1)}$, and CF_4-$Ar^{(2)}$.

The fit in the case of CF_4-CF_4 is very good in total, in spite of the fact that in the range 10-25 cm^{-1}, where the potential is the main factor, the value of δ(CILS) was not that good. It is still clear the fit in the case of CF_4-$Ar^{(2)}$, where the combination rules by Pena were used, is better than that obtained by the simple combination rules.

6.2 EXPERIMENTAL MOMENTS

(i) The Two-Body Experimental Moment

The zeroth, second, fourth, and the sixth moments were calculated for both CF_4-CF_4 and CF_4-Ar.

Table 6.4 shows a comparison between the experimental and theoretical zeroth moment.

TABLE 6.4

A Comparison Between the Experimental and Theoretical Zeroth Moment of the Two-Body Spectrum for CF_4-CF_4, CF_4-$Ar^{(1)}$ and CF_4-$Ar^{(2)}$,

$M_0(\mathring{A}^9)$

	Theoretical (SR)	Total Theoretical	Experimental
CF_4-CF_4			
Present work	145.72	149.12	148.36±25
Shelton and Tabisz (1980)	166		266
CF_4-$Ar^{(1)}$	50.98	60.11	57.58± 7.5
CF_4-$Ar^{(2)}$	78.82	82.63	57.58± 7.5

TABLE 6.5

A Comparison Between the Experimental and Theoretical Higher Moments of the Two-Body Spectrum for CF_4-CF_4, CF_4-$Ar^{(1)}$, and CF_4-$Ar^{(2)}$

		Theoretical (SR)	Total Theoretical	Experimental
CF_4-CF_4	M_2	291.98	396.71	407.1±23
	M_4	5118.78	13996.14	13804.42±2512
	M_6	0.2500088×10^6	0.15553×10^7	$(0.21731 \pm 0.0657) \times 10^7$
CF_4-$Ar^{(1)}$	M_2	173.08	463.36	364.55±20
	M_4	5025.96	29857.56	17908.15±3800
	M_6	0.5743376×10^6	0.37965×10^7	$(0.21739 \pm 0.1024) \times 10^7$
CF_4-$Ar^{(2)}$	M_2	376.1	498.1	368.74±26
	M_4	17225.96	27768.5	19965.35±6000
	M_6	0.3099724×10^7	0.44887×10^7	$(0.32204 \pm 0.208) \times 10^7$

Table 6.4 shows the good agreement between the experimental and total theoretical zeroth moments in the case of CF_4-CF_4 and CF_4-Ar. Again the difference between the moments of the first two columns is due to collision induced rotational spectrum.

Table 6.5 shows a comparision the same type for higher moments.

In the case of CF_4-CF_4, the experimental and total theoretical higher moments agree within the experimental error.

In the case of CF_4-Ar, the agreement is not satisfactory in general, and the reason is because of applying the combination rules results in inadequate potentials.

Still, in general, the combination rules by Pena work better than using the simple combination rules (δ(CILS) and δ(total)).

(ii) The Three-Body Experimental Moment

For CF_4-CF_4, Table 6.6 shows a comparison between the three-body experimental and theoretical zeroth and second moments for this and other studies.

TABLE 6.6

A Comparison Between the Experimental and Theoretical Zeroth and Second Moments of the Three-Body Spectrum for CF_4-CF_4

Group	Method	$M_0(\text{Å}^9)$	$M_2(\text{Å}^9\ PS^{-2})$
This work	Experimental	13.6 ± 1.8	34.63 ± 1
Shelton et al. (1982)	Experimental	28.8 ± 6	60.25 ± 18
Shelton et al. (1982)	Calculations using L-J (6-12) Potential	29.16	32.65

Table 6.6 shows good agreement between the second experimental and theoretical moments in this work, but there is a discrepancy between the zeroth moment. Again the ratio of M_0^3/M_0^2 for CF_4-CF_4 is about 9%, so the neglect of the three-body effect for CF_4-Ar (Eqn. (3.10)) is justified as in the SF_6-X cases.

6.3 CONCLUSIONS

(1) In the Case of CF_4-CF_4

(i) The experimental moments are in good agreement with the total theoretical ones.

(ii) The total fit is good (δ(total)), but still δ(CILS) is a little bit high, which is reason to believe that the L-J (6-12) potential is not the best type to explain the interactions between the CF_4 molecules.

(2) In the Case of CF_4-Ar

(i) The combination rules by Pena are better than the simple combination rules (δ(CILS) and δ(total)).

(ii) Attempts should be made to develop a potential for CF_4-Ar, instead of using two different potentials and a combination rule.

Figures 6.1-6.3

Figures 6.1-6.3 The experimental two-body, translational, and dimer spectra for CF_4-CF_4, CF_4-Ar(1), and CF_4-Ar(2) respectively.

. The experimental two-body spectrum.

□ The theoretical translational spectrum.

⊙ The theoretical dimer spectrum.

FIGURE 6.1

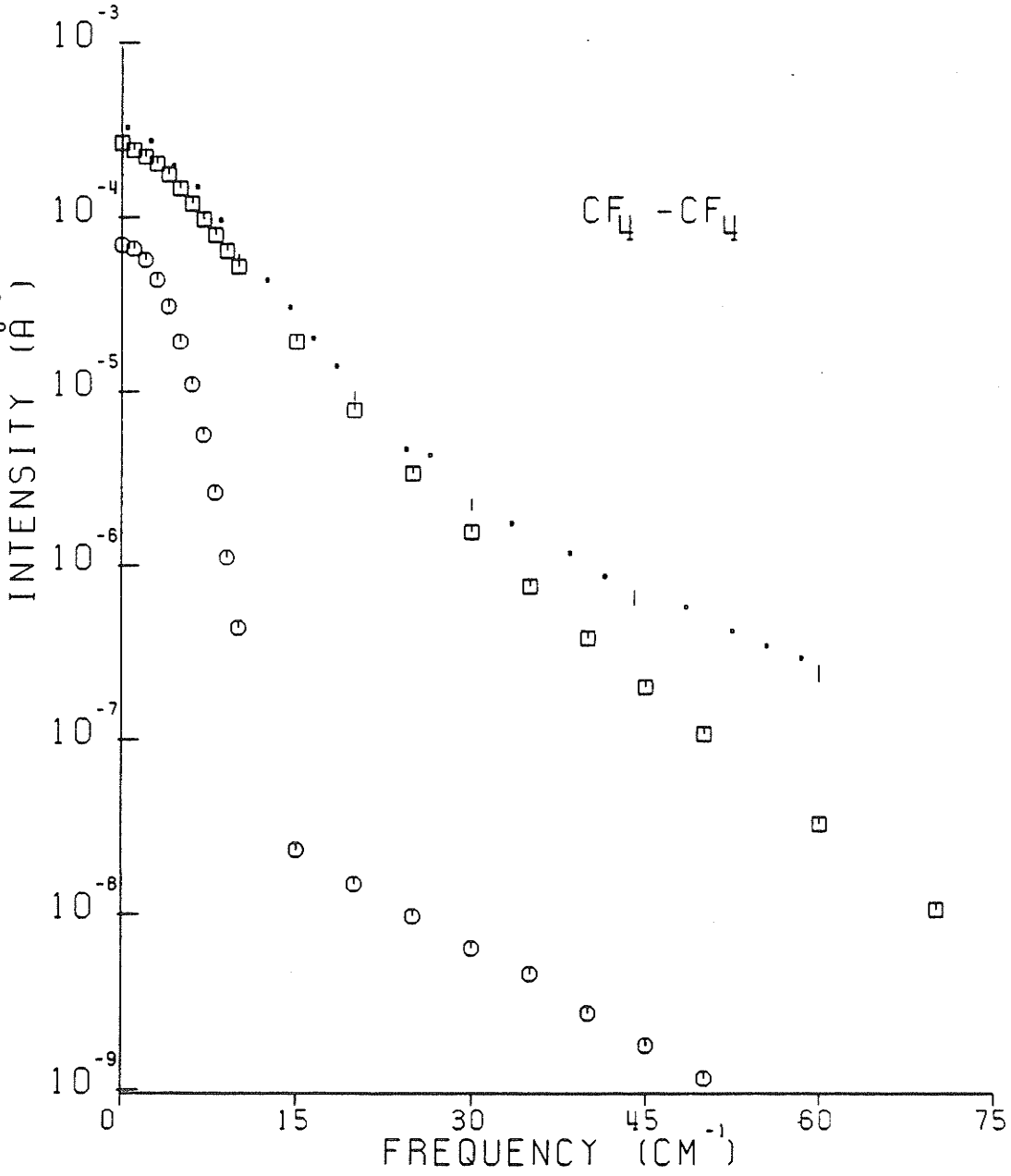
$CF_4 - CF_4$
INTENSITY (A^6)
10^{-3}
10^{-4}
10^{-5}
10^{-6}
10^{-7}
10^{-8}
10^{-9}
0
15
30
45
60
75
FREQUENCY (CM^{-1})

FIGURE 6.2

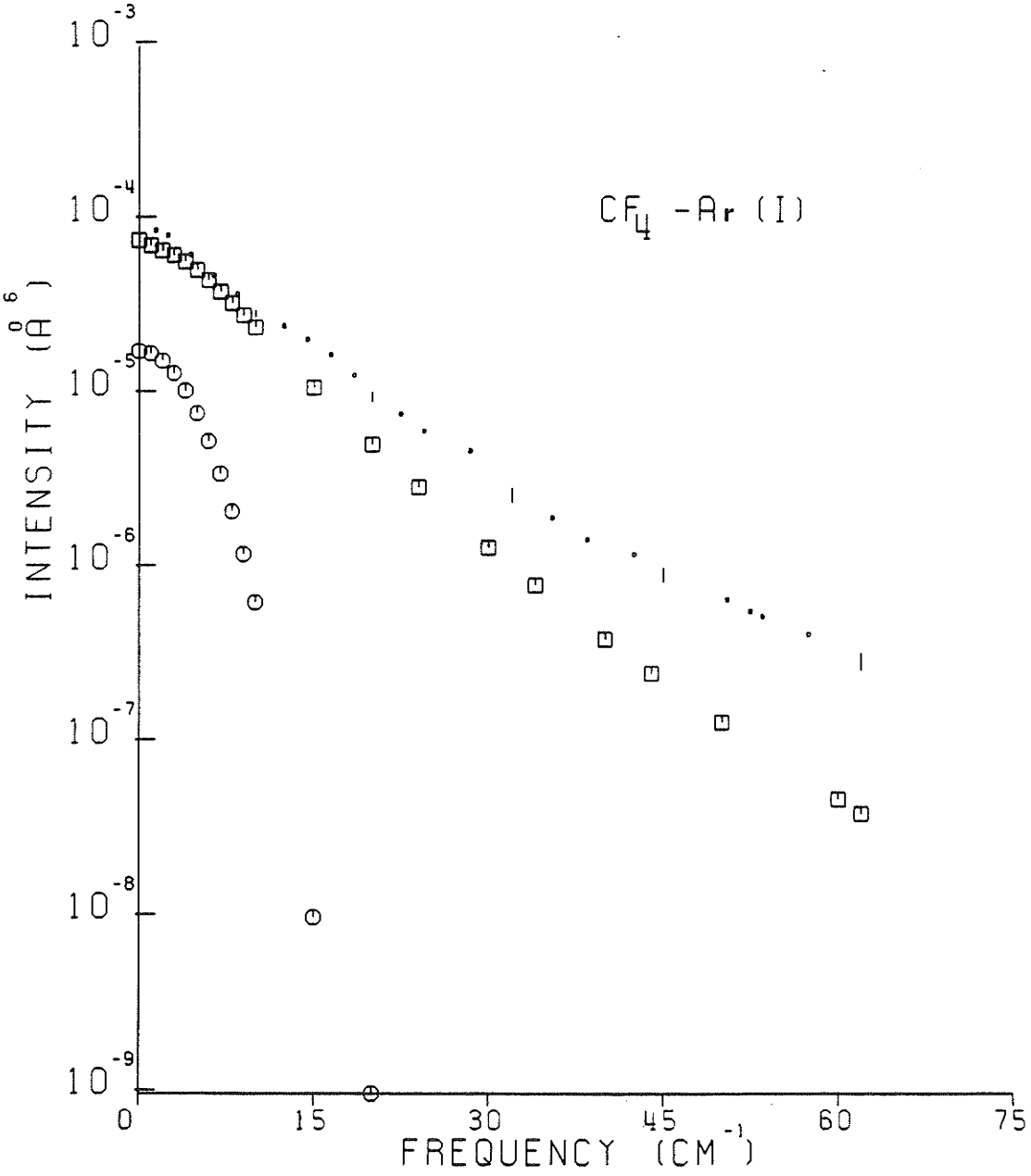
CF_4 -Ar (I)
INTENSITY (A^6)
10^{-3}
10^{-4}
10^{-5}
10^{-6}
10^{-7}
10^{-8}
10^{-9}
0
15
30
45
60
75
FREQUENCY (CM^{-1})

FIGURE 6.3

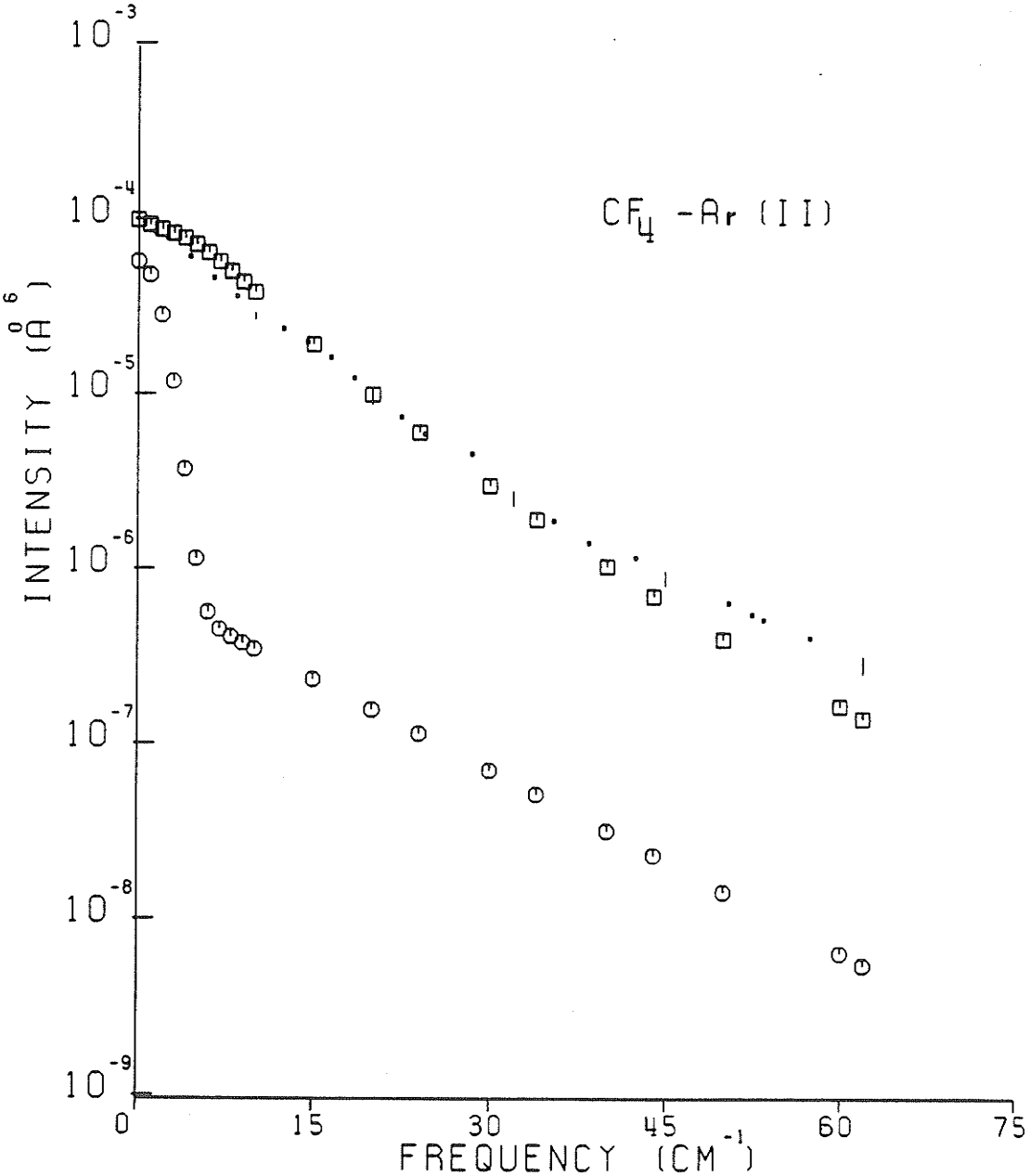
CF_4 -Ar (II)
INTENSITY (A^6)
10^{-3}
10^{-4}
10^{-5}
10^{-6}
10^{-7}
10^{-8}
10^{-9}
0
15
30
45
60
75
FREQUENCY (CM^{-1})

Figures 6.4-6.6

Figures 6.4-6.6 The experimental two-body, total theoretical, translational, and rotational spectra for CF_4-CF_4, CF_4-Ar(1), and CF_4-Ar(2) respectively.

. The experimental two-body spectrum.

- The total theoretical spectrum.

□ The theoretical translational spectrum.

* The theoretical rotational spectrum.

FIGURE 6.4

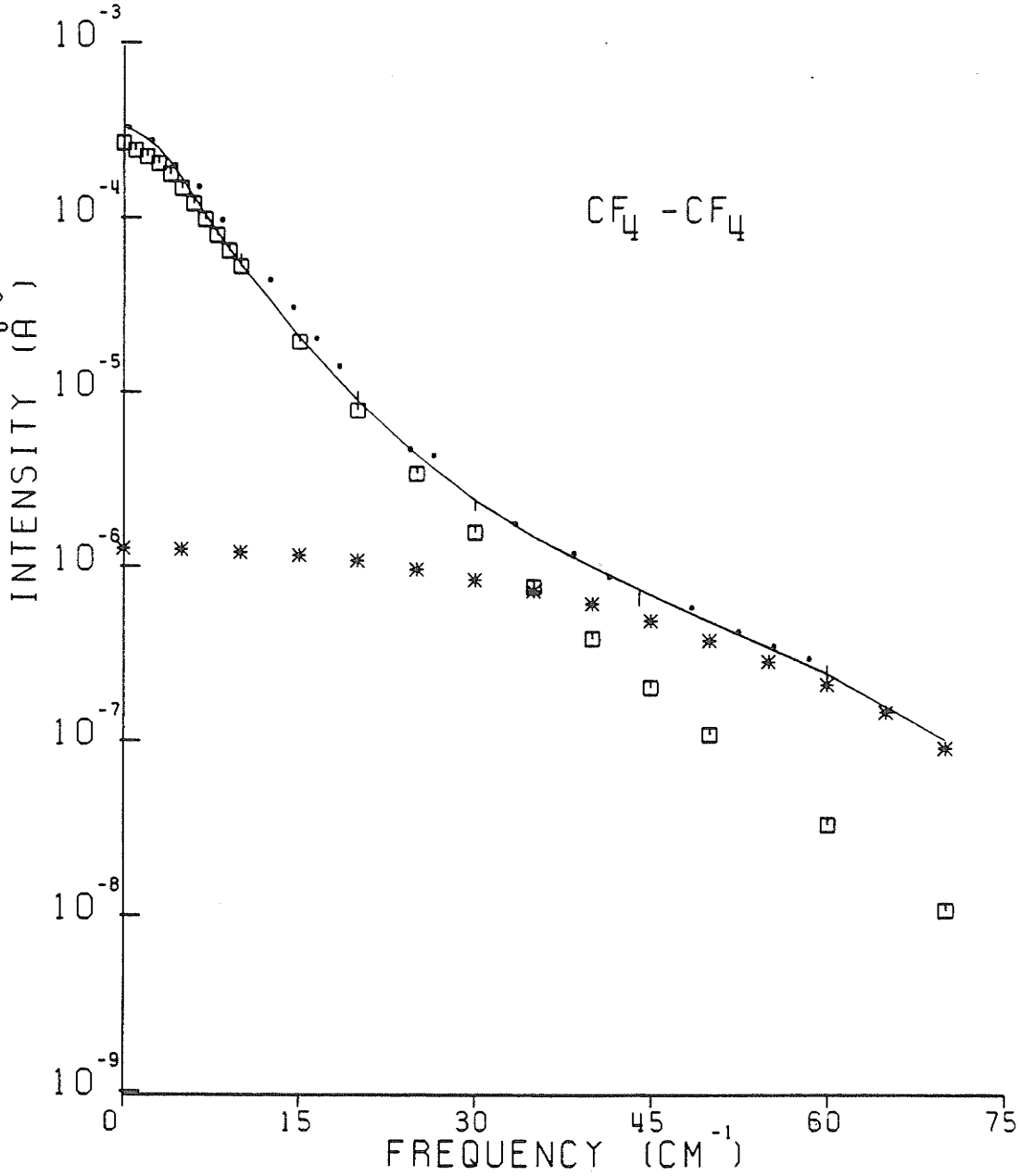
10^{-3}
10^{-4}
10^{-5}
10^{-6}
10^{-7}
10^{-8}
10^{-9}
INTENSITY ($A^{0\,6}$)
CF_4 -CF_4
0
15
30
45
60
75
FREQUENCY (CM^{-1})

FIGURE 6.5

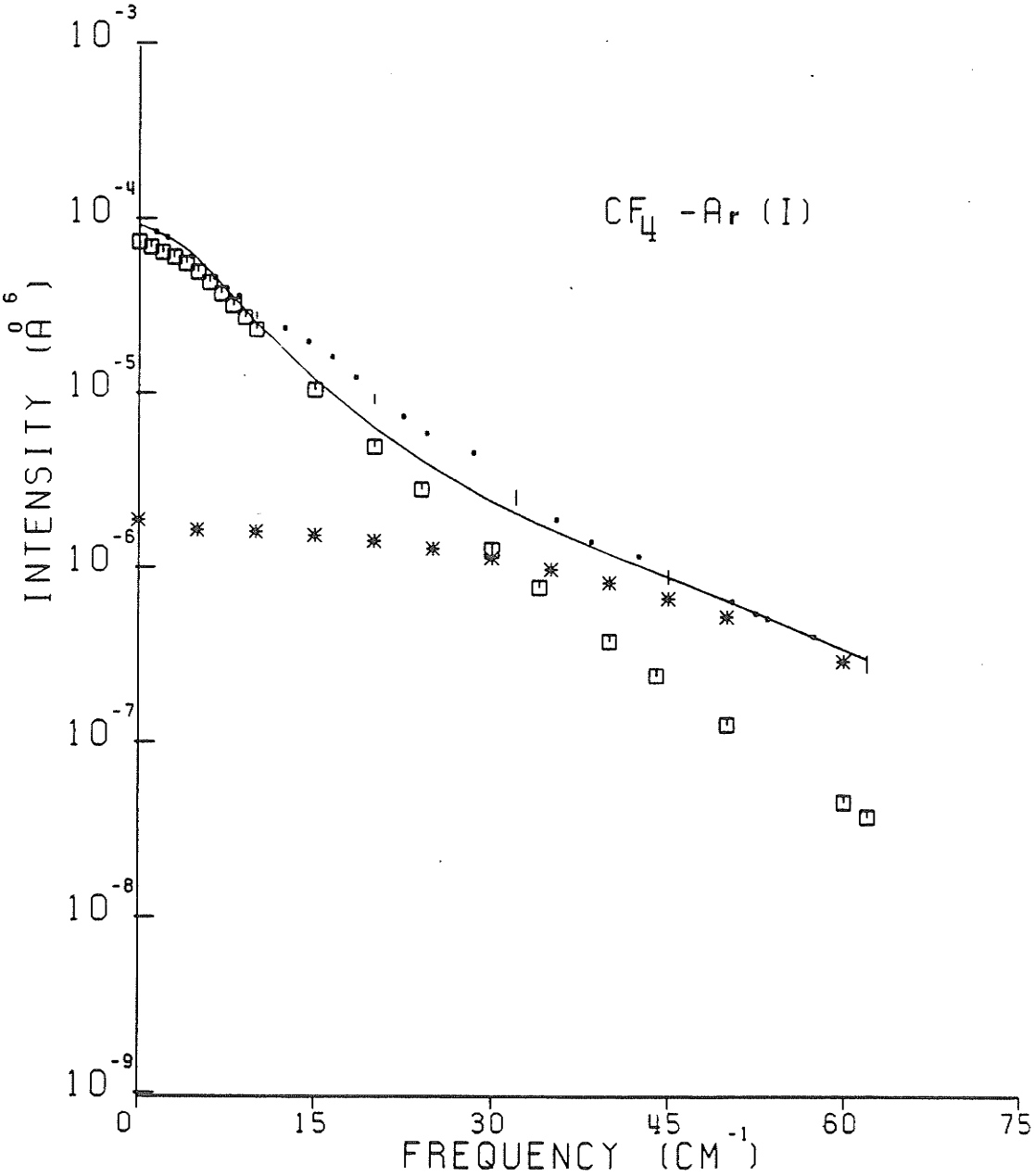
CF_4 -Ar (I)
INTENSITY (A^{06})
10^{-3}
10^{-4}
10^{-5}
10^{-6}
10^{-7}
10^{-8}
10^{-9}
0
15
30
45
60
75
FREQUENCY (CM^{-1})

FIGURE 6.6

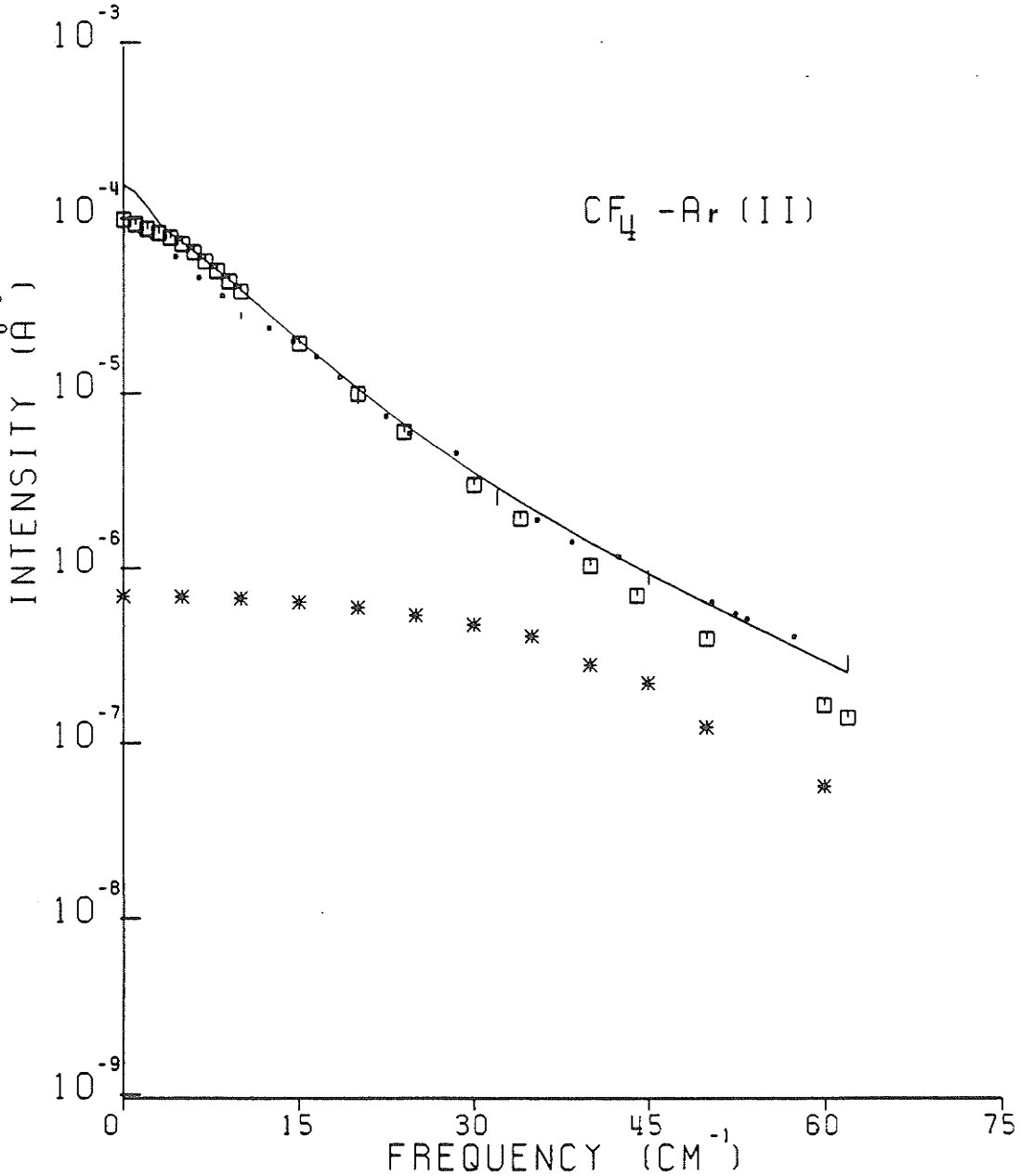
CF_4 -Ar (II)
INTENSITY (A^6)
10^{-3}
10^{-4}
10^{-5}
10^{-6}
10^{-7}
10^{-8}
10^{-9}
0
15
30
45
60
75
FREQUENCY (CM^{-1})

CHAPTER 7

CH_4 AT DIFFERENT TEMPERATURES

CH_4 is the ideal candidate to study collision-induced light scattering, since the translational and rotational motions can be studied separately. In the case of SF_6 and CF_4, there is almost total overlap between the two components. For CH_4 the spectrum consists essentially of an intense pure translational component and a weaker induced rotational wing.

CILS spectrum of gaseous CH_4 has been studied as a pure gas (Shelton and Tabisz, 1980) and in mixture with Ar and Xe (Penner et al., 1985) at room temperature in this laboratory. A consistency in the magnitude of the dipole-quadrupole polarizability $\underset{\sim}{A}$ of CH_4 was found in analyzing both pure and mixture spectra, a value of $A = 0.88 \pm 0.05$ $\mathring{A}^4$.

Nevertheless, scattering by gases has never been systematically studied as a function of temperature before.

This chapter will analyze the measurement of the spectrum of CH_4 in the range 130-295 K (performed in Firenze (Italy)) through calculations done here. The translational spectrum was calculated using two methods, the classical line shape (described in Chapter 2), which requires the pair polarizability and the intermolecular potential to be identified, and the Birnbaum-Cohen model for line shape of the collision-induced absorption spectrum (Birnbaum and Cohen, 1976). As before, the spectrum of bound dimers appears as a low frequency feature. Prengel and Gornall (1976) have given a detailed discussion of the CH_4 dimer spectrum at 300 K and 115 K.

7.1 EXPERIMENT

The experiments reported here were performed by A. Guasti, M. Zoppi, and F. Barocchi at the Istituto di Elettronica Quantistica del C.N.R. in Firenze and the apparatus used is described in detail elsewhere (Bafile et al., 1988); the gas sample was contained in a pressure cell (Mazzinghi and Zoppi, 1983) housed in an Air Products cryogenic cooling system. Excitation of the spectra was achieved with an argon ion laser operating at 1 w at 5145 Å. Experiments were performed in the depolarized geometry as the geometry used in Chapter 2.

A common procedure (Tabisz, 1979; Shelton et al., 1982) is to record spectra at a number of densities and then apply a virial expansion of the intensity at a large number of frequencies to separate two-, and three-body correlation components of the total spectrum. Such an approach was impractical in the present case. The necessity to record precise data for an extremely broad spectrum, frequently under low signal conditions, requires long observation times. This circumstance, coupled with the stability problems with the crystal system at low temperature, prevented collection of data for a thorough density analysis. Consequently, another approach was adopted; gas pressures were chosen so that the experiment was always performed in a thermodynamic state, for which the intensity varied essentially as the density square and thereby the two-body correlation spectrum was measured directly.

For example, at T = 295 K, the spectra were recorded from 4-15 cm^{-1} with a gas pressure of 10 bar. At high frequency shifts, 10-130 cm^{-1}, pressures were increased to 40 bar and to 90 bar for

100-550 cm^{-1}. The same approach was applied to the spectra recorded at lower temperatures, 250, 203, and 163 K.

The spectrum at 130 K was that of the saturated vapour pressure 3.48 bar. Confidence in the procedure was gained from the fact that the two- and three-body spectra were known to behave similarly (Barocchi et al., 1977; Shelton et al., 1982). Also the three-body spectrum contributes only at low frequencies (Barocchi et al., 1977).

Spectra were recorded at different pressures in overlapping frequency regions to ensure continuity in intensity calibrations as well as quadratic density dependence.

The spectral slit widths were 0.6 cm^{-1} (4-10 cm^{-1}), 1.0 cm^{-1} (4-20 cm^{-1}), and 2.4 cm^{-1} (10-600 cm^{-1}).

To calibrate intensities in absolute terms, low pressure H_2 was used as an external intensity standard and the light scattered at 20 cm^{-1} from CH_4 was compared to the intensities of the $S_0(0)$ and $S_0(1)$ lines of H_2.

Table 7.1 shows the intensities at 20 cm^{-1} at different temperatures.

Figures 7.1-7.5 show the experimental spectra for temperatures 295, 250.5, 203, 163.4 and 130.8 respectively.

7.2 THEORETICAL SPECTRA

Two different approaches were used, both under the assumption that there is no translation rotational coupling. We will discuss each method separately.

TABLE 7.1

Intensity D_{II} at 20 cm^{-1} Frequency Shift

T (K)	D_{II} (10^{-5} $Å^6$)
295	5.4 ± 0.3
250.5	5.6 ± 0.2
203.0	5.8 ± 0.5
163.4	5.9 ± 0.3
130.8	5.85 ± 0.3

7.2.1 Classical Line Shape Analysis

Eqns. (2.31) and (2.32) were used as before to calculate the intensity of the translational spectrum as a function of frequency for different temperatures. The quantum nature of the collision dynamics are expected to become increasingly important with decreasing temperature. The spectra can be calculated once the intermolecular potential U(r) and the pair polarizability β(r) are known.

Dimer spectra were calculated as mentioned in Section 2.2. Again the effect of bound dimers relative to the translational component increases with decreasing temperature, and can be calculated using Eqns. (2.46) and (2.48).

7.2.1a The Pair Polarizability β(r)

The model for the pair polarizability anisotropy β(r) (Meinander et al., 1985) was derived from the first four even classical moments of the depolarized pure translational spectra of the inert

gases and CH_4 at room temperature, the formula used is in Eqn. (2.17).

The values of the parameters for CH_4 are

$$\alpha_0 = 2.642\ \text{Å}^3 \quad , \quad \gamma = 19.2 \times 10^{-62}\ C^4\ m^4\ J^{-3}$$

$$C_6 = 129.6 \text{ a.u. and } B^* = 2580$$

7.2.1b The Intermolecular Potential U(r)

An intermolecular potential was derived for CH_4 molecules by Righini et al. (1981) using solid state data, the second virial coefficient, and the known long-range dispersion forces. It was modified by Meinander and Tabisz (1983), who added the first anisotropic dispersion term to the model and modified the repulsive C-C interaction parameters so the experimental second virial coefficients were reproduced. This modified RMK-potential was used to construct an effective isotropic potential (Reed and Gubbins, 1973), which reproduces the angular average of the pair distribution function g(r) at 295 K (Penner et al., 1985).

$$g(r) = \exp\ (-U_{eff}(r)\ /k_B T)$$

$$= \frac{1}{(4\pi)^2} \iint \exp\ (-U(r, \Omega_1, \Omega_2)\ /k_B T)\ d\Omega_1\ d\Omega_2. \qquad (7.1)$$

This numerical isotropic potential was described in the HFD form, namely,

$$U(x) = \varepsilon \{C\ X^y \exp\ (-AX) - F(X)\ (C_6 X^{-6} + C_8 X^{-8} + C_{10} X^{-10})\}$$

where $f(X) = \exp\ [-(D/X - 1)^2] \quad x \leq D$

$= 1 \qquad\qquad X > D \qquad (7.2)$

and $X = r/r_{min}$.

This potential was used at all temperatures, at first, with the parameters calculated at 295 K to calculate the theoretical spectra. However an effective intermolecular potential at each experimental temperature was found necessary. The parameters at each temperature are shown in Table 7.2.

7.2.1c Rotational Spectra

CH_4 is a tetrahedral molecule, where the dipole-quadrupole $\underset{\sim}{A}$ and the dipole-octopole ($\underset{\sim}{E}$) polarizabilities are non-zero. The rotational lines due to $\underset{\sim}{A}$ and $\underset{\sim}{E}$ at 295 K were broadened with gaussians of HWHM of 20 and 25 cm^{-1} respectively; the widths were assumed to vary as $\sqrt{T}$ for lower temperatures. The rotational spectrum was added to the (translational + dimer) one, and the values of A and E were adjusted to produce agreement with the experimental intensity in the range where the rotational spectrum is dominant.

Comparison Between the Experimental and Theoretical Spectra

Figs. 7.6-7.10 show the comparison between the experimental profiles and the calculations. Overall the agreement is very good and the principal behaviour of the experimental data is reproduced. The low frequency translational profile is well reproduced at all temperatures, except from 0-30 cm^{-1} at 295 K and 250 K.

At high frequency shifts where the induced rotational component dominates, the experimental intensity is well reproduced over very broad frequency ranges to 560 cm^{-1} at 295 K, 400 cm^{-1} for 250.5 and 203 K, 300 cm^{-1} for 163.4 and 100 cm^{-1} for 130.8 K. The effect of using the effective potential appropriate to each temperature

TABLE 7.2

Effective Potential Parameters

	T(K) 295.0	250.5	203.0	163.4	130.8
C	0.106941×10^8	0.894842×10^7	0.8429702×10^7	0.7476459×10^7	0.6226944×10^7
y	2.67164	2.52848	2.513727	2.442912	2.312344
a	16.14407	15.96006	15.89286	15.76464	15.5703
C_6	1.016033	1.018077	1.020732	1.023577	1.026516
C_8	0.6867825	0.6896673	0.7034269	0.697673	0.7023532
C_{10}	0.4700447	0.4730498	0.4769775	0.4814949	0.4865795
D	1.248246	1.250609	1.252382	1.254463	1.256861
ε(K)	180.43	181.2526	182.3238	183.6378	185.222
r_m(Å)	4.1465	4.141981	4.136119	4.129256	4.121379
σ(Å)	3.6915	3.687125	3.680639	3.673404	3.665473

may be seen by comparing Figs. 7.10 and 7.11. In Fig. 7.11 the profile is calculated for 130 K using the isotropic potential derived for 295 K; the agreement is clearly worse.

To compare the experimental and theoretical profiles in detail we will consider the comparison in three different regions, low frequency shifts, mid frequencies and high frequency shifts.

1. Low Frequency Shifts

The low frequency spectrum has a large contribution from dimers. This can be appreciated from Table 7.3 where the moments from the translational spectrum, the sum rules and the quantum mechanical corrected Wigner-Kirkwood terms are shown. The difference between the moment calculated from the sum rules and the translational spectrum increases with decreasing temperature, especially for the zeroth moment. This difference is 86% at 130 K. The quantum mechanical corrections produce further changes, especially for higher moments.

Figs. 7.12-7.16 show clearly the difference between the experimental data and the free-free profile and hence show the importance of the dimer spectrum. The effect of dimers is negligible beyond 30 cm^{-1} at all temperatures.

2. Mid Frequency Range

The least satisfactory agreement between theory and experiment occurs at mid frequencies for temperature < 295 (40-160 cm^{-1}) for several possible reasons. First, this is the region where quantum mechanical corrections to higher moments are important and are available only up to the fourth moment. Secondly, the parameters, especially B and r_0 in the scaling law were calculated

TABLE 7.3

Calculated Spectral Moments

T (K)		M_0 (10^2 Å^9)	M_2 (10^3 Å^9 ps^{-2})	M_4 (10^5 Å^9 ps^{-4})	M_6 (10^8 Å^9 ps^{-6})
295.0	a)	1.81	3.87	6.71	4.24
	b)	2.14 (18%)	4.00 (3%)	6.76 (1%)	4.25 (0.1%)
	c)	2.13 (18%)	4.02 (4%)	7.10 (6%)	
250.5	a)	1.82	3.44	5.40	3.15
	b)	2.26 (25%)	3.63 (6%)	5.50 (2%)	3.15 (0%)
	c)	2.26 (25%)	3.65 (6%)	5.88 (9%)	
203.0	a)	1.83	3.00	4.18	2.21
	b)	2.50 (36%)	3.30 (10%)	4.35 (4%)	2.22 (1%)
	c)	2.48 (35%)	3.33 (11%)	4.82 (16%)	
163.4	a)	1.85	2.65	3.33	1.61
	b)	2.86 (55%)	3.11 (17%)	3.60 (8%)	1.65 (3%)
	c)	2.84 (54%)	3.14 (19%)	4.18 (26%)	
130.8	a)	1.86	2.36	2.73	1.23
	b)	3.46 (86%)	3.08 (31%)	3.16 (16%)	1.31 (7%)
	c)	3.42 (84%)	3.13 (33%)	3.95 (44%)	

at 295 K, and are now used for lower temperatures. Thirdly, the use of an effective isotropic potential instead of the true anisotropic potential can affect the collision dynamics and consequences of the line shape. A full quantum mechanical calculation could settle these questions.

3. High Frequency Shifts

The rotational spectrum dominates this region. Table 7.4 will show the values of A and E in this and other studies.

The average values of this work agree with the work done before in this laboratory.

It is evident from Figs. 7.6-7.10 that some intensity remains beyond the $\underset{\sim}{E}$ spectrum and possibly the multipole series should be

TABLE 7.4

The Values of A and E

Group	Method	T (K)	A ($\mathring{A}^4$)	E ($\mathring{A}^5$)
This work	Experimental	295	0.83	2.00
		250.5	0.9	2.42
		203.0	0.9	2.56
		163.4	0.86	2.65
		130.8	0.9	3.0
	Average*		0.88±0.03	2.5±0.26
Buckingham and Tabisz (1978)	Bond Polarizability model		1.0	-1.0
Shelton and Tabisz (1980)	Experimental	295	1.0	2.5
Penner et al. (1985)		295	0.88±0.05	
Isnard et al. (1976)	Virial coefficient		2.35	
Rajan and Lalita (1974)	N.M.R.		2.71 0.88 0.89	
Buck et al. (1981)	Molecular beam scattering		2.67	

* The error mentioned is the average deviation.

taken to higher terms. As a result, the value of E reported here may be considered as an upper limit.

Table 7.5 shows the values of δ(CILS) and δ(total) for each case.

It seems from Table 7.5 that the whole model works for all temperatures, especially at T = 295, 163.4, and 130.8 K. To

TABLE 7.5

The Values of δ(CILS) and δ(total)

T(K)	δ(CILS)	δ(total)
295	1.619	1.28
250.5	4.64	2.73
203	4.54	2.56
163.4	2.95	1.92
130.8	2.49	2.01

improve the model, one could change B and r_0 as parameters in the fit, since they describe the overlap interaction, which is very temperature sensitive.

7.2.2 Birnbaum-Cohen (BC) Model

A very useful model for the line shape in pressure-induced absorption has been developed by Birnbaum and Cohen (1976), and has been previously shown to be capable of approximating the line shape closely. The model correlation function is given by

$$C(y) = \exp\left[\tau_1^{-1}\left[\tau_2 - (\tau_2^2 + y^2)^{\frac{1}{2}}\right]\right] \qquad (7.3)$$

where $y = (t^2 - i\beta\hbar t)^{\frac{1}{2}}$

The model line shape at frequency $\omega' = \omega_{if} \pm \omega$ is given by

$$\Gamma(\omega) = \int_{-\infty}^{\infty} e^{i(\omega_{if}-\omega)y} C(y)\, dy$$

$$= S \frac{\tau_1}{\pi} \frac{1}{1+(\tau_1 \omega')2} \exp\left(\frac{\tau_2}{\tau_1} + \tau_0 \omega'\right) Z K_1(Z) \qquad (7.4)$$

where $\tau_0 = \frac{\beta h}{2}$ $\qquad$ $\tau_3^2 = \tau_2^2 + \tau_0^2$

and $Z = \frac{\tau_3}{\tau_1} \sqrt{1+(\tau_1 \omega')^2}$.

$K_1(Z)$ is the modified Bessel function, with the asymptotic properties

$$Z K_1(Z) \to 1 \text{ as } Z \to 0$$

and $K_1(Z) \to \sqrt{\frac{\pi}{2Z}} e^{-Z}$ as $Z \to \infty$

The model was applied to the translational absorption spectrum of He-Ar, the S(0) rotational line of H_2 at 77 K, and the unresolved rotational band of N_2 (Birnbaum and Cohen, 1976). In all cases, the theory fits the spectra and accounts for the spectral features. Also for H_2-He (Borysow and Frommhold, 1983) collision-induced absorption was fitted with satisfactory agreement at temperatures from 50-300 K.

Significant improvements are possible by combining the BC and so-called K_0 model in the form (Borysow and Frommhold, 1983)

$$G_{c\ell}(\omega) = \frac{S'}{1+\varepsilon} \left(\frac{\tau_1}{1+\omega^2 \tau_1^2} \exp\left(\frac{\tau_2}{\tau_1}\right) [X K_1(X)] + \varepsilon\tau_3 \right.$$

$$\left. * \exp\left(\frac{\tau_3}{\tau_4}\right) K_0(y)\right) \frac{1}{\pi} \qquad (7.5)$$

where $X = \frac{\tau_2}{\tau_1} (1+\omega^2 \tau_1^2)^{\frac{1}{2}}$, $\qquad y = \frac{\tau_3}{\tau_4} (1+\omega^2 \tau_4^2)^{\frac{1}{2}}$,

$G_{c\ell}(\omega)$ is the classical spectral line shape,

K_0, K_1 are modified Bessel functions

and the parameters τ_1, τ_2, τ_3, τ_4, ε and S are adjusted to match the classical line shape.

This model is not prefered for systems that have considerable dimer contributions because the spectrum has to be calculated for each interaction (free-free, free-bound, and bound-bound). Moreover, there are many parameters to adjust, and our philosophy is to decrease the number of parameters as much as possible in order to compare in a physically meaningful way the theoretical spectrum with the experimental, not just to fit it to the experimental spectrum.

As a test, the BC model was used to calculate the translational spectrum where τ_1 and τ_2 can be calculated using the following equations

$$\int_{-\infty}^{\infty} \Gamma(\omega)\, d\omega = 1 \qquad (7.6)$$

$$M_n = (-i)^n \frac{\partial^n C(y)}{\partial y^n}\Big|_{t=0} = \int_{-\infty}^{\infty} \omega^n \Gamma(\omega)\, d\omega \quad . \qquad (7.7)$$

With Eqns. (7.3) and (7.4) one can find

$$S = M_0 \qquad (7.8)$$

$$M_2 = \frac{1}{\tau_1\tau_2}\left(1 + \left(\frac{1}{\tau_1} + \frac{1}{\tau_2}\right)\frac{\tau_0^2}{\tau_2}\right) M_0 \qquad (7.9)$$

$$M_4 = \left(\frac{3}{\tau_1^2\tau_2^2} + 18\,\frac{\tau_0^2}{\tau_1^2\tau_2^4} + 6\,\frac{\tau_0^2}{\tau_1^3\tau_2^3} + 6\,\frac{\tau_0^4}{\tau_1^3\tau_2^5}\right.$$

$$+ 15 \frac{\tau_0^4}{\tau_1^2 \tau_2^6} + \frac{3}{\tau_1^3 \tau_2^3} + 18 \frac{\tau_0^2}{\tau_1^5 \tau_2^5} + 15 \frac{\tau_0^4}{\tau_1^7 \tau_2^7} + \frac{\tau_0^4}{\tau_1^4 \tau_2^4}) M_0 \quad , \quad (7.10)$$

So, if the values of the first three even moments are known, S, τ_1, and τ_2 can be determined.

To make it easier, instead of starting by solving an equation of the 7th order, one can start by solving for τ_1 and τ_2 classically at first, to the first order in h, where

$$C(y) = 1 + i\, t \frac{\tau_0}{\tau_1 \tau_2} - \frac{t^2}{2} \frac{1}{\tau_1 \tau_2} + i \frac{t^3}{2} \tau_0 \frac{\tau_1 + \tau_2}{\tau_1^2 \tau_2^3}$$

$$+ \frac{t^4}{8} \frac{\tau_1 + \tau_2}{\tau_1^2 \tau_2^3} + \ldots \qquad (7.11)$$

From this, one can easily find the relations:

$$\frac{M_2}{M_0} = \frac{1}{\tau_1 \tau_2} \qquad (7.12)$$

$$\frac{M_4}{M_0} = 3 \frac{\tau_1 + \tau_2}{\tau_1^2 \tau_2^3} \quad . \qquad (7.13)$$

Solving Eqns. (7.12) and (7.13), one can find

$$\tau_1^2 = \frac{M_0}{M_2} \left(\frac{1}{3} \frac{M_4 M_0}{M_2^2} - 1\right)$$

$$\tau_2 = \frac{M_0}{M_2} \frac{1}{\tau_1} \qquad (7.14)$$

Starting from these values for τ_1 and τ_2, and using Eqns. (7.7) and (7.8), one can find the values of τ_1 and τ_2 by iteration. Once these three parameters are known, Eqn. (7.2) can be used to calculate the spectral line shape.

For comparison with the experiment, the rotational spectra used in the previous line shape analysis, with the values of A and E kept the same as before for different temperatures, were added to the translational spectra.

Figs. 7.17-7.21 show that this method gives satisfactory results only at 203 K, but in general the line shape calculated by this method was higher than the experimental one, especially at mid-range frequencies. Here we believe that M_6 begins to have an effect on the profile while only M_0, M_2 and M_4 were used to calculate the spectrum. The relative importance of the various moments change with temperature and could explain the good fit at 203 K.

7.3 EXPERIMENTAL MOMENTS

Since calculations using classical line shape analysis works better than using the BC model, we will compare the experimental moments with the calculated spectrum from the first method.

Table 7.6 shows a comparison between the experimental and theoretical zeroth moments for each temperature.

The experimental and total theoretical zeroth moments agree in general for all cases, but better for T = 250.5 and T = 203 K than for the rest of the cases. But that does not mean a better fit, δ(total) is the better overall measure of agreement.

The induced rotational moments are higher, the lower the

TABLE 7.6

A Comparison Between the Experimental and Theoretical Zeroth Moments for CH_4

		M_0 ($\AA^9$)		
T(K)	Theoretical (SR)	Rotational	Total Theoretical	Experimental
295	213.13	1.67	214.77	192.24 ± 10
250.5	224.36	2.41	226.77	227.42 ± 16
203	246.12	2.5	248.63	244.62 ± 20
163.4	279.26	2.76	282.02	272.4 ± 24
130.0	326.67	3.91	330.58	340.66 ± 33

temperature, but the contribution of the rotational moment is small in general for the zeroth moment.

Table 7.7 shows a comparison of the same type for higher moments.

The error in M_4 and M_6 is very high at T = 163.8 and 130 K, so we have little to say about them.

The agreement in M_2 is best at T = 163.4 K (≃ 2%) and worst at T = 130.8 (33%) and about 12% for the rest. The values of the higher moments are higher than expected at T = 163.4, but the reason is obvious (Fig. 7.4) from the bump at high frequency shifts, but the experimental error was very high.

7.4 CONCLUSIONS

(1) Models for both the induced pure translational and rotational scattering work well over a range from room temperature to that of the saturated vapour.

TABLE 7.7

A Comparison Between the Experimental and Theoretical Higher Moments for CH_4

T(K)		Theoretical (SR)	Total Theoretical	Experimental
295	M_2	4018.34	6127.87	5310.07±65
	M_4	0.7100149×10^{6}	0.90413×10^{7}	$(0.6860767\pm0.0592)\times10^{7}$
	M_6	0.4245418×10^{9}	0.58367×10^{11}	$(0.3720344\pm0.05806)\times10^{11}$
250.5	M_2	3616.07	6461.61	5811.26±44
	M_4	0.5760191×10^{6}	0.110925×10^{8}	$(0.7541836\pm0.046)\times10^{7}$
	M_6	0.3056436×10^{9}	0.680225×10^{11}	$(0.4181184\pm0.06816)\times10^{11}$
203.0	M_2	3221.32	5645.73	5003.38±23
	M_4	0.4538272×10^{6}	0.77901×10^{7}	$(0.4508614\pm0.0156)\times10^{7}$
	M_6	0.2037772×10^{9}	0.38928×10^{11}	$(0.1890966\pm0.0209)\times10^{11}$
163.4	M_2	2981.86	5299.11	5356.02±832
	M_4	0.3806209×10^{6}	0.63881×10^{7}	$(0.2139319\pm0.209177)\times10^{9}$
	M_6	0.14434×10^{9}	0.27006×10^{11}	$(0.1347149\pm0.13469)\times10^{10}$
130.8	M_2	2899.9	5777.52	4242.89
	M_4	0.34689×10^{6}	0.67762×10^{7}	$(0.2823266\pm0.2307)\times10^{7}$
	M_6	0.0000726×10^{9}	0.24431×10^{11}	$(0.7421259\pm0.71824)\times10^{10}$

(2) It was essential to use an effective potential appropriate to each temperature to reproduce the profile well. For example, at 130 K, the discrepancy between theory and experiment is as much as 40% if the effective potential is not employed. These results provide an important test of the RMK-potential for CH_4 over a range of reduced temperature from 0.7 to 1.6.

(3) The values of the three parameters in the pair polarizability giving the translational scattering have not been adjusted in calculations. As a result, the validity of the scaling of the parameter B has been shown to hold approximately over this wide temperature range.

(4) The fact that the values of A = 0.88 $\mathring{A}^4$ and E = 2.5 $\mathring{A}^5$ result in a reproduction of the induced rotational spectrum at all temperatures unequivocally confirms the applicability of the long-range model of the induction mechanism.

(5) Although a rough model was employed to represent the bound state profile, the agreement with the experiment with no adjustable parameters is impressive up to a dimer population which changes the zero moment by 86%.

Figures 7.1-7.5

The experimental spectra for CH_4-CH_4 at T = 295, 250.5, 203, 163.4, and 130.8 K respectively.

FIGURE 7.1

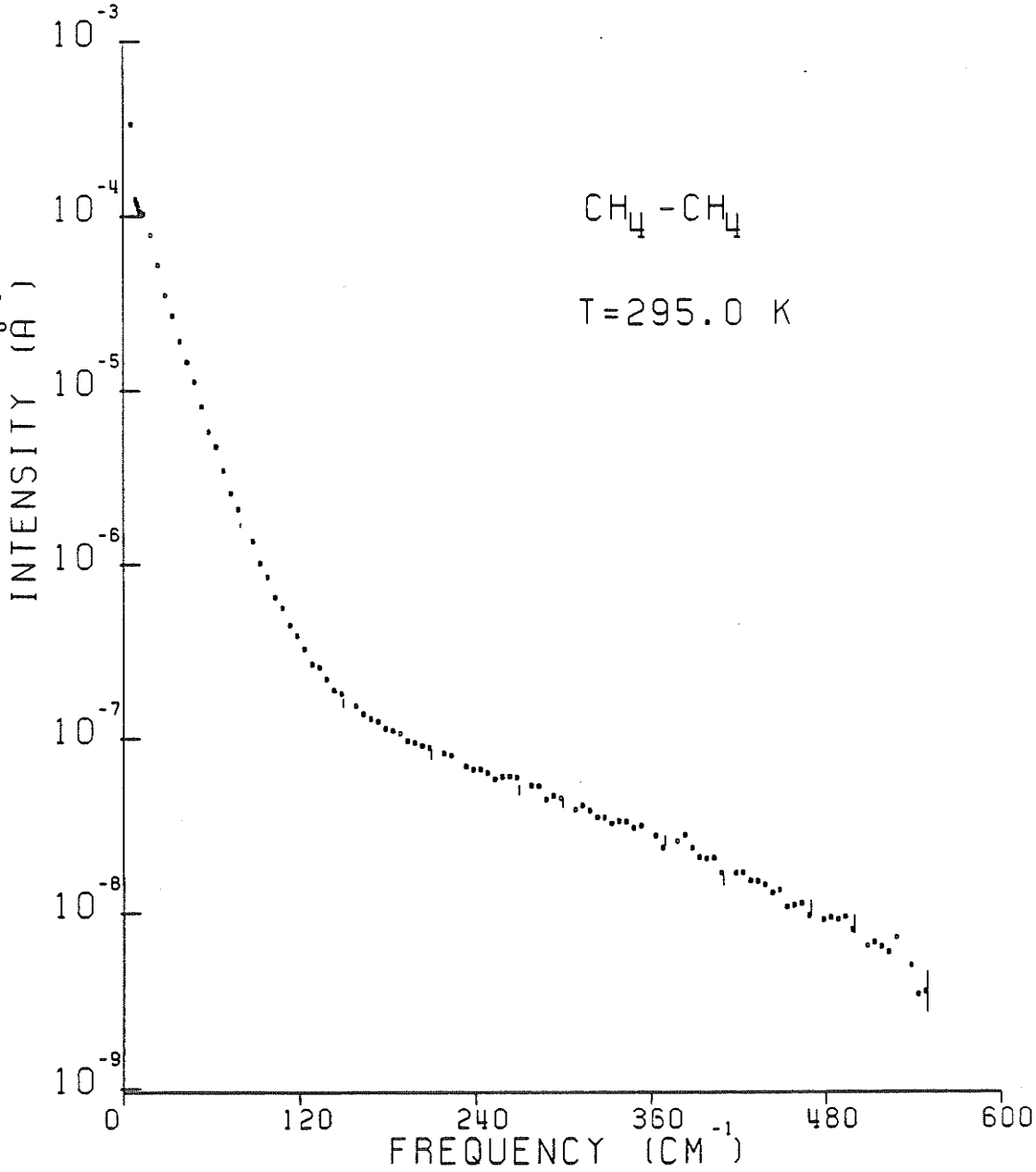
10^{-3}
10^{-4}
10^{-5}
10^{-6}
10^{-7}
10^{-8}
10^{-9}
INTENSITY (A^6)
$CH_4 - CH_4$
T=295.0 K
0
120
240
360
480
600
FREQUENCY (CM^{-1})

FIGURE 7.2

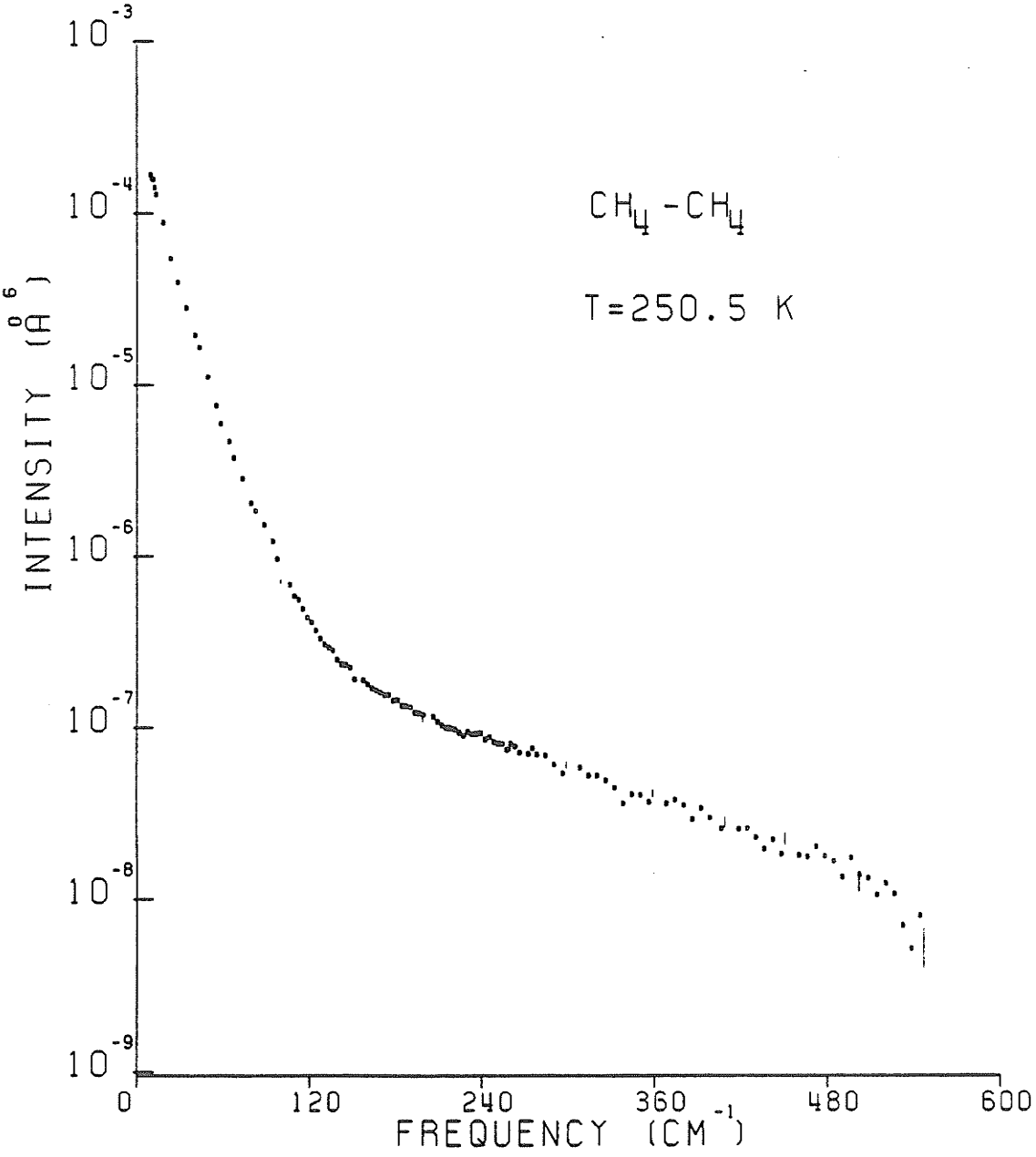
10^{-3}
10^{-4}
10^{-5}
10^{-6}
10^{-7}
10^{-8}
10^{-9}
INTENSITY (A^{6})
$CH_4 - CH_4$
T=250.5 K
0
120
240
360
480
600
FREQUENCY (CM^{-1})

FIGURE 7.3

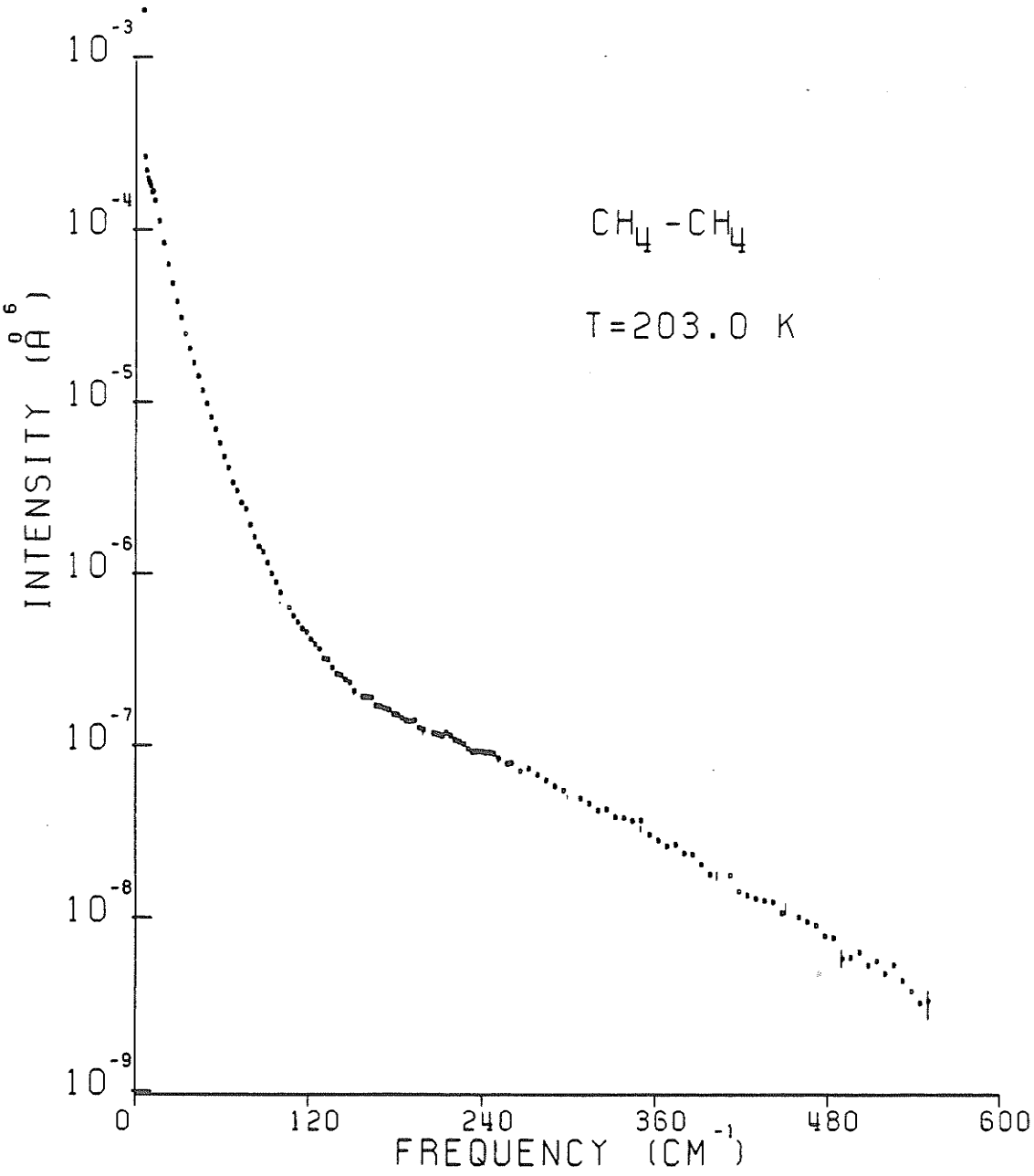
$CH_4 - CH_4$
T=203.0 K
INTENSITY (A^6)
10^{-3}
10^{-4}
10^{-5}
10^{-6}
10^{-7}
10^{-8}
10^{-9}
0
120
240
360
480
600
FREQUENCY (CM^{-1})

FIGURE 7.4

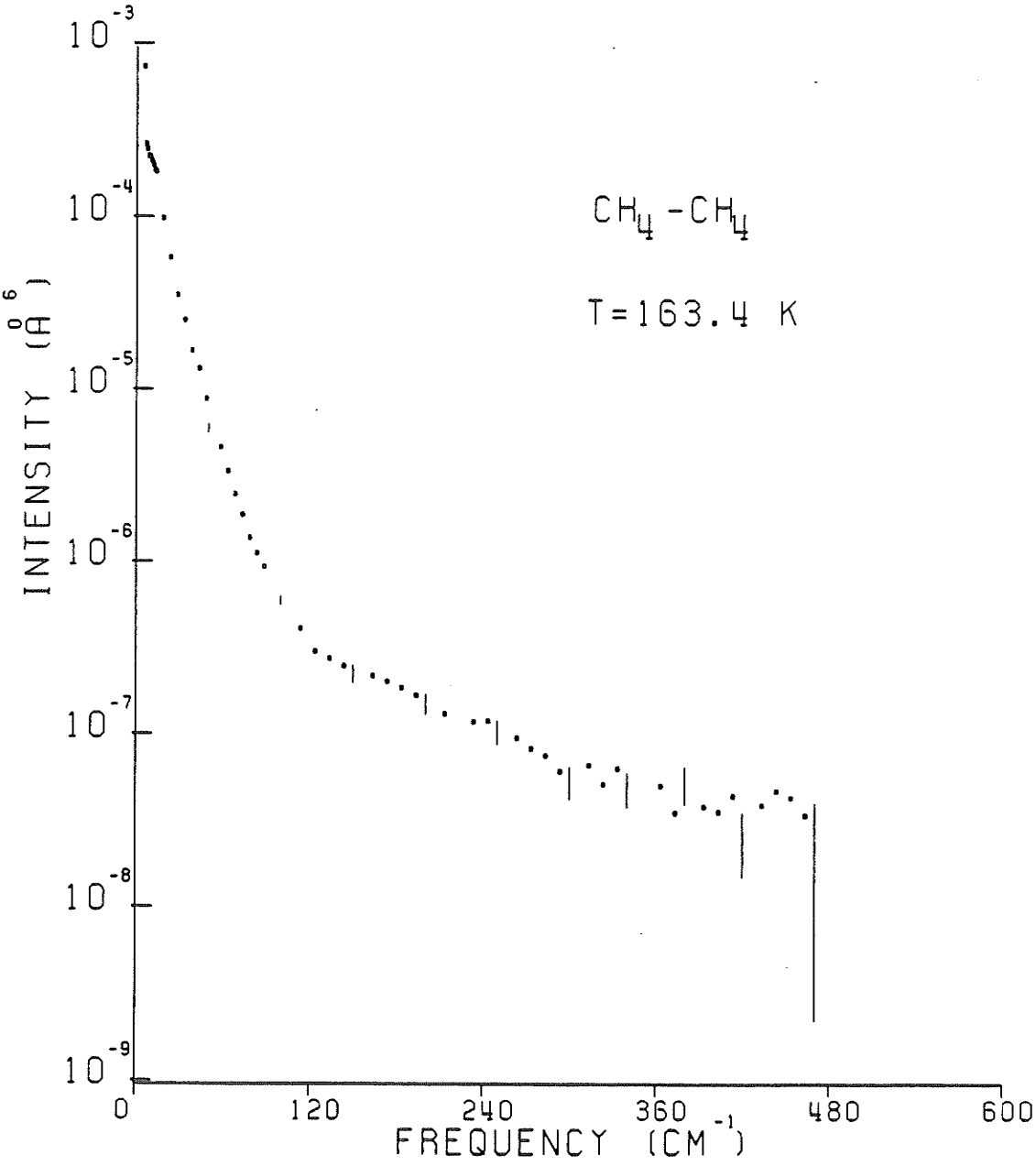
10^{-3}
10^{-4}
10^{-5}
10^{-6}
10^{-7}
10^{-8}
10^{-9}
INTENSITY (A^6)
$CH_4 - CH_4$
T=163.4 K
0
120
240
360
480
600
FREQUENCY (CM^{-1})

FIGURE 7.5

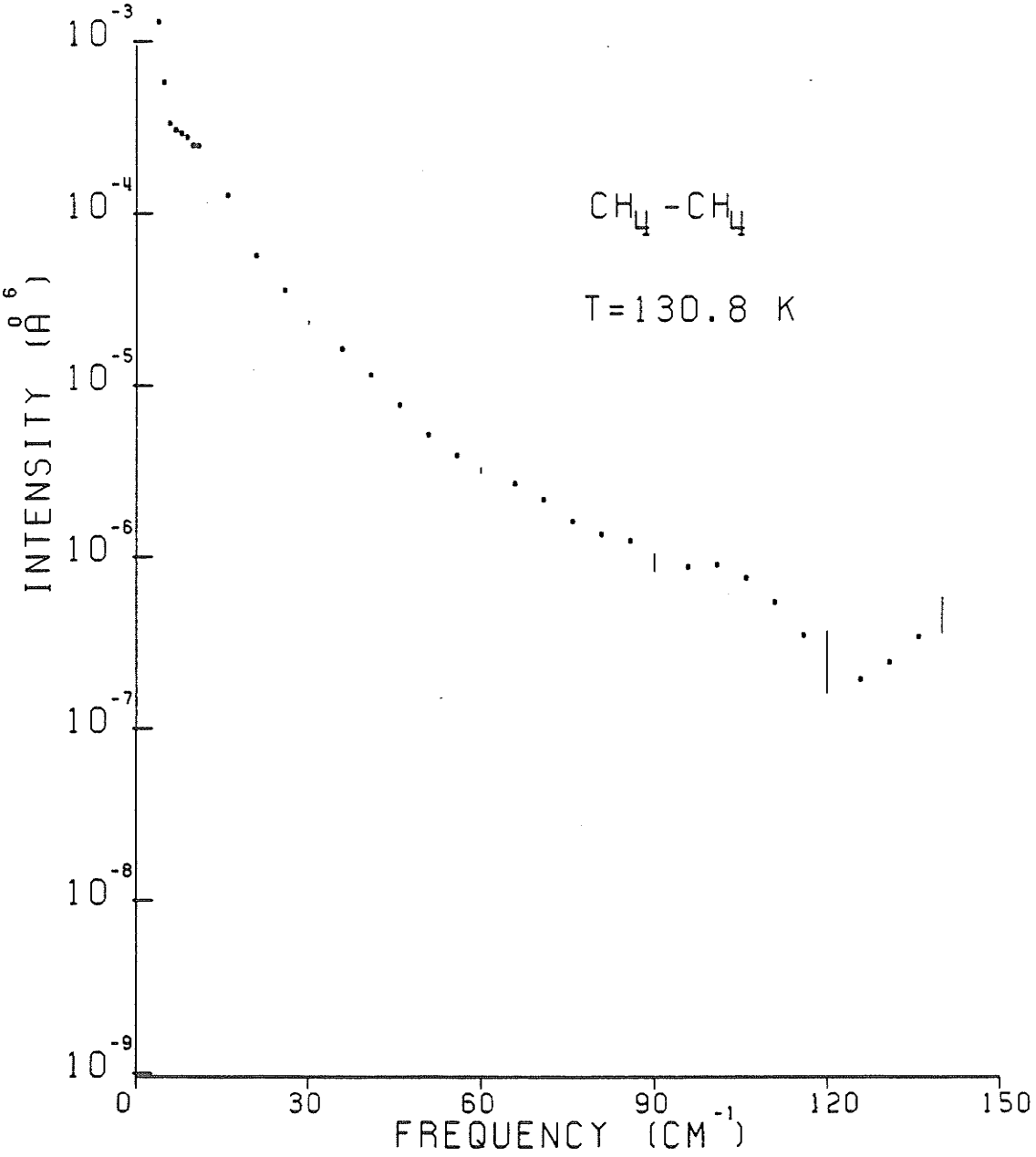
10^{-3}
10^{-4}
10^{-5}
10^{-6}
10^{-7}
10^{-8}
10^{-9}
INTENSITY ($Å^6$)
$CH_4 - CH_4$
T=130.8 K
0
30
60
90
120
150
FREQUENCY (CM^{-1})

Figures 7.6-7.10

Figures 7.6-7.10 The experimental, total theoretical, (translational + dimer), and rotational spectra for CH_4-CH_4 at temperatures of 295, 250.5, 203.0, 163.4, and 130.8 K respectively.

. The experimental spectrum.

- The total theoretical spectrum.

□ The theoretical translational plus dimer spectrum.

* The theoretical rotational spectrum.

FIGURE 7.6

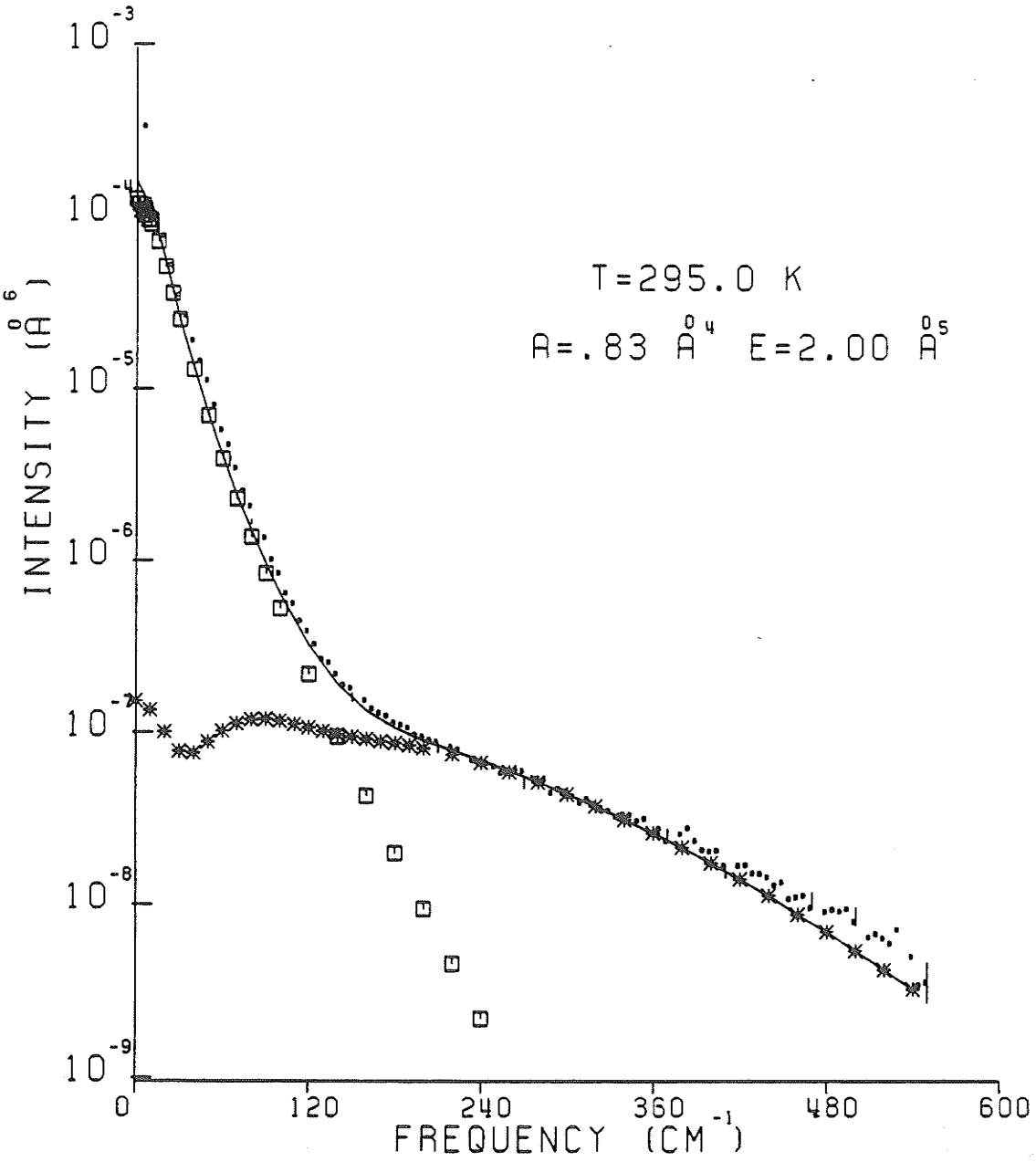
T=295.0 K
A=.83 Å⁴ E=2.00 Å⁵
INTENSITY (Å⁶)
10⁻³
10⁻⁴
10⁻⁵
10⁻⁶
10⁻⁷
10⁻⁸
10⁻⁹
0
120
240
360
480
600
FREQUENCY (CM⁻¹)

FIGURE 7.7

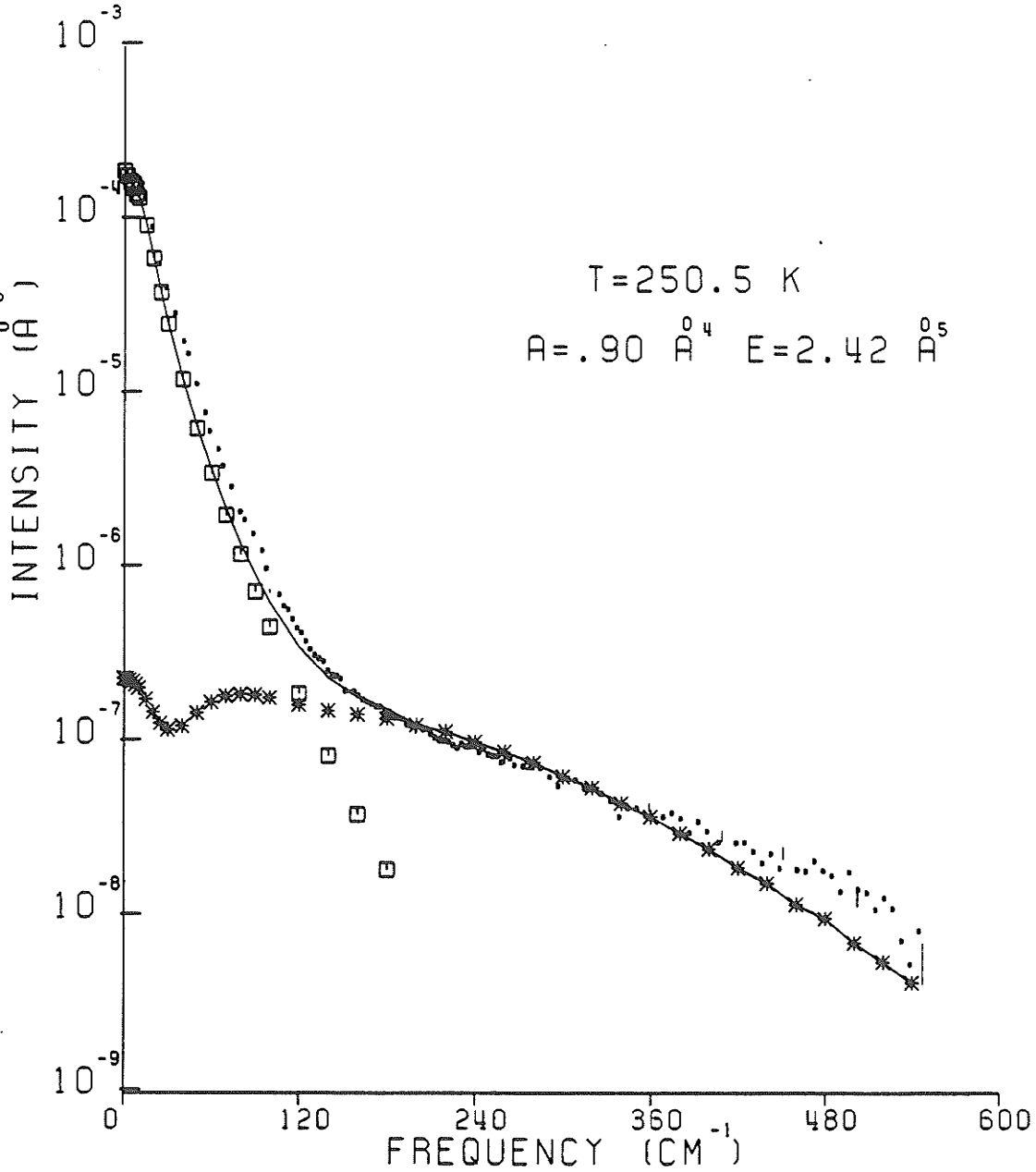
T=250.5 K
A=.90 Å⁴ E=2.42 Å⁵
INTENSITY (Å⁶)
10⁻³
10⁻⁵
10⁻⁶
10⁻⁷
10⁻⁸
10⁻⁹
0
120
240
360
480
600
FREQUENCY (CM⁻¹)

FIGURE 7.8

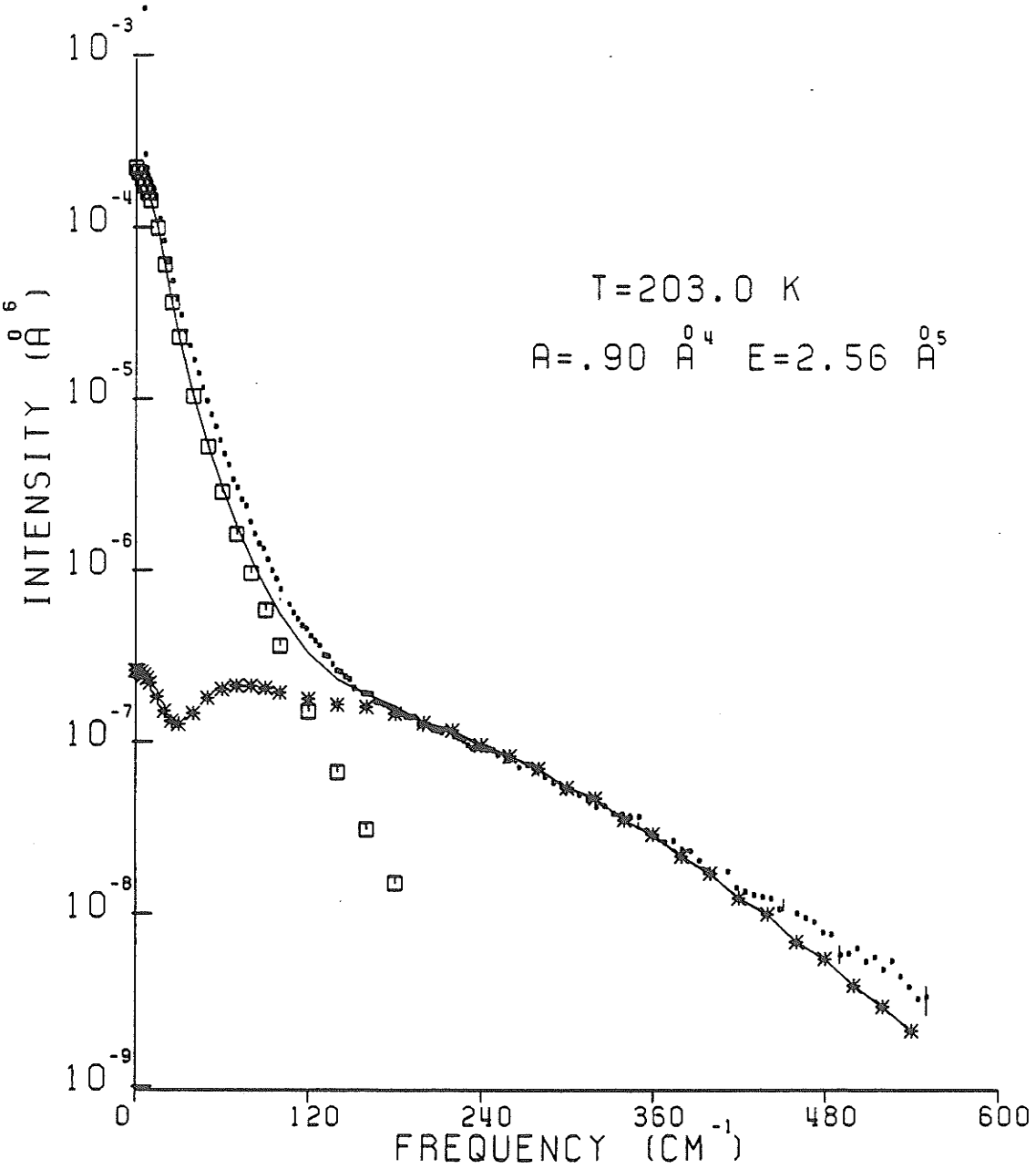
T=203.0 K
A=.90 Å⁴ E=2.56 Å⁵
INTENSITY (Å⁶)
10⁻³
10⁻⁴
10⁻⁵
10⁻⁶
10⁻⁷
10⁻⁸
10⁻⁹
0
120
240
360
480
600
FREQUENCY (CM⁻¹)

FIGURE 7.9

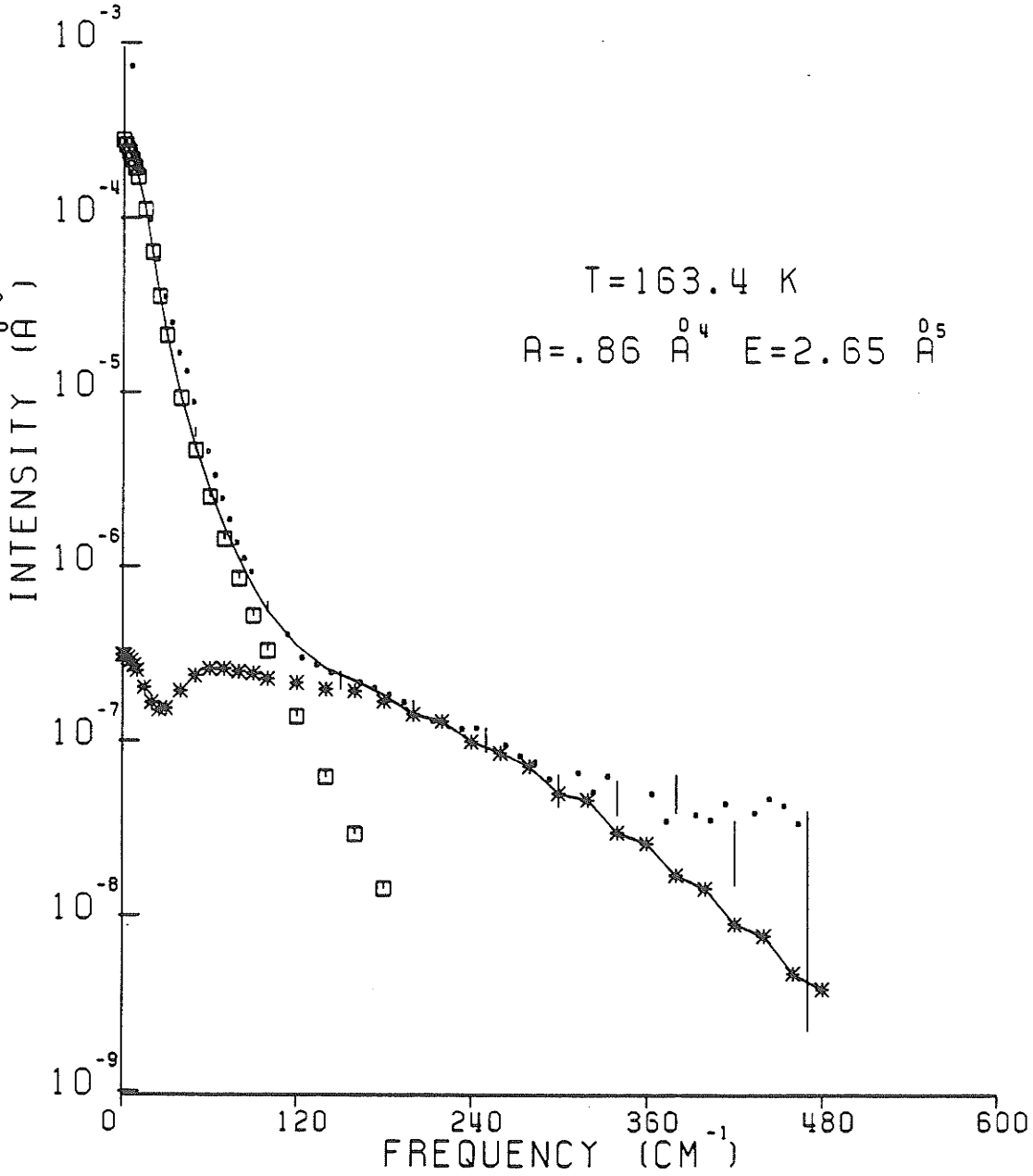
T=163.4 K
A=.86 Å⁴ E=2.65 Å⁵
INTENSITY (Å⁶)
10⁻³
10⁻⁴
10⁻⁵
10⁻⁶
10⁻⁷
10⁻⁸
10⁻⁹
0
120
240
360
480
600
FREQUENCY (CM⁻¹)

FIGURE 7.10

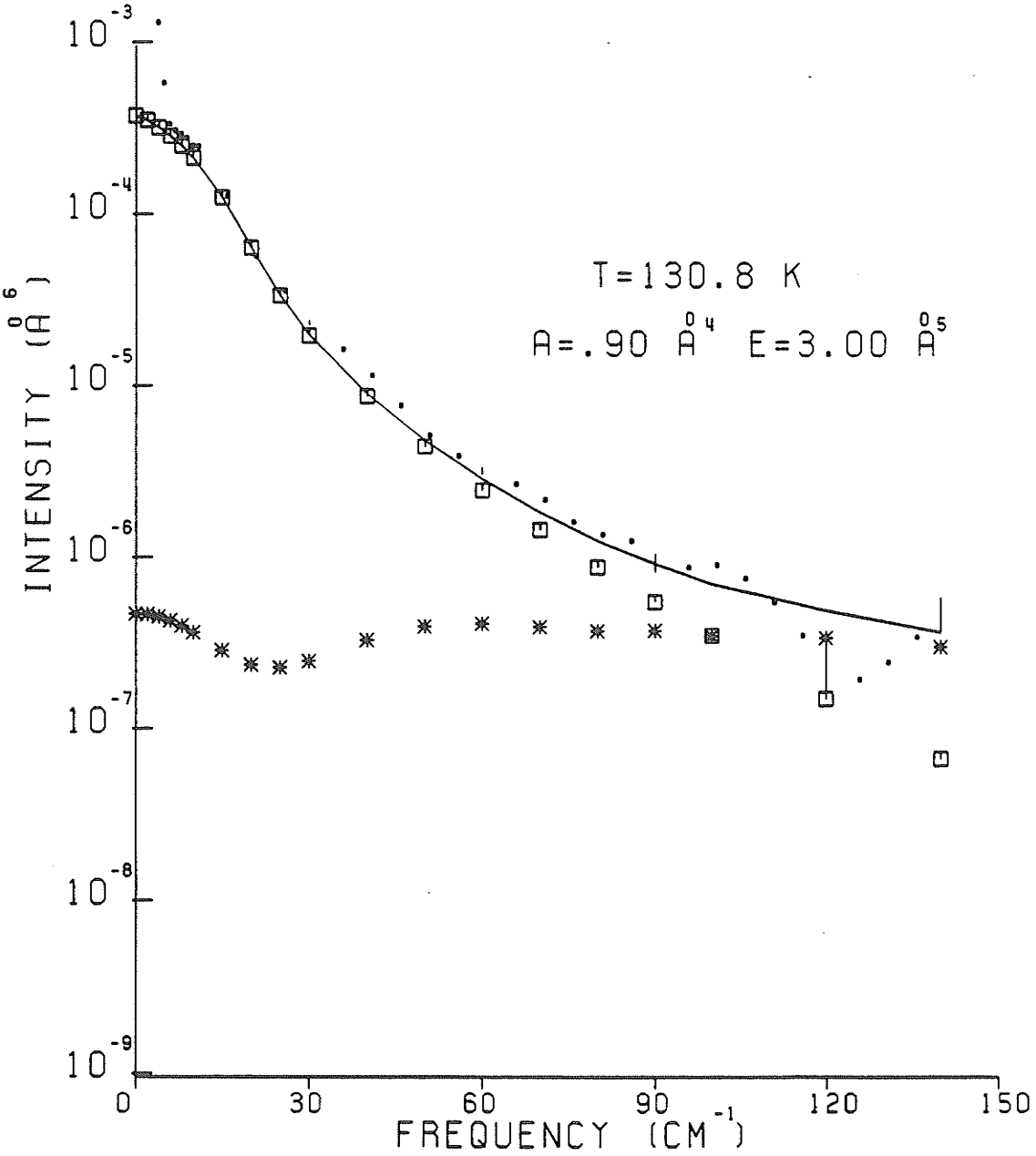
T=130.8 K
A=.90 Å⁴ E=3.00 Å⁵
INTENSITY (Å⁶)
10⁻³
10⁻⁴
10⁻⁵
10⁻⁶
10⁻⁷
10⁻⁸
10⁻⁹
0
30
60
90
120
150
FREQUENCY (CM⁻¹)

Figure 7.11

The experimental spectrum at 130.8 K with theoretical calculations performed with an effective potential appropriate to 295 K.

. The experimental spectrum.

- The total theoretical spectrum.

—·— The theoretical translational plus dimer spectrum.

– – The theoretical rotational spectrum.

FIGURE 7.11

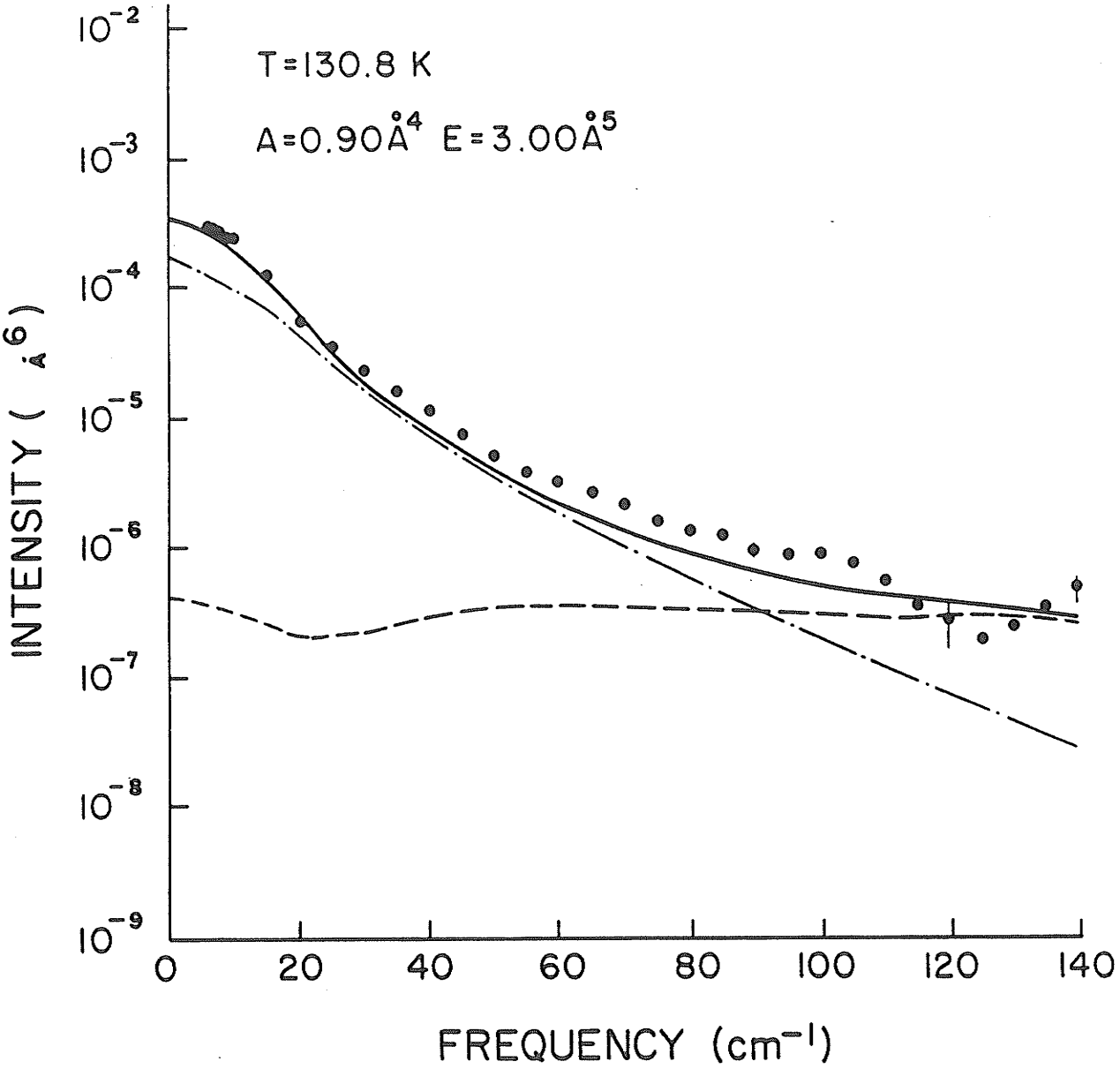
T=130.8 K
A=0.90Å⁴ E=3.00Å⁵
INTENSITY (Å⁶)
10⁻²
10⁻³
10⁻⁴
10⁻⁵
10⁻⁶
10⁻⁷
10⁻⁸
10⁻⁹
0
20
40
60
80
100
120
140
FREQUENCY (cm⁻¹)

Figures 7.12-7.16

Figures 7.12-7.16 The experimental, total theoretical, and translational spectra in the range (0-50 cm^{-1}), at T = 295, 250.5, 203.0, 163.4, and 130.8 K respectively.

. The experimental spectrum.

- The total theoretical spectrum.

—.— The translational spectrum.

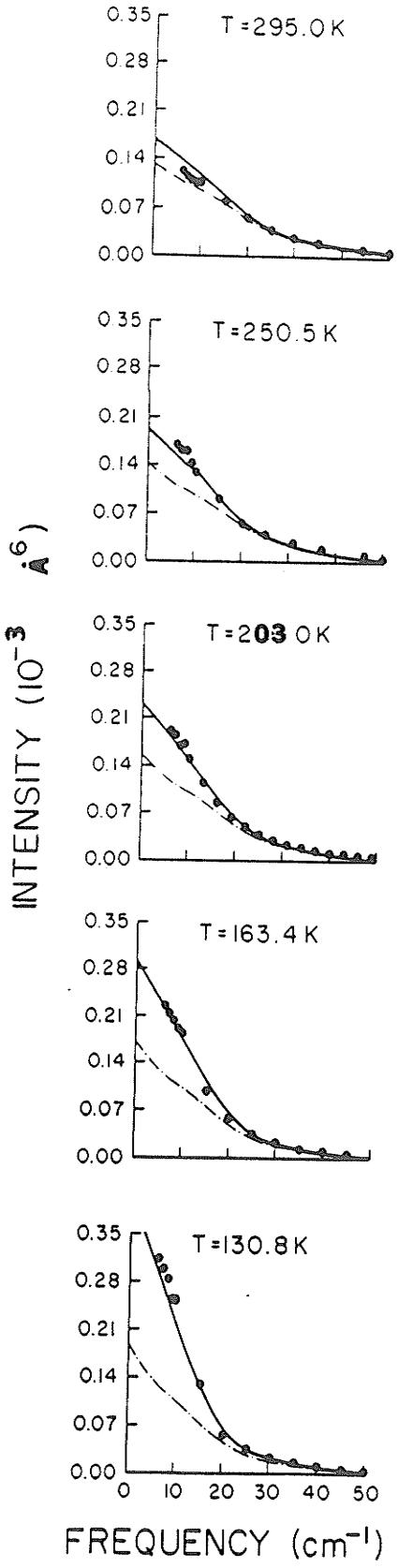

FIGURES 7.12-7.16

Figures 7.17-7.21

Figures 7.17-7.21 The experimental, total theoretical, translational, and rotational spectra at T = 295, 250.5, 203, 163.4, and 130.8 K respectively, where the theoretical spectra were calculated using the Birnbaum-Cohen model.

. The experimental spectrum.

- The total theoretical spectrum.

□ The translational spectrum.

* The rotational spectrum.

FIGURE 7.17

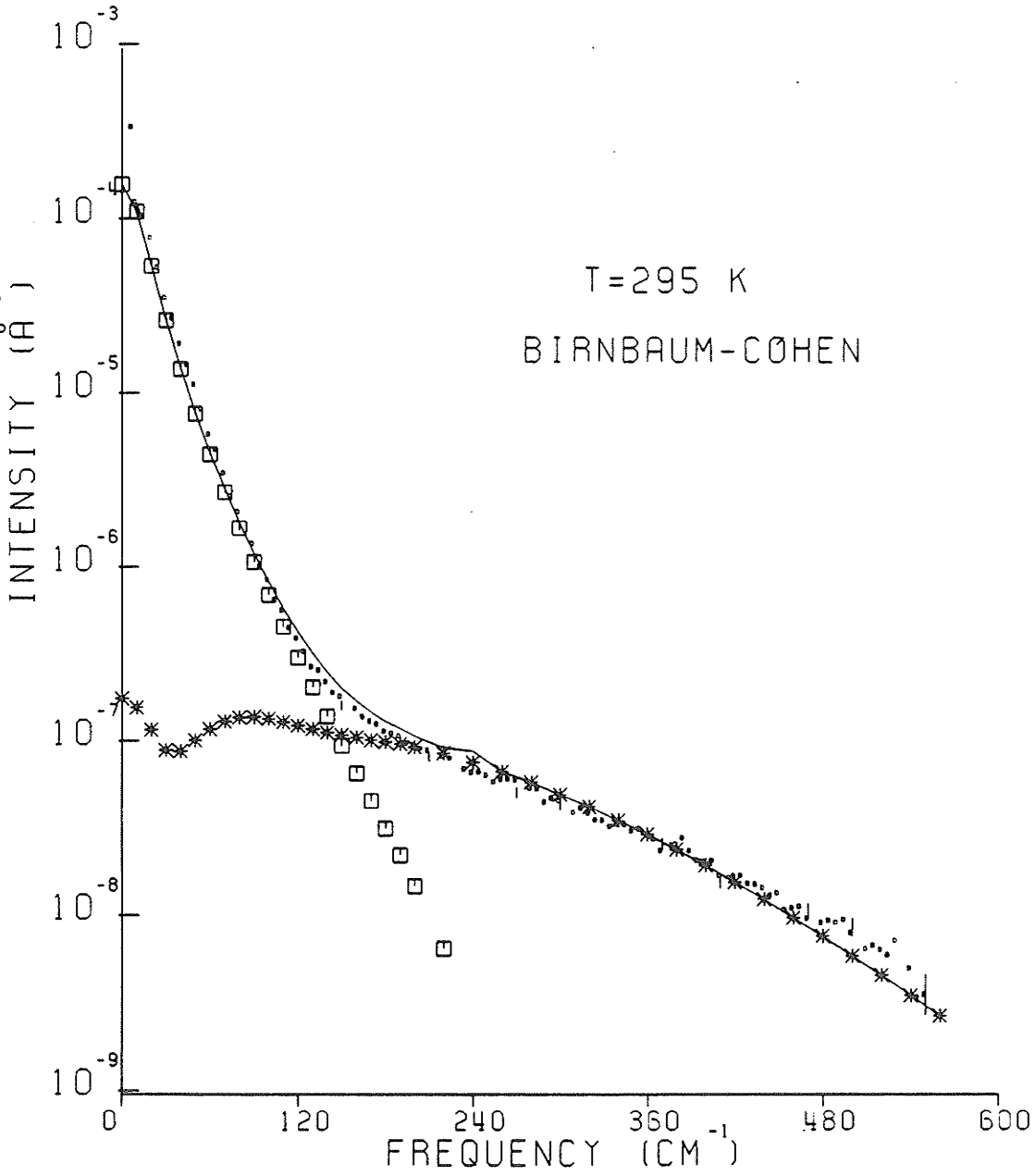
T=295 K
BIRNBAUM-COHEN
INTENSITY ($A^{\circ 6}$)
10^{-3}
10^{-4}
10^{-5}
10^{-6}
10^{-7}
10^{-8}
10^{-9}
0
120
240
360
480
600
FREQUENCY (CM^{-1})

FIGURE 7.18

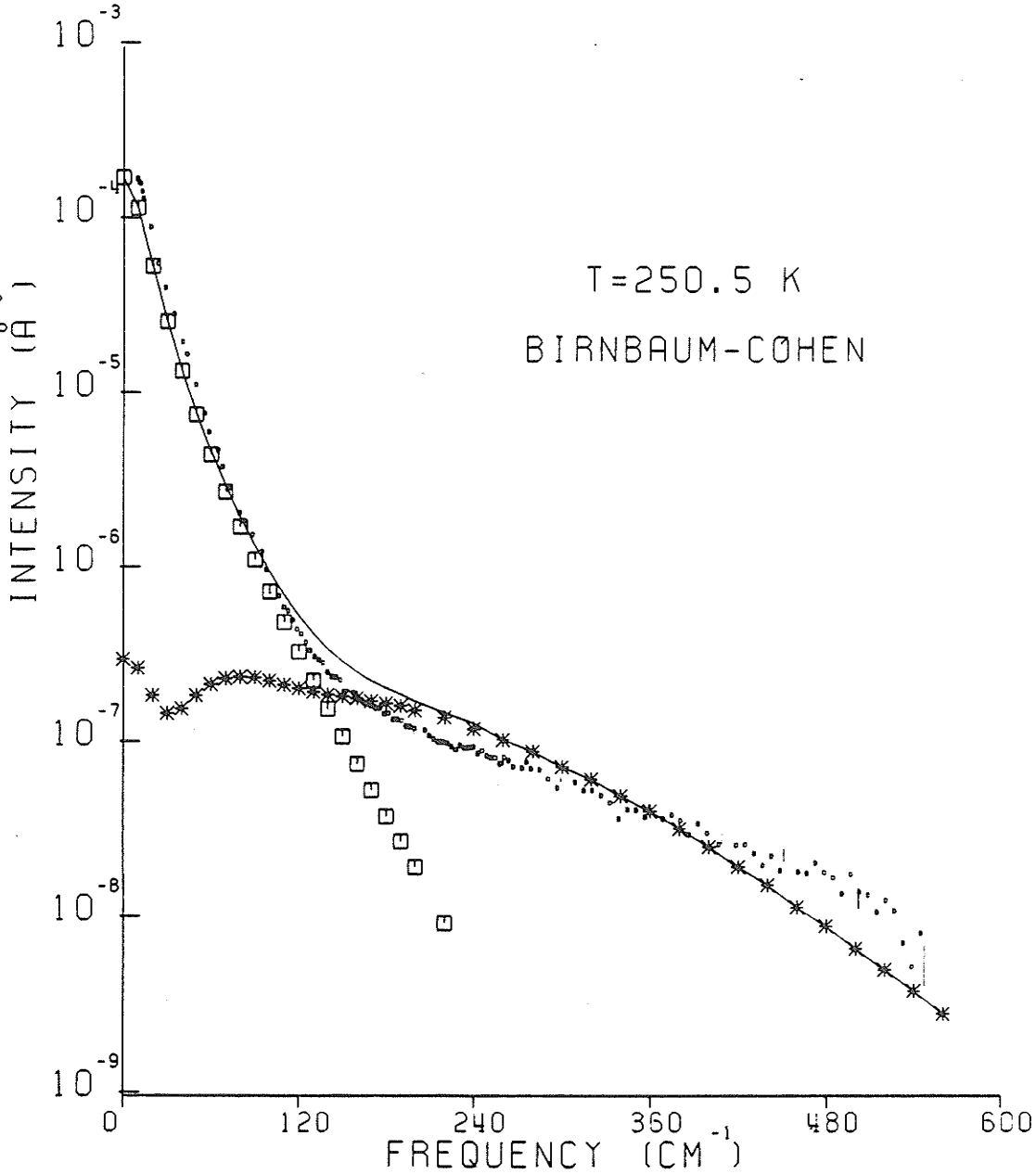
T=250.5 K
BIRNBAUM-COHEN
INTENSITY (A^6)
10^{-3}
10^{-4}
10^{-5}
10^{-6}
10^{-7}
10^{-8}
10^{-9}
0
120
240
360
480
600
FREQUENCY (CM^{-1})

FIGURE 7.19

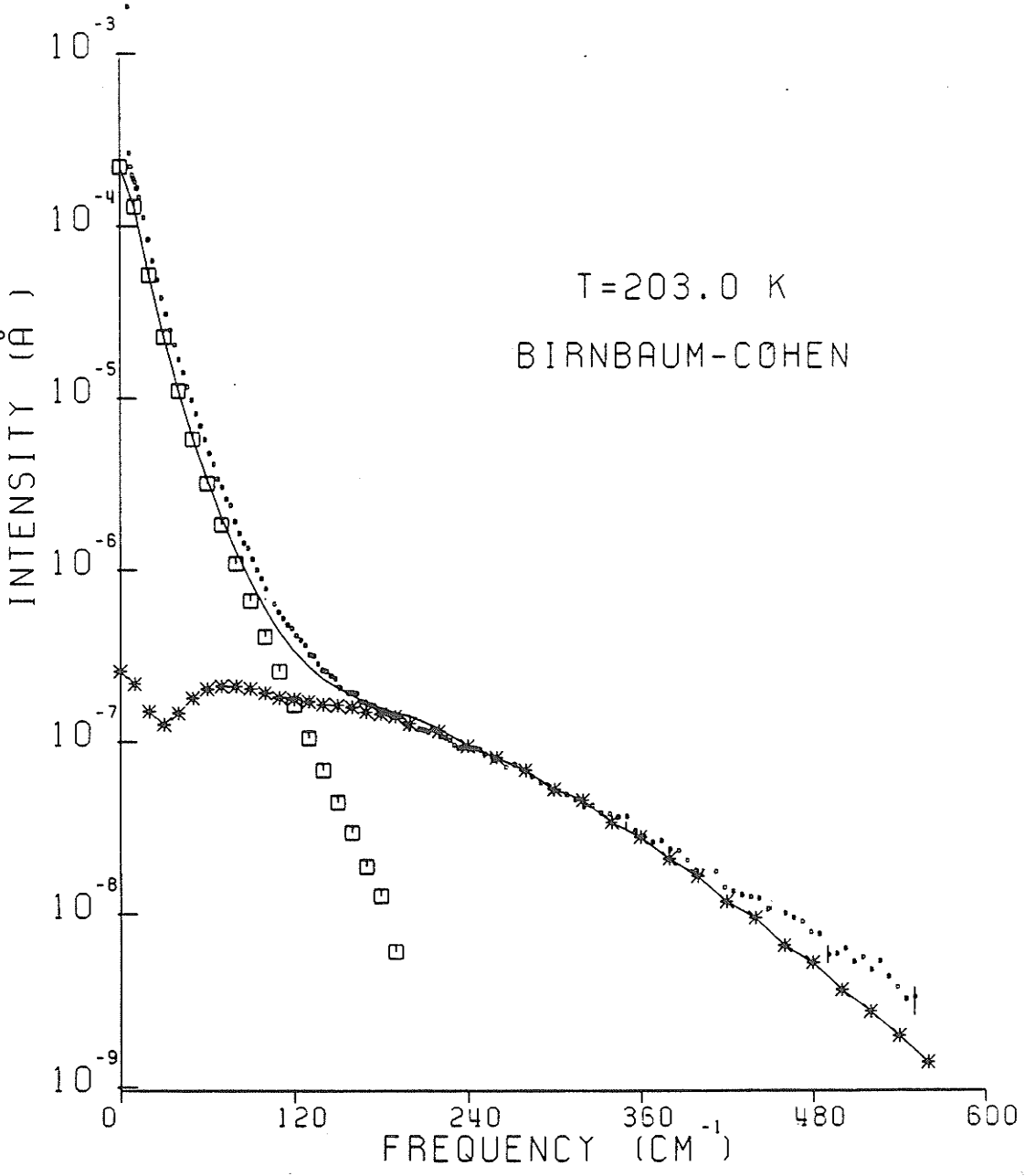
T=203.0 K
BIRNBAUM-COHEN
INTENSITY ($\AA^6$)
10^{-3}
10^{-4}
10^{-5}
10^{-6}
10^{-7}
10^{-8}
10^{-9}
0
120
240
360
480
600
FREQUENCY (CM^{-1})

FIGURE 7.20

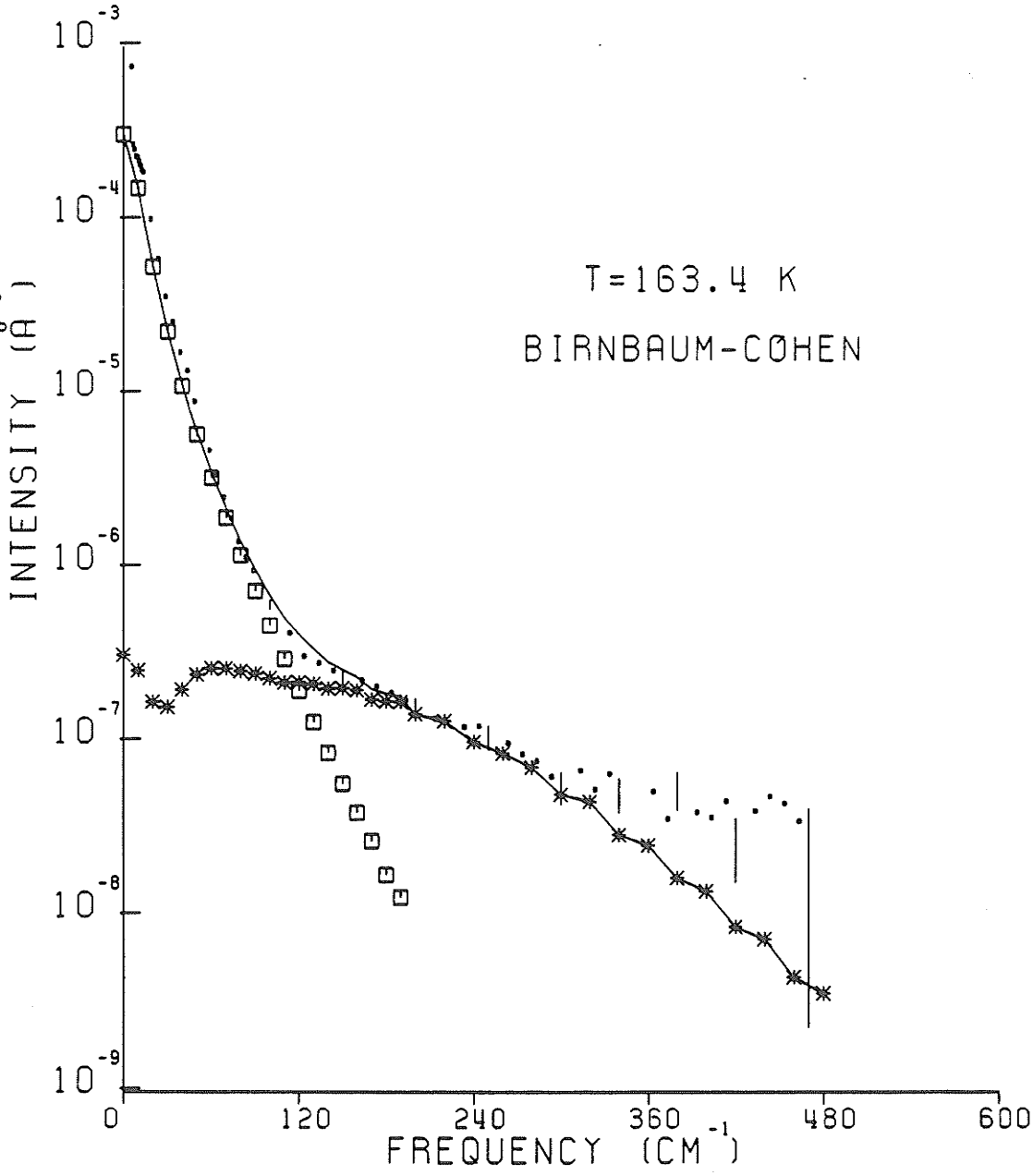
T=163.4 K
BIRNBAUM-COHEN
INTENSITY (Å^6)
10^-3
10^-4
10^-5
10^-6
10^-7
10^-8
10^-9
0
120
240
360
480
600
FREQUENCY (CM^-1)

FIGURE 7.21

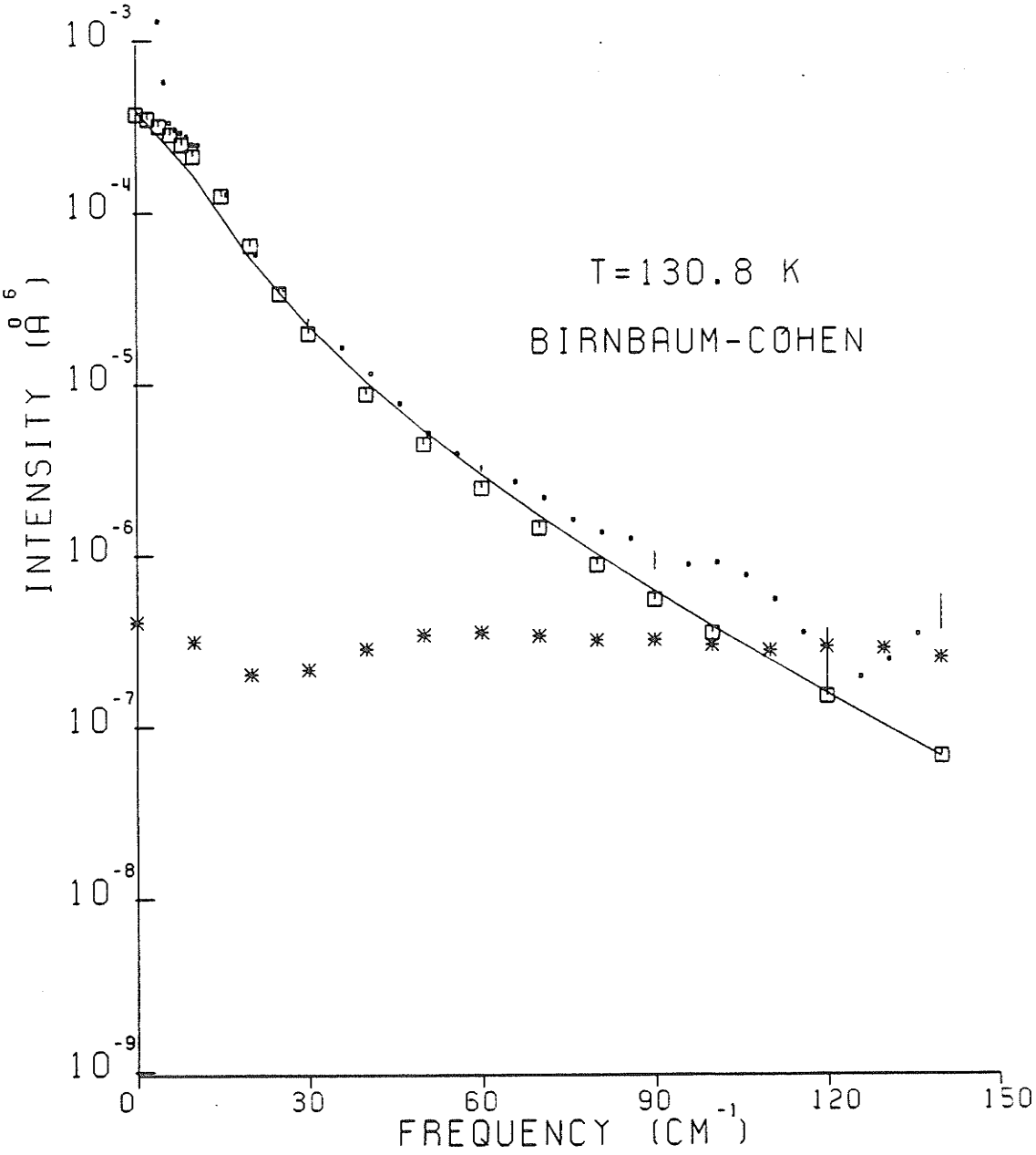
T=130.8 K
BIRNBAUM-COHEN
INTENSITY (Å^6)
10^-3
10^-4
10^-5
10^-6
10^-7
10^-8
10^-9
0
30
60
90
120
150
FREQUENCY (CM^-1)

CHAPTER 8

CONCLUSIONS

The spectrum of collision-induced light scattering of molecules can be accounted for by the free-free interactions which contribute most to the low and mid frequency ranges, the bound-bound interactions which have a narrow feature at low frequency shifts, and the collision-induced rotational scattering which accounts for the intensity and shape of the spectrum at high frequency shifts. There could be a strong overlap between the translational and rotational spectra as in the case of SF_6, a moderate overlap as in the case of CF_4 or as in the case of CH_4, the rotational wing can clearly extend beyond the translational component over a broad frequency range.

This thesis dealt with the three kinds of interactions in the different frequency ranges and these are our conclusions:

1. Line shape calculations for collision-induced translational (free-free) scattering worked very well at room temperature whereas at lower temperatures, it held only approximately because some of the parameters can be temperature dependent.
2. The bound-bound scattering spectrum was calculated roughly but the agreement with the experiment is impressive, even at lower temperatures where the dimer intensity contribute about 45% of the total intensity of the spectrum.
3. The higher order polarizability tensors that were taken to calculate the collision-induced rotational spectrum accounted

well for the intensity and shape of the rotational spectrum, higher order polarizabilities were not usually necessary.

4. The spectrum of collision-induced light scattering of molecules can play a role in developing intermolecular potentials, as for the case of SF_6-Xe.

As mentioned before, the theoretical calculations depend on two important factors, the pair polarizability, and the form of intermolecular potential. More detailed conclusions regarding both can be formulated.

1. The model for the pair polarizability with no adjustable parameters worked very well at room temperature for all species.
2. At lower temperatures (CH_4), the model for $\beta(r)$ still worked, but there was some discrepancy between the theoretical and experimental spectra because some of the parameters, B and r_0, were fixed, while it is believed both can be temperature dependent.
3. The HFD potential is a suitable form of SF_6.
4. The form and parameters of the intermolecular potential have to be known for different kinds of interactions in order to determine high order polarizabilities accurately, as in the case of SF_6-Kr, SF_6-Ar, and SF_6-Ne.
5. In calculating the theoretical spectra at different temperatures, it is important to refine an isotropic effective potential at each temperature as in the case of CH_4.
6. It is not recommended to combine two different potentials for two different molecules to get a potential for the mixture, but if there is no other option, the combination rules by Pena work better than just the simple combination rules.

A summary of the properties and potential quantitatively specified in the thesis is as follows:

(1) The average value of the dipole-octopole polarizability for SF_6 is E = 10.7 ± 2.5 $\mathring{A}^5$.

(2) A new M2SV intermolecular potential for the SF_6-Xe mixture has been developed.

(3) The average values of the dipole-quadrupole polarizability A = 2.5 ± 0.3 $\mathring{A}^4$, and the dipole-octopole polarizability E = 2.5 ± 0.3 $\mathring{A}^5$ for CF_4, agree with the values obtained in this laboratory and give a spectrum which fits well the experimental spectrum.

(4) The average value of the dipole-quadrupole polarizability A = 0.88 ± 0.03 $\mathring{A}^4$ for CH_4, which agrees with the values reported earlier in this laboratory and with the ab initio calculations; the average value of the dipole-octopole polarizability E = 2.5 ± 0.26 $\mathring{A}^5$ for CH_4, agrees with the value obtained earlier in this laboratory.

As for future work, we recommend:

(1) Quantum mechanical trajectory calculations of the spectrum are necessary at lower temperatures.

(2) More refined potentials are needed for tetrahedral molecules and their mixtures as done for the cases for SF_6 mixtures.

REFERENCES

Bafile et al., 1983 — Bafile, U., Magli, R., Barocchi, F., Zoppi, M. and Frommhold, L. 1983. Molec. Phys. 49, 1149.

Bafile et al., 1988 — Bafile, U., Ulivi, L., Zoppi, M. and Barocchi, F. 1988. Phys., Rev. A 37, 4133.

Barocchi et al., 1977 — Barocchi, F., Neri, M. and Zoppi, M. 1977. Molec. Phys. 34, 1391.

Barocchi and Zoppi, 1978 — Barocchi, F. and Zoppi, M. 1978. Phys. Lett. A 66, 99.

Barocchi and Zoppi, 1980 — Barocchi, F. and Zoppi, M. 1980. Intermolecular Spectroscopy and Dynamical Properties of Dense Systems. Edited by J. Van Kranandok. North Holland.

Barocchi et al., 1981 — Barocchi, F., Moraldi, M., Zoppi, M. and Poll, J.D. 1981. Molec. Phys. 43, 1193.

Barocchi et al., 1982 — Barocchi, F., Moraldi, M. and Zoppi, M. 1982. Molec. Phys. 45, 1285.

Barocchi et al., 1983 — Barocchi, F., Zoppi, M., Bafile, U. and Magli, R. 1983. Chem. Phys. Lett. 95, 135.

Birnbaum and Cohen, 1975 — Birnbaum, G. and Cohen, E.R. 1975. J. Chem. Phys. 62, 3807.

Birnbaum and Cohen, 1976 — Birnbaum, G. and Cohen, E.R. 1976. Can. J. Phys. 54, 593.

Borysow and Frommhold, 1983 — Borysow, J. and Frommhold, L. 1983. Phenomena Induced by Intermolecular Interactions. Edited

by G. Birnbaum (Plenum Press), 67.

Buck et al., 1981 — Buck, U., Schleusener, J. Malik, D.J. and Secrest, D. 1981. J. Chem. Phys. 74, 1707.

Buckingham, 1956 — Buckingham, A.D. 1956. Trans. Faraday Soc., 52, 1035.

Buckingham, 1967 — Buckingham, A.D. 1967. Adv. Chem. Phys. 12, 107.

Buckingham and Dunmur, 1968 — Buckingham, A.D. and Dunmur, D.A. 1968. Trans. Faraday Soc., 64, 1776.

Buckingham and Tabisz, 1977 — Buckingham, A.D. and Tabisz, G.C. 1977. Optics Lett., 1, 220.

Buckingham and Tabisz, 1978 — Buckingham, A.D. and Tabisz, G.C. 1978. Molec. Phys. 36, 583.

Buckingham and Clarke, 1979 — Buckingham, A.D. and Clarke, K.L. 1979. Chem. Phys. Lett. 57, 321.

Certain and Fortune, 1971 — Certain, P.R. and Fortune, P.J. 1971. Chem. Phys. Letters, 55, 5818.

Dacre, 1982 — Dacre, Peter D. 1982. Molec. Phys. 45, 17.

Dalgarno and Kingston, 1960 — Dalgarno, A. and Kingston, A.E. 1960. Proc. R. Soc. A 259, 424.

Dymond, 1969 — Dymond, J.H. 1969. The Virial Coefficient of Gases. Clarendon, Oxford.

El-Sheikh, 1985 — El-Sheikh, S.M. 1985. M.Sc. Thesis, U. of M.

El-Sheikh et al. 1985 — El-Sheikh, S.M., Meinander, N. and Tabisz, G.C. 1985. Chem. Phys. Letters 118, 151.

Fieschi and Fumi, 1953 — Fieschi, R. and Fumi, F.G. 1953. Nuovo Cimento

X, 865.

Frommhold, 1987 — Frommhold, Lother. 1987. A Bibliography on Collision-Induced Light Scattering. University of Texas, Austin.

Gharbi and Leduff, 1980 — Gharbi, A. and Leduff, Y. 1980. Molec. Phys., 40, 545.

Hirschfelder et al., 1954 — Hirschfelder, J.O., Curtiss, C.F. and Bird, R.B. 1954. Molecular Theory of Gases and Liquids. (Wiley, New York) 525, 675.

Holzer and Leduff, 1974 — Holzer, W. and Leduff, Y. 1974. Phys. Rev. Letters, 32, 205.

Holzer and Ouillon, 1971 — Holzer, W. and Ouillon, R. 1971. Chem. Phys. Letters, 24, 589.

Holzer and Ouillon, 1976 — Holzer, W. and Ouillon, R. 1976. Proc. 5th Intl. Conf. on Raman Spectroscopy. Edited by E.D. Schmid, Schulz, Freiburg, P. 424.

Isnard et al., 1976 — Isnard, P., Robert, D. and Galatry, L. 1976. Molec. Phys. 31, 1789.

Kielich, 1969 — Kielich, S. 1969. I.E.E.E. J. Quant. Electronics 5, 562.

Leduff et al., 1987 — Leduff, Y., Ouillon, R., Chandrasekharan, V. and Silvi, B. 1987. Molec. Phys., 62, 1065.

Lu and Shelton, 1987 — Lu, Z. and Shelton, D.P. 1987. J. Chem. Phys. 87, 1967.

MacCormack and Schneider, 1951 — MacCormack, K.E. and Schneider, W.G. 1951. J. Chem. Phys. 19, 849.

Maitland et al., 1981 Maitland, G.E., Rigby, M., Smith, E.B. and Wakeham, W.A. 1981. Intermolecular Forces, Their Origin and Determination.

Martin et al., 1982 Martin, M.L., Trengove, R.D., Harris, K.R. and Dunlop, Peter J. 1982. Ber. Bunsenges. Phys. Chem. 86, 626.

Mazzinghi and Zoppi, 1983 Mazzinghi, P. and Zoppi, M. 1983. Rev. Sci. Instrum. 54, 11.

McCoubrey and Singh, 1959 McCoubrey, J.C. and Singh, N.M. 1959. Trans. Faraday Soc. 55, 1826.

Meinander and Tabisz, 1983 Meinander, N. and Tabisz, G.C. 1983. J. Chem. Phys. 79, 1.

Meinander et al., 1985 Meinander, N., Penner, A.R., Bafile, U., Barocchi, F., Zoppi, M., Shelton, D.P. and Tabisz, G.C. 1985. Molec. Phys. 54, 493.

Meinander et al., 1986 Meinander, N., Tabisz, G.C. and Zoppi, M. 1986. J. Chem. Phys. 84, 3005.

Meinander and Tabisz, 1986 Meinander, N. and Tabisz, G.C. 1986. J. Quant. Spectroscopy Radiat. Transfer 35, 39.

Monchick et al., 1963 Monchick, L., Yun, K.S. and Mason, E.A. 1963. J. Chem. Phys. 39, 654.

Monchick and Green, 1975 Monchick, L. and Green, S. 1975. J. Chem. Phys. 63, 2000.

Neumann, 1984 Neumann, Martin. 1984. Molec. Phys. 53, 187.

O'Brien et al., 1973 O'Brien, E.F. Gutshick, V.P., McKoy, V. and McTague, J.P. 1973. Phys. Rev. A 8, 690.

Pack et al., 1982 Pack, R.T., Valentini, J.J. and Cross, J.B.

1982. J. Chem. Phys. 77, 5486.

Pack et al., 1984 — Pack, R.T., Piper, E., Pfeffer, G.A. and Toennies, J.P. 1984. J. Chem. Phys. 80, 4940.

Parker and Pack, 1976 — Parker, G.A. and Pack, R.T. 1976. J. Chem. Phys. 68, 1585.

Pena et al., 1982 — Pena, M. Diaz, Pando, C. and Renuncio, J.A.R. 1982. J. Chem. Phys. 76, 1.

Penner, 1983 — Penner, A.R. 1983. M.Sc. Thesis, U. of M.

Penner et al., 1985 — Penner, A.R., Meinander, N. and Tabisz, G.C. 1985. Molec. Phys. 54, 479.

Pleich, 1983 — Pleich, R. 1983. Ph.D. Thesis, University of Vienna.

Poll, 1980 — Poll, J.D. 1980. Intermolecular Spectroscopy and Dynamical Properties of Dense Systems. Edited by J. Van Kranandok (North Holland), 45.

Poll and Hunt, 1981 — Poll, J.D. and Hunt, J.L. 1981. Can. J. Phys. 59, 1449.

Posch, 1982 — Posch, A.H. 1982. Molec. Phys., 46, 1213.

Powels et al., 1983 — Powels, J.G., Dore, J.C., Deraman, M.B. and Osag, E.K. 1983. Molec. Phys. 30, 1.

Prengel and Gornall, 1976 — Prengel, A.T. and Gornall, W.S. 1976. Phys. Rev. A 13, 253.

Rajan and Lalita, 1974 — Rajan, S. and Lalita, K. 1974. J. Magn. Reson. 16, 115.

Reed and Gubbins, 1973 — Reed, T.M. and Gubbins, K.E. 1973. Applied

Statistical Mechanics. (McGraw-Hill), 386.

Righini et al., 1981 — Righini, Roberto, Maki, Kazno and Klein, Michael L. 1981. Chem. Phys. Letters 80, 1981.

Rose, 1959 — Rose, M.E. 1959. Elementary Theory of Angular Momentum. Wiley, New York.

Samson and Ben-Reuven, 1976 — Samson, R. and Ben-Reuven, A. 1976. J. Chem. Phys., 65, 3586.

Samson et al., 1976 — Samson, R., Pasmanter, R.A. and Ben-Reuven, A. 1976. Phys. Rev. A., 14, 1224 and 1238.

Santafa et al., 1978 — Santafa, J., Urieta, J.S. and Losa, C.G. 1978. Chem. Phys. 28, 187.

Shelton, 1979 — Shelton, D.P. 1979. Ph.D. Thesis, U. of M.

Shelton and Tabisz, 1980 — Shelton, D.P. and Tabisz, G.C. 1980. Molec. Phys. 40, 299.

Shelton et al., 1982 — Shelton, D.P., Tabisz, G.C., Barocchi, F. and Zoppi, M. 1982. Molec. Phys. 46, 21.

Shelton, 1986 — Shelton, D.P. 1986. J. Chem. Phys. 1, 84.

Shelton and Lu, 1988 — Shelton, D.P. and Lu, Zhangfong. 1988. Phys. Rev. A 37, 3813.

Shelton and Ulivi, 1988 — Shelton, D.P. and Ulivi, L. 1988. J. Chem. Phys. 89, 149.

Sigmund et al., 1972 — Sigmund, P.M., Silberberg, I.H. and McKetta, J.J. 1972. J. Chem. Eng. Data 15, 168.

Silberstein, 1917 — Silberstein, L. 1917. Phil. Mag. 33, 92, and 521.

Stone, 1975 — Stone, A.J. 1975. Molec. Phys. 29, 1461.

Stone, 1976	Stone, A.J. 1976. F. Phys. A. 2, 485.
Tabisz, 1979	Tabisz, G.C. 1979. Molecular Spectroscopy. Specialist Periodical Report. Chemical Society of London, 6, 136.
Thibeau, 1968	Thibeau, M. and Oksengorn, B. 1968. Molec. Phys. 15, 579.
Thibeau et al., 1977	Thibeau, M., Gharbi, A., Leduff, Y. and Sergiescu, V. 1977. J. Phys. (Paris), 38, 641.
Watson and Ramaswamy, 1936	Watson, H.E. and Ramaswamy, K.L. 1936. Proc. Royal Soc. A 156, 144.